



XA04N2808

INIS-XA-N--235

**OECD Standard Problem**

**OECD-CSNI-ISP 29**

**"Distribution of Hydrogen within the  
HDR-Containment under  
Severe Accident Conditions"**

**- Final Comparison Report -**

**H. Karwat**

**Lehrstuhl für Reaktordynamik**

**und Reaktorsicherheit**

**Technische Universität München**

**August 1992**



Work performed under contract with Gesellschaft für Reaktorsicherheit (GRS) mbH, Köln (contract number 73010 / UA 670) within the frame of BMFT-funded research work.

## Table of Contents

	Page
Summary	iii
<b>1. Introduction</b>	<b>1</b>
<b>2. The HDR Test Facility and the Main Features of the Experiment</b>	<b>4</b>
2.1 Available Instrumentation	5
2.2 The Initial and Operating Conditions of Experiment E11.2	6
2.3 Performance of the Experiment	8
<b>3. The Analytical Task</b>	<b>9</b>
<b>4. Chronology of the Activity</b>	<b>11</b>
<b>5. Submitted Contributions and Applied Simulation Models</b>	<b>11</b>
<b>6. Comparison of Calculated with Measured Parameters</b>	<b>13</b>
6.1 Containment Pressure	14
6.2 Temperatures of the Containment Atmosphere	14
6.3 Gas Concentrations	15
6.4 Steam Concentrations	16
6.5 Containment Sump Temperatures	17
6.6 The Period of Water Spray on the Outside of the Steel Shell	17
<b>7. Overall Assessment of the Results</b>	<b>18</b>
<b>8. Conclusions and Recommendations</b>	<b>22</b>
References	27
Tables	29
Figures	53
Appendix I	144
Appendices II A, B, C , H, J	157

## Summary

The present report summarizes the results of the International Standard Problem Exercise ISP-29, based on the HDR Hydrogen Distribution Experiment E11.2. Post-test analyses are compared to experimentally measured parameters, well-known to the analysts. This report has been prepared by the Institute for Reactor Dynamics and Reactor Safety of the Technical University Munich under contract with the Gesellschaft für Anlagen- und Reaktorsicherheit (GRS) which received funding for this activity from the German Ministry for Research and Technology (BMFT) under the research contract RS 792. The HDR experiment E11.2 has been performed by the Kernforschungszentrum Karlsruhe (KfK) in the frame of the project "Projekt HDR-Sicherheitsprogramm" sponsored by the BMFT.

Ten institutions from eight countries participated in the post-test analysis exercise which was focussing on the long-lasting gas distribution processes expected inside a PWR containment under severe accident conditions. The gas release experiment was coupled to a long-lasting steam release into the containment typical for an unmitigated small break loss-of-coolant accident. In lieu of pure hydrogen a gas mixture consisting of 15 % hydrogen and 85 % helium has been applied in order to avoid reaching flammability during the experiment.

Of central importance are common overlay plots comparing calculated transients with measurements of the global pressure, the local temperature-, steam- and gas concentration distributions throughout the entire HDR containment. The comparisons indicate relatively large margins between most calculations and the experiment.

Having in mind that this exercise was specified as an "open post-test" analysis of well-known measured data the reasons for discrepancies between measurements and simulations were extensively discussed during a final workshop. It was concluded that analytical shortcomings as well as some uncertainties of experimental boundary conditions may be responsible for deviations. Several processes have been identified to deserve more close consideration. The long-lasting absorption of energy by relatively cold containment structures and the associated prediction of long acting heat-sources and - sinks as well as the predictability of the temperature of the sump water collected during the experiment and the impact of an instrument cooling system extracting relatively large amounts of energy during the experiment were the main objects of the discussion. Several important recommendations concerning future activities have been identified.



## 1. INTRODUCTION

A variety of codes has been generated which predict the thermalhydraulic containment behaviour as a basis for important design decisions. Conservation equations together with a number of constitutive relationships form the essential mathematical basis which must be solved by suitable numerical solution procedures. In general, the numerical solution of every fluiddynamic code is to a considerable extent dependent on the user's decisions how to apply the code in terms of nodalisation, the choice of empirical constants or correlations and the selection of the available code versions when he sets up his "Analytical Simulation Model" (ASM) of the object. It is the validity not only of the code, but of the "Analytical Simulation Model" which must be verified by the comparison to measured evidence, generated by suitable experiments or actual plant data. Many experiments have been performed, the data of which have been documented within reports or sometimes on magnetic tapes. However, not every individual experiment is suitable for validation purposes.

Some experiments served as a basis for International Standard Problem (ISP) exercises. They are exceptionally well documented and nowadays form the main structure of a containment code validation matrix.

A standard problem is defined as a task to predict in advance by means of computer simulation models the course of a carefully specified experiment carried out to demonstrate certain technical-physical phenomena. Such tasks have been executed since 1972 in the field of the simulation of various engineered reactor safety systems (e.g. of the Emergency Core Cooling Systems or of the containments of Light Water Reactors) within the national or international frame. They have been sponsored either by the Committee for the Safety of Nuclear Installations (CSNI) of the OECD (Organisation for Economic Cooperation and Development) or the CEC (Commission of the European Communities).

The main objective of a standard problem activity with respect to the behaviour of a reactor safety system is the assessment of the predictive accuracies by comparing calculated results of several code users to the measured reality of a well specified experiment. Preferably, this may be done in performing "best-estimate"-type calculations to establish a meaningful basis for comparisons.

Specific standard problem objectives are:

- (I) to provide a comparison of best-estimate computer code calculations with experimental data under controlled conditions,
- (II) to contribute to a better engineering understanding of postulated accident events and their interactions with mitigating systems,
- (III) to provide a unique opportunity for code users to verify their methods of applying codes on the basis of experimental measurements.

Code verification is primarily a task for institutions developing codes; it requires considerable financial resources for performing a large number of calculations and comparing relevant experimental results with calculated ones. The ISP activity should be considered as a supplementary activity, validating proper code application by experts other than the code developer.

The "blind" pretest prediction of the PHDR-Containment test T31.5 (a DBA-type blowdown test with a long subsequent cooldown phase) showed considerable uncertainties with respect to the analytical simulation of the thermohydraulic state of the containment after termination of the blowdown event /KAR89/. A similar observation was made by those participants who undertook an attempt to predict the very first hydrogen distribution experiment carried out as a continuation of the Standard Problem test T31.5. Certain shortcomings have been identified which were held responsible for the deviations between measured parameters and predicted parameters. Long term natural convection flow simulation requires a different simulation approach compared to the task to predict the highly transient containment pressurization process at the beginning of an accident.

Participants in both activities felt a strong need for more experimental evidence for longlasting processes governing the results of probabilistic risk analyses. They recommended the execution of another International Standard Problem focusing mainly on the long-lasting natural convection effects. A typical small break LOCA blowdown with up to a 24 h period of analyses of natural convection phenomena was considered as an interesting test condition.

With the agreement of the Federal Ministry for Research and Technology (BMFT) who sponsored the HDR-based Safety Research Programme a test out of a series of 5 hydrogen distribution tests (the E11-series) has been offered to the members of the Principal



Working Group No. 4 and its particular Task Group on Severe Accident Phenomena in the Containment during meetings held in April 1989 and October 1989. Both groups felt it too early to attempt another "blind" pre-test prediction of such an experiment immediately after learning about the result of ISP-23 with respect to long-term containment behaviour. The group instead recommended to support an "open" exercise to give code developers and code users an opportunity to improve their code application skillness.

On this basis the Federal Republic of Germany formally submitted the experiment E11.2 as basis for an "open" Standard Problem to the Principal Working Group No. 4. The experiment E11.2 was run to study the distribution of hydrogen inside a pressurized water reactor (PWR) containment. The objectives of the experiment E11.2 were the following:

- determine the temperature distribution during the entire transient
- study the distribution of energy during and after the SBLOCA-phase
- measure the steam/air/hydrogen distribution within the containment atmosphere under severe accident conditions initiated by a SBLOCA

Out of the entire series of hydrogen distribution tests E11.1-5 the experiment E11.2 was chosen to serve as the basis for an International Standard Problem ISP-29. This selection was done before the test results have become available. The main reason for the selection of E11.2 was due to the fact that the adopted experimental procedure for E11.2 obviously was based on the most simple sequence of events characterizing a possible severe accident scenario. Furthermore, it was anticipated that the location of the small break LOCA simulation and the subsequent release of hydrogen gas into the HDR containment for the test E11.2 was more typical in view of the possible conditions existing within a large PWR containment than all the applied operating conditions of other experiments, e.g. that chosen to execute experiment E11.4. Another important aspect was, that the ratio between heat absorbing internal concrete masses and the involved free volume is more typical within the upper section of the HDR containment than for the lower section.

The main features of the operational procedure for experiment E11.2 are leaning towards an analytical prediction obtained in connection with the German Risk Analysis, Phase B. In particular, the timing of the thermal conditioning of the containment and the hydrogen release period has been selected on basis of numerical calculations, strongly linked to a particular severe accident sequence. However, the energy actually transferred with the steam from internal and external sources was not in full agreement with commonly applied scaling

aspects based on the ratio of the free volume of the HDR test facility to that of a full-size PWR.

## 2. THE HDR TEST FACILITY AND THE MAIN FEATURES OF THE EXPERIMENT

The HDR test facility has been described in detail on occasion of the International Standard Problems ISP-16 and ISP-23. The main features of the test facility are shown in fig. 2.1. The facility is described by the documents /SCH82/ and /SCH82a/, the leaktightness characteristic of the HDR containment has been checked in 1990 and proven to be largely unchanged compared to the test results obtained earlier in 1984 (see fig. 2.2).

The experiment has been started by injecting steam for more than 12 hours into the compartment 1.805 at an elevation of 17,55 m according to the compartment configuration shown in cross section in fig. 2.3. Three injection lines have been provided:

- 1 pipe connects the energy reservoir of the former HDR reactor pressure vessel with compartment 1.805
- 1 line connects to an external steam source
- 1 line connects to the reservoir for the hydrogen/helium mixture.

The mass flow rate originating from the reactor pressure vessel-reservoir is shown in fig. 2.4, the specific enthalpy of the discharged steam is shown in fig. 2.5.

Considerably more steam has been injected from a source outside the HDR-facility according to the mass flow rates given in fig. 2.6. The specific enthalpy of the external steam supply is shown in fig. 2.7.

From the figures 2.4 to 2.7 it is evident, that the pre-conditioning of the containment lasted for approximately 740 minutes. Between 740 minutes and 772 minutes a mixture of 15 % hydrogen and 85 % helium (termed "light gas") has been released at the location of the first steam injection through the third line. Fig. 2.8 and 2.9 show the mass flow rate and the specific enthalpy of the "light gas" as function of time.

After termination of the "light gas" release a second steam injection took place. Now the steam has been released into the compartment R1.405 at the -1,1 m elevation. The second steam injection period ended at 958 minutes after starting the experiment (location see fig. 2.10).

At 975 minutes in time spraying of the containment steel shell from the outside was initiated with a flow rate of 5.83 kg/s. The temperature of the external spray water is given as time function shown in fig. 2.11.

A summary of the major operational events of the experiment E11.2 is given by table 1 and by fig. 2.12.

A list of all HDR containment compartments and flow paths connecting these compartments during experiment E11.2 has been provided to the ISP-participants either in form of tables or as information stored on a tape. Similar information has been made available to participants to the former ISP-23 activity. The status of doors and flaps of all flow connection during experiment E11.2 is described by the attached tables 2/1 to 2/3.

Additional information on the details of the flow path geometry, the concrete and metal surface associated to each compartment and a possible nodalisation scheme has also been given by a tape. The thermal properties of structural materials present within the HDR containment are given by the attached tables 3/1 to 3/3.

## **2.1 Available Instrumentation**

The details of the installed instrumentation of the containment have been documented within the task specification /KAR90/. The main measured physical parameters recorded were:

- local atmospheric and structural temperatures
- local composition of the atmosphere (air, steam, hydrogen)
- pressures
- heat transfer coefficients at selected positions within the containment
- heat transfer coefficients at selected positions of the containment steel shell
- local convective flow velocities

A complete list of all measured containment data available for comparison to calculated parameters has been provided by Appendix A to the ISP-29 Specification ("PHDR Requirements for Calculational Results of E11 Computations") giving exact information on the location of each sensor resp. of each gas sampling device.

Temperatures of the containment atmosphere, heat transfer data and steel shell temperatures have been registered with a frequency of 1 Hz. Other variables (e.g. pressure, humidities, velocities, mass flow rates, gas concentrations) have been stored with a sampling frequency of 0.166 Hz. Some data have been recorded with a frequency of 625 Hz during the phases of the "light gas" release and the external steel shell spray operation /VAL89/.

## **2.2 The Initial and Operating Conditions of Experiment E11.2**

Within the frame of the PHDR research project an opportunity was given to several interested institutions to submit "blind post-test prediction results" of the experiment E11.2. These calculations had to be based on the communicated as-measured initial and operating conditions of the experiments E11.2 and E11.4. The submitted predictions showed unexpectedly large deviations to the measured pressure vs. time history /WOL91/. Subsequent discussions took place during the first preparatory workshop of the ISP-29 exercise to understand the reasons for these deviations, because the same initial conditions and the same steam discharge rates were given to the nominated ISP-29 participants as basis for the "open" recalculation of E11.2.

Several possible reasons have been addressed. It was found that an instrument cooling system activated during the E11-series of experiments had extracted between 10 to 15 % of the total energy transferred by the steam into the containment (see fig. 2.13). The energy loss by instrument cooling has been measured integrally by the temperature difference of the auxiliary coolant system of the HDR-facility which was connected to several instruments requiring cooling. Main contributors were the humidity sensors which were located close to the gas sampling points (see Appendix A of the ISP-29 specification /KAR90/). PHDR suggested a local distribution of energy sinks (caused by the instrument cooling) according to the location of gas sensors. Some uncertainty still exists with respect to the quality of the thermal isolation of the involved coolant lines, which may have also contributed to the relatively large overall energy extraction through the auxiliary coolant system.

The major reason for the deviation between most "blind" predictions and the measured pressure transient however was supposed to stem from an error in the communicated steam release rates. Some inconsistencies concerning the energy transfer from the external steam source into the containment had been discovered in March 1991. There was a discrepancy between the data provided by the specification for the external steam mass flow rate and the associated specific enthalpy on one side, and the measured data of the

pressure sensors in the external steam injection line (supplying energy for the E11-experiments) close to the pipe exit into the containment on the other side. One possible explanation was that the mass flow calibration according to the orifice measurement rules provided by the norm DIN 1952/ISO 5167 had been invalidated.

Subsequent investigation by PHDR has revealed that

- the calibration of the orifice in the steam discharge line had been invalidated for unknown reasons;
- the mass flow control was based on wrong mass flow measurements;
- one had to conclude on a considerably reduced mass and energy flow into the containment

As a consequence, the HDR-Project had undertaken an activity to recalibrate the orifice under E11.2 experimental conditions. It had even been envisaged to repeat the experiment should the recalibration efforts fail.

Four independent problems have been identified by HDR during their recalibration studies invalidating the earlier communicated steam release rates. They have been reassessed on the basis of the recalibration of the flow orifice. The recalibrated integral release has been cross-checked by a comparison to the measured mass of condensate water at the end of the experiment. Reasonable agreement was found resulting in the external steam release rate now shown in fig. 2.6.

The "as-measured" thermal initial conditions (temperatures, relative humidity) are given in tables 4/1 to 4/4. The actually applied steam release rates and the light gas (15 % hydrogen and 85 % helium) injection rates have also been provided in digital form by a revised tape mailed to nominated participants in July 1991.

The gas sampling system has been started at 680 min extracting a locally existing air-steam-gas mixture through 42 pipes, each with an internal diameter of 4 mm and a length of 60 meters. The instrument cooling system was operated for the entire duration of the experiment continuously extracting energy according to fig. 2.13.

Altogether, the calibration error of the mass flow measurement of the external steam line and the instrument cooling system caused a factual reduction of the total enthalpy input from internal and external sources into the containment during the experiment E11.2 as

shown by fig. 2.14. This largely explains the reasons for the deviations between "blind" predictions and the measured pressures mentioned above, published earlier at several occasions (e.g. /WOL91/).

### 2.3 Performance of the experiment

The execution of the experiment E11.2 has been described in detail by a test protocol /WEN89/, which also served as the basis for the ISP-29 specification. The experiment was executed as specified (with the exception of the reduced external steam supply rate).

From the phenomenological point of view the experiment E11.2 may be subdivided into 3 distinct phases:

- the containment heat-up phase which is to a certain extent oriented towards the energy release rates of an unmitigated small break loss-of-coolant accident.
- The hydrogen gas release phase immediately coupled to the second low elevation steam release. At least the hydrogen release rates may be considered as a representative volume-scaled simulation of a risk-relevant core melt scenario. The second steam release period was originally anticipated to be representative for a slow sump evaporation after core melt discharge into the sump water.
- A cooldown period enhanced by spraying water into the gap between the containment steel shell and the surrounding external concrete structure.

The main interest of the ISP-29 concentrates on containment internal natural convection flows and heat absorption processes by structures. Of particular interest was the second phase of the experiment during which the "light gas" distribution (15 % hydrogen and 85 % helium) occurred.

The reliability of the experimental data and the accuracy of the measured parameters have been assessed in detail by the experimentalist /WEN91/. Particular attention has been given to the gas concentration measurements which provided the information about the distribution of the injected "light gas", the air and the steam as well. It should be noted that the gas concentration measurement was based upon the measurement of the local hydrogen concentration in combination with humidity, temperature and pressure measurements. A maximum absolute error of the measured hydrogen concentration of 0,12 vol.% (for a nominal value of 2,12 vol.%) has been reported. These values correspond to a maximum absolute error of 0,8 vol.% "light gas" (for a nominal value of 14,1 vol.% "light gas"). In face of

the complexity of the gas concentration measurement procedure the reported error bands for the measured gas concentrations appear to be somewhat optimistic. However, even a duplication of the anticipated error bands would allow to consider the generated data base as being well suited to serve for a comparison to calculated parameters.

### **3. THE ANALYTICAL TASK**

The participants to this standard problem exercise had the opportunity to analyse in detail the local distribution of air, steam and "light gas" based on a full knowledge of the experimental data, provided on a tape. Hence, the main aim of ISP-29 was to investigate into the capabilities of the code users to set-up an appropriate analytical simulation model to reproduce the experimental evidence ("open exercise").

The formation of local transient gas concentrations may be considered as the most important integral result of the longlasting natural convection process dominating the entire free volume of the containment. Hence, in performing such calculations careful attention must also be given to the simulation of the energy addition caused by the anticipated longlasting unmitigated small break loss-of-coolant accident and the associated energy absorption by structure.

Out of a total number of more than 420 sensors a limited number of parameters have been specified to serve for comparison within the frame of this exercise. Tables 5, 6/1 and 6/2 show the selected sensors which found the agreement of the participants to the first preparatory workshop. They may allow an overall assessment of the integral results of the comparative calculations submitted by the participants. The safety relevance of ISP-29 is seen in the gas distribution process as characterized by the locally measured gas and steam concentration transients. 43 parameters including 19 local gas concentrations have been chosen for the comparison. The reduction was necessary to limit the exercise within the frame usual for ISP-exercises. Subjecting all measured parameters to a comparison would have been useful to open a more in-depth scientific discussion of analytical shortcomings.

On the other hand, experience with previous containment standard problems has shown that parameters like local heat transfer coefficients, local velocities and temperatures of structures have often been disregarded by participants from the data submitted for the comparison. Either incompatibility of the chosen analytical simulation model (ASM) with the location of measured data or anticipated large discrepancies between measured and calcu-

lated data have been told as reasons. Participants agreed in the selected parameter field as a reasonable compromise on occasion of the preparatory workshop.

Having this in mind, the discussion of the result of the ISP-29 submissions will preferably focus on the quality of analytical simulations for the 3 distinct phases of the experiment.

During the heat-up phase (1st phase) of the containment structures absorb energy from the released steam. Local temperature fields are generated which cause a temperature stratification within the containment atmosphere. In particular, in the vicinity of the steam release location the containment internal structures are warmed-up resulting in a typical distribution of heat sources and heat sinks for the subsequent development of the buoyancy-driven gas distribution process. The analysis of this first phase will best be assessed on basis of the calculated overall pressure transient and the local atmospheric temperatures.

For the gas distribution phase (2nd phase) the most important parameters are the local "light gas", steam and air concentration transients. They may be considered as important indicators for the integral convection loops developing under the given thermal conditions of the containment internal atmosphere (stratification) and temperature distribution at the surfaces of the internal metallic and concrete structures. The late low-level steam release (into compartment R1.405) to a certain extent promotes the generation of a new convection pattern which is evident from the observed changes of the local concentration transients thereafter.

The effect of the local instrument cooling on the thermalhydraulic behaviour of the HDR-containment has been a major topic for discussions during the execution of this exercise and afterwards. A direct impact on the pressure-time history and an influence on locally generated convection loops and atmospheric temperature distributions must be assumed, but is difficult to quantify. The local cooling effect might have been large within areas of high temperatures while it might be negligible in other areas. Clearly, instrument cooling and its associated uncertainties might have complicated the analytical task.

For the cooldown period the evolution of the pressure transient as a representative overall parameter for the energy status of the containment temperature was of importance. Progressing steam condensation influenced the "light gas"-distribution as well.



#### 4. CHRONOLOGY OF THE ACTIVITY

The experiment E11.2 was proposed to the CSNI-Working Group No. 4 "Confinement of Accidental Radioactive Releases" on occasion of its annual meeting in October 1989. PWG4 submitted this proposal to CSNI which endorsed the execution of ISP-29 in November 1989.

The exercise was performed according to the following chronology:

Endorsement by CSNI	November 1989
Mailing of the preliminary specification	April 1990
Nomination of participants	May 1990
First preparatory workshop	19./20. June 1990
Communication of experimental data of the experiment E11.2	30. June 1990
Release of the completed specification including the experimental data tape	18. July 1990
Special workshop discussing the results of some pre-test predictions submitted to PHDR	29./30. November 1990
Temporary suspension of the exercise due to inconsistencies in the energy input data	Mid March 1991
Resumption of the exercise after definitive assessment of the energy release data relevant for experiment E11.2	31. July 1991
Submission of calculated results	1. February 1992
Release of the preliminary comparison report	29. May 1992
3rd workshop to discuss the results and conclusions of the preliminary comparison report	24/25. June 1992
Presentation of the Final Report to the CSNI-Principal Working Group No. 4	September 1992

#### 5. SUBMITTED CONTRIBUTIONS AND APPLIED SIMULATION MODELS

Ten international institutions representing eight countries made an attempt to analyse the HDR experiment E11.2 and submitted calculated results according to the agreed list of physical parameters requested by the task specification. Five different thermal-hydraulic containment codes have been involved in the activity.

Table 7 provides an overview on the participating institutions, the involved experts and the participating countries. An identifier has been given to each contribution to distinguish the results within the comparative plots. 6 participants used the CONTAIN-Code in either the

version 1.11 or 1.12. Two participants submitted more than one set of calculated parameters. Upon request these participants identified a preferred "base case" the data of which have been processed in the form of common overlay plots presented within this report. Where appropriate important findings of sensitivity studies have been communicated they will be mentioned separately.

More information about the applied computer programs, the adopted nodalisation concepts and some other details identifying the empirical treatment of important physical parameters are summarized by tables 8/1 to 11/2. The processed information has been extracted from the reports submitted by the participants describing their analytical modelling approach. Summary descriptions of the involved codes are given in Appendix A of this report.

Tables 8/1 and 8/2 depict important features which characterize the Analytical Simulation Models (ASM) which the participants have generated using the indicated code version. The inner free containment volume has been represented by a number of control volumes ranging between 9 and 56. The control volumes were interconnected by 14 up to 130 flow junctions. Both parameters (control volumes and flow junctions) are representative for the degree of sophistication which was attempted by the ASM set-up.

The external gap between the steel shell and the surrounding concrete was simulated by several control volumes ranging between 1 and 9. Interesting is also the wide range of the number of specified heat structures describing the inner containment structural design as evident from tables 8/1 and 8/2.

Tables 9/1 and 9/2 provide some information concerning other specific features of the ASMs. Table 9/1 summarizes information given for the application of the CONTAIN-code. The items of interest cover the handling of the heat transfer to structures and the heat conduction inside structures as well as the specification of flow loss coefficients to be decided upon by the code users. Table 9/2 provides the same information for the application of codes other than CONTAIN.

With revision 2 (August 1990) the participants to the ISP-29 exercise have been informed about the overall heat losses caused by the instrument cooling system (see also fig. 2.13 of this report). During certain periods of the experiment the heat losses by instrument cooling reduced the global energy added from the external steam source by nearly 30 % and caused even net cooling of the containment during the gas release period (see fig. 21.4). Hence, some analysts spent considerable efforts in proper modelling of the instrument cool-

ing effects. Tables 10/1 and 10/2 give an overview on the modelling aspects of the instrument cooling as applied by users of the CONTAIN code (table 10/1) and of other codes (table 10/2). Some participants attempted an integral simulation of the cooling effects while others used more sophisticated concepts to study the impact on natural convection flow circuits and gas concentration distributions. Locations with high atmospheric temperatures must be considered as to contribute more to local cooling than the low temperature regions.

Tables 11/1 and 11/2 provide additional information characterizing particularities of the generated ASMs. Past experience obtained on occasion of the ISP-23 follow-up activity has indicated the importance of the numerical subdivision of the large dome compartment. Subdivision in several control volumes may have an impact on the proper simulation of convection loops possibly existing in parallel within a large space which is unrestricted by structures. This problem is to be seen in close connection with the proper choice of a flow resistance factor for such areas.

Two participants submitted more than 1 set of calculated numerical results. Some information has been provided about the result of their sensitivity studies performed before they decided to submit the contribution. The results of these sensitivity studies and other additional studies performed after the deadline for submissions have been summarized by the participants and are included in this report as appendix II.

Figures 5.1 to 5.10 show the nodalisation concepts chosen by the participants to set-up their thermohydraulic ASM. These figures illustrate the considerable differences in the adopted nodalisation concepts and give an impression about more or less sophisticated flow path networks generated by connecting the computational cells. Only GRS provided a specific scheme describing a separate flow network simulating a specific condensate flow pattern (fig. 5.11). Upon further request on occasion of the final workshop held in June 1992 most participants submitted tabular information showing the allocation of HDR compartment numbers to the adopted nodalisation scheme.

## **6. COMPARISON OF CALCULATED WITH MEASURED PARAMETERS**

The participants were asked to submit calculated information according to the list of parameters given by the task specification /KAR90/. To facilitate an easy identification of the individual contributions each common overlay plot has been limited to show only 5 calculated contributions in comparison with the relevant measured parameter. Each contribution is identified by capital letters according to table 7.

Average error bands of the measured data have been indicated in /WEN91/ to amount for pressures  $\pm 0.02$  bar, for temperatures of the containment atmosphere  $\pm 0.5$  °C and for local gas concentrations up to  $\pm 4$  vol.%, the latter value dependent on the location of the gas sensors.

## 6.1 Containment Pressure

Figure 6.1 shows the results of calculated absolute containment pressures in comparison to the measured transient. In terms of containment overpressure considerable deviations between measured and calculated values of several submissions may be noted up to the moment the containment cooling process started at about 975 minutes. After this point in time the deviations become somewhat smaller.

The global pressurization of the containment may be considered as the important indicator of the energy status of the free atmosphere inside the containment. In so far, the result is indicative for general shortcomings of the overall energy balance for most codes. These shortcomings must be identified in more detail should any progress in the long term application of the involved codes be the next goal for code improvement work.

## 6.2 Temperatures of the Containment Atmosphere

Figures 6.2 to 6.11 show the results of calculated atmospheric temperatures in comparison to the measured information deduced from comparable sensors at several locations within the HDR containment. Figures 6.2 to 6.11 are presented in sequence starting at the 6 m elevation in the lower level of the containment ending at the dome of the containment at the 48 m elevation.

The containment heat-up phase ends at approx. 700 minutes into the experiment when the external steam mass flow rate was reduced to approx. 1.2 kg/s. The reduced steam mass flow rate was obviously not sufficient to maintain the pressure and the temperatures at the high level reached at 700 minutes. Hence, we may consider the time period up to 700 minutes as the "conditioning period" of the containment before a massive hydrogen release into the containment could be expected.

Assessing the common overlay plots with respect to the simulation of the conditioning period it is evident that in simulating the experiment E11.2 too much energy was transferred into the lower sections of the containment. There are a few calculated transients for the

6 m, the 12 m and the 16.5 m elevation which are more close to the measured transients (e.g. the results of the GOTHIC model and the FUMO model). But the general trend of the overestimation of the atmospheric temperatures in the lower sections of the containment and the corresponding underestimation at higher elevations is easily to be recognized from all contributions. This means that the temperature stratification which existed within the HDR-containment during the experiment E11.2 at the beginning of the "light gas" injection period was not correctly simulated by most models. This trend of underestimating an existing temperature stratification is only changed at the moment when the second late steam injection in the lower section of the containment is started at about 770 minutes into the experimental transient. After initiating the late steam injection the heat-up of the lower containment section took place. The upper sections of the containment were mixed with the low temperature atmosphere pushed upwards by the lower section steam release.

### 6.3 Gas Concentrations

"Light gas" injection started at 740 minutes into the experiment E11.2. Figures 6.12 to 6.22 show the results of measured versus calculated gas concentration transients over the period between 600 and 1000 minutes into the experiment. The transient evaluation of gas concentrations has been compared to measurements taken from a large number of sensors positioned at various elevations within the containment.

Assessing the results of the overlay plots it is evident that after starting the "light gas" injection all codes simulate too much convection into the lower regions of the containment drastically increasing the computed gas concentrations below the 17.5 m elevation of the gas release location contrary to the measured evidence. In compensation, calculated gas concentrations are considerably lower than the measured concentration transients at the higher elevations. Only in the middle section in the vicinity of the gas release elevation the calculated gas concentration transients are somewhat similar to all the measured transients.

To fully merit the importance of the gas concentration predictions the distribution of the gas concentration within the containment is of importance. The time period during which the local flammability status must be predicted is of particular importance. To visualize the situation figure 6.23 shows the measured gas concentration profiles at distinct points in time for the stair case region (80° sector, top picture) and the spiral stair case region (280° sector, bottom picture). The point of release of the "light gas" was in the neighbourhood of 80° sector of the containment. Obviously, the gas concentrations reached high values very early in

the vicinity of the gas release point. The reliability of the gas concentration sensor CG1431 at the 30.6 m elevation in the upper diagram of figure 6.23 remains subject to further discussion. This sensor indicates an increase of gas concentrations only at approx. 772 minutes (32 minutes after starting the "light gas" injection) as evident from figure 6.24. The delayed increase of this local gas concentration coincides with the begin of the late second steam injection into the lower compartment of the HDR containment. Fig. 6.25 shows the transient evolution of air concentrations of the 80° sector, with a corresponding decrease of the air concentration at the same time. It seems possible, that a local gas pocket has been mobilized by an alteration of the convection pattern or a gas plume passed without affecting the gas sensor during this period.

The measured concentration profiles are compared to the calculated concentration profiles for the stair case region (80° sector) and for the spiral stair case area (280° sector). Figures 6.26 to 6.35 show the results at selected points in time (5, 15, 25, 35 and 60 min) after start of the hydrogen/helium gas injection.

For the addressed points in time it is evident that too much gas is mixed into the lower section of the containment which on the other hand is lacking within the upper regions. Obviously, the same trends as observed for the transient temperature simulations dominate the calculated gas concentration process in comparison to the measured evidence.

#### **6.4 Steam Concentrations**

The predictions of gas concentration distributions aims for an assessment of the flammability status of the containment atmosphere. The presence of steam in a post LOCA atmosphere inside the containment is an important factor. It is influential on the mode of combustion and if steam concentrations are large enough it even inhabits flammability. Hence, the comparison of measured versus calculated steam concentration transients is of similar safety relevance as the comparison of gas concentrations.

Figs. 6.36 to 6.43 show common overlay plots calculated for the experiment E11.2 for various elevations. Again, large discrepancies between measured and calculated steam concentrations are evident. In particular, during the "conditioning period" much more steam transport into the lower elevations of the containment has been simulated than actually occurred. These tendencies continue to influence the results also for the period of "light gas" injection and distribution. Even, if we find reasonable agreement between calculations and measurements of particular calculations (e.g. for the conditioning phase in the lower elev-

ations) for certain sensors the same calculations show even more disagreement for other sensors (e.g. results generated with the same ASM for the higher elevations). Overall, it must be concluded that steam concentration as well as gas concentration results could not be considered as a reliable basis should it serve for a subsequent prediction of an expected combustion mode.

## 6.5 Containment Sump Temperatures

Figs. 6.44 and 6.45 show the comparison between calculated and measured sump temperatures at two elevations. In order to understand the measurements of both sensors a lower level containment atmosphere temperature must be consulted. Although not specified for code comparison purposes the sensors of the atmospheric temperatures at the lowest levels (sensors CT2101 and CT3301) have been plotted in fig. 6.46. These temperatures show the same quality. The latest steam injection phase is indicated by very small increase of the temperature between 750 and approx. 1000 min. From these measurements it can be concluded, that water collected within the sump obviously has been cooled down very efficiently by the cold structures of the lower containment when reaching the sump.

The comparison between calculated and measured sump temperatures shows that several codes do not correctly model the cooldown of the condensate when reaching the sump level. Problems may be associated to the analytical treatment of the thermal non-equilibrium between the atmospheric phase and the liquid phase.

## 6.6 The Period of Water Spray on the Outside of the Steel Shell

The common overlay plots for the global parameters pressure, the atmospheric temperatures, the steam concentration transients and the sump temperatures cover the entire duration of the experiment. Particular interest has been expressed for a detailed comparison of the gas concentration transients for this period in time. As evident from figs. 6.36 to 6.43 the local steam concentrations are considerably reduced by condensation on the inside of the externally cooled steel shell dome.

The gas concentration transients are shown by common overlay plots for the period between 950 min and 1300 min (when most simulations were terminated) by figs. 6.47 to 6.49. Not all submissions cover this time period. Therefore, only one common overlay plot is shown for the addressed gas concentration sensors.

Common overlay plots for measured and calculated gas concentration profiles are shown for 1000, 1200 and 1300 min (figs. 6.50 to 6.52). The upper diagrams show the common overlay plots for the stair case (80 °) sector while the profiles for the spiral stair area (280 °) are shown by the lower diagrams. All the comparative plots showing gas concentrations as well as the comparisons of the steam concentrations indicate that during the period of external spray cooling serious simulation problems existed. The safety relevance of these observations should be a matter of discussion for the envisaged workshop.

Most of the Western type PWR-containments have installed internal water spray cooling as a mechanism for the long term pressure reduction within a containment. The findings of this exercise however have been obtained from an experiment with external spray cooling. A question exists: Which process of both, the external shell cooling or the internal spray cooling is more challenging to the analytical simulation models?

Three condensation rate measurements were specified for comparison to calculated transients. Only two submissions attempted to present calculated condensation rates. They are shown in fig. 6.53. It is interesting to note that the two calculations shown for the parameter CF0450 (steel shell condensation at 32 m elevation) decrease to very low values at the moment the external spray cooling period started. In general, simulated condensation rates are too low when compared to the measurement CF0450. Markable deviations are evident for the measurement CF6601 may be related to the local thermal-hydraulic conditions at the 12.5 m elevation relevant for heat exchange with the concrete. One participant presented a calculation for the condensate collector CF7402 for which the measurement was missing (see fig. 6.54). The submissions dedicated to the parameter "condensation rates" are a typical example for the limitations of an in-depth discussion of analytical simulation problems (see also section 3 "the analytical task").

## 7. OVERALL ASSESSMENT OF THE RESULTS

The International Standard Problem ISP-29 was the first exercise out of a series of OECD/CSNI-sponsored containment standard problems which was exclusively devoted to shed some light into the capabilities of Analytical Simulation Models (ASM) to describe the longlasting distribution of hydrogen gas inside a containment of a pressurized water reactor. Earlier ISPs were focussing on phenomena typical for design basis accident conditions. Only ISP-23 gave a first indication about possible shortcomings of long term containment behaviour predictions. These indications have been confirmed by the subsequent asses-



sment of code predictions submitted for an early hydrogen distribution scoping experiment performed by the HDR-Project in the context of the containment experiment T31.5. A final PHDR-Evaluation Report on the PHDR Benchmark Exercise on the long-term H<sub>2</sub>-aspects of T31.5 is in preparation.

Both, the ISP-23 exercise as well as the supplementary PHDR-organized code comparison exercise on the hydrogen distribution scoping experiment were performed as "blind" post test predictions. In contrast, the present document describes the results of "open" post test analyses of the HDR-experiment E11.2 the results of which were known to the participants in detail. One would have expected to see calculated results in more close agreement to the measured evidence. The achieved agreement (or disagreement) may be considered as the best possible results obtained by the adopted analytical simulation models nowadays.

The comparisons of calculated with measured gas concentrations and of the atmosphere temperatures demonstrate that for this experiment too much energy- and gas transport was simulated to occur within the HDR-containment. The reason for this is most likely to be seen in problems concerning the absorption of energy during the blowdown phase by the involved containment structures. Similar shortcomings have been observed already on occasion of the earlier International Standard Problem ISP-23 in connection with the assessment of the cooldown period (up to 20 min) of the containment experiment T31.5. One should note however that experiment T31.5 was initiated by a large break LOCA simulation lasting over 50 s blowdown time only. The problems associated to the energy exchange between the containment atmosphere and the containment structures are also evident from the comparison of the measured and calculated overall containment pressure. This parameter may be considered as being indicative for the overall energy status of the containment atmosphere. A margin of uncertainties of the involved ASMs as evident from fig. 6.1 cannot be considered as a satisfactory result of a best possible post test analysis. The margins for the observed local temperature simulations are consistently indicating energy distribution problems within the containment atmosphere. Thermal non-equilibrium between the containment atmosphere and condensate formed at containment internal structures may have amplified the simulation difficulties.

As mentioned before, the existence of a powerful instrument cooling system has complicated the analytical simulation procedure. Sensitivity studies have confirmed the improvements between calculated and measured global pressure transients if instrument cooling is taken into account (see annexes). On the other hand resulting improvements in calculated

and measured local temperature and gas concentration transients are not easy to assess in general. Taking into account additional local cooling within high temperature areas might even have amplified calculated convective flow rates promoting mixing of the atmosphere.

Unfortunately, a detailed investigation into these problems is not possible within the frame of this activity. On one hand, the underlying experiment is an integral experiment focusing mainly on the integral overall behaviour of the containment. On the other hand, a number of additional local measurements have been performed for which a comparison to calculated parameters is strongly linked to the ASM adopted by the code user. Previous experience with comparisons to locally relevant parameters has shown the inherent limitations. For ISP-29 these limitations have been confirmed what is drastically shown by the common overlay plots for condensation rates.

Doubtless, the parameters with the highest safety relevance are the distributions of "light gas" concentration and steam concentration. In order to evaluate the result of the ISP-29 from this point of view it is interesting to assess the conditions under which the HDR-containment would have reached flammability conditions. Such an assessment makes sense if the released "light gas" is considered as a representative simulant of hydrogen.

Figs. 6.55 and 6.56 show the measured gas concentrations at various elevations throughout the containment for the 80° sector (stair case) and the 280° sector (spiral stair). Other local gas concentrations not included in these diagrams for this period of time are close to 0 vol.%. Figs. 6.57 and 6.58 show the steam concentrations measured for the same locations and elevations as those shown for the gas sensors. Altogether, it is evident that at relevant elevations with a strong increase of early gas concentrations the mixture of air, steam and gas would not have been combustible because of high steam concentrations well above 50 vol.%. From the combustion point of view the situation is classified as "steam inertisation".

In general, the lower limit for steam concentrations causing inertisation is considered to be around 50 vol.%. The ternary diagram for hydrogen-air-steam mixtures provides this information (see fig. 6.59), which is slightly pressure and temperature dependent (see also fig. 6.60).

Looking more close to the measured gas- and steam concentration distribution it is evident that a flammability status may have been reached at the moment the local steam concentrations fall below the 50 vol.% threshold. The second necessary condition for reaching flammability is a local gas concentration in the neighbourhood of 10-12 vol.%. From the

figs. 6.55 to 6.58 shown it is evident that a location represented by the gas concentration sensor CG1092 may have been the location with the first possibility for ignition. At approx. 780 min the measured steam concentration rapidly falls below the 50 vol.% limit while the local gas concentration was measured to be somewhat above 10 vol.% at this moment. Obviously, this was the earliest possible moment of ignition if the containment would have been equipped with a large number activated igniters.

For the relevant time interval (approx. 780 min) and for this location (represented by the gas sensor CG1092) an attempt has been made to assess the margins of code calculations from which flammability would have been concluded. As an example fig. 6.61 shows a common overlay plot comparing the measured gas concentration transient (CG1092) with the results of CONTAIN-calculations only. Fig. 6.62 shows the corresponding common overlay plot for steam concentrations in good time resolution. Based on ternary diagram limits the flammability would have been predicted to occur at this location for a time interval between 25 min (contribution K) and 80 min (contribution A) after gas injection was started. The calculations E, F, G, H and K approach the flammability condition by a continuous reduction of the local steam concentration at increasing gas concentrations. Only calculation A simulated the flammability arrival at nearly constant gas concentrations but monotonously falling steam concentrations.

The results obtained from calculations based on other codes are shown in figs. 6.63 and 6.64. Here, flammability would have been predicted only by calculation C at 79 min after gas injection started. Table 11 summarizes the findings from a comparison of calculated flammability conditions and the measured situation at a location represented by the gas sensor CG1092. Gas and steam concentrations as simulated for this location are listed for the moment at which flammability was estimated from a comparison of the calculated conditions with the limits given by the ternary flammability diagram. The calculated containment pressure and the temperature (the calculated temperature transient most close to the location of the gas sensor CG1092 was the temperature associated to sensor CT0420) complement the information on gas- and steam concentrations. Gas concentrations at which de-inertisation at this location was predicted vary between 6.5 vol.% and 11 vol.% (compared to a measured value of 12 vol.%). De-inertisation, dependent on the actual steam concentration, was calculated ranging between 39 and 48 vol.% (compared to the measurement at 50 vol.%). Other parameters of importance for the judgement about possible combustion effects are the containment pressure and the local temperature. The calculated pressure variation cover the range between 0.17 and 0.22 MPa (compared to the

measured pressure of 0.196 MPa). Temperatures varied between 90 °C and 109 °C (compared to 107 °C as measured at sensor CT0432). Unfortunately the sensor CT9202 close to the gas concentration sensor CG1092 was not subject of the requested comparison. Sensor CT9202 indicates a local temperature of approx. 110 °C for this moment.

For the time being the flammability evaluation remains restricted to the discussion of the point in time at which ignition would have been predicted in comparison to the most likely moment at which the flammability conditions have been reached during the experiment E11.2. Any further assessment of the possible combustion mode caused by ignition over the entire containment would become irrelevant due to the large discrepancies observed for the locally predicted gas- and steam concentration distributions during the time period of interest (see section 6.3).

The preceding discussion may serve as an example to evaluate the safety and risk relevance of ISP-29 overall results. It shows that the large discrepancies documented for most transient parameters finally result in a margin of uncertainty in predicting the moment of flammability at the location CG1092 of approx. 40 min deduced from all submitted calculations. Certainly, this assessment requires further consideration. In particular, it is at the moment even unclear what kind of consequences ignition at the location CG1092 would have caused for the rest of the HDR-containment. An in-depth assessment would require to look in more detail at gas and steam concentrations simulated for other locations. It would also require to consult findings of more recent large scale multicompartment combustion experiments performed at elevated pressures and steam concentrations.

## **8. CONCLUSIONS AND RECOMMENDATIONS**

The submitted contributions, the modelling approaches and the overall results have been discussed on occasion of a workshop held in Garching on June 24/25th, 1992. The workshop was attended by experts which had submitted contributions and by experts which had been nominated as participants but which for one reason or the other could not submit calculations according to the specified deadlines.

The final discussion confirmed the particular importance of the exercise in view of safety and risk oriented studies required to identify the potential dangers stemming from the release and accumulation of large amounts of hydrogen during severe accidents. Understanding the local distribution of released hydrogen, steam and air inside a containment is a pre-requisite for any credible estimation of the consequences of a subsequent combustion

process, should it happen spontaneously or deliberately. The participants in the workshop unanimously noted that the exercise was very helpful in identifying shortcomings of the present analytical simulation models offering them the opportunity to learn about possible areas of improvements for their codes and the way how to use them.

The experiment has been assessed as to be performed under conditions relevant for a typical scenario which could be expected during a severe accident. An important feature of the experiment was the conditioning phase which can be interpreted as a longlasting blow-down, volumetrically scaled to an unmitigated small break LOCA of a large pressurized water reactor. The interrelations between the steam release periods and the hydrogen release period have been discussed as being a relevant phenomenological sequence of events. Finland and Italy were specifically interested in the impact of the external steel shell spray cooling on the containment internal processes.

The analytical task was specified as well as possible providing finally all the demanded major information required for an adequate treatment of the analytical task. In spite of considerable effort on the part of the experimental team, some difficulties remain in specifying all the detailed information required for an adequate analytical treatment of this type of experiment. One specific item of the experiment, not typical for full-size plant behaviour, was the comparatively large portion of energy extracted during the experiment by the instrument cooling system. Several experts involved in the exercise questioned the impact of the locally extracted amount of cooling energy on the calculated temperature and gas concentration distributions. For future exercises, should they be based on experiments with similar cooling problems, a more detailed background information on this experimental item would be helpful. In addition, more information about the temperature distribution within containment structures at the beginning of the experiment should be available to the analyst.

The overall results of the "post-test" analyses exercise were considered to be of utmost importance for learning processes for both, the analysts as well as the experimentalist. Compared to the results submitted within the frame of the "pre-test" predictions the results of the post-test analyses showed a reasonably good agreement between the calculated and the measured overall pressure transients. This improvement was essentially related to the application of a realistic energy input function for the "post-test" analyses taking into account also the instrument cooling. The former "pre-test" analyses /WOL91/ were based on a wrong steam discharge function and did not take into account the energy removed during the experiment by the instrument cooling system.

The other process-determining parameters relevant for the safety issue of this exercise, in particular the calculated gas concentration distributions, showed relatively large deviations from the measured transient parameters. Taking into account that the exercise was specified as an "open post-test" analysis of well-known measured data, the workshop discussed extensively the qualification of the lumped parameter (LP) codes for this type of phenomena. It was concluded that for the moment Analytical Simulation Models based on the lumped parameter approach must be considered as unreliable and inaccurate to describe the PHDR-experiment E11.2 which was essentially governed by buoyancy-driven natural convection processes and a high degree of thermal stratification. As far as the long term pressure evolution is concerned hitherto used model approaches may be sufficient. However, temperature - and gas concentration-distributions are not adequately described if afterwards the result would have been used to base a prediction of subsequent combustion processes on such distribution calculations.

Having this in view, the workshop extensively discussed possible reasons responsible for the observed analytical deficiencies. Several processes have been identified to deserve more close considerations before overall improvements of the Analytical Simulation Models should be expected. The long term absorption of energy by relatively cold containment structures and the associated prediction of longacting heat-sources and -sinks as well as the predictability of the temperature of the sump water collected during the experiment were the main object of the discussion. In so far, reference was also made to the result of the former International Standard Problem ISP-23 /KAR89/ and the conclusions and recommendations drawn therefrom with respect to the 20 minutes range predictions and associated "blind" post-test analyses of the HDR-experiment T31.5. Only very limited improvements have obviously been achieved since 1989 in both code performance and experimental methods.

Connected to the problems with the simulation of heat absorption by structures it was indicated that an improved knowledge about the thermal properties (thermal conductivity, heat capacity) of commercially used reinforced concrete could be very helpful. More specific for the PHDR-experiments of the E11-series, the distribution of instrument cooling heat losses was an additional item possibly relevant for some shortcomings of the presented ISP-29 analyses.

The influence of nodalisation schemes on the ability of existing lumped parameter codes to make accurate predictions requires further considerations. More reliable code user guide-

lines should be made available to the code users to minimize the potential for wrong user decisions when setting up Analytical Simulation Models. There is no value in code users applying input data which deviates from the given facts of the apparatus to be simulated without full physical or engineering justification. As an example, some participants made an attempt to largely reduce the flow areas interconnecting the HDR-compartments or those junctions resulting from a fictitious subdivision of the large containment dome volume in order to numerically reduce calculated convection flows and to improve the agreement between measured and calculated gas concentrations. At other occasions the flow loss coefficients have been modified far beyond the margins experienced and documented within the relevant engineering literature. If at all - such deviations from real data, even if classified as "parametric studies" should only be performed if adequate physical or technical justification supports such studies. Otherwise, such calculations remain questionable numerical attempts to cover shortcomings of the applied simulation method.

Merits and limits of a transition from the use of lumped parameter codes to Finite Element Methods (FEM) or to 3D-thermohydraulic codes have been discussed. The reasons for the difficulties encountered with this exercise may be to do with physical phenomena (plumes, temperature inversion etc. ) which are not included in the standard lumped parameter codes, or indeed, it may be that the specification of some boundary conditions is still uncertain. Hence, any firm recommendation to abandon lumped parameter codes was considered to be premature at the time being.

- Having these observations and the associated conclusions in mind the workshop addressed some recommendations for future activities. It was proposed to complement long term integral containment behaviour research work by some separate effects studies.
- One area could be an investigation into the behaviour and determination of flow loss coefficients for large area flow junctions under low flow conditions typical for containment systems. This problem is also of importance if users of lumped parameter codes attempt to subdivide large free volumes (e.g. the dome compartment of a PWR) into a number of fictitious subvolumes, interconnected by difficult to specify flow junctions.
- A small study contract should be devoted to assess thermal properties of commercial concrete in dependence of the concrete composition, of the amount and structuring of inserted rebars and last not least in dependence of concrete humidity.
- In order to assess the importance and understanding of the experiment E11.2 it was recommended to perform an evaluation of the entire series of hydrogen distribution experi-

ments executed in the frame of the HDR research project. This recommendation was supported by some first very promising comparisons of measured and post-test calculated parameters shown for the HDR hydrogen distribution experiment E11.4 by two participants (see also Annexes II B and II C) and published also by /WOL92/ on other occasion. Principle Working Group No. 4 and CSNI have been encouraged to contact the German Bundesministerium für Forschung und Technologie (the sponsor of the HDR-experiments) in this connection.

- To improve the predictive accuracy and reliability of Analytical Simulation Models the guidelines regarding the use of codes should more clearly define the limits of their legitimate and useful application (e.g. choice of nodalisation schemes, selection of correlations etc.). The results of code-specific sensitivity studies, which every code user should make with his code, might help to reduce or quantify the unavoidable user impact on generated numerical results.
- Finally, the workshop recommended to select another experiment, possibly a simpler one, as basis for a future International Standard Problem to allow monitoring of code improvement results. It would be useful to have another ISP based on a sequence with the injection of gas and steam located in the upper part of a containment building, allowing again the possibility of a thermally stratified containment atmosphere. In this context, the workshop took note of a presentation by representatives from NUPEC (Japan) describing two experiments out of a series of hydrogen distribution experiments from which one might be selected as an additional future ISP basis.



## References

- /KAR89/ Karwat H.  
Comparison Report on International Standard Problem No. 23: Rupture of a Large Diameter Pipe within the HDR-Containment  
December 1989, CSNI-Report No. 160, Vols. 1 and 2
- /KAR90/ Karwat H.  
OECD Standard Problem ISP-29: Distribution of Hydrogen within HDR-Containment under Severe Accident Conditions - Task Specification  
April 1990, (4. Revision 7/91)
- /SCH82/ Schall M., Valencia L.  
Data compilation on the HDR-containment for input data processing for pre-test calculations  
PHDR - Report No. 3.279/82, January 1982
- /SCH82a/ Schall M.  
Design report for the HDR-containment experiments V21.1 to V21.3 and V42 to V44 with specifications for the pre-test computations  
PHDR - Report No. 3.280/82, January 1982
- /SCH82b/ Schall M.  
Auslegungsbericht für Containment-Versuche V21.1-3, V42-V44  
PHDR-Arbeitsbericht Nr. 3.191/80, January 1982
- /VAL89/ Valencia L., Wolf L.  
Preliminary Design Report "Hydrogen Distribution Experiments E11.1-E11.5  
PHDR-Working Report No. 10.003/89, March 1989
- /WEN89/ Wenzel H.H., et al.  
Versuchsprotokoll - Wasserstoffverteilungs-Versuche HDR-Versuchsgruppe CON, Versuch E11.2  
PHDR-Arbeitsbericht No. 10.010/89
- /WEN91/ Wenzel H.H., et al.  
Quality considerations of major direct and indirect measured quantities during experiments of test group E11  
PHDR - Working Report No. 10.025/91, June 1991
- /WOL91/ Wolf L., Valencia L.  
Results of the PHDR Computational Benchmark Exercises on Hydrogen Distribution Experiments E11.2 and E11.4  
Proceedings Workshop on Hydrogen Behaviour and Mitigation, Brussels, 4/8. March 1991, EUR 14039en, p. 81-95
- /WOL92/ Wolf L. et al.  
Comparisons between HDR-H<sub>2</sub>-Distribution Experiments E11.2 and E11.4  
Proc. 19th Water Reactor Safety Information Meeting, Bethesda, USA, Oct. 1991, NUREG/CP-0119, Vol. 2, p. 139-168, April 1992

Detailed working reports provided by the participants in connection with the ISP-29 submissions

- /BRA92/ S.J.K. Bradley, M.I. Robertson  
MELCOR calculations for ISP-29  
Report No. AEA RS 5236, February 1992
- /ELL92/ P. Ellicott  
Short Report on the Winfrith-CONTAIN Submissions to the ISP-29  
(WinfrithReport), April 1992
- /HOL92/ H. Holzbauer  
International Standard Problem Exercise ISP-29  
Offene Nachrechnung des Versuchs E11.2  
(Battelle-Bericht), Januar 1992
- /HÜT92/ B. Hüttermann  
ISP-29 - Post calculation of HDR test E11.2 with RALOC  
GRS-A- , August 1992
- /MAN92/ M. Manfredini, F. Orioli, S. Paci  
OECD-CSNI ISP-29: Post-test Analysis using the FUMO Computer Code  
RL 531(92), January 1992
- /NIL92/ L. Nilsson  
CONTAIN 1.11 Calculation of the HDR Hydrogen Distribution Test E11.2  
Studsvik Report, STUDSVIK/NS-92/4, January 1992
- /SIL92/ A. Silde  
OECD Standard Problem OECD-CSNI-ISP-29 (CONTAIN 1.12 Calculation)  
February 1992
- /TIL92/ J. Tills  
CONTAIN Analysis of the HDR Facility for ISP-29 Containment Modeling Division  
Sandia National Laboratories (without date and report number)
- /VEL92/ E.J. Velema  
International Standard Problem ISP-29 (Hydrogen Distribution Inside a  
PWR-Containment Under Severe Accident Conditions)  
ECN-Petten, NP-R&V-92-02, Januari 1992

## Tables

0.0	Start small LOCA and simultaneously (1-2 minutes later) release of external steam with a constant mass flow rate of 2.06 kg/s (originally specified 3.3 kg/s)
693.82	End of LOCA and reduction of the external steam mass flow rate to 1.20 kg/s
739.4	Start of gas mixture injection
749.98	End of external steam release
772.3	End of gas injection
772.93	Start of external steam release in R1405 (mass flow rate 2.06 kg/s)
958.77	End of external steam release
975.0	Start of outer spray period with a mass flow rate of 21 t/h = 5.83 kg/s
1095.0	Increase of mass flow rate to 26.5 t/h = 7.36 kg/s
1155.0	Increase of mass flow rate to 33 t/h = 9.17 kg/s
1185.0	Increase of mass flow rate to 38.5 t/h = 10.69 kg/s
1203.0	End of spray period and start of natural cooldown
1300.0	End of Distribution Experiment
1445.0	End of natural cooldown period

**Table 1: Chronology of Operational Events of Experiment E11.2**

No.	From Subcompartment No.	To	Vent No.	Required State	Remarks
<b>Elevator Doors</b>					
1	1410	1406	53	OPEN	- 1,1 m plane
2	1410	1503	253	OPEN	+ 4,5 m plane
3	1410	1606	-	CLOSED	+ 10,0 m plane
4	1410	1707	-	CLOSED	+ 15,0 m plane
5	1410	1805	-	CLOSED	+ 20,6 m plane
6	1410	1903	-	CLOSED	+ 25,3 m plane
7	1410	11004	-	CLOSED	+ 30,8 m plane
<b>Room Doors</b>					
8	1308	1302	25	OPEN	Lead door
9	1308	1303	13	OPEN	
10	1308	1304	27	OPEN	
11	1308	1305	33	OPEN	
12	1406	1401	89	CLOSED	
13	1406	1403	60	OPEN	
14	1406	1404	236	OPEN	
15	1406	1407	54	OPEN	
16	1406	1409	199	OPEN	
17	1503	1504	67	CLOSED	from 1504 wall
18	1503	1520	70	CLOSED	from 1520 wall
19	1511	1508	147	OPEN	Lead door
20	1501	1512	192	OPEN	
21	1511	1514	193	OPEN	secured
22	1604	1607	209	OPEN	secured
23	1604	1608	210	OPEN	Lead door, secured
24	1611	1602	86	OPEN	secured
25	1611	1603	163	OPEN	secured
26	1606	1605	167	OPEN	Lead door, secured
27	1611	1609	87	OPEN	secured
28	1707	1702	90.1	OPEN	
29	1707	1702	90.2	OPEN	Redundant/gap
30	1707	1703	91	OPEN	Lead door, secured
31	1804	1802	137.2	CLOSED	sealed
32	1902	1802	137.1	CLOSED	sealed

Table 2/1: State of Vents and Doors in the Containment

No.	From Subcompartment No.	To	Vent No.	Required State	Remarks
<b>Maintenance Flaps in Staircase</b>					(in ceiling from:)
32	1308	1406	52	OPEN	secured
33	1406	1501	121.3	OPEN	secured
34	1503	1606	120.3	OPEN	secured
35	1606	1707	119.3	OPEN	secured
36	1707	1805	118.3	OPEN	secured
37	1805	1903	217.3	OPEN	secured
38	1903	11004	117.3	OPEN	secured
<b>Maintenance Flaps in Spiral Staircase</b>					(in ceiling from:)
39	1511	1611	231	OPEN	secured
40	1611	1708	131.1	OPEN	secured
41	1708	1804	213	OPEN	secured
42	1804	1902	216	OPEN	secured
43	1902	11004	122.1	OPEN	dismantled
<b>Other Flaps or Doors</b>					
44	1603	1611/1708	162/133	OPEN	flap wall
45	1603	1704	140	OPEN	secured
46	1802	11004	127	OPEN	secured
47	1704	1906	113.1	CLOSED	dism.small lead door
48	1704	11004	95	CLOSED	concrete
<b>Loose Metallic Covers</b>					
49	1301	1201	48	CLOSED	accessible
50	1301	1201	49	CLOSED	accessible
51	1301	1201	50	CLOSED	accessible
52	1301	1201	51	CLOSED	accessible
53	11004	1906	115	CLOSED	accessible for SHAG
54	11004	1903	116	CLOSED	accessible for SHAG
55	11004	1902	129	CLOSED	accessible
56	11004	1508	177	OPEN	0.79 m <sup>2</sup>
57	1603	1508	178	CLOSED	4 m x 0,7 m
58	1603	1508	179	CLOSED	1,8 m x 0,56 m

Table 2/2: State of Vents and Doors in the Containment

No.	From Subcompartment No.	To	Vent No.	Required State	Remarks
<b>Zinc Sheat Metal Walls</b>					
60	1302	1301	85	CLOSED	As built
61	1302	1304	79	CLOSED	As built
62	1406	1401	56	OPEN	
<b>Errected Brick Walls</b>					
63	1301	1308	21	OPEN	As built
64	1401/1408	pipe shaft	151.1	CLOSED	As built ( 310°)
65	1502	pipe shaft	151.2	CLOSED	As built (320°C)
66	1512	1513	93.3	CLOSED	As built
67	1607	1513	93.2	CLOSED	Already quite slipped
68	1611	pipe shaft	-	CLOSED	As built (320°C)
69	1609	1602	-	CLOSED	As built
70	1708	1703	-	CLOSED	As built
71	1703	pipe shaft	-	CLOSED	As built (320°)
72	1802	pipe shaft	-	CLOSED	As built (320°)
73	1406	1404	197	OPEN	Pipe storage
74	1406	1405	198	OPEN	
75	1603	1701u	143	OPEN	

Table 2/3: State of Vents and Doors in the Containment

## 1. HDR-Concrete

$$\lambda = 2.1 \text{ W/m} \cdot \text{K (humidity 2,85 \%)}$$

$$\rho = 2225 \text{ kg/m}^3$$

$$c_p = 879 \text{ J/kg} \cdot \text{K}$$

## 2. HDR-Paint

### a) Floor covering (protection)

$$\lambda = 0.288 \text{ W/m} \cdot \text{K}$$

$$\rho = 1540 \text{ kg/m}^3$$

$$c_p = 1280 \text{ J/kg} \cdot \text{K}$$

### b) Floor and wall paint

$$\lambda = 0.2 \text{ W/m} \cdot \text{K}$$

$$\rho = 1250 \text{ kg/m}^3$$

$$c_p = 1550 \text{ J/kg} \cdot \text{K}$$

The floor was first prepared with the covering (a) and then treated with the floor and wall paint (b) (giving a total thickness of 1.5 mm).

In the case of the walls the paint was applied directly (thickness: 0.15 mm)

$\lambda$  = thermal conductivity

$c_p$  = spec. heat capacity

$\rho$  = density

**Table 3/1: Thermal Properties of HDR Internal Structures**



### 3. HDR Steel Shell

Material St E36, No. 1.0854

$$\rho = 7840 \text{ kg/m}^3$$

Temperature	°C	20	100	200	300
Thermal Conductivity	W/m·K	42	43	43	42
Specific Heat Capacity	J/kg·K	460	490	520	560

### 4. HDR Metal Internals

	$\rho$ kg/m <sup>3</sup>	$\lambda$ W/m·K	$c_p$ J/kg·K
Steel	7850	50.0	460
Brass	8560	92.0	390
Zinc	7140	109.0	376
V2A Steel	7880	21.0	500
Lead	11340	35.0	130
Aluminium	2700	209.0	896
Copper	8930	372.0	383
Cast-Iron	7280	55.8	540

**Table 3/2: Thermal Properties of HDR Internal Structures**

5.  $\alpha$ -Blocks

## Concrete

$\lambda$  = 1.6 W/m·K dry and 2.2 W/m·K by 7.35 % humidity

$c_p$  = 1.090 J/kg·K

$\rho$  = 2300 kg/m<sup>3</sup>

## Paint

$\lambda$  = 0.465 W/m·K

$\rho$  = 1733 kg/m<sup>3</sup>

## Lead

$\lambda$  = 34.75 W/m·K

$c_p$  = 128.12 J/kg·K

$\rho$  = 11.430 kg/m<sup>3</sup>

## Insulation: Silicon RTV 615

$\lambda$  = 0.19 W/m·K

$c_p$  = 1.256 J/kg·K

$\rho$  = 1020 kg/m<sup>3</sup>

**Table 3/3: Thermal Properties of HDR Internal Structures**

Room No.	Temperature [°C]	Humidity [%]
13004	30.8	36.4
12004	30.9	37.3
11004	34.3	30.9
1906	35.5	28.5
1905	46.4	14.5
1904	46.4	46.6
1367	28.3	42.4
1903	31.4	39.9
1902	35.5	28.5
1901	53.0	9.28
1357	29.6	42.4
1805	27.0	42.4
1804	29.8	37.7
1803	46.4	14.5
1802	22.0	57.9
1801	27.0	46.6
1708	20.1	66.9
1707	21.1	56.9
1347	21.1	56.9
1706	17.9	64.0
1704	43.5	17.7
1703	17.9	64.0
1702	20.4	64.0
1701o	65.8	5.6
1701u	65.8	5.6

**Table 4/1: Initial Conditions of the HDR-Facility**

<b>Room No.</b>	<b>Temperature [°C]</b>	<b>Humidity [%]</b>
1611	19.5	68.2
1609	19.8	64.9
1608	25.1	53.2
1607	25.1	53.2
1337	20.1	61.5
1606	21.1	60.7
1605	28.5	60.7
1604	21.1	60.7
1603	25.7	47.7
1602	19.8	46.9
1514	19.5	70.3
1513	30.7	58.9
1512	22.0	58.9
1511	19.5	70.3
1508	20.1	62.5
1507	22.0	58.9
1506	20.3	58.9
1505	22.0	58.9
1504	22.0	58.9
1327	20.4	60.4
1503	21.2	59.6
1520	20.4	60.4
1502	20.4	60.4
1501	22.0	58.9
1410	23.2	52.7

**Table 4/2: Initial Conditions of the HDR-Facility**

Room No.	Temperature [°C]	Humidity [%]
1409	19.8	68.1
1408	19.8	68.1
1407	22.0	59.2
1317	20.4	62.2
1406	21.2	64.2
1405	19.8	68.1
1404	22.0	59.2
1403	19.8	68.1
1401	20.3	69.2
1311	27.8	42.0
1308	27.8	42.0
1307	20.2	61.4
1305	27.8	42.0
1304	27.8	42.0
1303	20.2	61.4
1302	20.2	61.4
1301	20.2	61.4
1203	20.0	100.0
Sump		
1202	20.0	100.0
1201	24.4	61.4

**Table 4/3: Initial Conditions of the HDR-Facility**

Thermocouple Denotation		Coordinates			Initial Temperatures
		R	$\phi$	z	
OT 27		1033	270	650	19.4
OT 28		970	71	- 350	20.4
OT 29		1033	315	2700	21.4
OT 31		632	270	4800	25.2
OT 32		632	0	4800	25.5
OT 33		632	66	4800	24.7
OT 34		632	210	4800	24.2
OT 35		986	270	4300	24.0
OT 36		986	0	4300	24.3
OT 37		986	66	4300	26.4
OT 38		986	210	4300	23.1
OT 39		1033	270	3800	21.2
OT 40		1033	0	3800	21.7
OT 41		1033	66	3700	21.1
OT 42		1033	210	3800	22.0
OT 43		1033	210	3100	21.1
OT 44		1033	0	3100	22.1
OT 45		1033	66	3100	21.1
OT 52		1033	270	3100	20.8
OT 55		1033	270	2700	20.2
OT 56		1033	66	2700	21.1
OT 57		1033	66	2500	21.1
OT 58		1033	270	2200	20.3
OT 59		1033	66	1500	19.9
OT 60		1033	270	1200	20.2
OT 61		1033	66	650	20.2
OT 3901		0	0	5070	26.7
OT 3902		1033	45	3100	20.5
OT 3903		1033	225	3100	21.0
OT 3904		1033	45	2700	20.3
OT 3905		1033	225	2700	20.8
OT 3906		1033	45	450	20.1
OT 3907		1033	225	450	19.4
OT 3908		1033	45	- 300	21.7
OT 3909		1033	225	- 300	19.5
OT 3911		1033	0	2700	21.6
OT 3912		1033	120	2700	21.5
OT 3913		1033	0	2700	21.1
OT 3914		1033	120	2700	21.8

Table 4/4: Initial Conditions of the HDR - Gap between Steel Shell and Concrete Containment

Pressure		Gas Concentrations		
CP	0401	CG	1038	Profile
Temperatures		CG	1043	Profile
CT	1101	CG	1146	Profile
CT	6603	CG	1053	Profile
CT	6604	CG	1011	Profile
CT	7701	CG	1066	
CT	7801	CG	1166	Profile
CT	8501	CG	1077	
CT	9302	CG	1078	
CT	0431	CG	1084	
CT	0432	CG	1085	
CT	0430	CG	1092	
Steam Concentrations		CG	1093	
CL	8066	CG	1431	Profile
CL	8077	CG	1432	
CL	8078	CG	1435	
CL	8084	CG	1436	Profile
CL	8085	CG	1430	
CL	8092	CG	1438	
CL	8093	Sump Temperatures		
CL	8338	CT	2103	
		CT	2106	
		Condensation Rates		
		CF	0450	
		CF	7402	
		CF	6601	

**Table 5: Sensors to which Calculated Parameters should be Submitted for the Comparison of Time Functions (Sensors marked with the Word "Profile" have only been utilized to compare Profiles according to tables 6/1+2)**

Time after start of hydrogen release (min)

5  
15  
25  
35  
60  
160  
260  
360  
460  
560

**Table 6/1: Points in time for which measured and calculated gas concentration profiles should be compared**

Stair Case (80°)  
(1. Profiles)

CG 1038  
CG 1146  
CG 1053  
CG 1066  
CG 1077  
CG 1085  
CG 1093  
CG 1431  
CG 1436  
CG 1438

Spiral Stair (280°)  
(2. Profiles)

CG 1043  
CG 1011  
CG 1166  
CG 1078  
CG 1084  
CG 1092  
CG 1432  
CG 1435  
CG 1430

**Table 6/2: Sensors from which the measured concentration profiles should be generated and compared to calculations**



Country	Institution	Experts	Code-Version	Disc Regist.	Ident.
Finland	VTT-Helsinki	A. Silde	CONTAIN 1.12	VTT	A
Germany 1	Battelle Frankfurt	H. Holzbauer	GOTHIC	BATF	B
Germany 2	GRS-Köln	B. Hüttermann	RALOC	GRSK	C
Italy	University Pisa	F. Oriolo / S. Paci	FUMO	UPI	D
Japan	JAERI, Tokaimura	K. Soda	CONTAIN 1.11	JAER	E
Netherlands	ECN-Petten	E. Velema	CONTAIN 1.12	ECN	F
Sweden	Studsvik, Nyköping	L. Nilsson	CONTAIN 1.11	STU	G
United Kingdom 1	AEE Winfrith	P. Ellicott	CONTAIN 1.11(UK)	WTC 1 and 2	H
United Kingdom 2	AEA Technology	M. Robertson	MELCOR	AEA 1, 2 and 3	J
USA	SANDIA Nat. Lab.	J. Tills	CONTAIN 1.12	SNL	K

Table 7: Post-Test Analyses - Contributions to the International Standard Problem ISP-29 (HDR Experiment E11.2)

Institution	Code Version	Nodalisation		Flow Junctions		Heat Structures	
		Inner Containment	External Gap	Inner Containment	External Gap	Inner Containment	External Gap
AAA - VTT	CONTAIN 1.12	46	6	110	7	225 25 (steel shell)	6 (25)
BBB - BATF	GOTHIC	47	9	97	10	92 43 (steel shell) 21 ( $\alpha$ -blocks)	9 (43)
CCC - GRS	RALOC-2.2	55	7	gas phase 130 liquid phase 54	gas ph. 11 liquid ph. 4	103 45 (steel shell)	10 (45)
DDD - UPI	FUMO	12 (+1 gas sam- pling node)	2	51 (+12 gas sam- pling junctions)	1 +2 vents	71 + 12 simulation instr. cooling	2
EEE - JAER	CONTAIN 1.11	25	2	71	1	137	2

Table 8/1: Main Features of the Generated Analytical Simulation Models (ASM)

Institution	Code Version	Nodalisation		Flow Junctions		Heat Structures	
		Inner Containment	External Gap	Inner Containment	External Gap	Inner Containment	External Gap
FFF - ECN	CONTAIN 1.12	29	not simulated	65	not simulated	93	-
GGG - STU	CONTAIN 1.11	36	1	68 + 1 vent	1 vent	147 8 (steel shell)	1 concrete 8 steel shell
HHH - WTC	CONTAIN 1.11 (UK)	35	3	79 + 1 vent	5	215	3
JJJ - AEA	MELCOR	31	not simulated	66	not simulated	124	not simulated
KKK - SNL	CONTAIN 1.12	9	4	25	7	128	16

Table 8/2: Main Features of the Generated Analytical Simulation Models (ASM)

Institution	CONTAIN-Version	Flow Loss Coefficients	Heat Transfer to Structures	Heat Conduction Inside Structures
AAA - VTT	1.12	2.0 in the dome area 5.0 (locally 20) all others	6.08 W/m <sup>2</sup> K to outside of steel shell $Nu_C = 0.13 \cdot Gr \cdot Pr^{0.33}$ natural convection $Nu_F = 0.037 Re^{0.8} \cdot Pr^{0.33}$ forced convection Radiation into gap taken into account	material properties accord. PHDR recommendation
EEE - JAER	1.11	?	convection and condensation model provided by CONTAIN	concrete $\lambda = 2.1$ W/mK steel shell $\lambda = 43$ W/mK
FFF - ECN	1.12	0.7 (for $A < 1$ m <sup>2</sup> ) 0.05 (for $A > 1$ m <sup>2</sup> )	11.5 W/m <sup>2</sup> K (to outer concrete shell)	concrete $\lambda = 2.1$ W/mK steel $\lambda = 43$ W/mK
GGG - STU	1.11	between 0.1 and 1.0	$Nu = 0.27 (Gr \cdot Pr)^{1/9}$ (laminar flow) $Nu = 0.14 (Gr \cdot Pr)^{1/3}$ (turbulent flow)	concrete $\lambda = 2.3$ W/mK (5 different groups of structures)
HHH - WTC	1.11 (UK) (Base Case)	0.75 (for almost all paths)	$Nu = 0.27 (Gr \cdot Pr)^{1/9}$ (laminar flow) $Nu = 0.14 (Gr \cdot Pr)^{1/3}$ (turbulent flow) $Nu = 0.37 Re^{4/5} Pr^{1/3}$ (forced flow) 6.08 W/m <sup>2</sup> K to outer concrete shell	concrete $\lambda = 2.1$ W/mK steel $\lambda = 50$ W/mK Ytong $\lambda = 0.55$ W/mK Alumin. $\lambda = 209.0$ W/mK
KKK - SNL	1.12	0.7 for all paths	Condense mode in CONTAIN activated. no forced convective input Orientation of concrete modeled (floor, roof, and wall)	Constant properties per PHDR specification for concrete ( $\lambda = 2.1$ W/mK) Non-uniform grids for concrete (typically 8-12 nodes) Uniform grids for steel shell (~4 nodes)

Table 9/1: Specific Features of the ASMs Generated with the CONTAIN Code

Institution	Code Version	Flow Loss Coefficients	Heat Transfer to Structures	Heat Conduction Inside Structures
BBB - BAT	GOTHIC	between 1.2 and 2.8 as recomm. by PHDR, but all containment internal flow areas reduced to 1/10	Uchida-correlation	material properties according to PHDR recommendation
CCC - GRS	RALOC	accord. Idelchik (flow direction dependent) average value 4.0, ranging between 1 and 15	convection Grigull radiation: Hottel-Egbert condensation: Fick's Law	material properties according to PHDR recommendation
DDD - UPI	FUMO	dependent on Re-Number and L/D-Ratio of Junction	specific DCMN-Correlation utilizing Uchida Correlation (see also Annex D) const. $\alpha = 5 \text{ W/m}^2\text{K}$ on the gap outside	Fourier Equation (coarse mesh method)
JJJ - AEA	MELCOR (Base Case)	20 (lower cell junctions) 2 elsewhere above blowdown elevation	Convection: uses Nusselt correlation for different flow regimes Radiation: equivalent band model Condensation: mass/heat transfer analogy	material properties according to PHDR recommendation

Table 9/2: Specific Features of the ASMs Generated with Codes other than CONTAIN

Institution	CONTAIN- Version	Instrument Cooling
AAA - VTT	1.12	distributed according to sensor locations with user defined heat fluxes at outside of slab, certain corrections for unisolated length of cooling pipes
EEE - JAER	1.11	not taken into account in submitted case
FFF - ECN	1.12	distributed according to sensor locations
GGG - STU	1.11	integral reduction of steam enthalpy injected from external steam source
HHH - WTC	• 1.11 (UK) (Base Case)	concentrated in lower pressure vessel cell by the assumption all energy extracted from room 1701 u
KKK - SNL	1.12	distributed according to sensor locations, weighted by containment temperature profile (~ 67 % in lower dome, 15 % in upper dome region, 18 % in RPV regions)

Table 10/1: Simulation of Instrument Cooling with the CONTAIN Code

Institution	Code-Version	Instrument Cooling
BBB - BAT	GOTHIC	distributed inside 9 out of a total of 47 fluid dynamic cells, but only for sensors above the 1700 elevation (cooled surfaces)
CCC - GRS	RALOC 2.2	weighted inside 17 out of a total of 55 fluid dynamic nodes with cooling surfaces
DDD - UPI	FUMO	simulated by 12 cooled heat slabs (1 mm thickness) coolant temperature const. 288 K inside heat slabs
JJJ - AEA	MELCOR (Base Case)	concentrated to blowdown shaft and pressure vessel cells (additional sensitivity calculations performed with cooling either within blowdown cell or within pressure vessel cell) (see also Annex J)

Table 10/2: Simulation of Instrument Cooling with Codes other than CONTAIN

Institution	CONTAIN- Version	Dome Nodalisation	Other Particularities of the ASM
AAA - VTT	1.12	12 cells	additional sensitivity studies (see also Annex A): - 44 cell dome nodalisation with reduced junction areas - loss coefficients modification of horizontal flow paths within dome area
EEE - JAER	1.11	1	- sensitivity study to assess local impact of instrument cooling - several other sensitivity studies (see Annex E)
FFF - ECN	1.12	5	The external gap is modelled as an integral part of the outer steel shell
GGG - STU	1.11	13	-
HHH - WTC	1.11 (UK) (Base Case)	4	1 additional sensitivity case with loss-coefficient changed from 0.75 to 5.0 for 8 out of 79 junctions (see also Annex H)
KKK - SNL	1.12	3	External sprays simulated by "pseudo water aerosol deposition" via code update. Gap heat transfer used structure connects for thermal link to containment, and net radiation enclosure models for shell to secondary concrete heat transfer

Table 11/1: Additional Information Characterizing Particularities of the Analytical Simulation Models and Sensitivity Studies  
(CONTAIN Code User)



<b>Institution</b>	<b>Code Version</b>	<b>Dome Nodalisation</b>	<b>Other Particularities of the ASM</b>
BBB - BAT	GOTHIC	6	-
CCC - GRS	RALOC	7	Flow areas of junctions inter-connecting fictitious dome sub-volumes largely reduced
DDD - UPI	FUMO	1	-
JJJ - AEA	MELCOR (Base Case)	7	14 sensitivity calculations performed and results described in the report /BRA92/. 2 additional sensitivity cases submitted as ISP-contribution (see also Annex J).

Table 11/2: Additional Information Characterizing Particularities of the Analytical Simulation Models and Sensitivity Studies

ASM-Basis	Contrib.	Time (min)	H <sub>2</sub> (equiv.) Vol.%	H <sub>2</sub> O Vol.%	Press. MPa	Temp. °C	Flammability not predicted because
CONTAIN 1.12	A	80	6,5	39	0,19	93	-
CONTAIN 1.11	E	28	6,5	40	0,17	90	-
CONTAIN 1.12	F	32	8	42	0,175	92	-
CONTAIN 1.11	G	30	7	41	0,170	90	-
CONTAIN 1.11 (UK)	H	28	11	48	0,180	102	-
CONTAIN 1.12	K	25	6,5	40	0,220	109	-
GOTHIC	B	-	-	-	-	-	Gas concentration too low
RALOC	C	79	8	42	0,192	99	-
FUMO	D	-	-	-	-	-	Steam concentration too high
MELCOR	J	-	-	-	-	-	Steam concentration too high
Experiment	-	39	12	50	0,196	107 (CT0432)	All other sensors later !

Table 12: Flammability Conditions (Simulated and Experimental) at Location of Gas Sensor CG 1092  
(Time after begin of "Light Gas" Injection)

## Figures

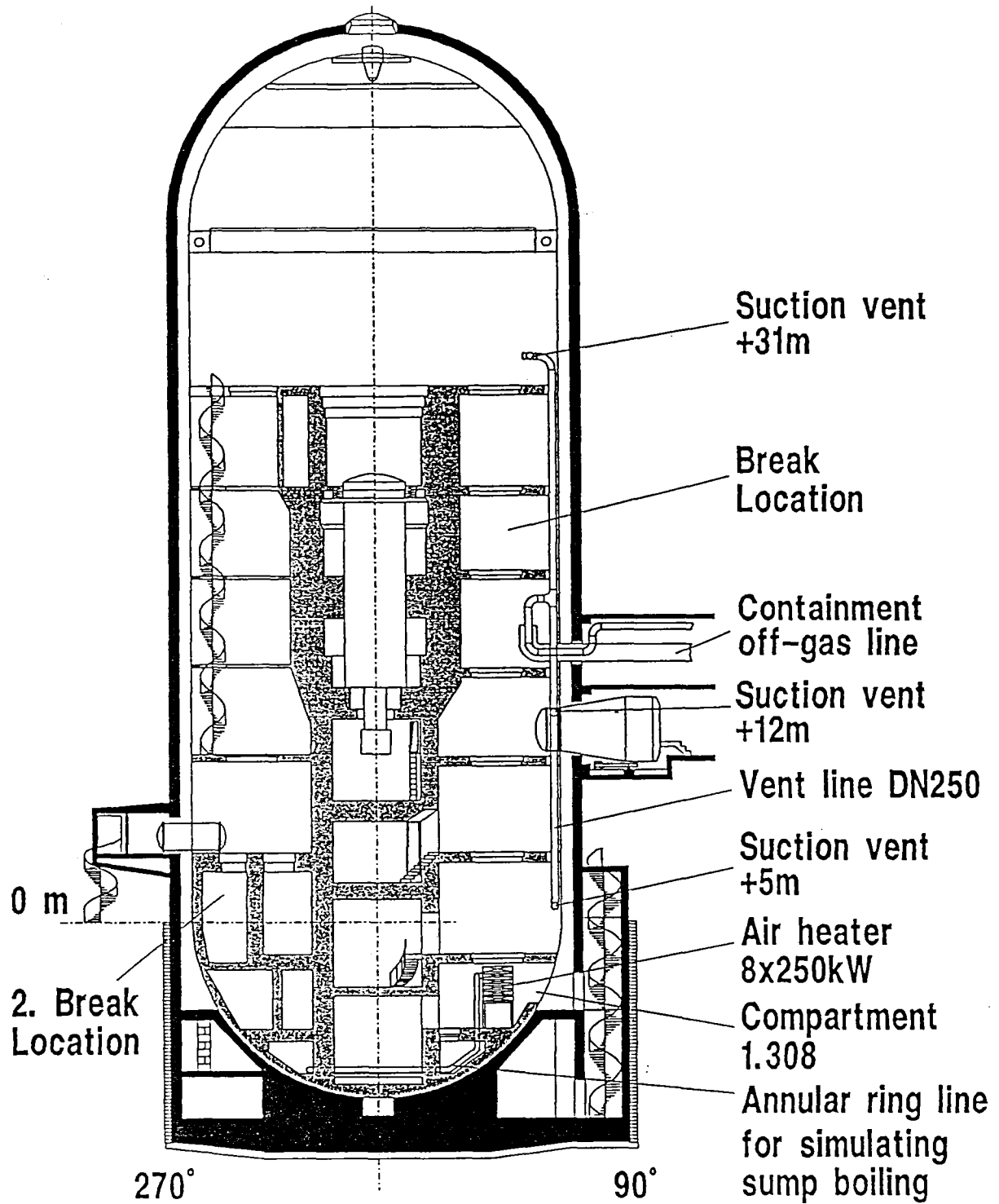


Fig. 2.1: Cross Section of the HDR-Containment showing main components of the facility

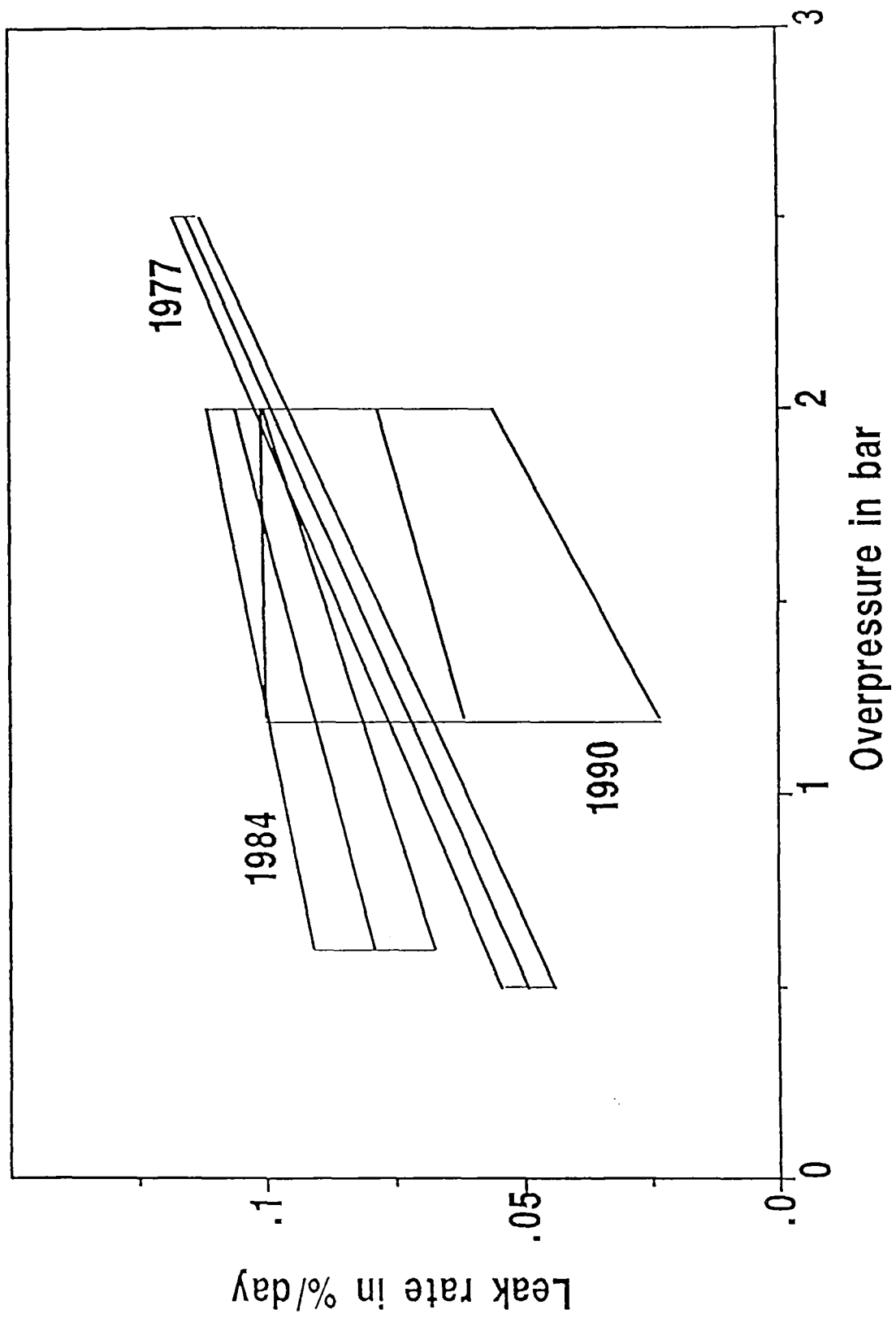


Fig. 2.2: Ranges of Measured Leakrates (Tests performed in 1977, 1984, 1990)

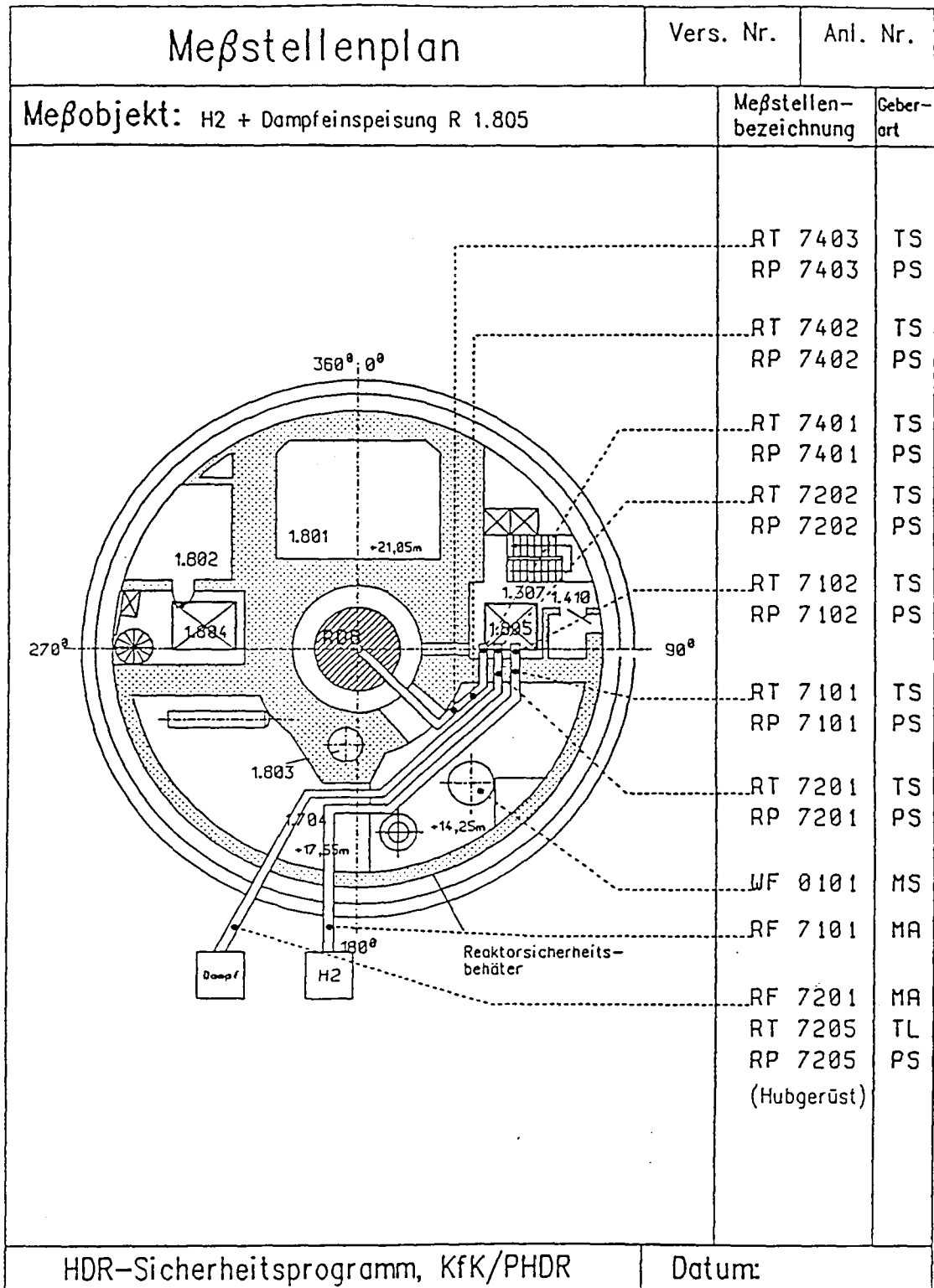


Fig. 2.3: Horizontal Cross Section Showing the Location of Steam and Hydrogen Release (First Period)

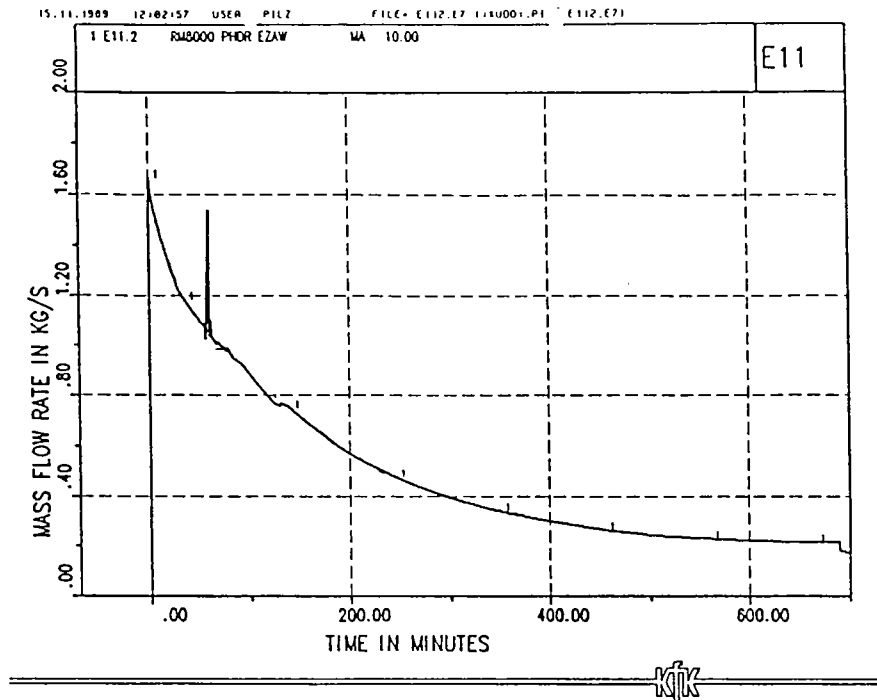


Fig. 2.4: Steam Mass Flow Rate from Reactor Pressure Vessel

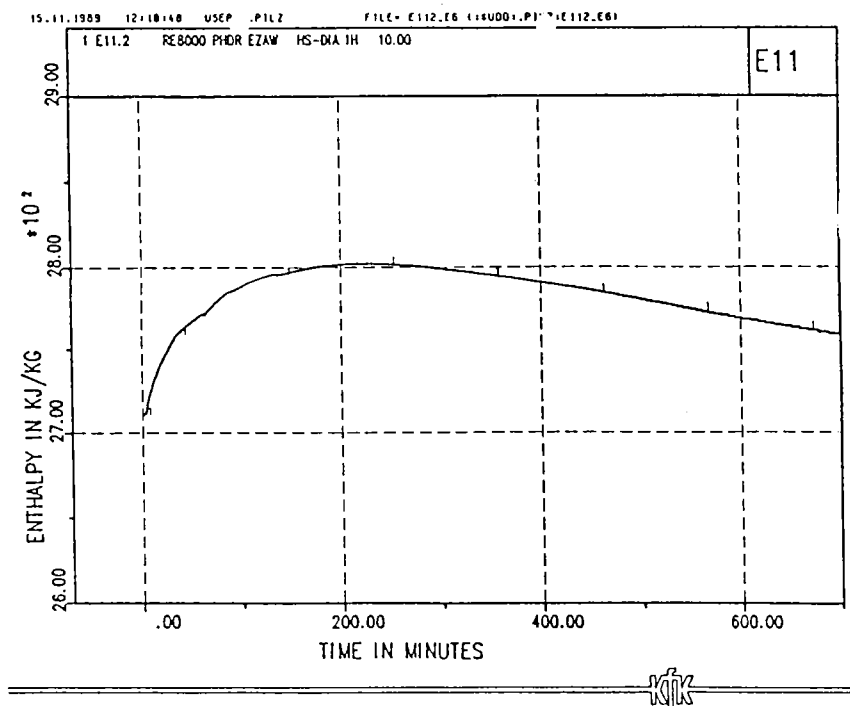


Fig. 2.5: Specific Enthalpy of Discharged Steam from Pressure Vessel

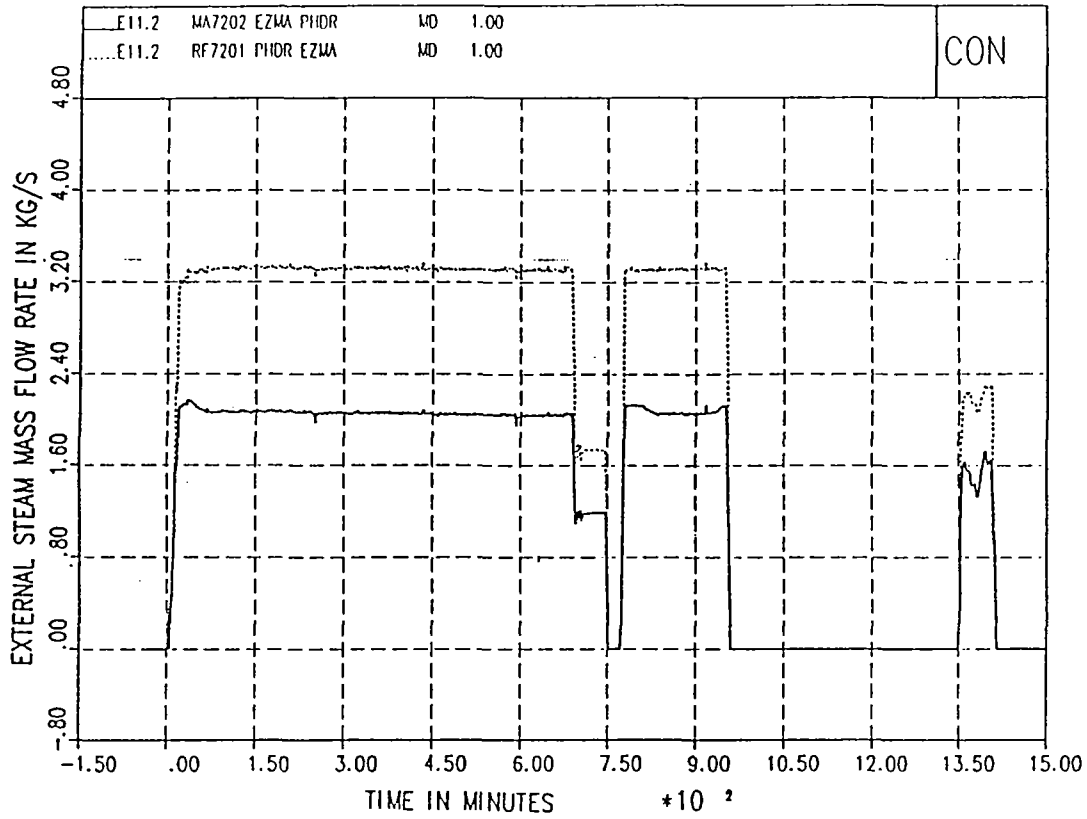


Fig. 2.6: Steam Discharge Rate from External Steam Source (Function MA7202 is representative for the orifice RF7201 shown in figs. 2 and 9)

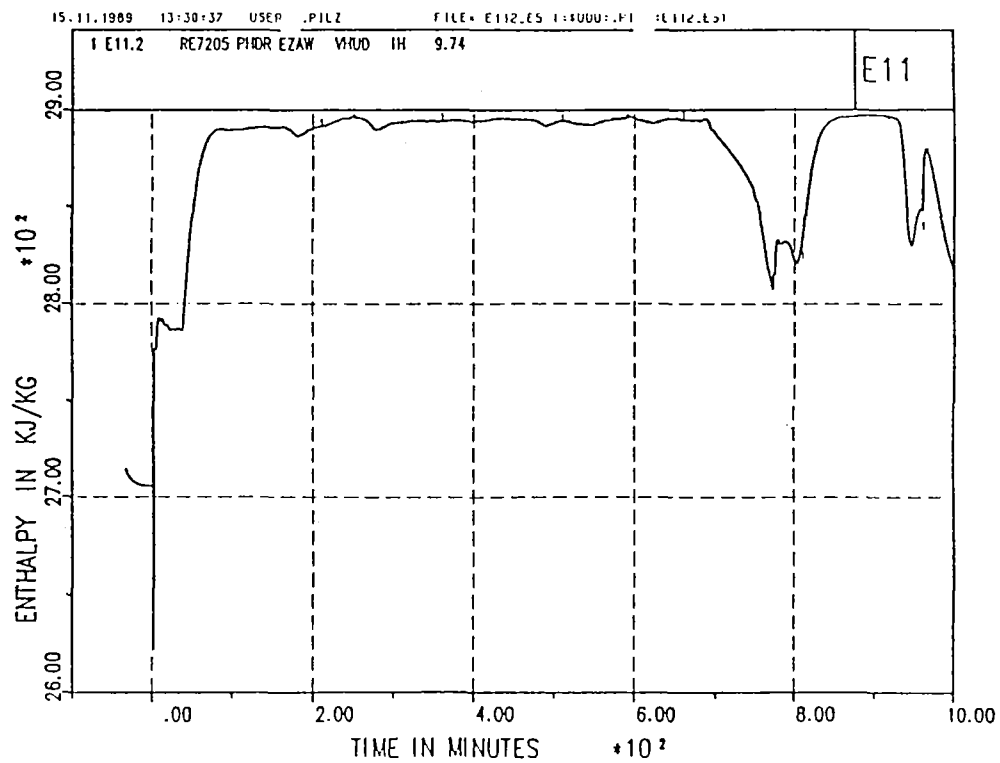


Fig. 2.7: Specific Enthalpy of Steam from External Source



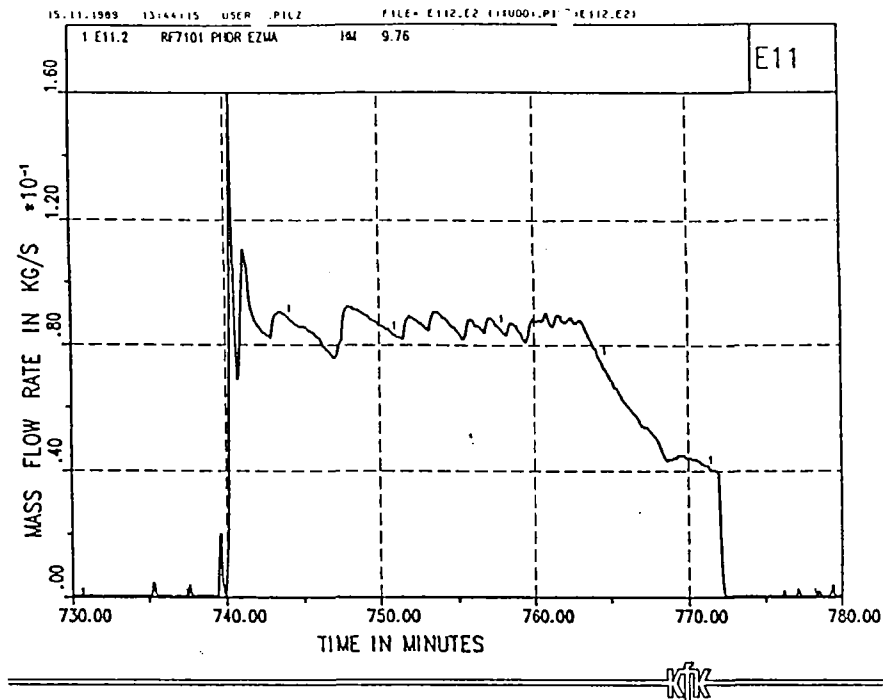


Fig. 2.8: Gas Mixture (15 vol.% Hydrogen, 85 vol.% Helium) Release Rate in R1.805

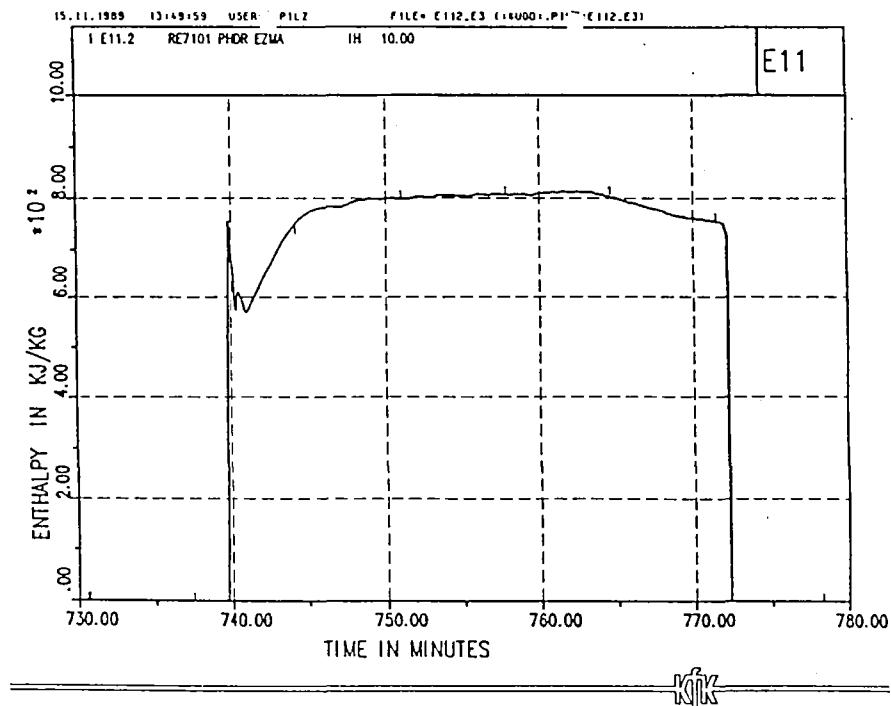


Fig. 2.9: Specific Enthalpy of Gas Mixture (15 vol.% Hydrogen, 85 vol.% Helium) Released in R1.805

Fig. 2.10: Horizontal Cross Section Showing the Location of Steam Release (Second Period)

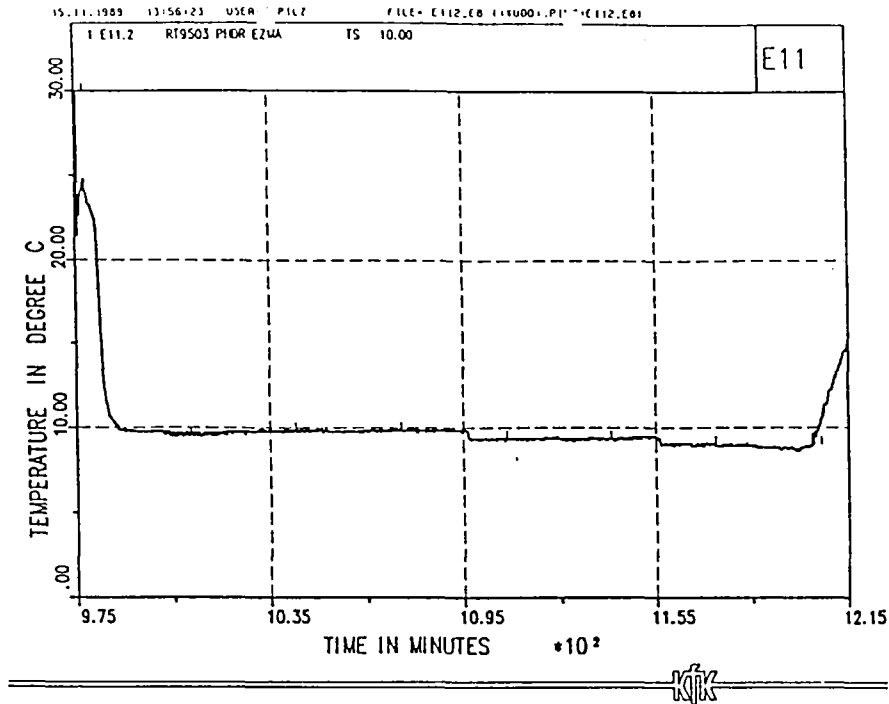


Fig. 2.11: Temperature Water Sprayed Externally onto the Containment Shell

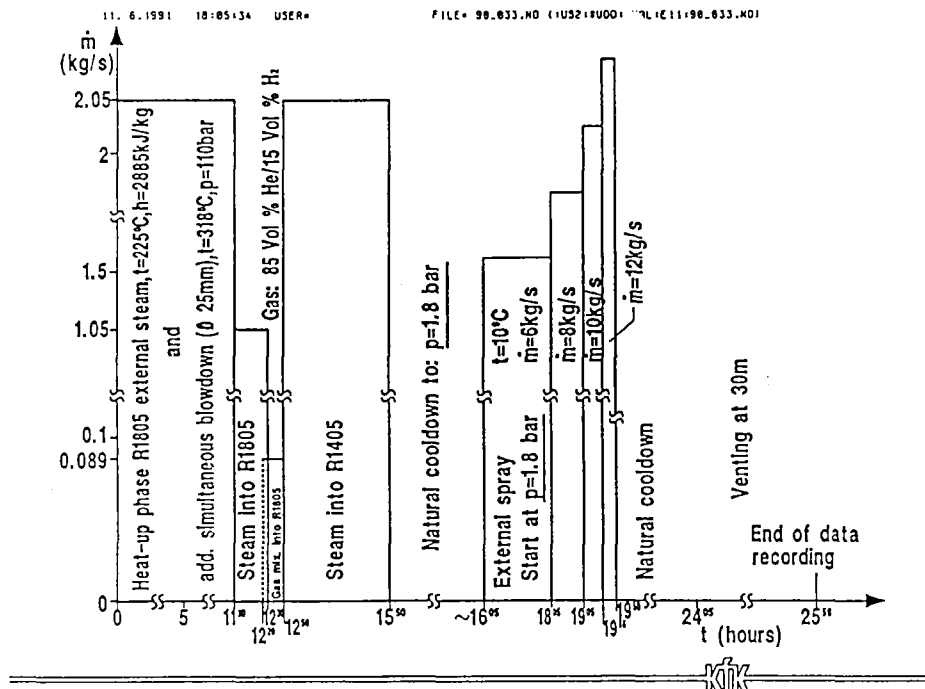


Fig. 2.12: Timing of the Experimental Procedure for E11.2

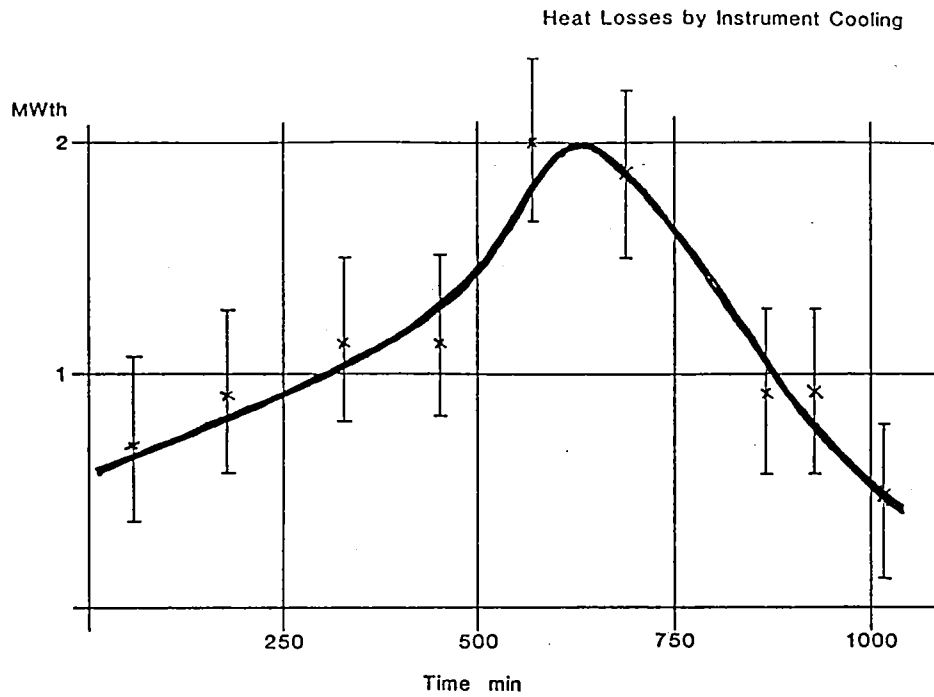


Fig. 2.13: Overall Heat Losses caused by Instrument Cooling deduced from Measurements taken from the Auxilliary Cooling System

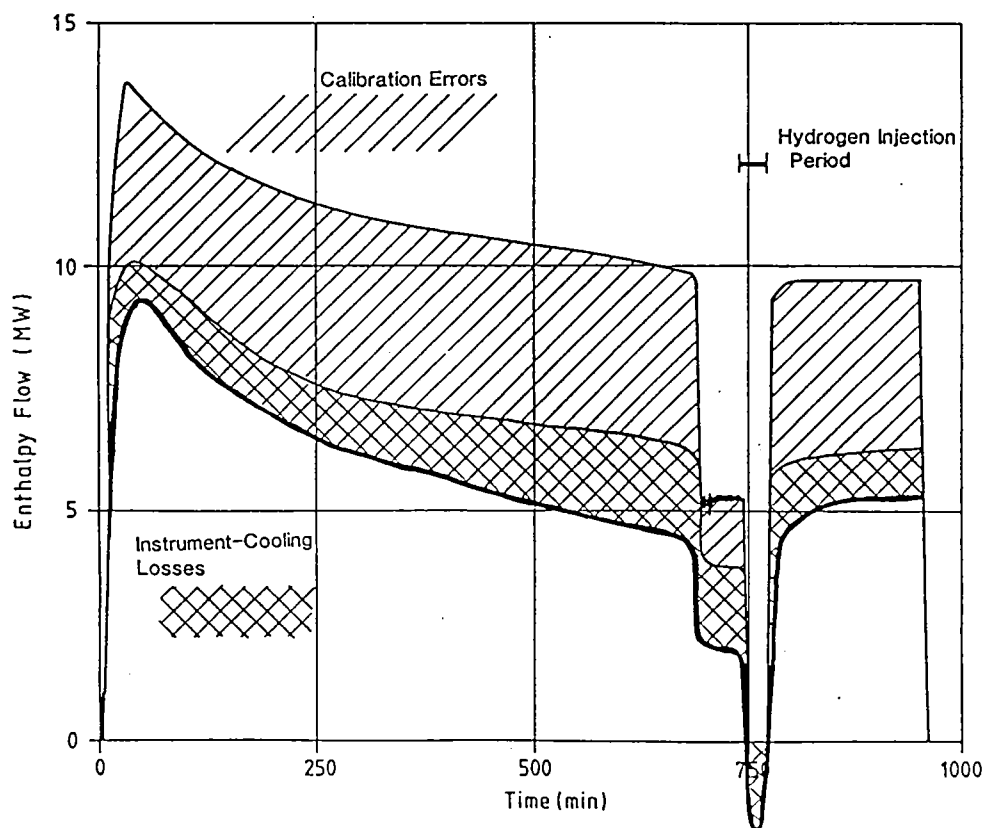


Fig. 2.14: Netto Energy Input into the HDR-Containment during Experiment E11.2 (Lower Solid Curve)

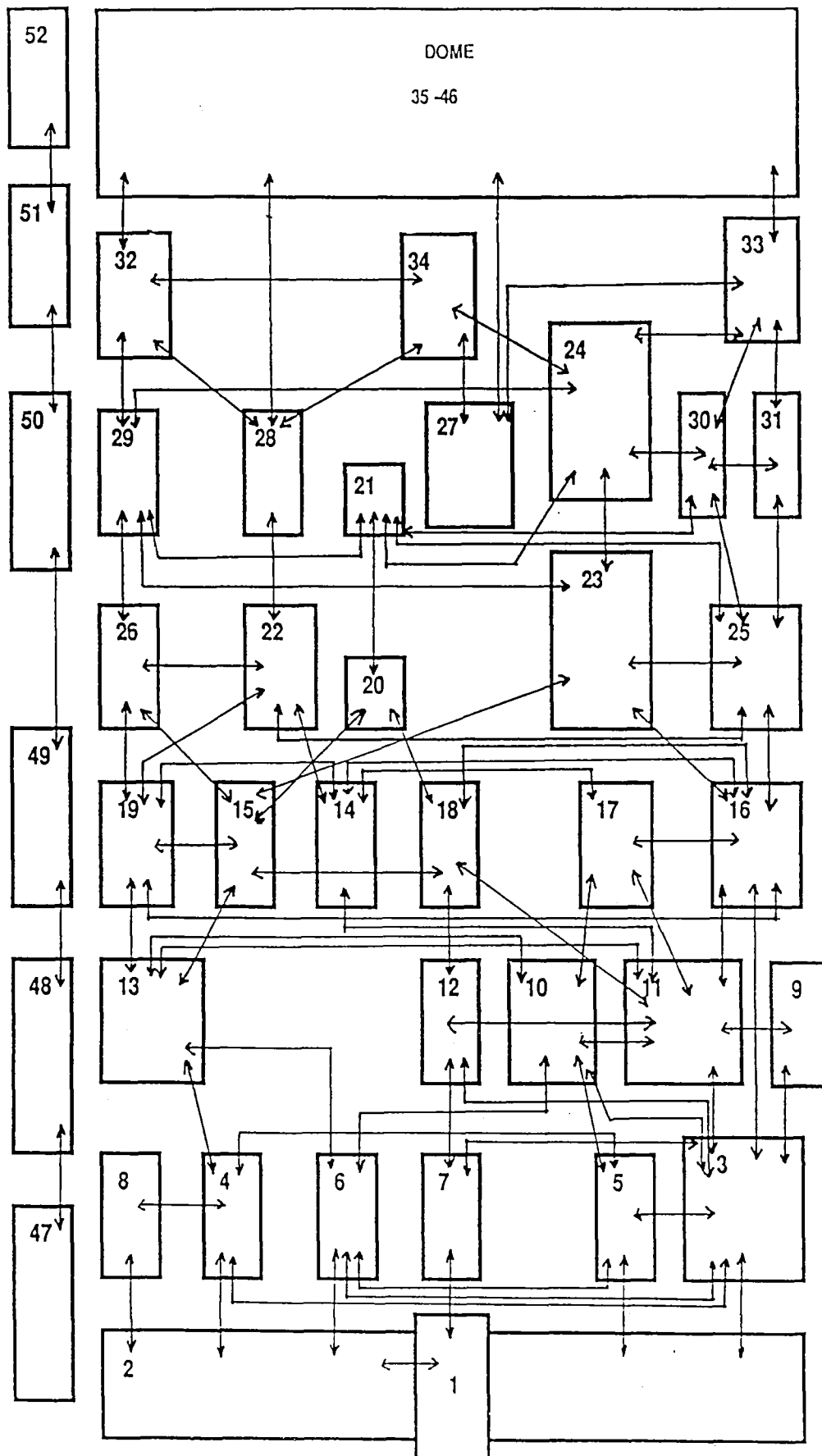
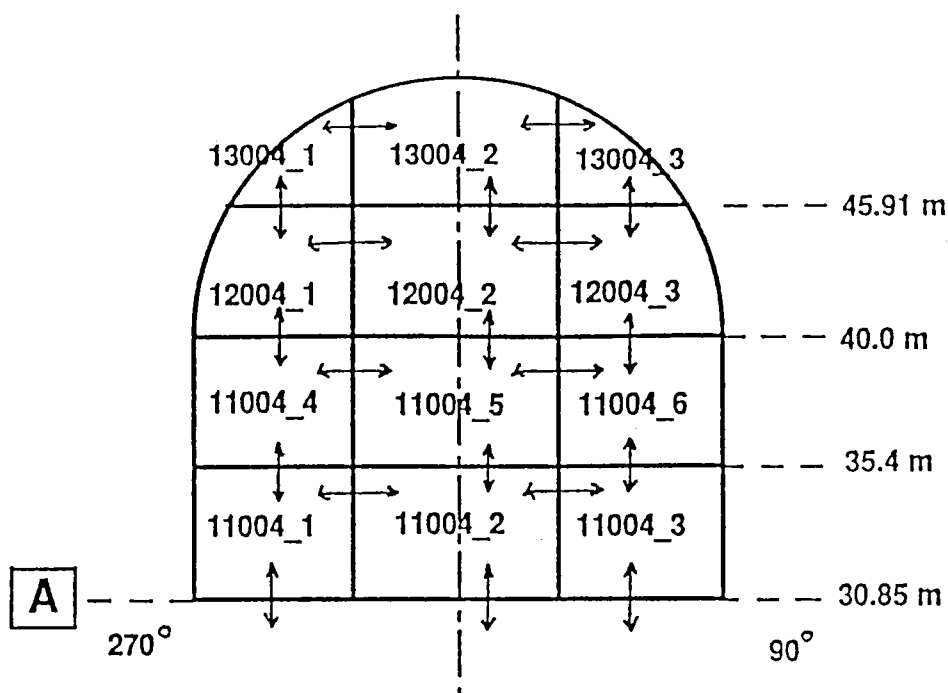


Fig. 5.1: Nodalisation Concept Adopted for the CONTAIN Version 1.12-Calculation (VTT - Helsinki)



CELL	HDR ROOMS	CELL	HDR ROOMS
1	1201, 1202, 1203, 1303	26	1708
2	1301, 1302, 1304, 1305	27	1801
	1307, 1308, 1311	28	1802
3	1401, 1406, 1317	29	1804
4	1403, 1409	30	1805
5	1404	31	1357
6	1405	32	1902, 1906
7	1407	33	1903, 1367
8	1408	34	1803, 1904, 1905
9	1410	35	11004_1
10	1501, 1506, 1507, 1512,	36	11004_2
	1513	37	11004_3
11	1502, 1520, 1503, 1505	38	11004_4
	1327	39	11004_5
12	1504	40	11004_6
13	1508, 1511, 1514	41	12004_1
14	1602, 1609	42	12004_2
15	1603	43	12004_3
16	1606, 1337	44	13004_1
17	1604, 1607, 1608	45	13004_2
18	1605	46	13004_3
19	1611	47-52	annular gap
20	1701 u	53	environment
21	1701 o		
22	1702, 1703, 1706		
23	1704 lower		
24	1704 upper, 1901		
25	1707, 1347		

Fig. 5.1A: Dome Nodalisation Concept Adopted for the CONTAIN Version 1.12-Calculations (VTT - Helsinki) and Correspondence between Nodalisation and HDR Room Numbers

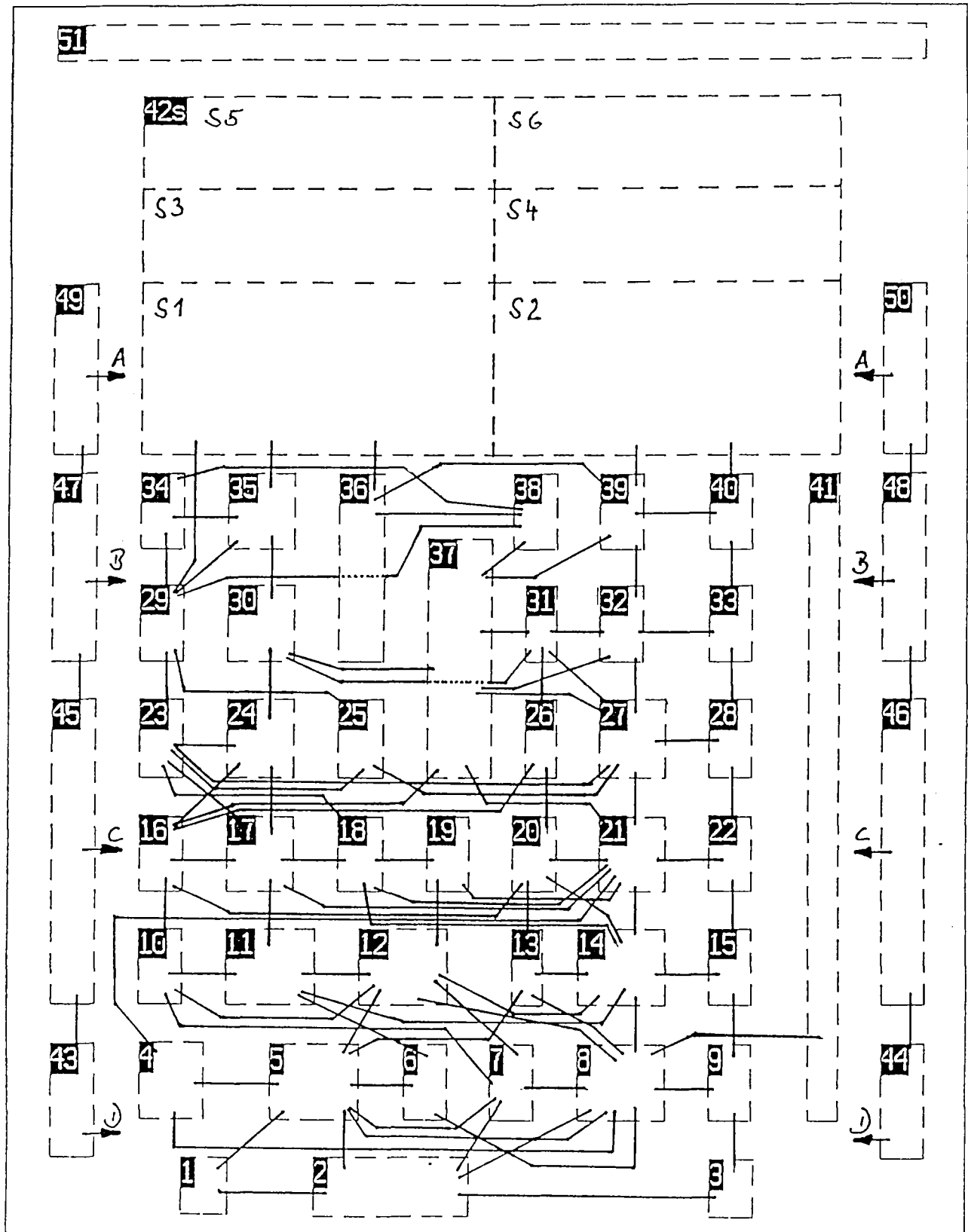


Fig. 5.2: Nodalisation Concept Adopted for the GOTHIC-Calculations  
(Battelle - Frankfurt)

## CONTROL VOLUMES

Vol. Nr.	HDR-Rooms	Volume (m <sup>3</sup> )
1	1202-03, 1303	78.00
2	REST 1200, 1300 Elevation	700.00
3	1307	58.00
4	1401	183.00
5	1404, 1407-09	296.00
6	1403	76.00
7	1405	95.00
8	1406	266.00
9	1317	63.00
10	1508, 1514	73.00
11	1511	222.00
12	REST 1500 Elevation	316.00
13	1504	28.00
14	1503	304.00
15	1327	61.00
16	1603	280.00
17	1611	192.00
18	1602, 1609	120.00
19	1604, 1607, 1608	112.00
20	1605	78.00
21	1606	183.00
22	1337	40.00
23	1703	83.00
24	1708	90.00
25	1702, 1706	73.00
26	1701 u	44.00
27	1707	119.00
28	1347	83.00
29	1802	125.00
30	1804	79.00
31	1701 o	64.00
32	1805	58.00
33	1357	68.00
34	1906	65.00
35	1902	90.00
36	1801	343.00
37	1704, 1901	805.00
38	1803, 1904, 1905	164.00
39	1903	71.00
40	1367	82.00
41	1410	113.00
42s	Dome	4800.00
43	Annular Gap - 5 m - 4.8 m	418.00
44	Annular Gap - 5 m - 4.8 m	418.00
45	Annular Gap 4.8 m - 17.55 m	280.00
46	Annular Gap 4.8 m - 17.55 m	280.00
47	Annular Gap 17.55 - 13.85 m	258.00
48	Annular Gap 17.55 - 30.85 m	258.00
49	Annular Gap 30.85 - 40 m	190.00
50	Annular Gap 30.85 - 40 m	190.00
51	Annular Gap 40 - 50 m	576.00

Fig. 5.2A: Correspondence between GOTHIC Nodalisation and HDR Room Numbers



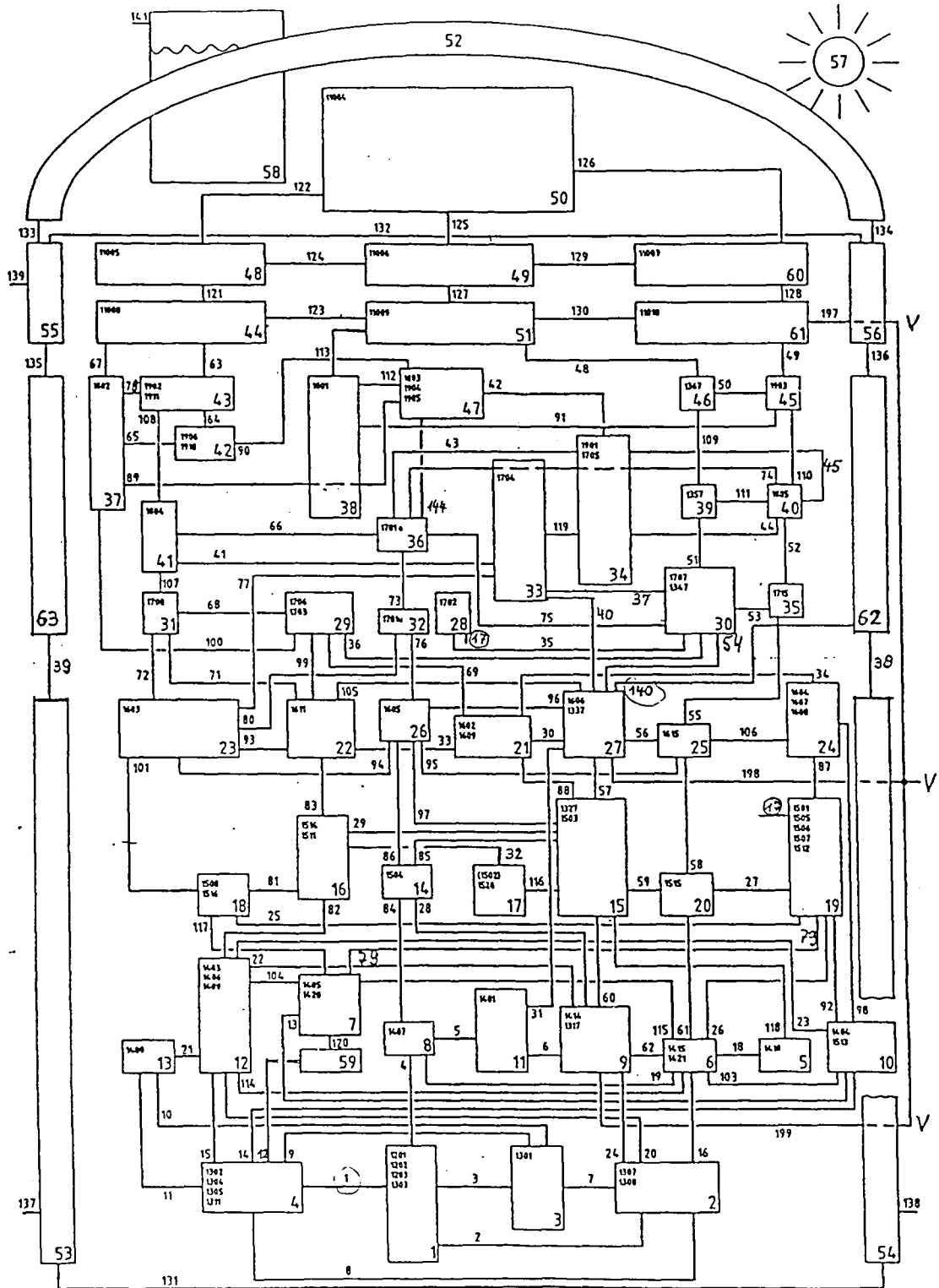


Fig. 5.3: Nodalisation Concept Adopted for the RALOC-Calculations showing Atmospheric Junctions (GRS - Köln)

## ISP 29

RALOC-63 zone numbers according to HDR-room numbers for the post-test-calculation of HDR test E11.2

zone-Nr.	HDR room number	zone-Nr.	HDR room number
1	1201, 1202, 1203, 1303, sump	34	1705, 1901, 1704 front
2	1307, 1308	35	1715
3	1301	36	1701 o
4	1302, 1304, 1305, 1311	37	1802
5	1410, lift	38	1801
6	1415, 1421	39	1357
7	1405, 1420, breakroom 2	40	1805, breakroom 1
8	1407	41	1804
9	1317, 1414	42	1906, 1910
10	1404, 1513	43	1902, 1911
11	1401	44	11008 over spiral staircase
12	1403, 1406, 1409	45	1903
13	1408	46	1367
14	1504	47	1803, 1904, 1905
15	1327, 1503, 1502 (part of)	48	11005
16	1511, 1514	49	11006
17	1520, former 1502	50	11004 dome high
18	1508, 1516	51	11009
19	1501, 1505, 1506, 1507, 1512	52	gap 40 m upwards
20	1515	53	gap left 15 m downwards
21	1602, 1609	54	gap right 15 m downwards
22	1611	55	gap left 30m-40m
23	1603	56	gap right 30m-40m
24	1604, 1607, 1608	57	environment
25	1615	58	spray water tank
26	1605	59	sump of 1405
27	1337, 1606	60	11007
28	1702	61	11010 over stair case
29	1703, 1706	62	gap right 15m-30m
30	1347, 1707	63	gap left 15m-30m
31	1708		
32	1701 u with nest		
33	1704 rear		

Fig. 5.3A: Correspondence between RALOC Nodalisation and HDR Room Numbers

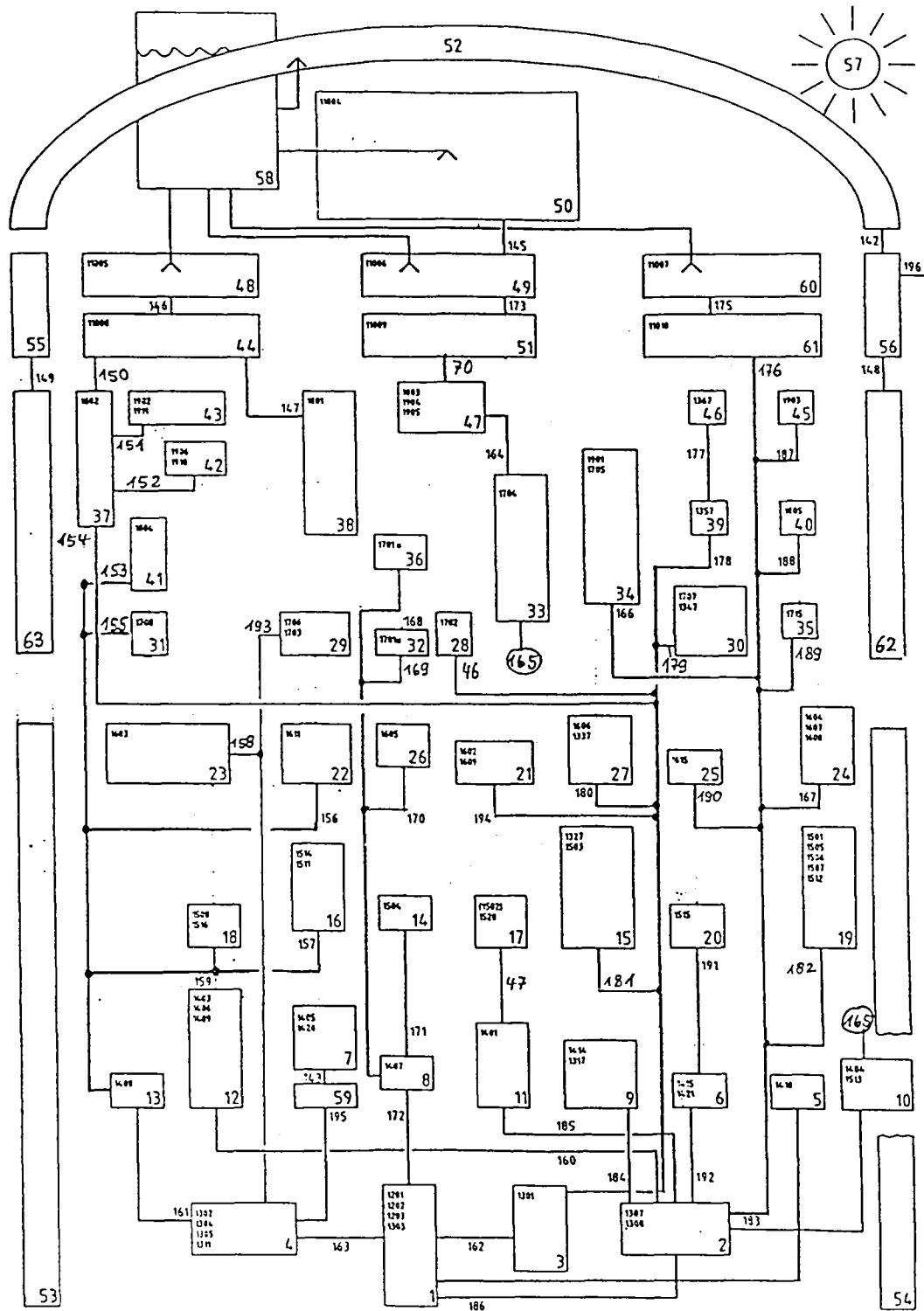


Fig. 5.3B: Nodalisation Concept Adopted for the RALOC-Calculations  
(Water Transport Junctions) (GRS - Köln)

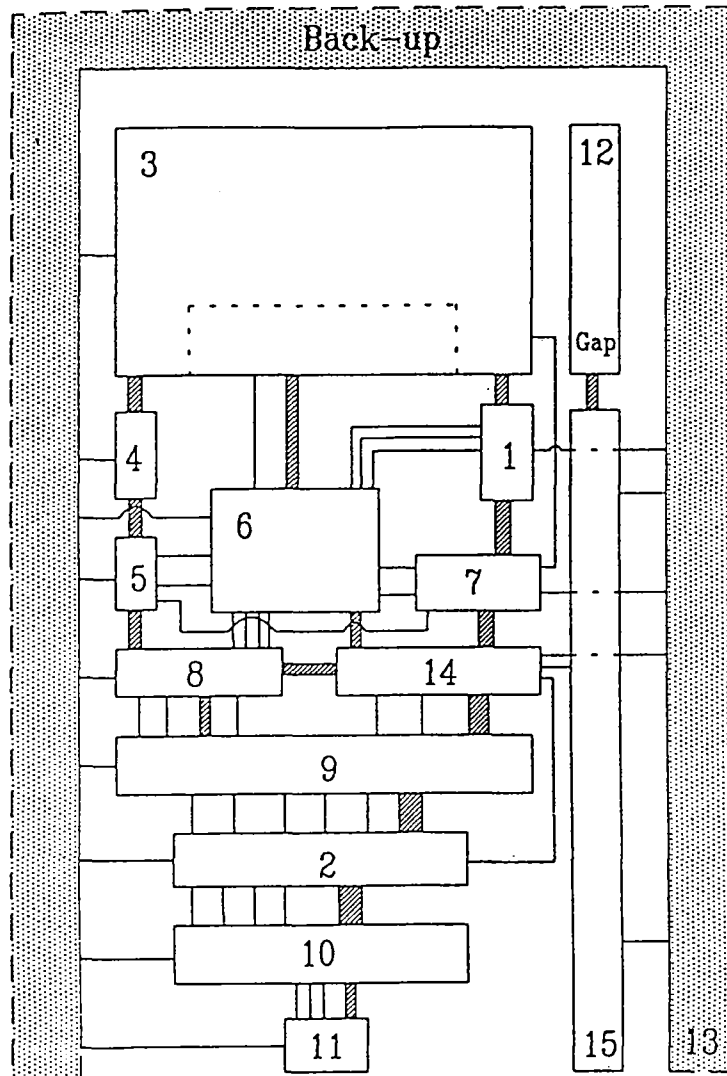


Fig. 5.4: Nodalisation Concept Adopted for the FUMO-Calculations  
(University of Pisa)  
blowdown compartment: node 1  
lower energy addition: node 2

<b>FUMO Node</b>	<b>HDR Compartments</b>
1	1357 1367 1805
2	1317 1401 1403 1404 1405 1406 1409
3	1801 1802 1803 1903 1904 1905 11004
4	1902 1906
5	1708 1804
6	1701 1704
7	1347 1702 1703 1706 1707
8	1602 1603 1609 1611
9	1327 1410 1501 1503 1504 1505 1506 1507 1508 1511 1512 1513 1514 1520
10	1301 1302 1304 1305 1307 1308 1311 1407 1408
11	1201 1202 1203 1303
14	1337 1604 1605 1606 1607 1608

Fig. 5.4A: Correspondence between FUMO Nodalisation and HDR Room Numbers

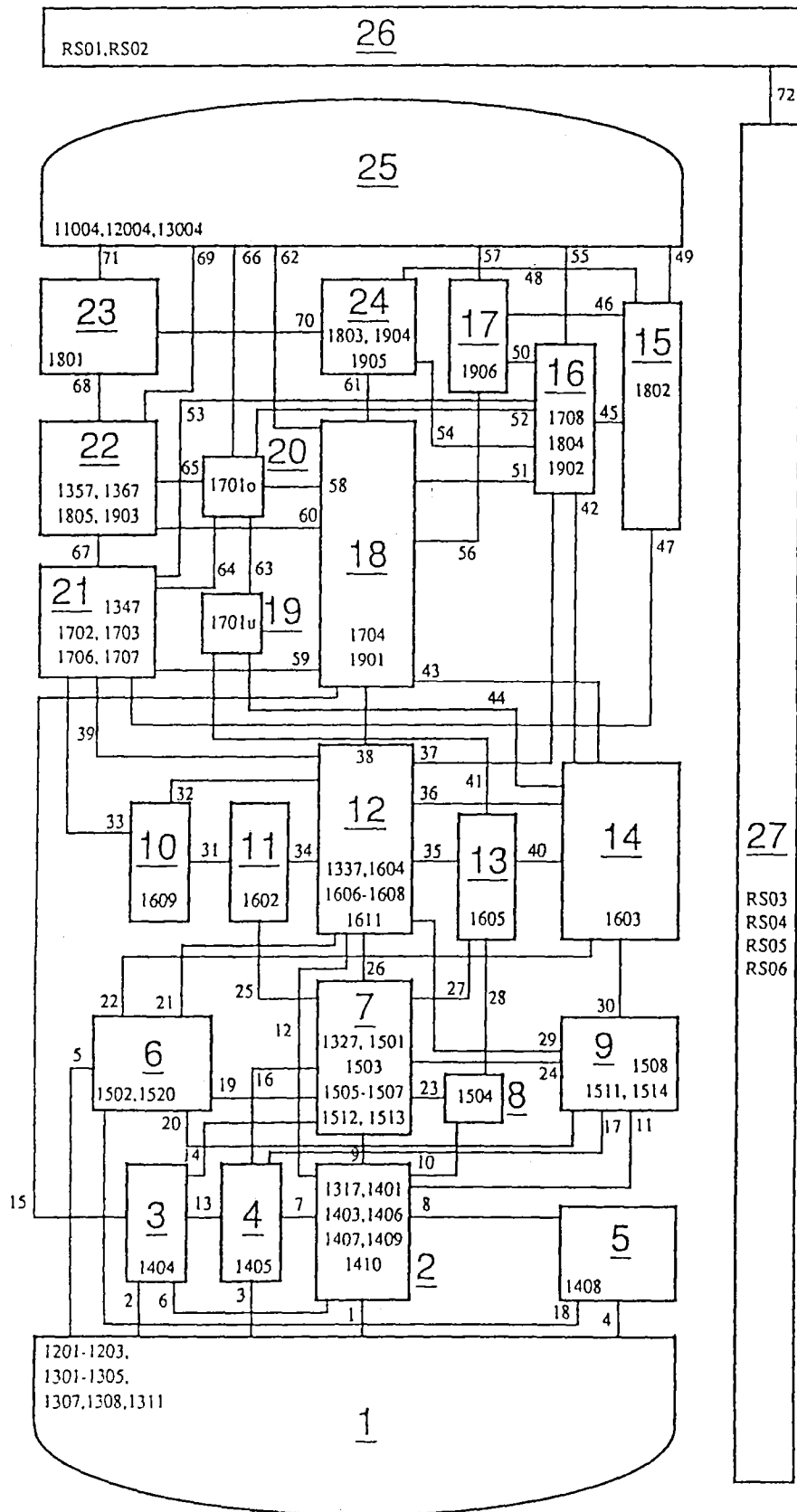


Fig. 5.5: Nodalisation Concept Adopted for the CONTAIN Version 1.11 (JAERI-Japan) showing Correspondence to HDR Room Numbers

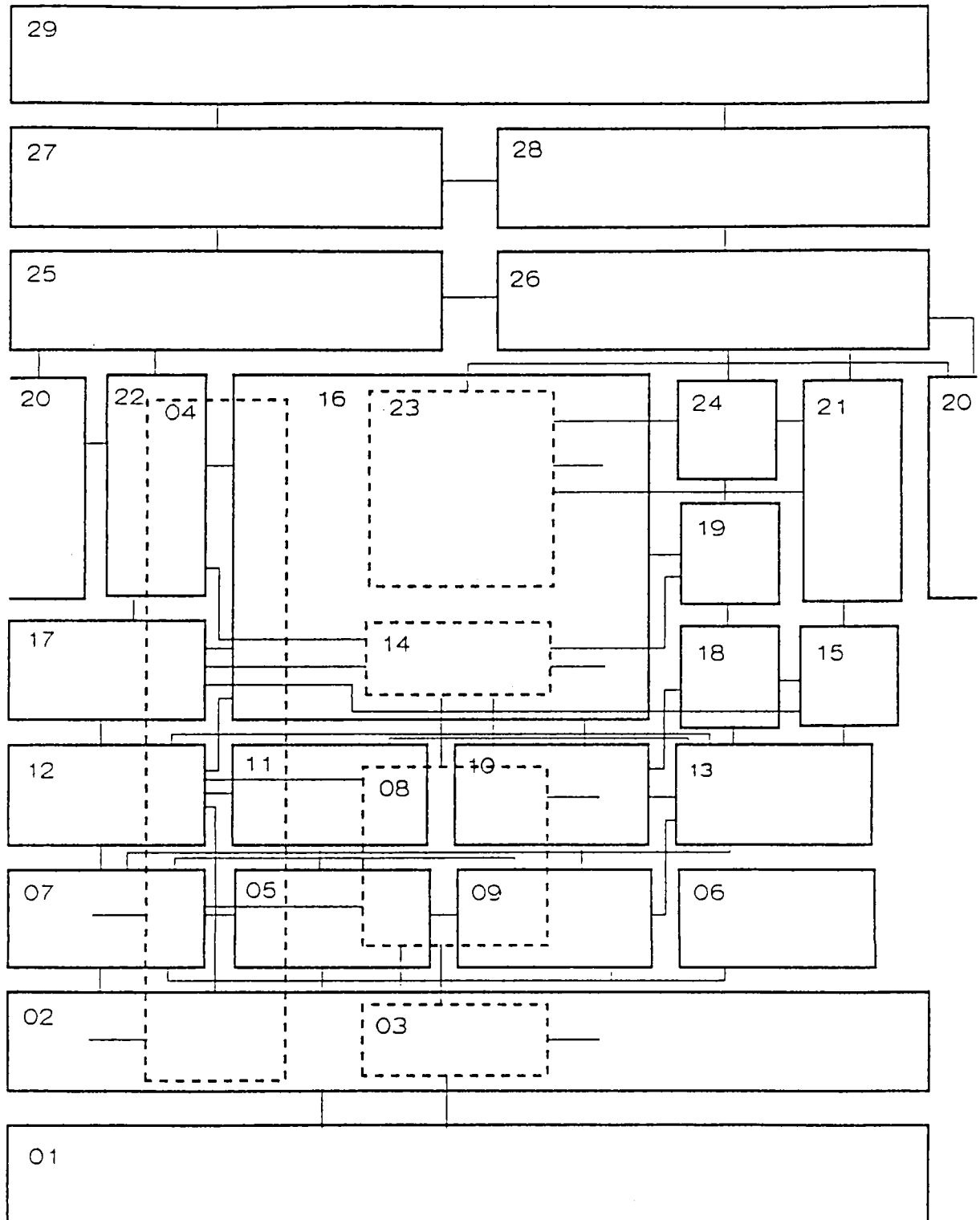


Fig. 5.6: Nodalisation Concept Adopted for the CONTAIN Version 1.12-Calculations (ECN - Petten)

No.	Compartments	Vol. [m <sup>3</sup> ]	Hght. [m]	Elev. [m]	Temp. [K]
01	1201-1203, 1301-1308, 1311, 1408	895.	4.0	-5.8	296.5
02	1401, 1403-1406, 1409, 1317	836.	4.5	-1.1	293.7
03	1407	84.	5.0	-3.0	295.0
04	1410	113.	31.9	0.0	296.2
05	1501, 1505-1507, 1512, 1513	196.	4.5	4.5	296.8
06	1502, 1520	120.	5.0	0.0	293.4
07	1503, 1327	385.	5.0	4.5	294.1
08	1504, 1605	106.	3.5	4.5	299.8
09	1508, 1511, 1514	295.	4.5	4.5	292.5
10	1603	280.	7.5	8.7	298.7
11	1604, 1607, 1608	112.	3.0	10.0	297.2
12	1606, 1337	223.	4.5	10.0	293.9
13	1602, 1609, 1611	312.	4.5	10.0	292.5
14	1701u, 1701o	108.	4.5	14.0	338.8
15	1703, 1706	102.	4.5	14.0	290.9
16	1704	793.	8.5	14.0	316.5
17	1702, 1707, 1347	256.	4.5	14.0	293.9
18	1708	90.	5.5	14.0	293.1
19	1804	79.	4.5	20.6	293.1
20	1801	343.	10.0	21.0	300.0
21	1802	125.	4.5	21.0	295.0
22	1805, 1903, 1357, 1367	279.	9.0	21.0	301.3
23	1803, 1904, 1905	164.	6.0	25.0	319.4
24	1902, 1906	155.	6.0	25.0	308.5
25	11004a	365.	9.1	30.9	307.3
26	11004b	365.	9.1	30.9	307.3
27	12004a	310.	5.9	40.0	303.9
28	12004b	310.	5.9	40.0	303.9
29	13004	450.	4.1	45.9	303.9
Total Volume		11245.			

Fig. 5.6A: Correspondence between CONTAIN Nodalisation and HDR Room Numbers



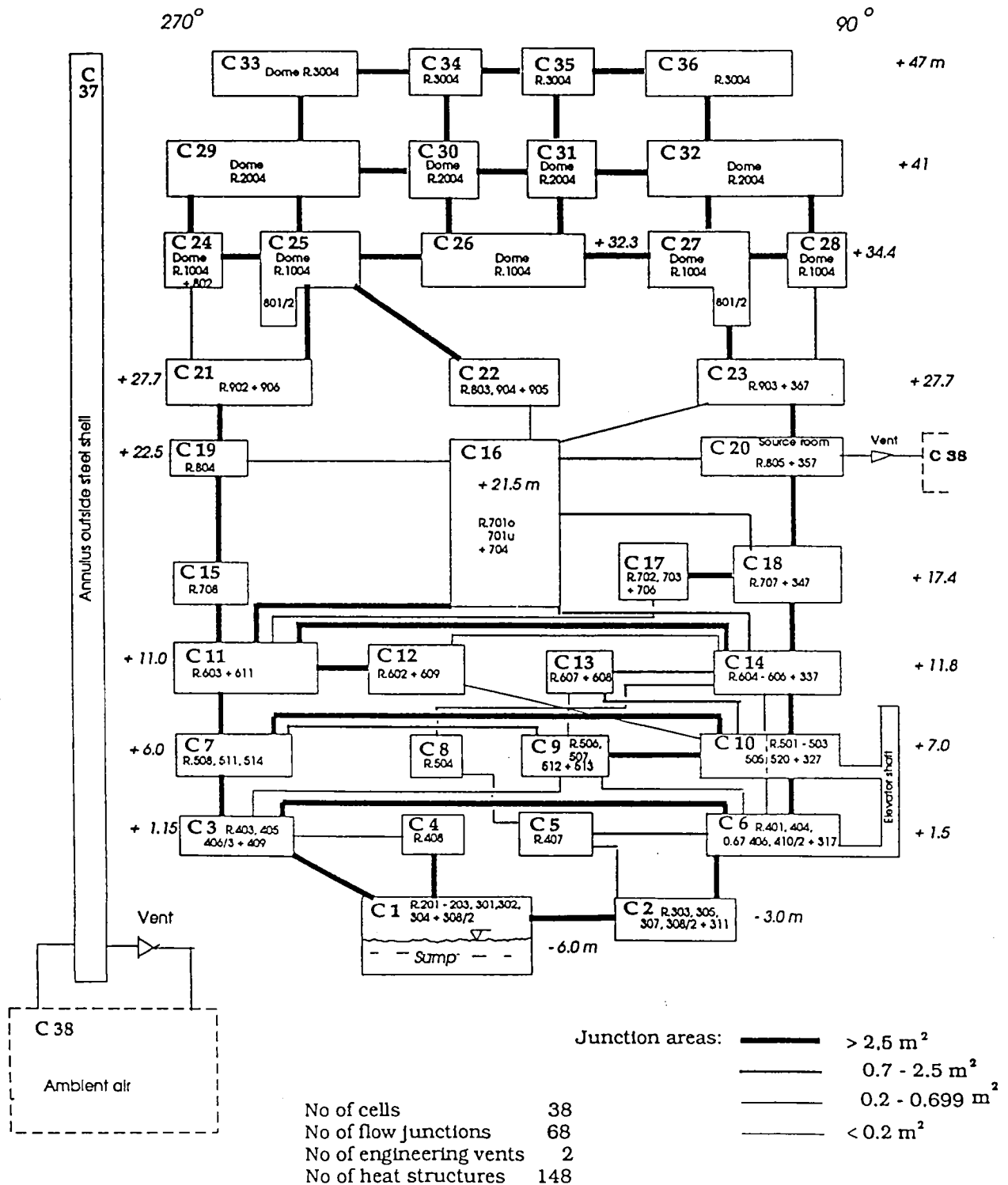


Fig. 5.7: Nodalisation Concept Adopted for the CONTAIN Version 1.11-Calculations (Studsvik - Nykoeeping)

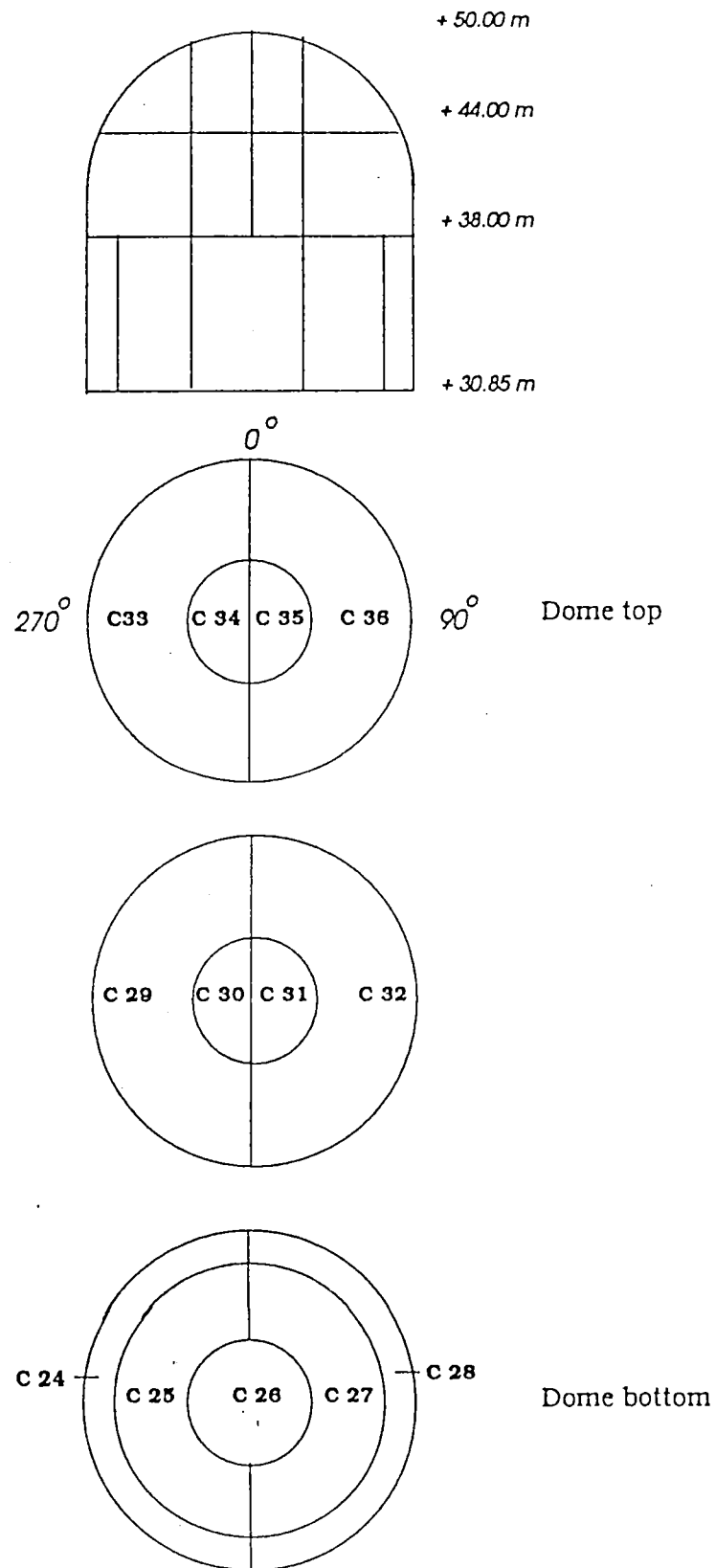


Fig. 5.7A: Nodalisation Concept Adopted for the CONTAIN Version 1.11-Calculations (Studsvik - Nykoeping) - Details of Dome Nodalisation

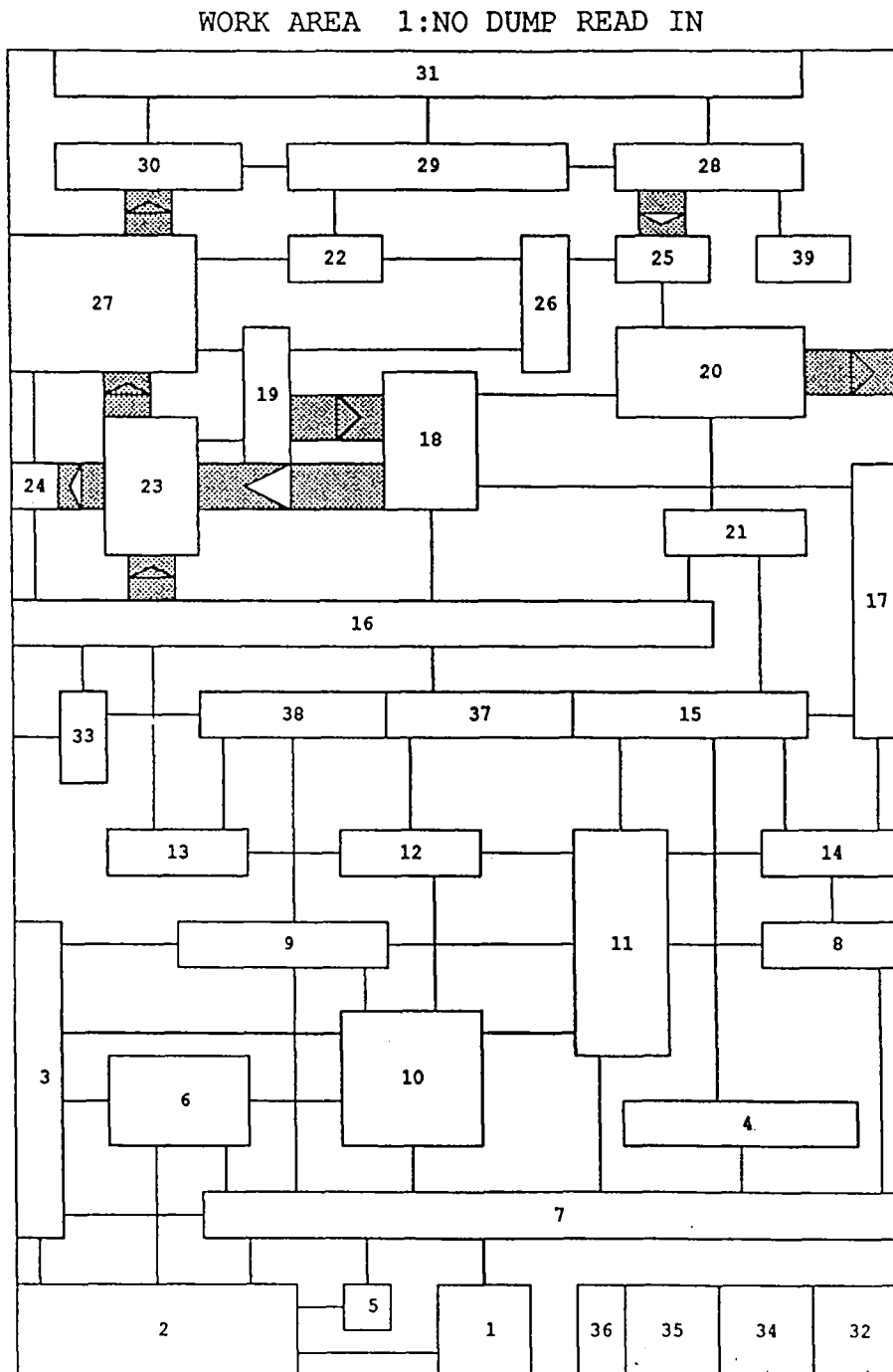


Fig. 5.8: Nodalisation Concept Adopted for the CONTAIN Version 1.11(UK)-Calculations  
(AEE - Winfrith)

Cell number	Room number(s)	comments
1	1201-3 1303	sump and bottom most rooms
2	1301-2 1304-5 1307-8 1311	
3	1405	lower source cell
4	1401	
5	1408	
6	1404	
7	1403 1406-7 1409 1317	
8	1504	
9	1508 1511 1514	
10	1501 1505-7 1512-13	
11	1503 1520 1327 1410	
12	1602 1607-8	
13	1609	
14	1605	
15	1603	
37	1611	
38	1604 1606 1337	
16	1702-3 1706-7 1347	
17	1701u	lower reactor vessel (heat sink)
18	1701o	
19	1704 1901	
33	1704	bottom half of large room 1704
20	1804	
21	1708	
22	1801	
23	1805	upper source cell
24	1357	stair case neighbouring source cell
25	1902 1904	
26	1904-5 1803	
27	1903 1367	cell between source cell and dome
28	11004	dome
29	11004	dome
30	11004	dome
31	12004 13004	top of dome
32		airgap (lower)
34		airgap
35		airgap (upper)
36		atmosphere
39	1802	dead end room

Fig. 5.8A: Correspondence between CONTAIN (UK) Nodalisation and HDR Room Numbers

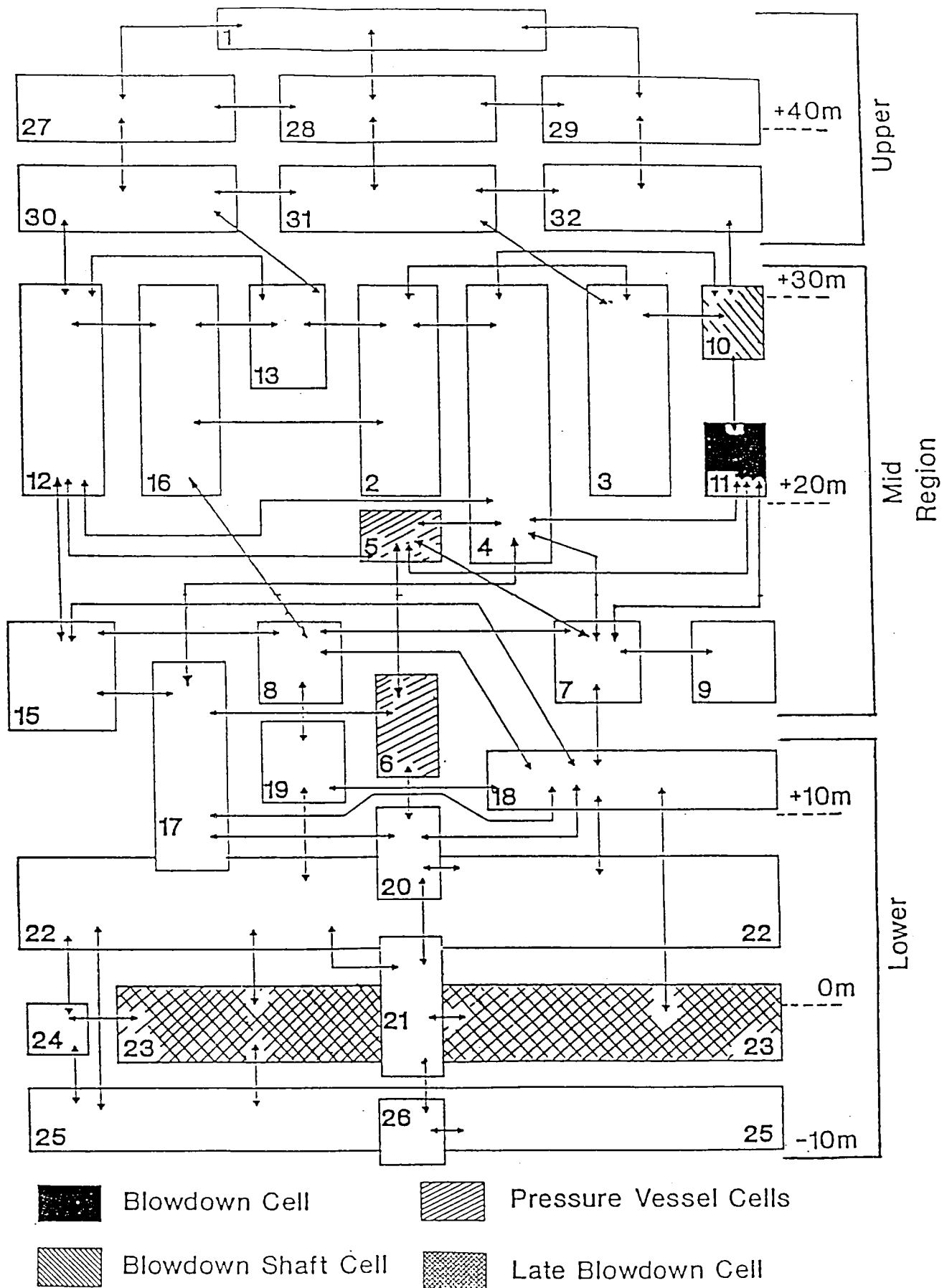


Fig. 5.9: Nodalisation Concept Adopted for the MELCOR-Calculations (AEA Technology)

CELL NUMBER	HDR ROOMS	COMMENT
1, 27, 28, 29, 30, 31, 32	11004	Upper dome split into 7 nodes.
2	1803 1904	
3	1801 1905	
4	1704	
5	1701o	
6	1701u	
7	1347 1707	
8	1703 1706	
9	1702	
10	1367 1903	
11	1357 1805	Blowdown cell
12	1804 1902	
13	1906	
15	1708	
16	1802	
17	1603	
18	1337 1604 1606 1607 1608 1611	
19	1602 1609	
20	1605	
21	1407 1504	
22	1327 1501 1502 1503 1505 1506 1507 1508 1511 1512 1513 1514	
23	1317 1401 1403 1404 1405 1406 1409 1410 1420 1421	Late blowdown cell
24	1408	
25	1201 1301 1302 1304 1305 1307 1308 1311	
26	1202 1203 1303	

Fig. 5.9A: Correspondence between MELCOR Nodalisation and HDR Room Numbers

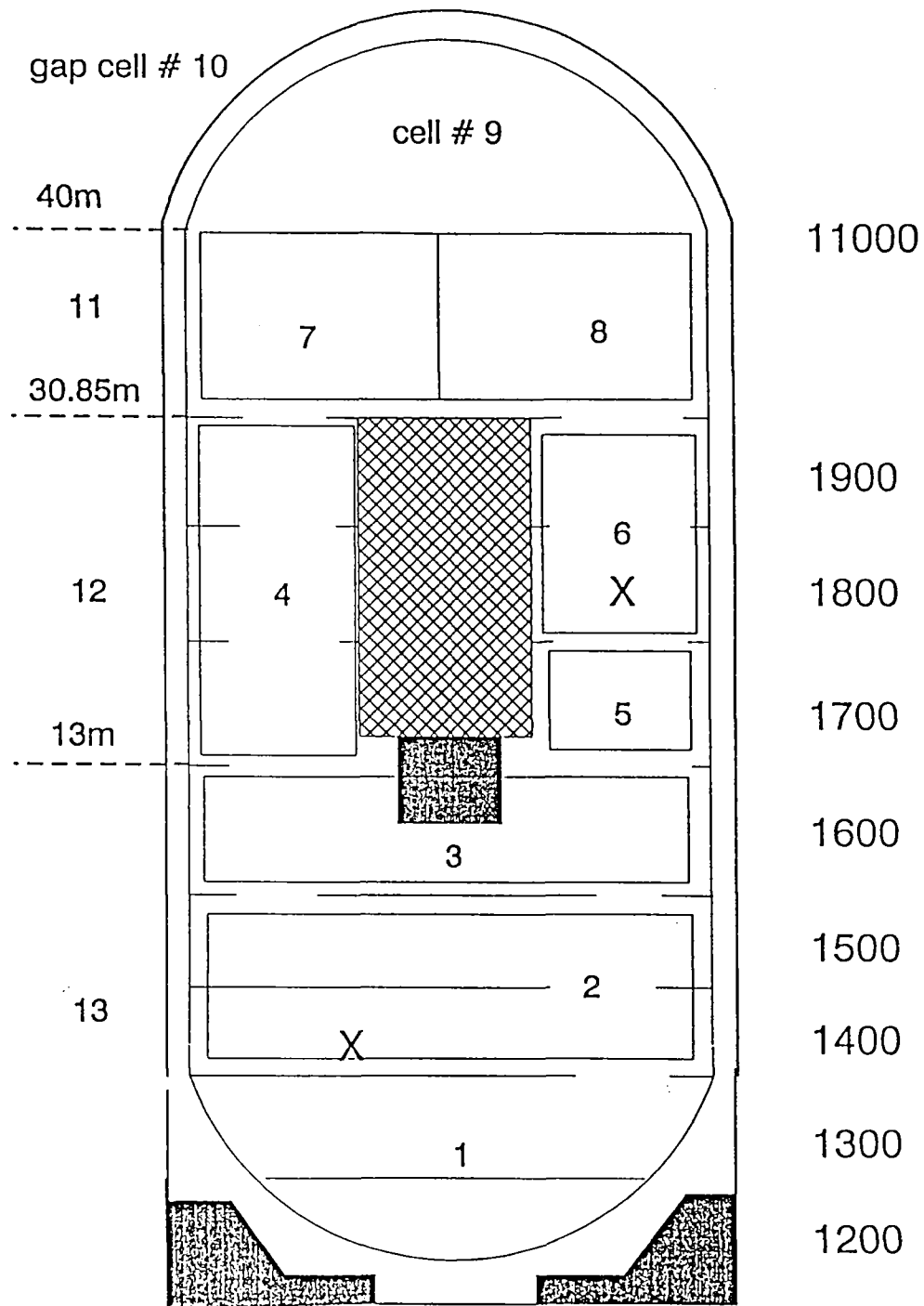
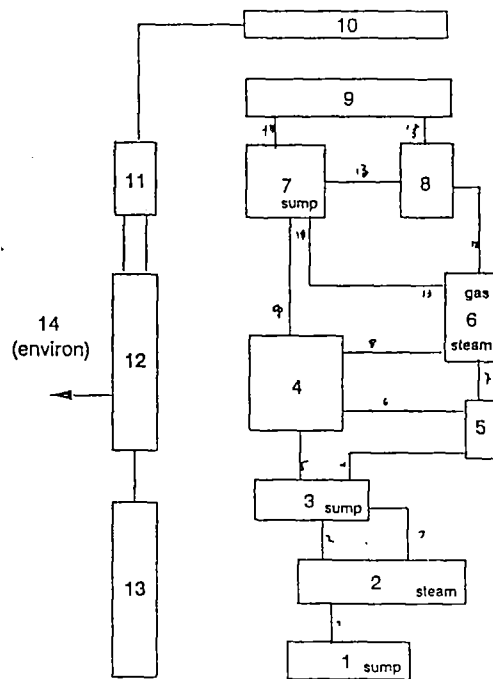


Fig. 5.10: Nodalisation Concept Adopted for the CONTAIN Version 1.12-Calculations (SANDIA National Laboratories)



CONTAIN Cell#	HDR Rooms	Volume m <sup>3</sup>	Elev. <sup>a</sup> m
1	1201,1202,1203,1301,1302,1303,1304, 1305,1307,1308,1311	836.0	-4.567
2	1405,1406,1407,1403,1409,1401,1410, 1408,1404,1317,1327,1501,1506,1507, 1512,1513,1502,1520,1503,1504,1505, 1508,1511,1514	2113.0	4.195
3	1603,1611,1602,1609,1606,1604,1607, 1608,1605,1337	1005.0	12.678
4	1701u,1701b,1704,1708,1703,1706,1702, 1803,1904,1905,1906,1802,1804,1901, 1902	1656.0	20.311
5	1707,1347	202.0	17.05
6	1805,1903,1357,1367	279.0	25.293
7	33332,33333 <sup>b</sup>	2146.8	34.133
8	33331 <sup>b</sup>	901.9	35.670
9	33334 <sup>b</sup>	2094.4	45.25
10	2011 <sup>c</sup>	588.16	45.25
11	2012,2022,2032 <sup>c</sup>	367.2	35.67
12	2013,2023,2033 <sup>c</sup>	654.3	22.42
13	2014,2015,2016,2024,2025,2026,2034, 2035,2036,2017,2027,2037 <sup>c</sup>	1033.6	3.34
14	environment	1.0e30	-----

<sup>a</sup> Elevation of cell mass centroid

<sup>b</sup> Nodalization of containment above 30.85m (Figure 1)

<sup>c</sup> Gap Nodalization (Figure 2)

Fig. 5.10A: Nodalisation Concept Adopted for the CONTAIN Version 1.12-Calculations (Scheme showing Junctions) (SANDIA National Laboratories) and Correspondence between Nodalisation and HDR Room Numbers



## OECD Standard Problem ISP-29

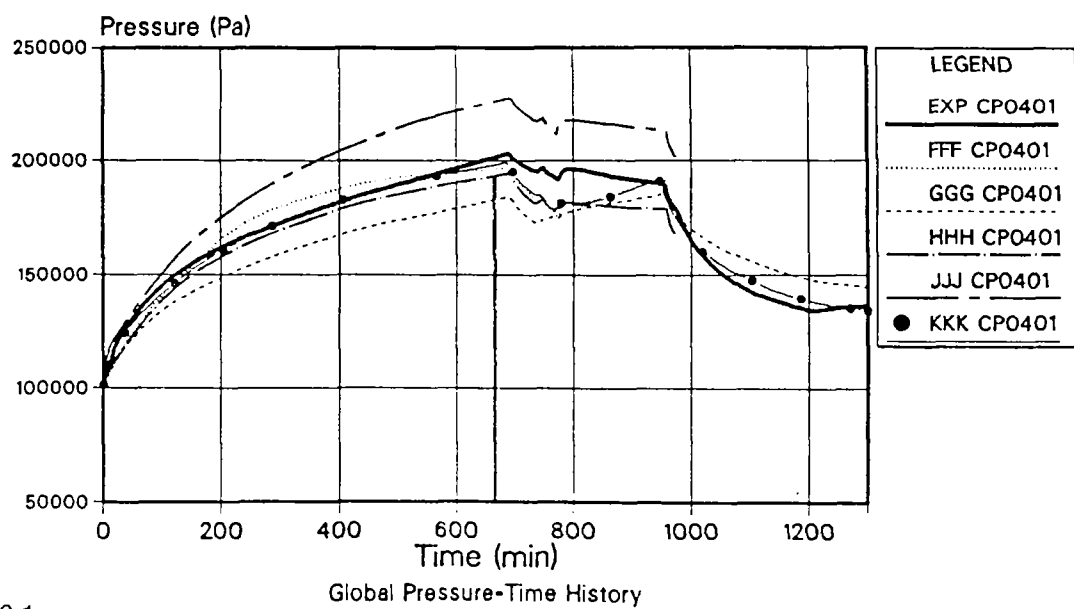
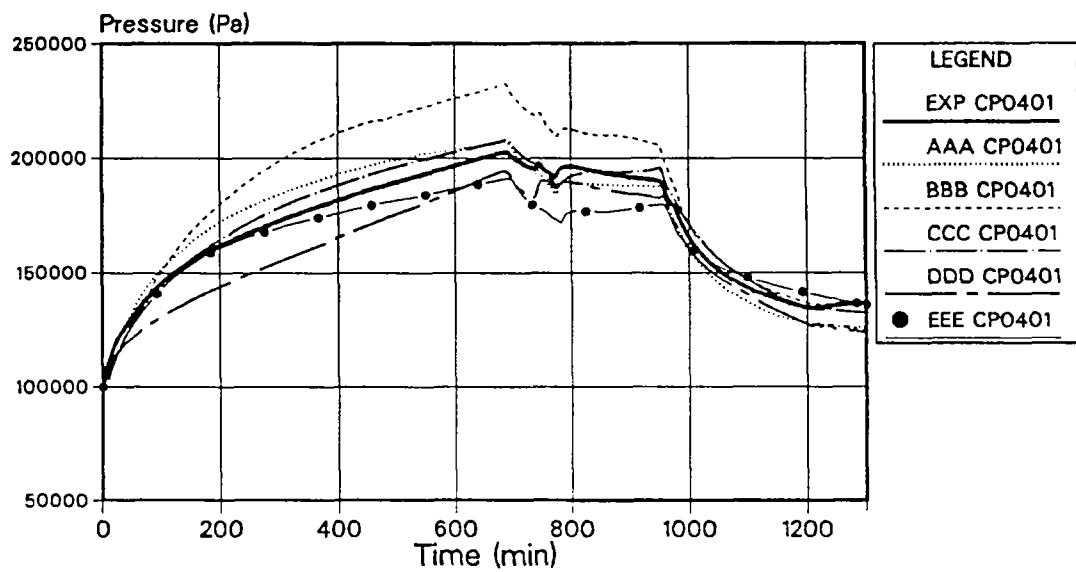
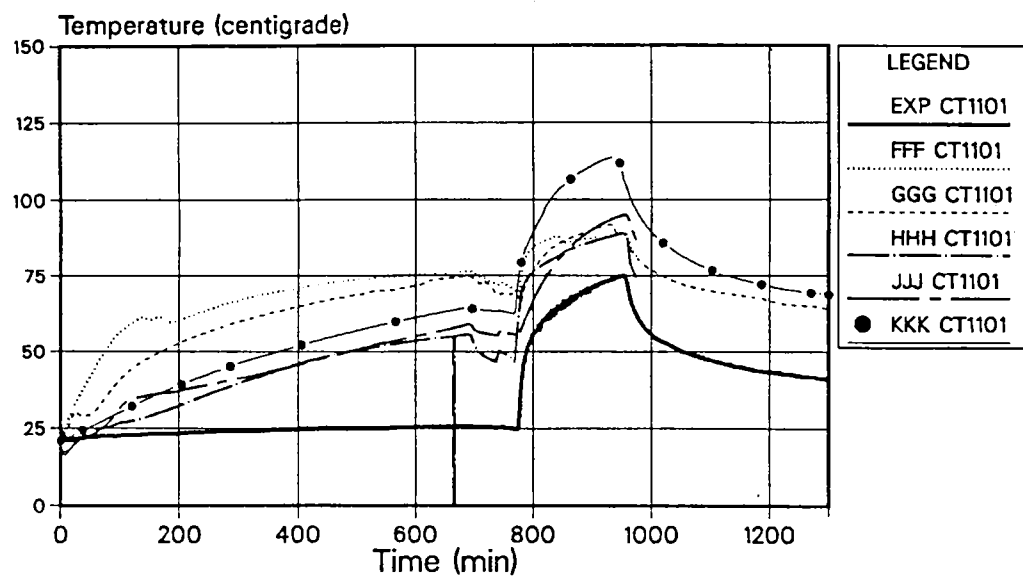
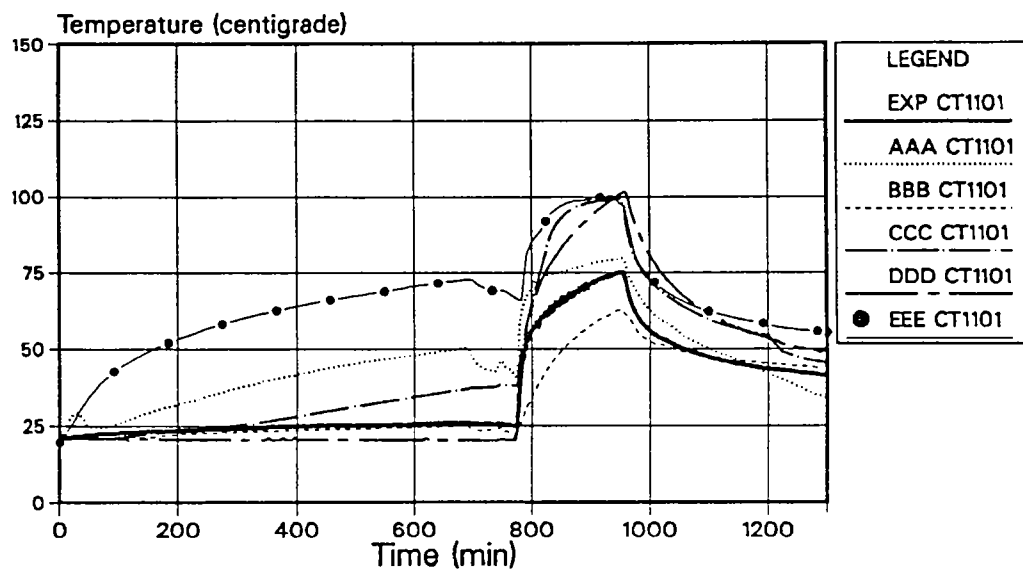


Fig. 6.1

Global Pressure-Time History

## OECD Standard Problem ISP-29



Containment Temperatures 6 m Elevation (280 degree)

Fig. 6.2

## OECD Standard Problem ISP-29

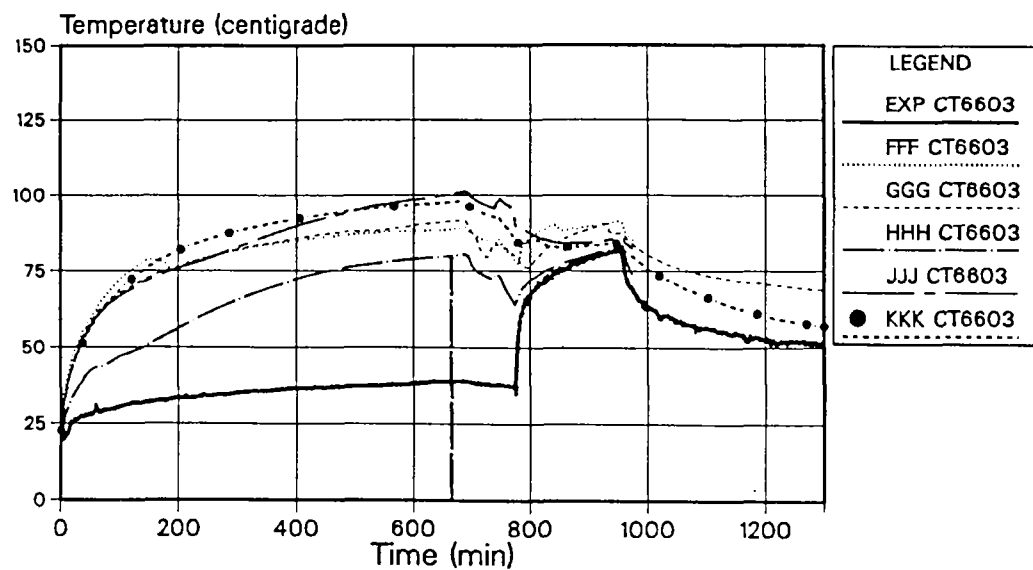
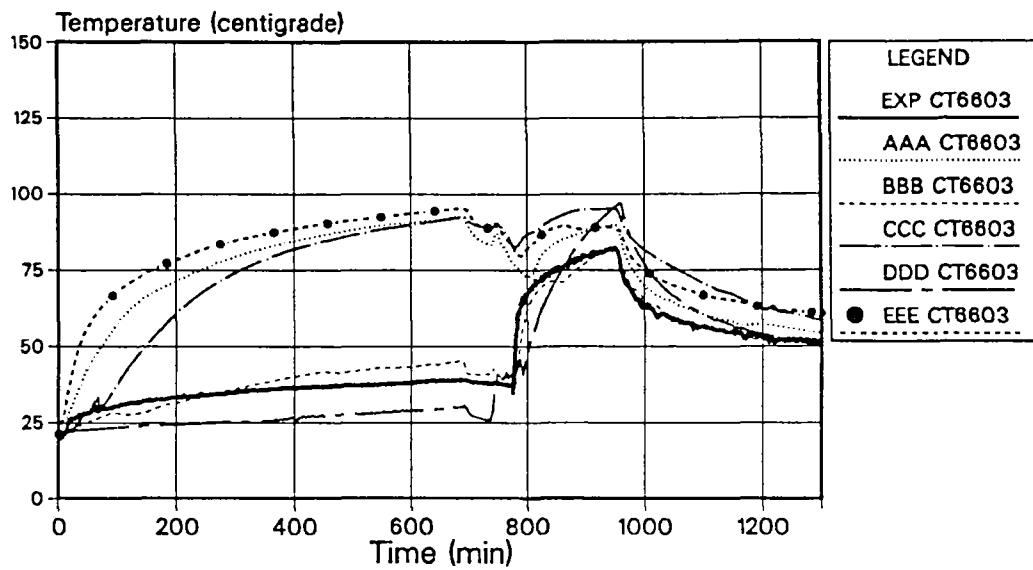


Fig. 6.3

Containment Temperatures 12 m Elevation (80 degree)

## OECD Standard Problem ISP-29

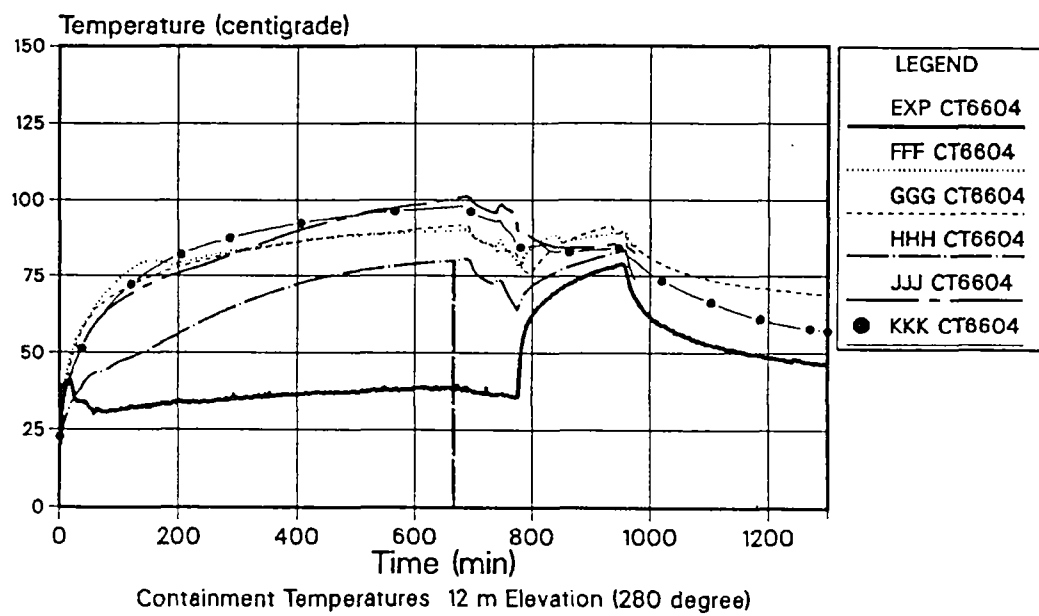
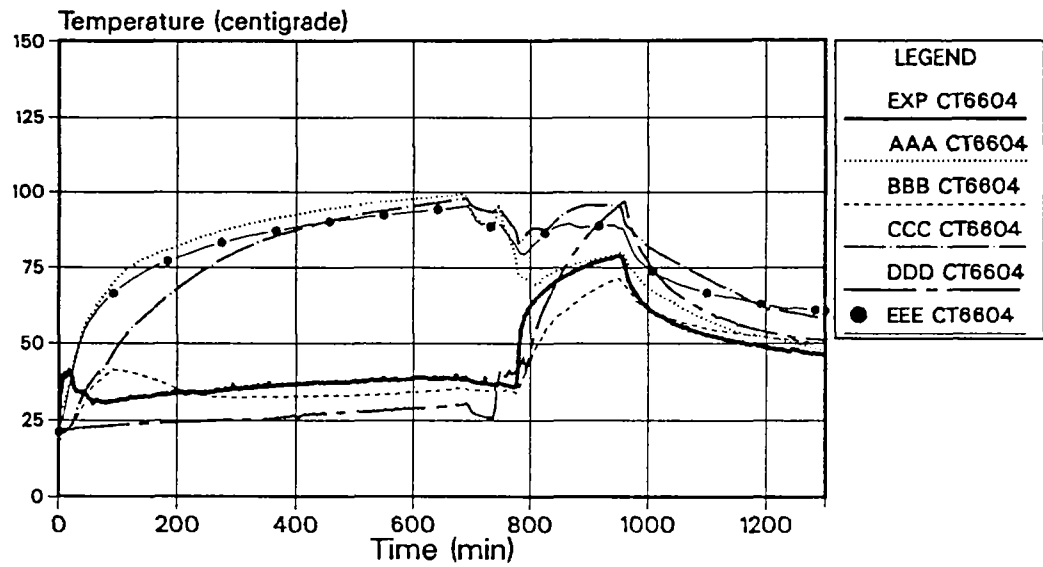


Fig. 6.4

Containment Temperatures 12 m Elevation (280 degree)

## OECD Standard Problem ISP-29

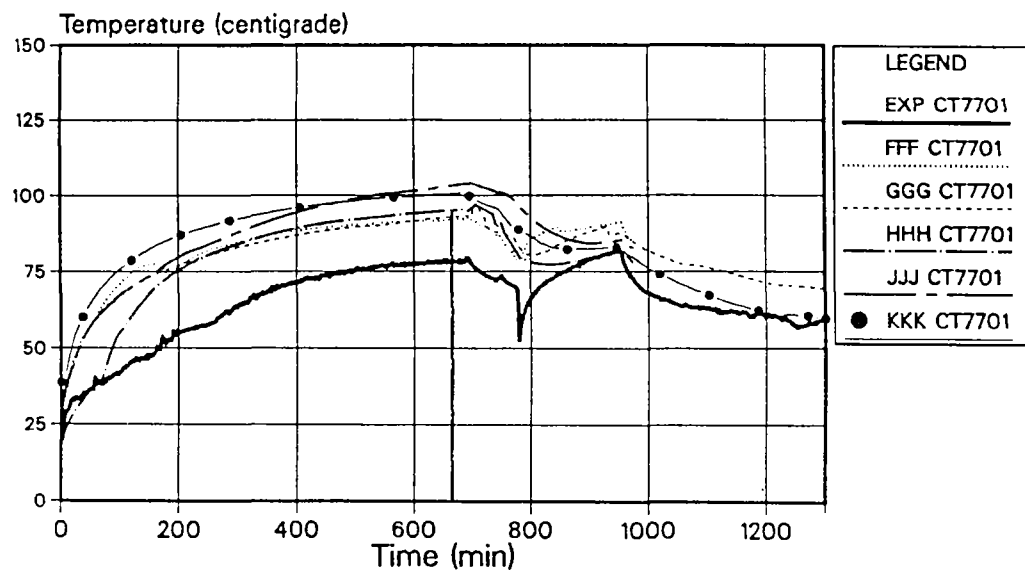
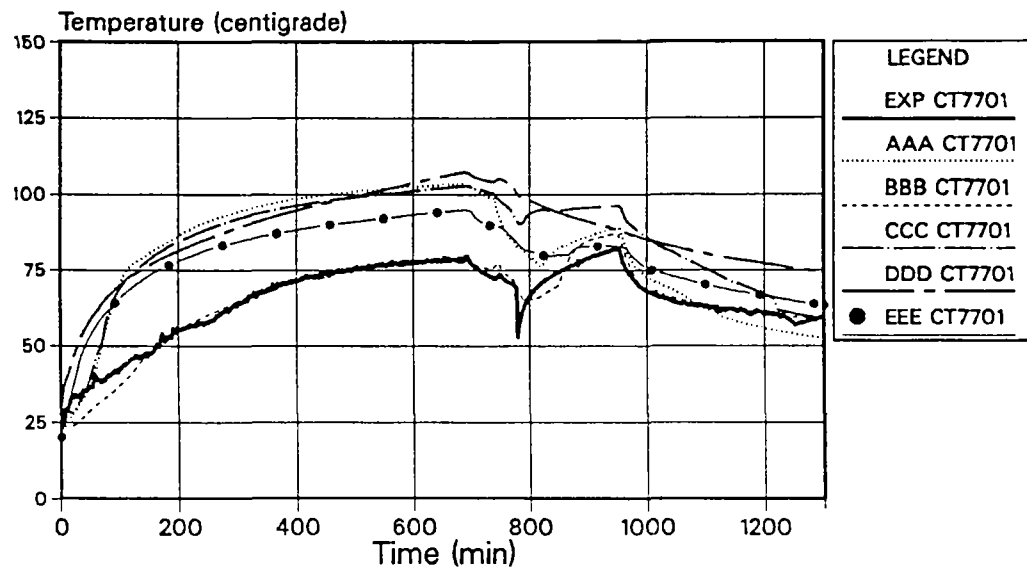


Fig. 6.5

Containment Temperatures 16.50 m Elevation (80 degree)

## OECD Standard Problem ISP-29

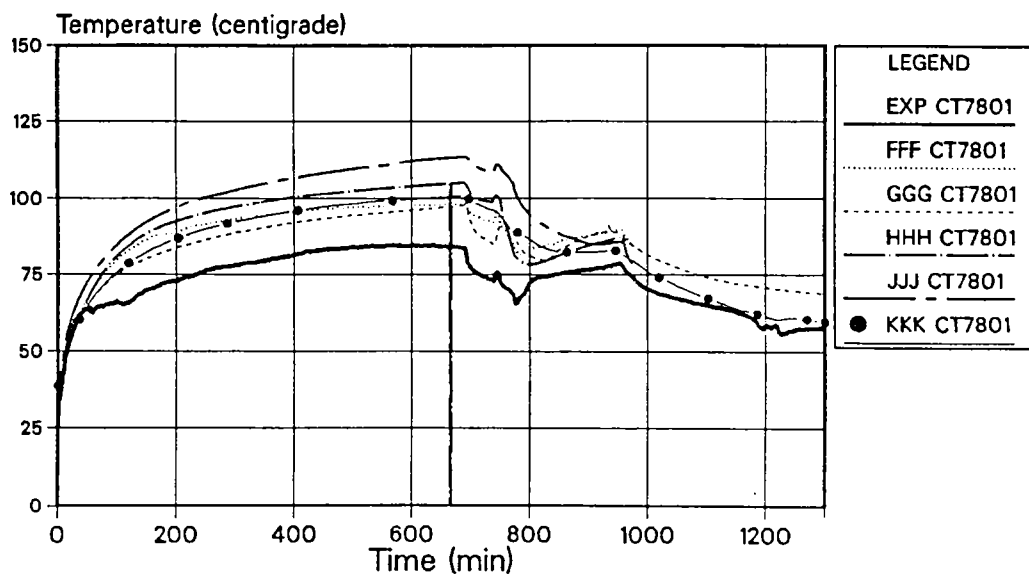
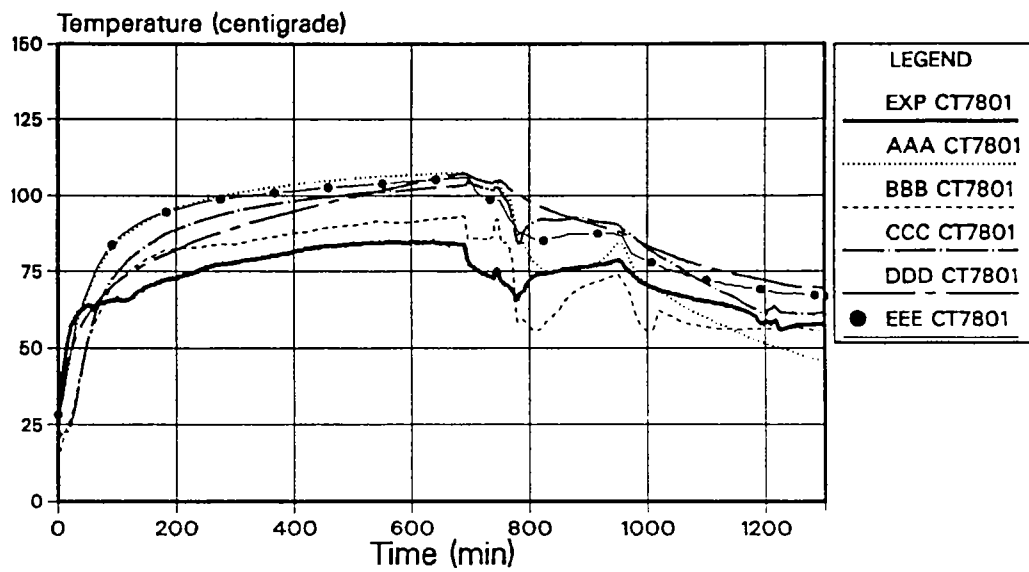


Fig. 6.6

Containment Temperatures 16.50 m Elevation (80 degree)

## OECD Standard Problem ISP-29

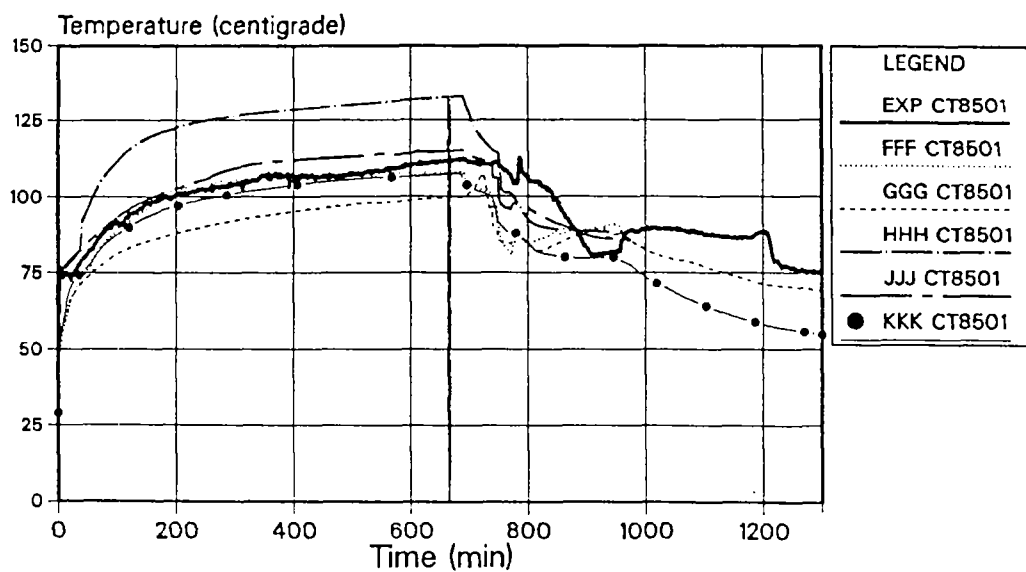
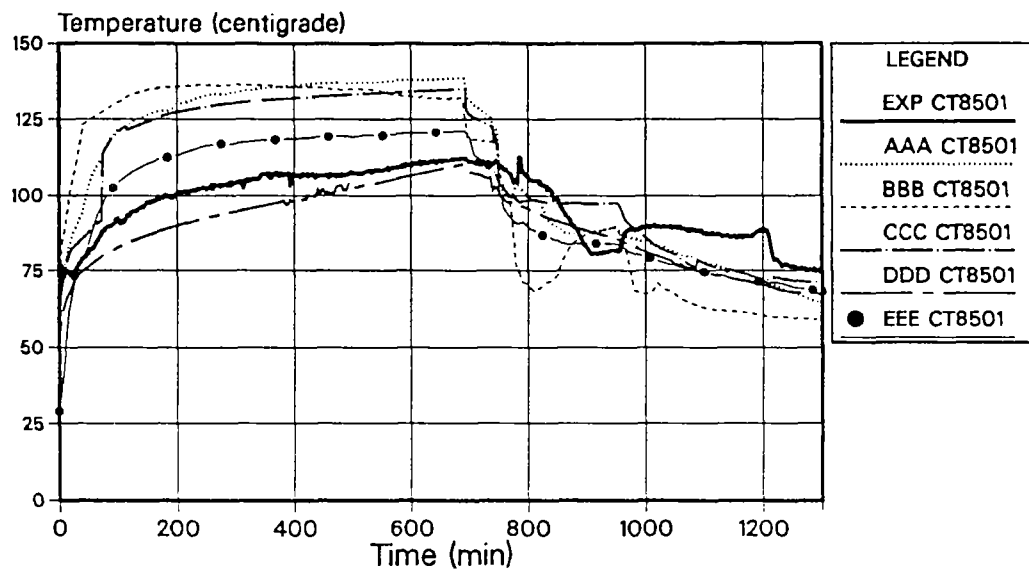


Fig. 6.7

Containment Temperatures 22.10 m Elevation (80 degree)

## OECD Standard Problem ISP-29

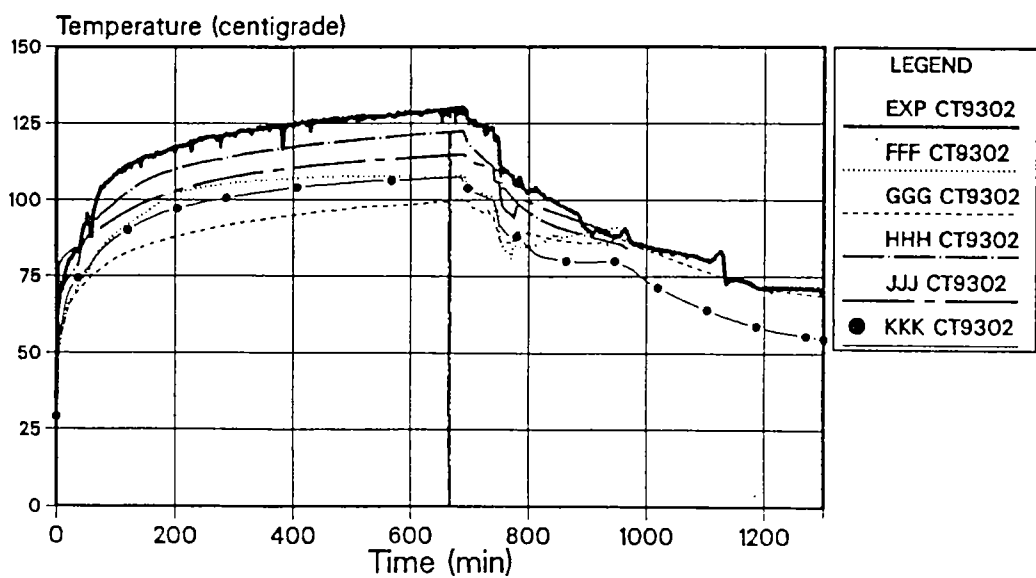
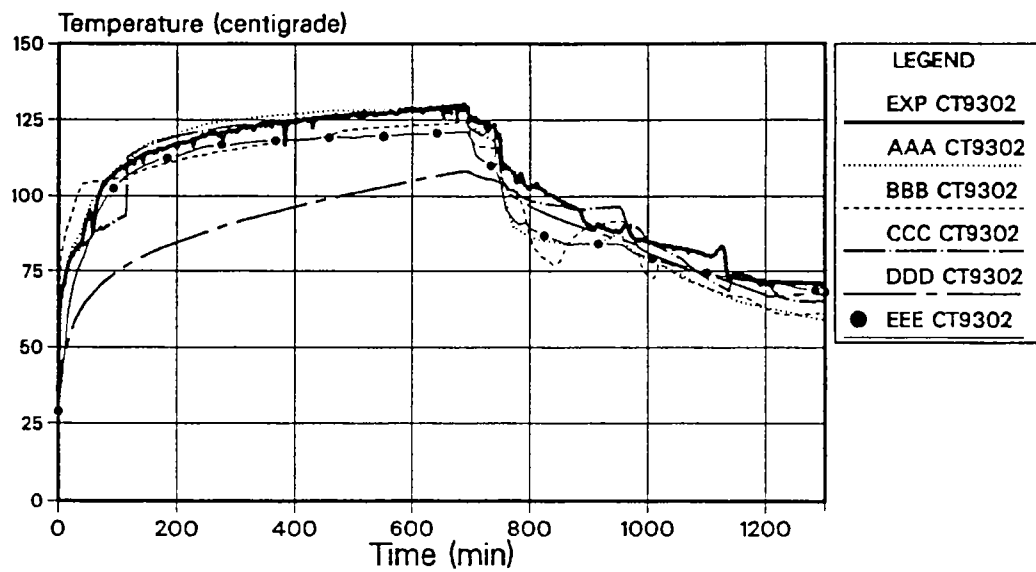


Fig. 6.8

Containment Temperatures 28.50 m Elevation (80 degree)



## OECD Standard Problem ISP-29

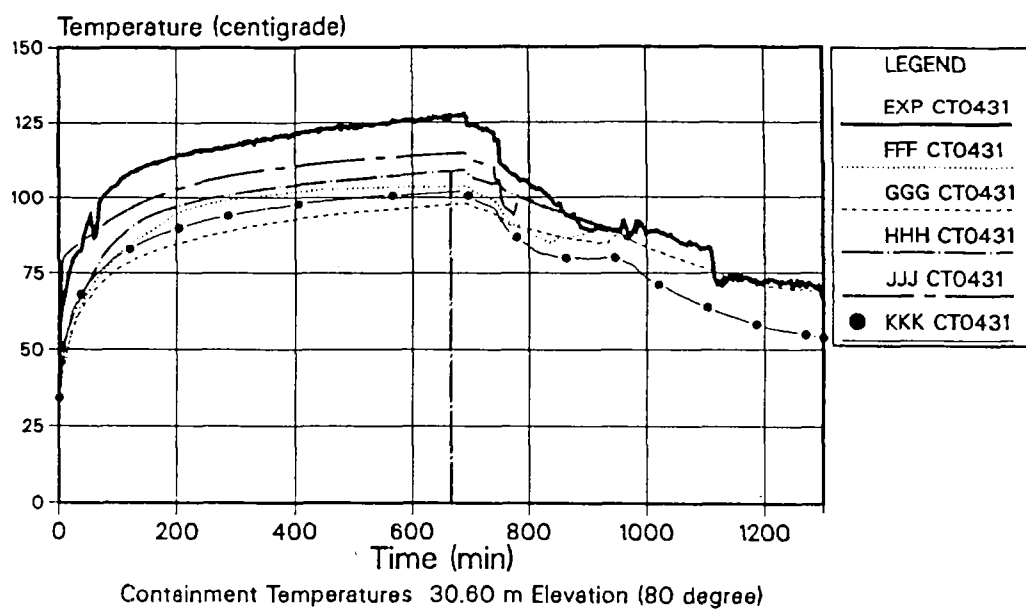
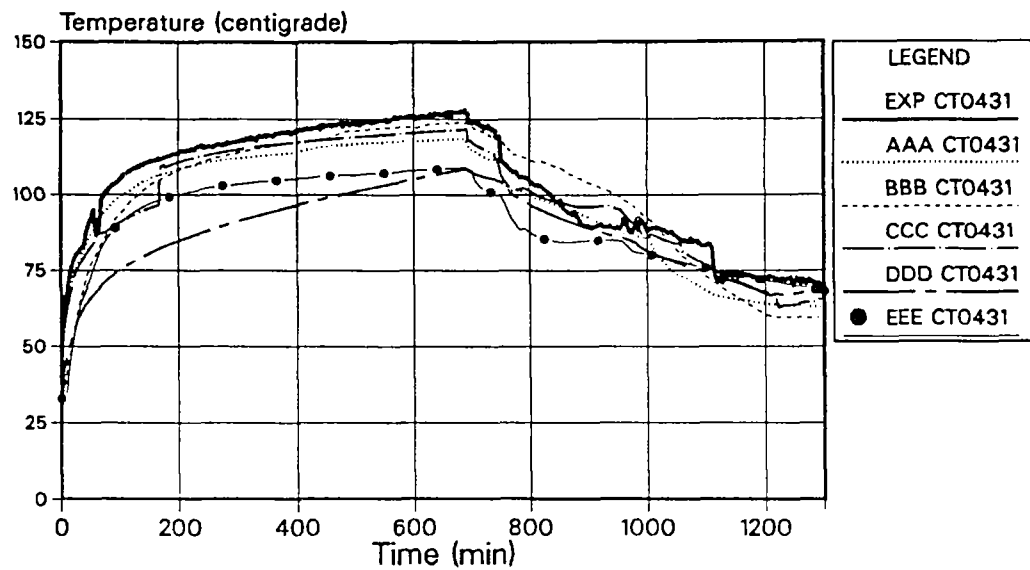
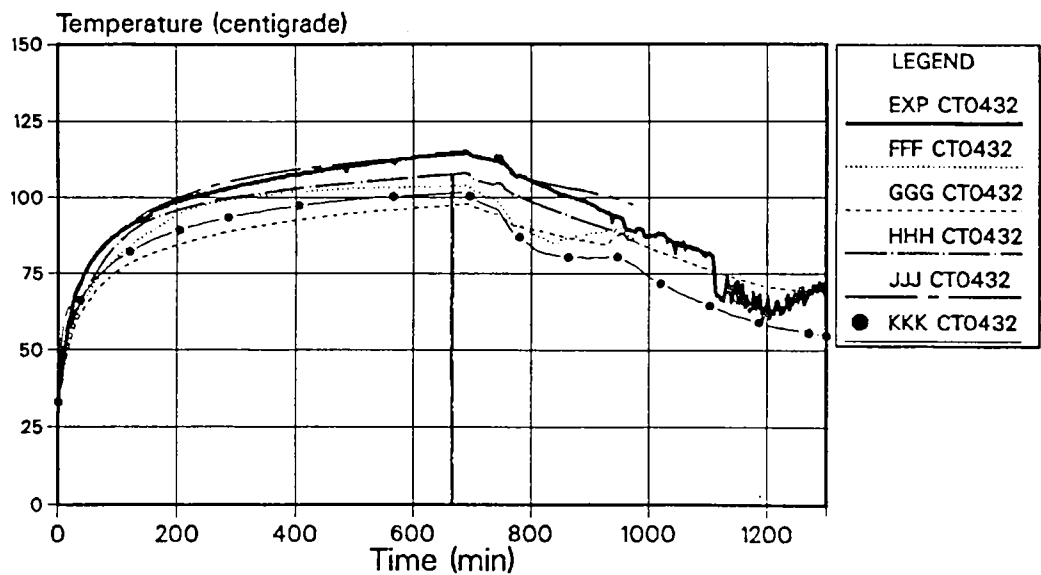
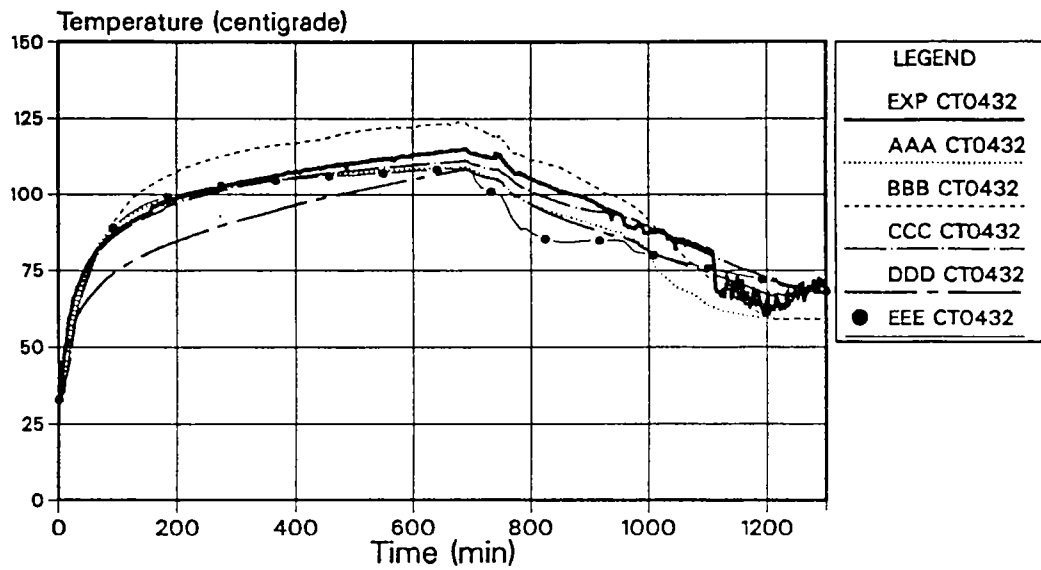


Fig. 6.9

Containment Temperatures 30.60 m Elevation (80 degree)

## OECD Standard Problem ISP-29



Containment Temperatures 31 m Elevation (280 degree)

Fig. 6.10

## OECD Standard Problem ISP-29

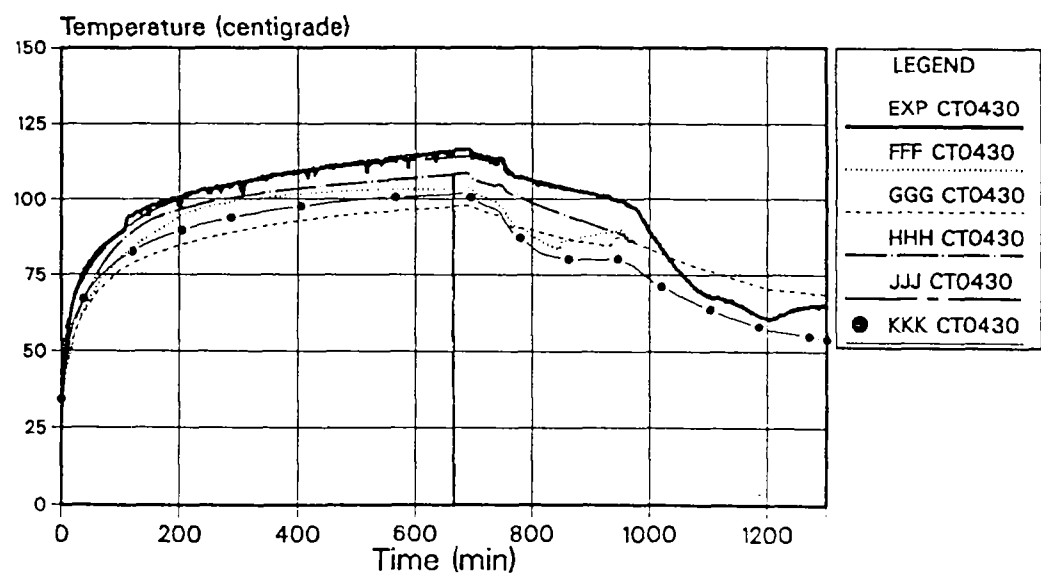
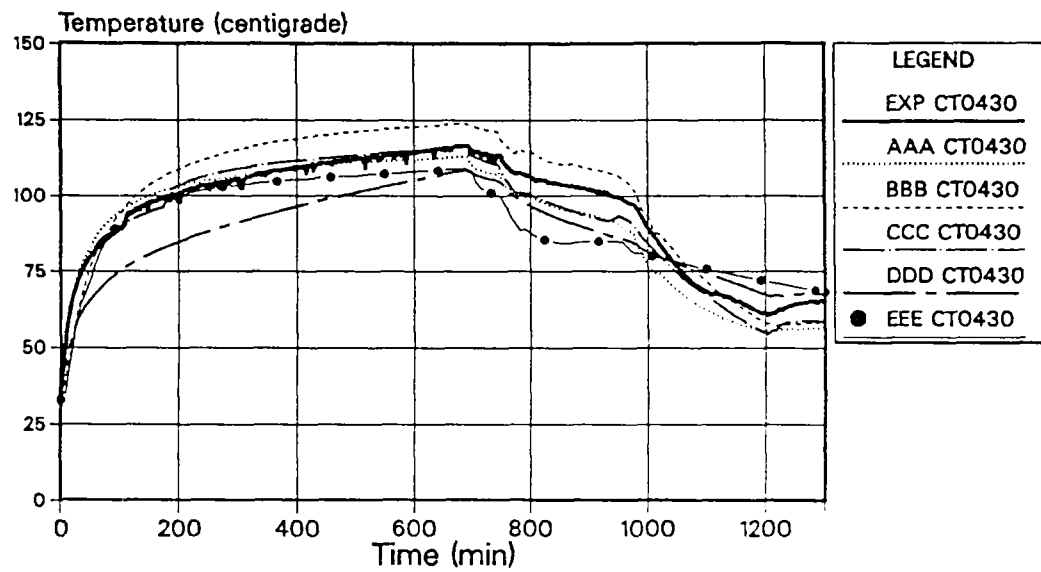


Fig. 6.11

Containment Temperatures 48 m Elevation (315 degree)

## OECD Standard Problem ISP-29

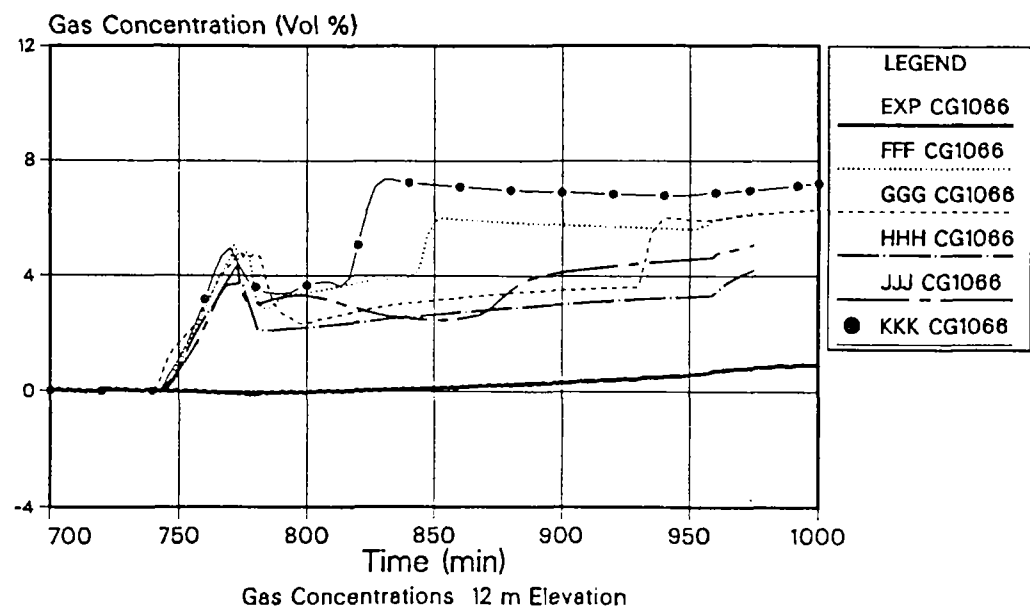
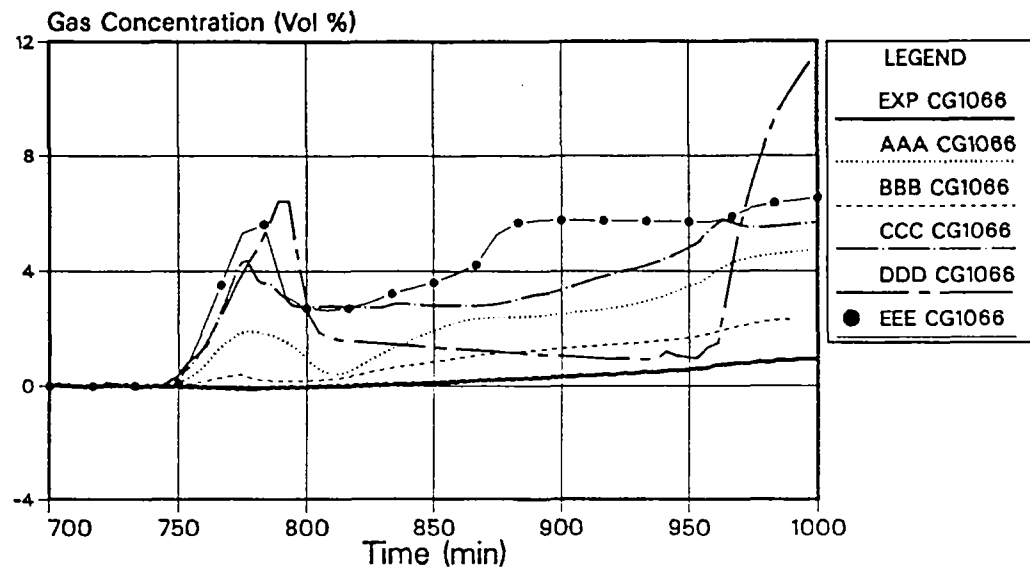


Fig. 6.12: Stair Case (80° Sector)

## OECD Standard Problem ISP-29

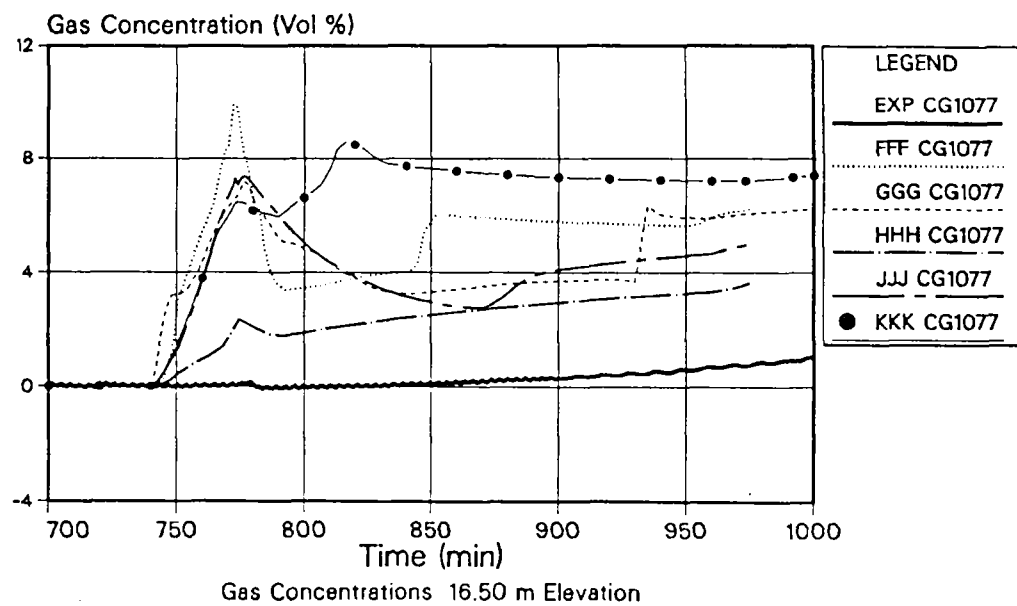
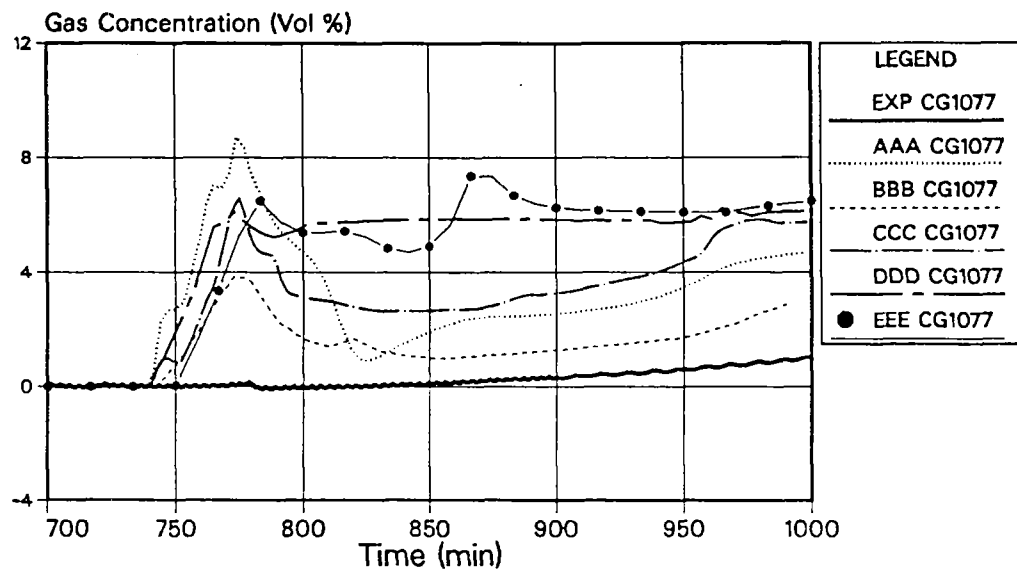


Fig. 6.13 Stair Case (80° Sector)

## OECD Standard Problem ISP-29

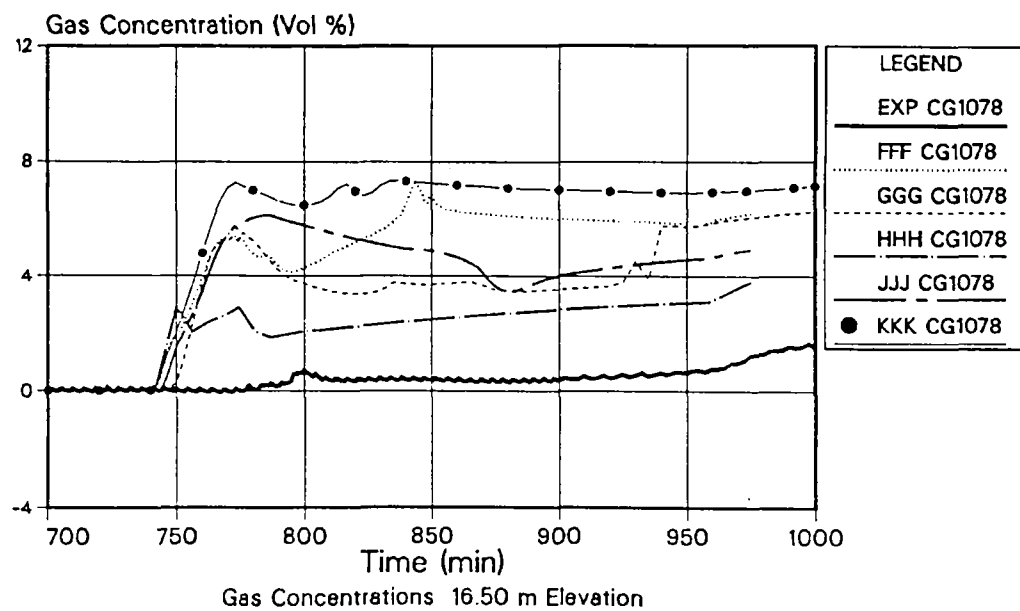
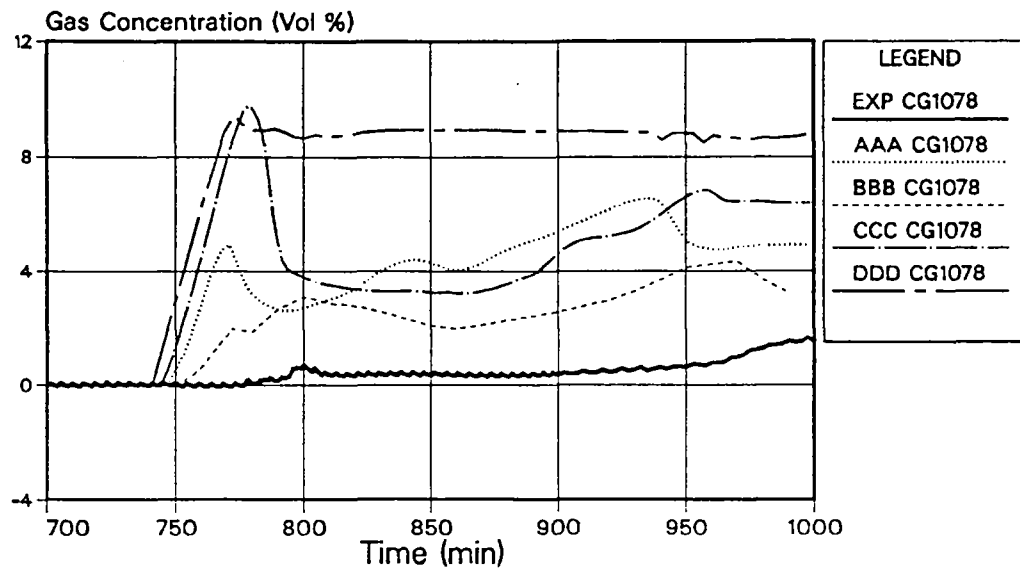


Fig. 6.14: Spiral Stair (280° Sector)

## OECD Standard Problem ISP-29

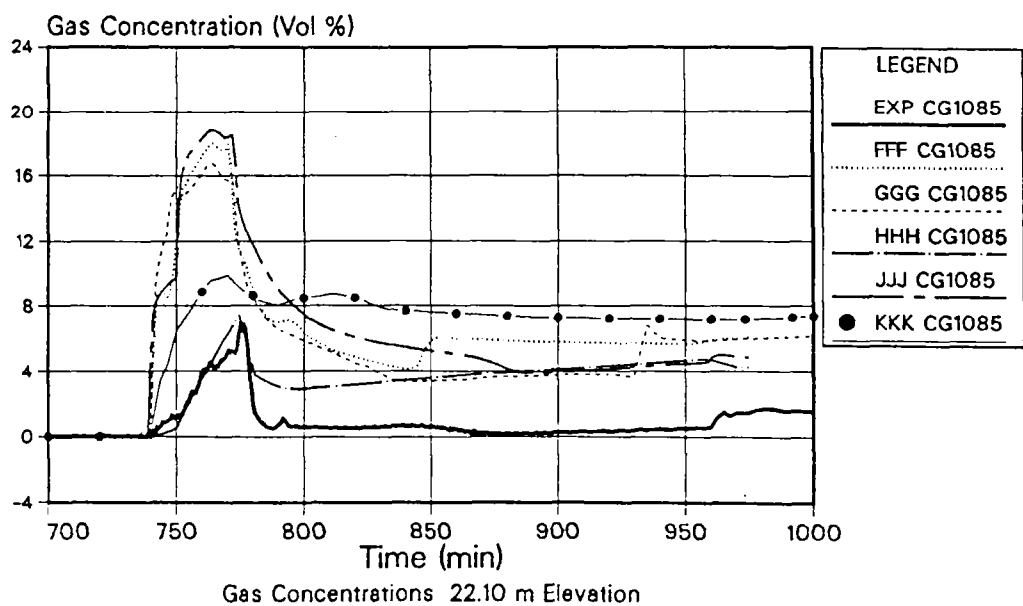
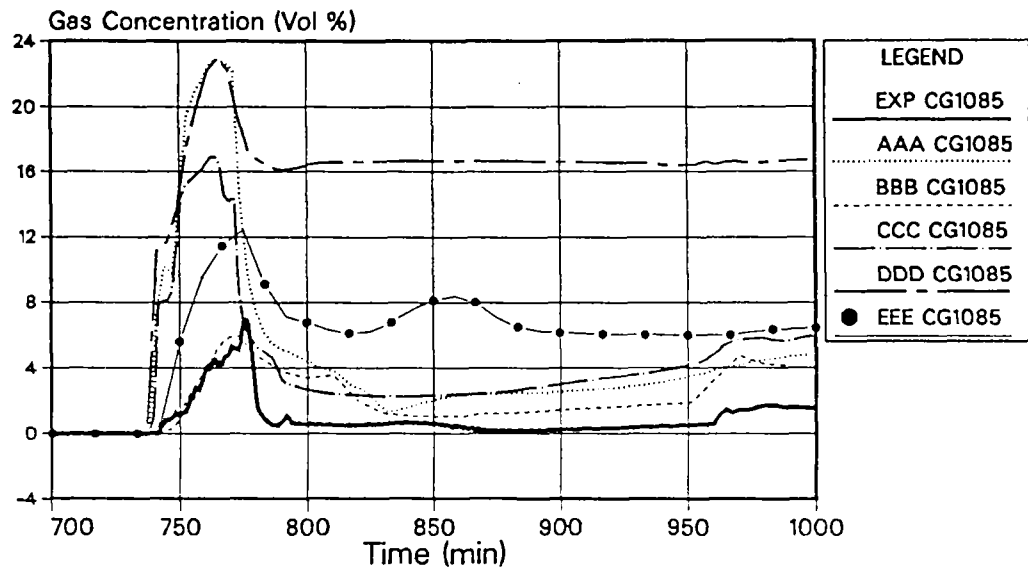


Fig. 6.15: Stair Case (80° Sector)

## OECD Standard Problem ISP-29

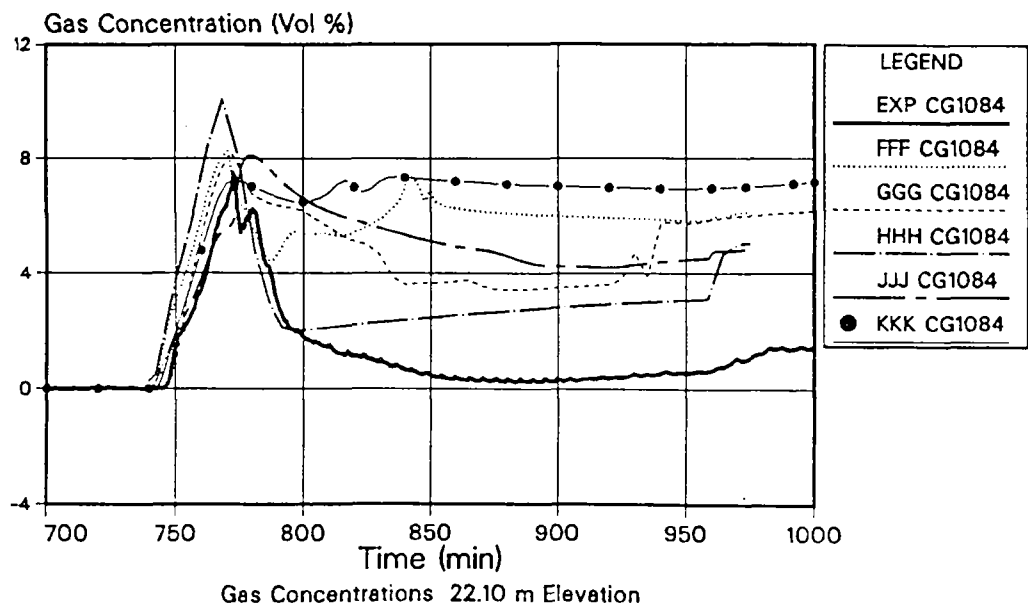
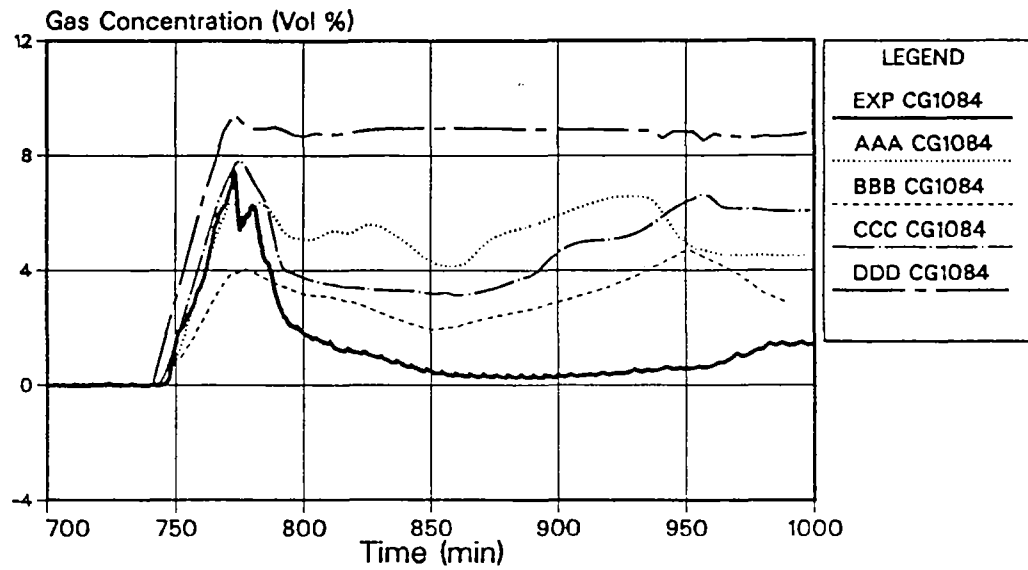


Fig. 6.16: Spiral Stair (280° Sector)



## OECD Standard Problem ISP-29

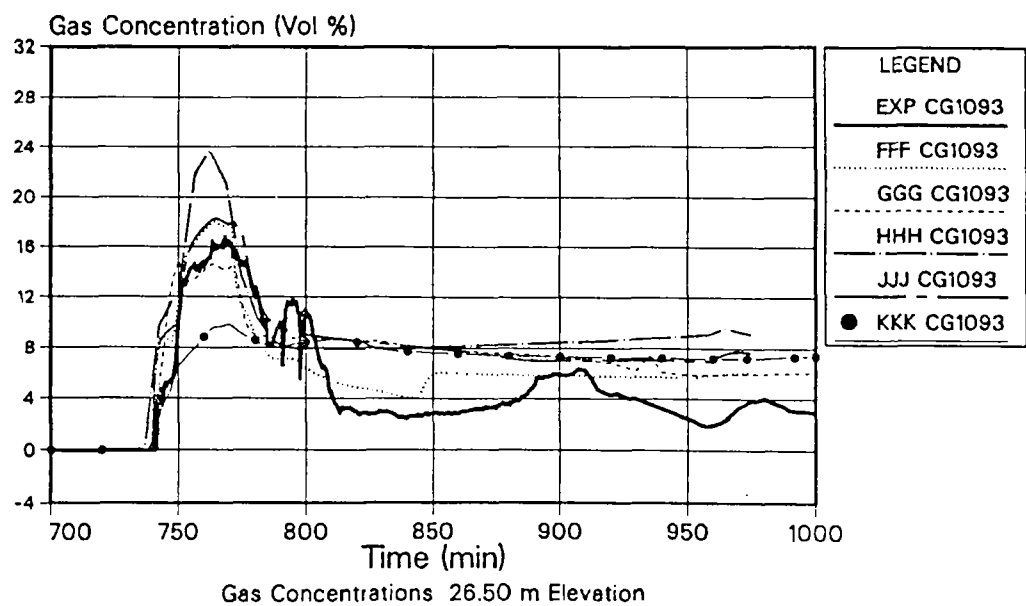
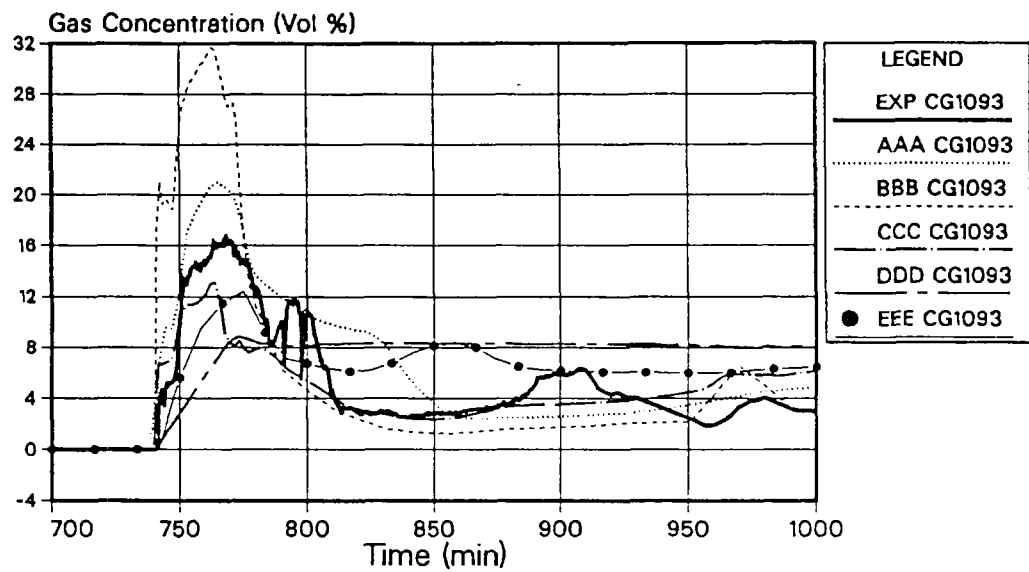


Fig. 6.17: Stair Case (80° Sector)

## OECD Standard Problem ISP-29

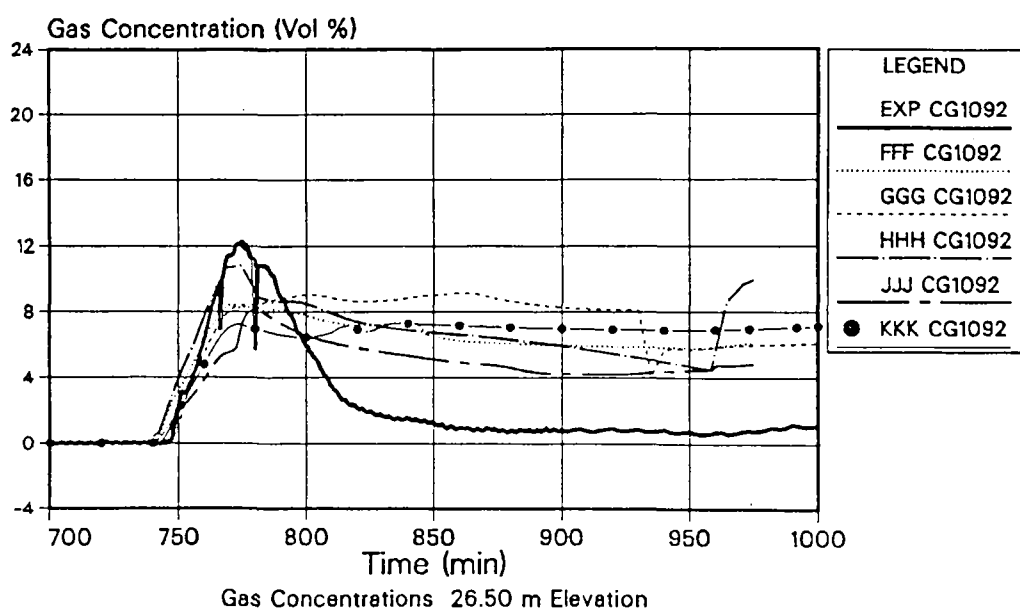
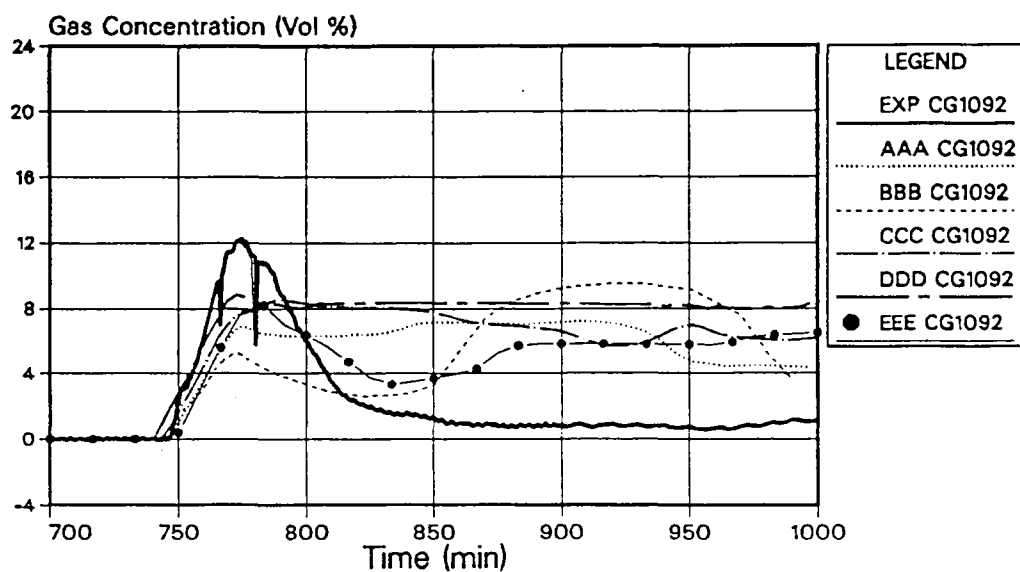


Fig. 6.18: Spiral Stair (280° Sector)

## OECD Standard Problem ISP-29

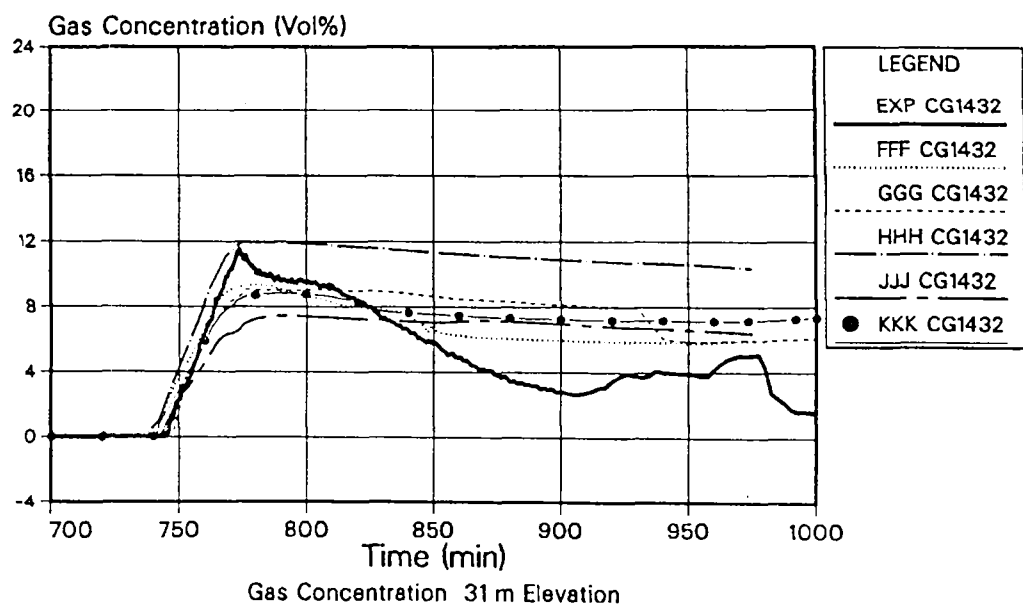
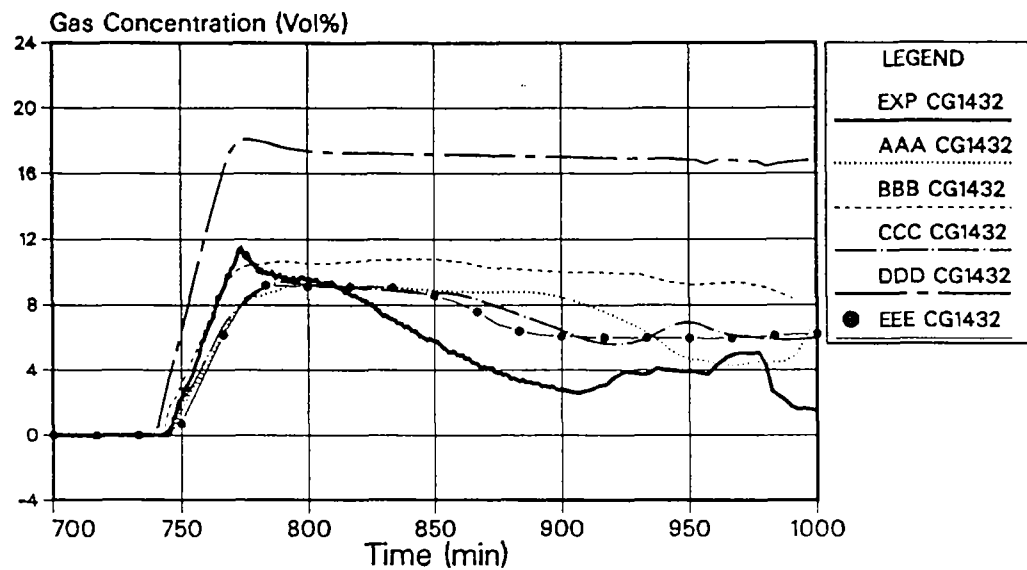


Fig. 6.19: Spiral Stair (280° Sector)

## OECD Standard Problem ISP-29

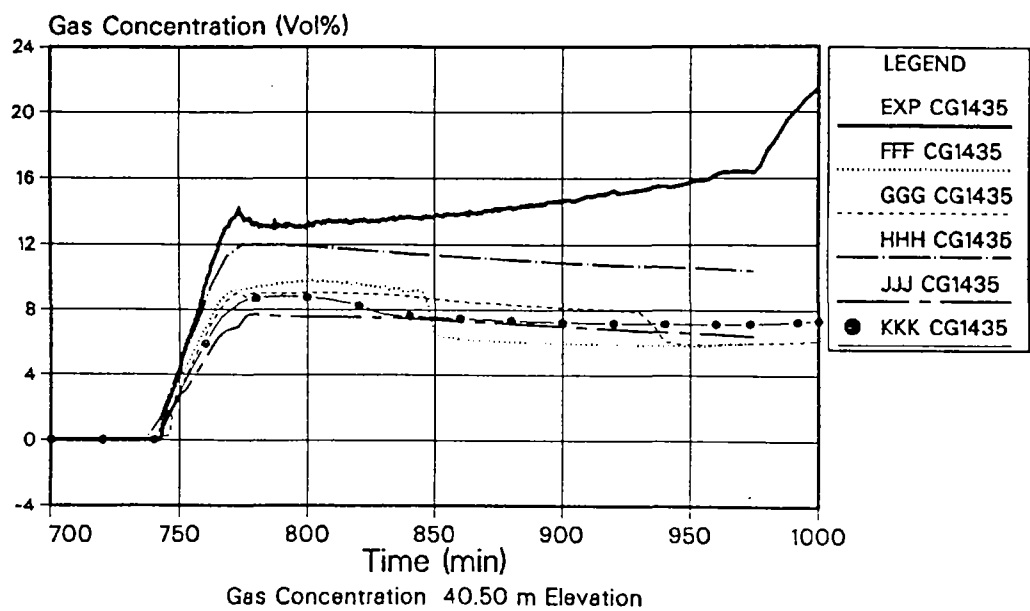
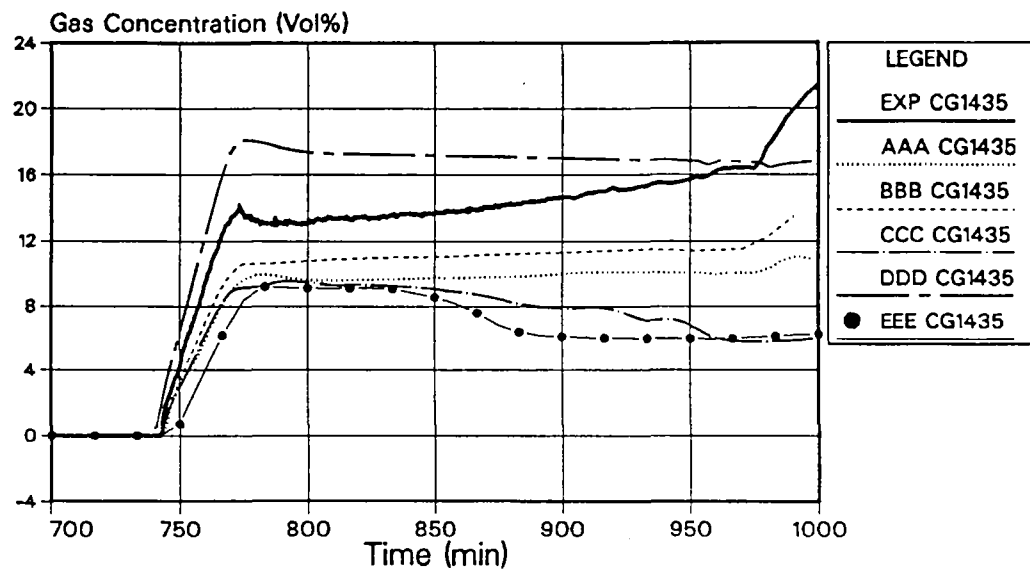


Fig. 6.20: Spiral Stair (280° Sector)

## OECD Standard Problem ISP-29

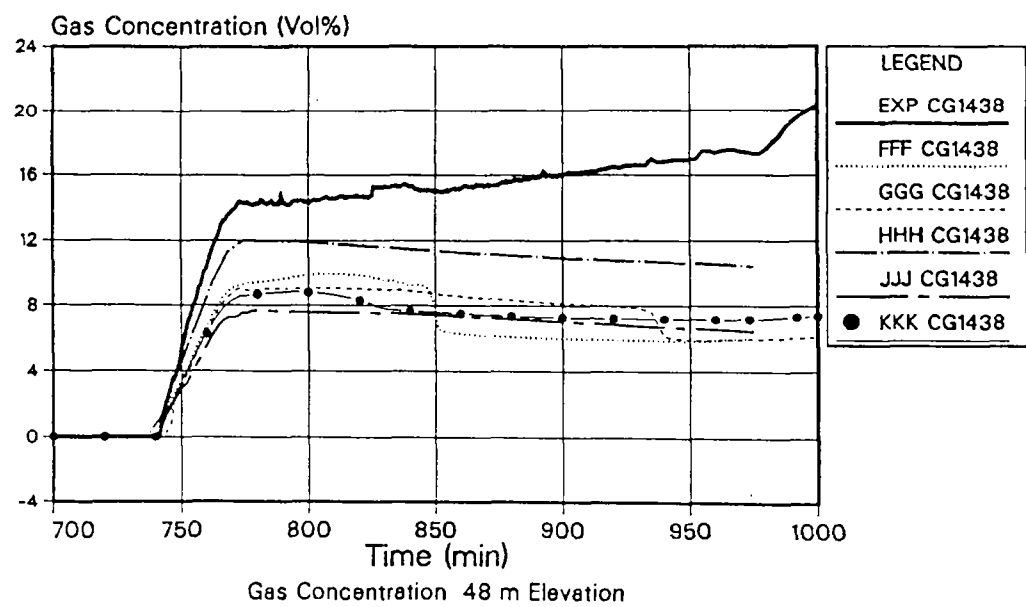
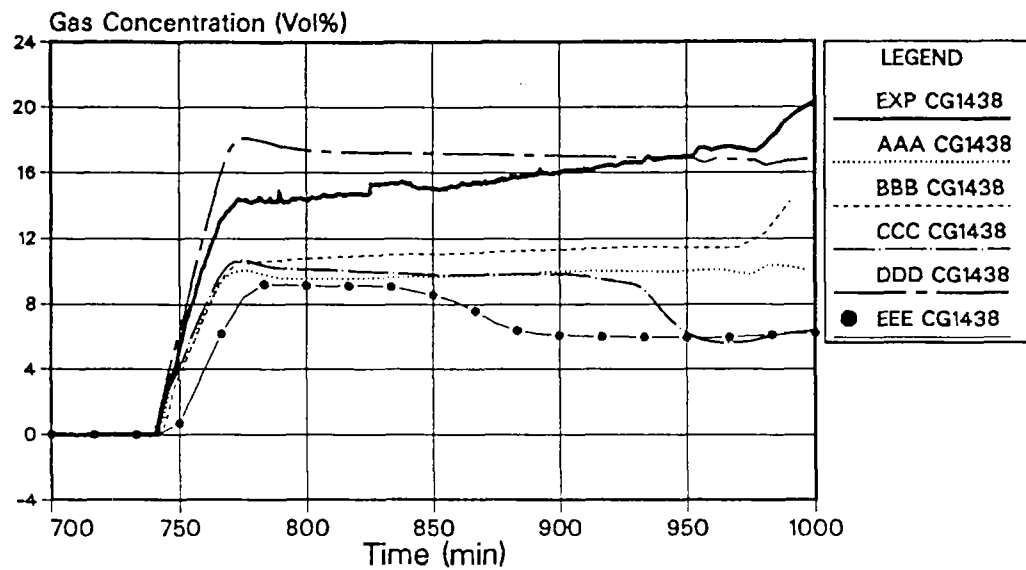


Fig. 6.21: Stair Case (80° Sector)

## OECD Standard Problem ISP-29

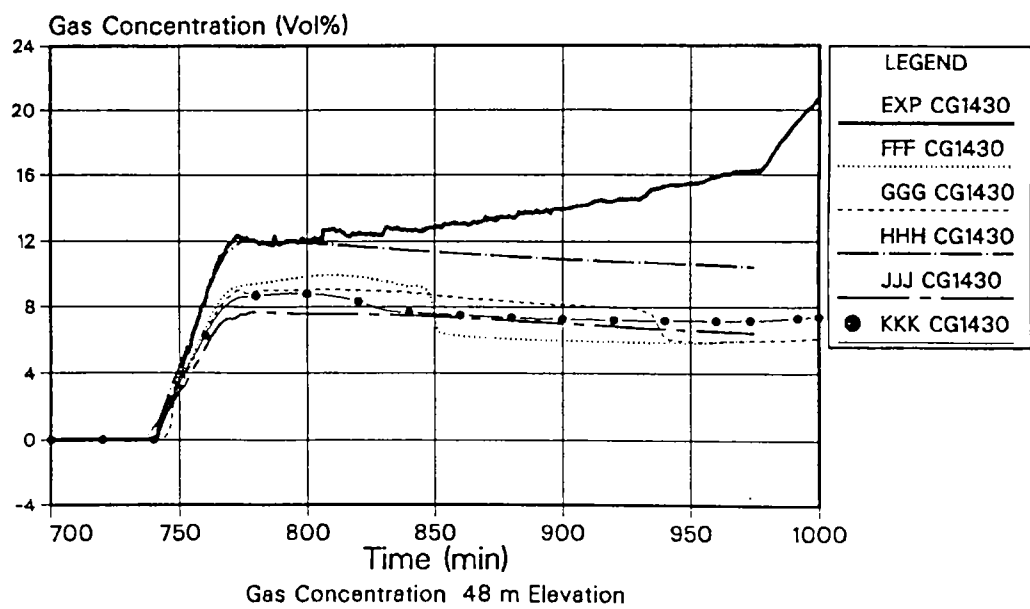
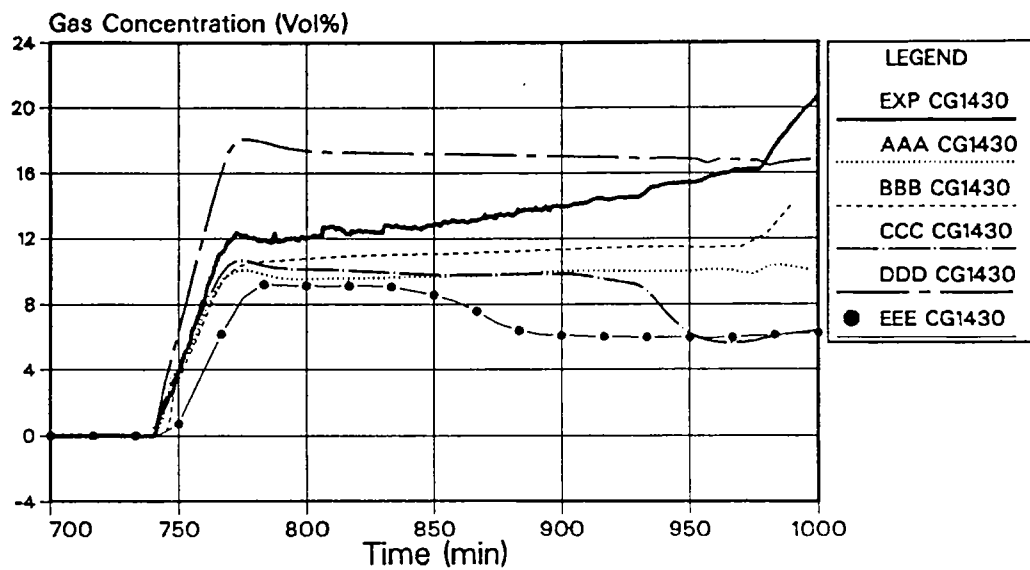


Fig. 6.22: Spiral Stair (280° Sector)

# OECD Standard Problem ISP-29 - Experimental Data

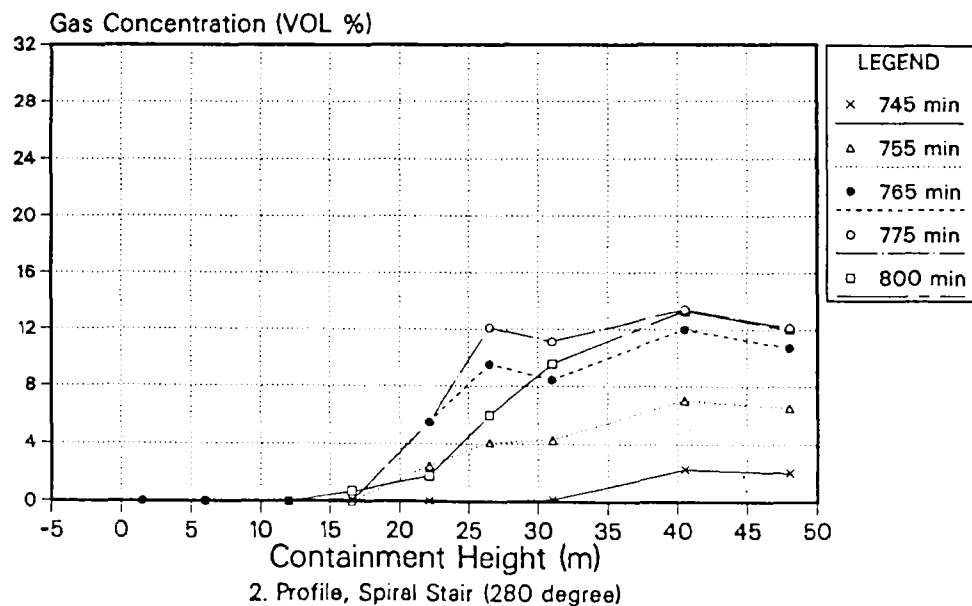
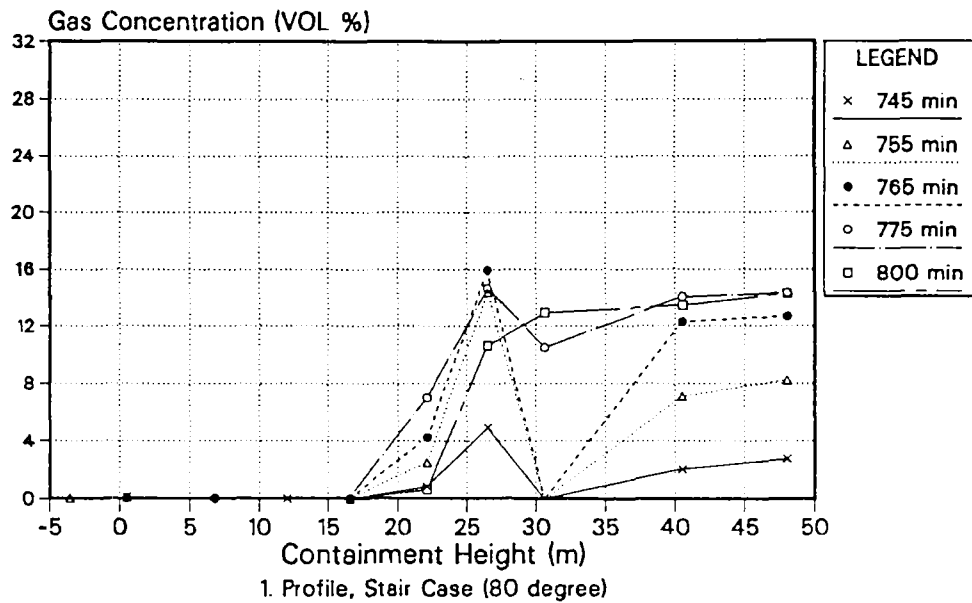


Fig. 6.23 Measured Gas Concentration Profiles at Various Points in Time

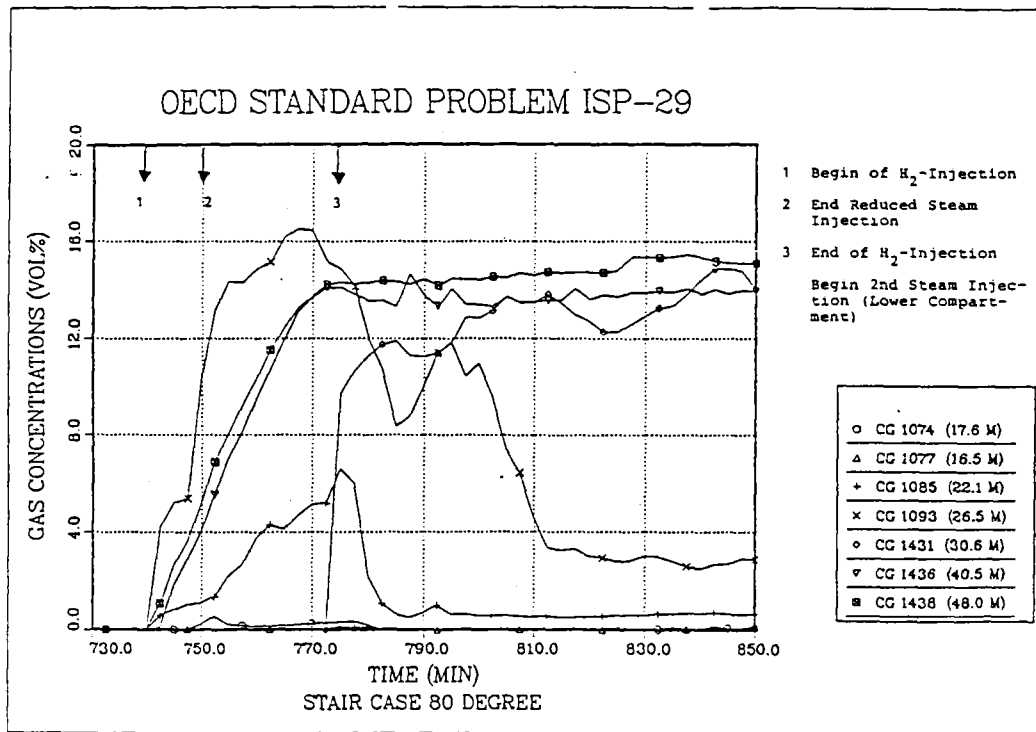


Fig. 6.24 Measured Local Gas Concentration Transients  
(Stair Case - 80° Sector)

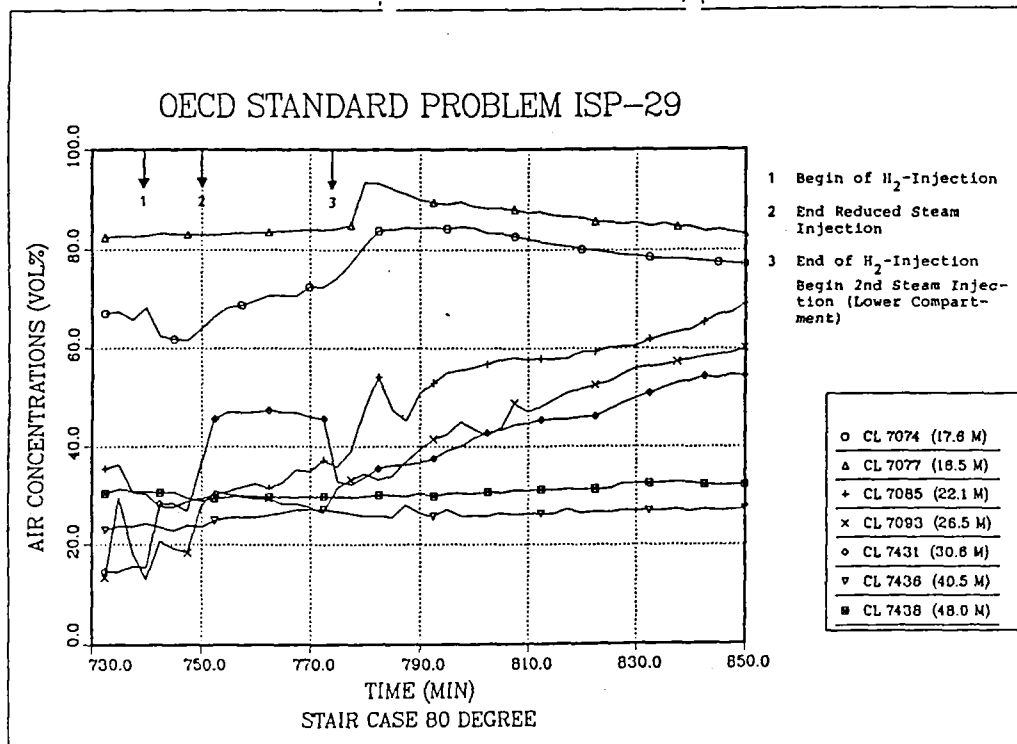


Fig. 6.25: Measured Local Air Concentration Transients  
(Stair Case - 80° Sector)



## OECD Standard Problem ISP-29

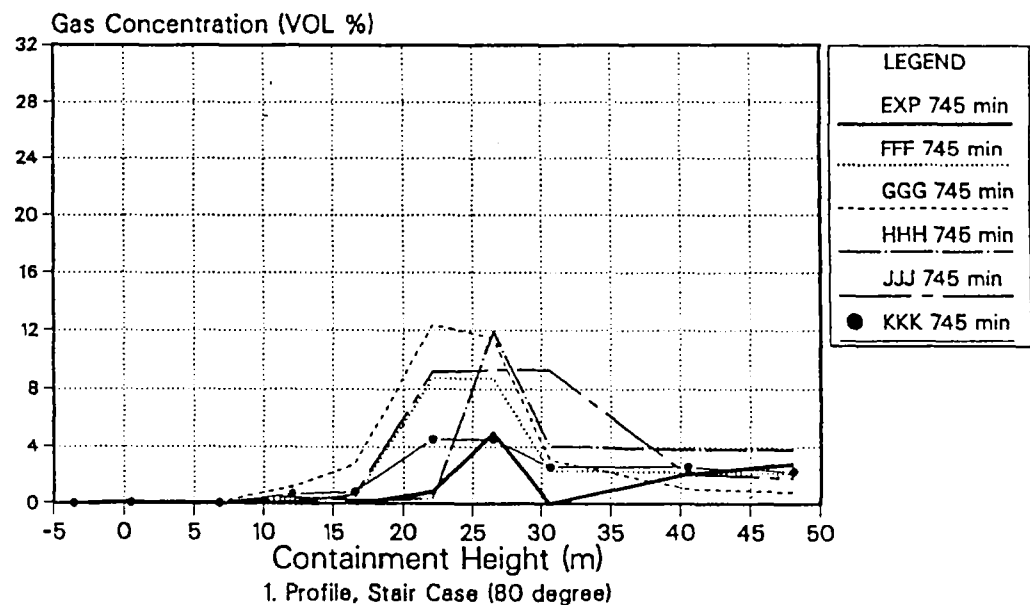
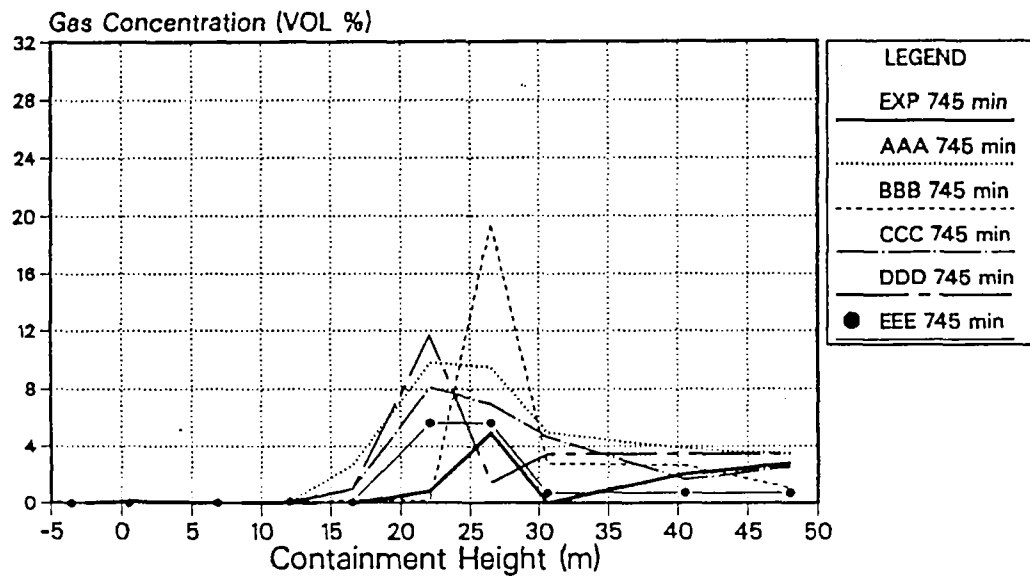


Fig. 6.26: Calculated Gas Concentration Profiles compared to the Measured Profile 5 min after starting gas release

## OECD Standard Problem ISP-29

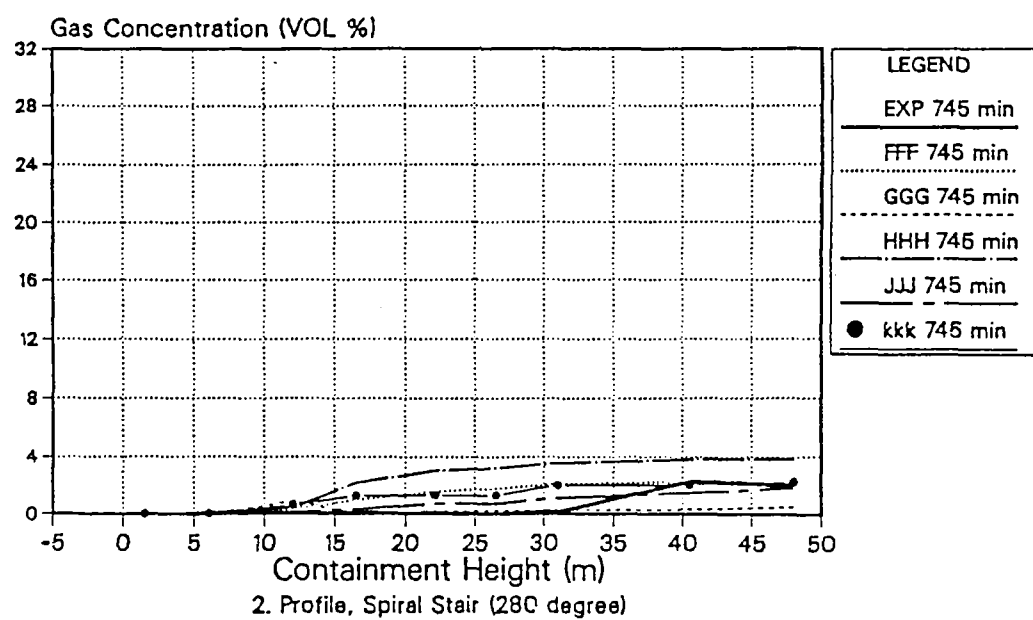
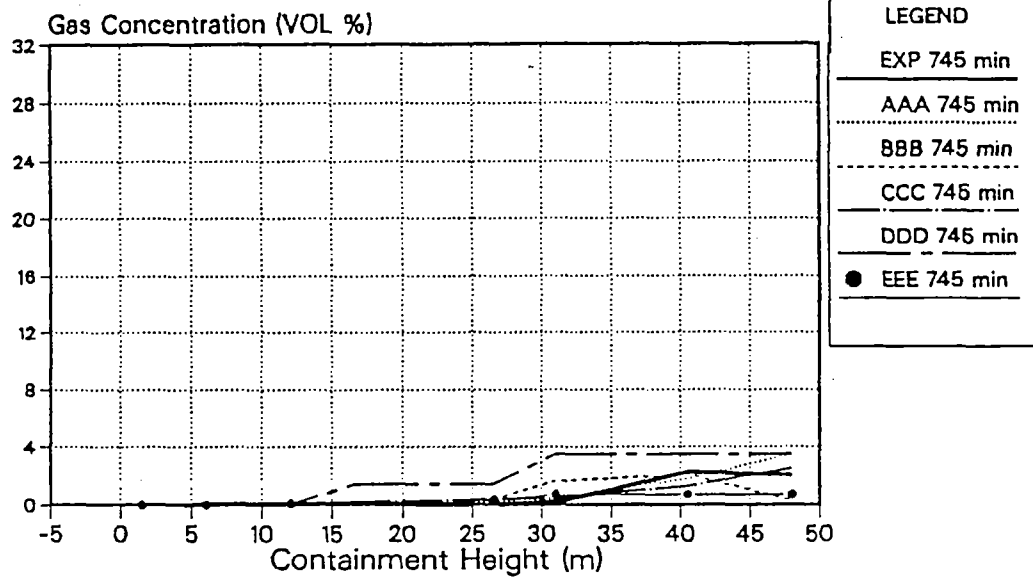


Fig. 6.27: Calculated Gas Concentration Profiles compared to the Measured Profile 5 min after starting gas release

## OECD Standard Problem ISP-29

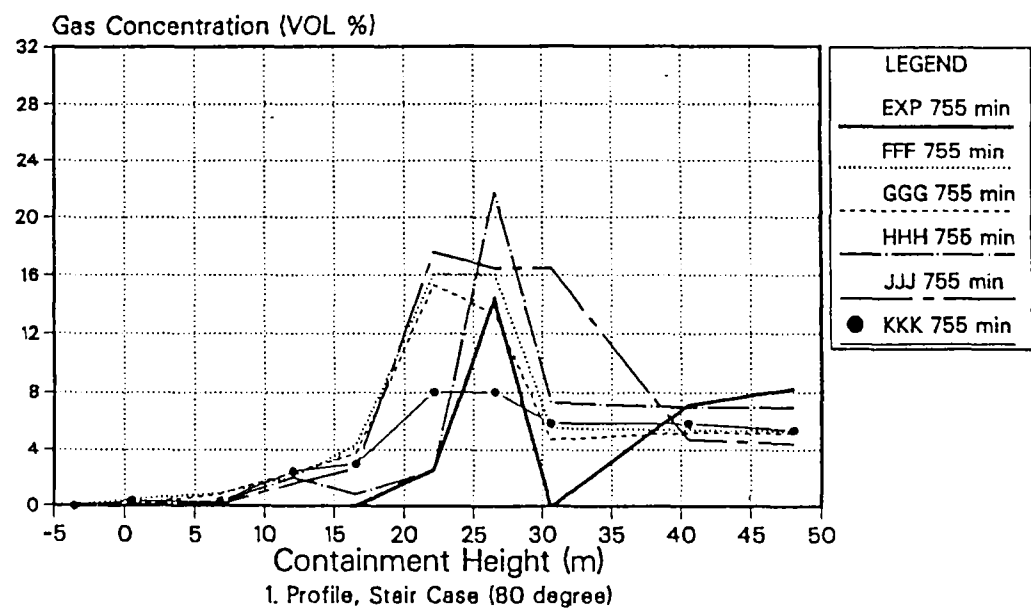
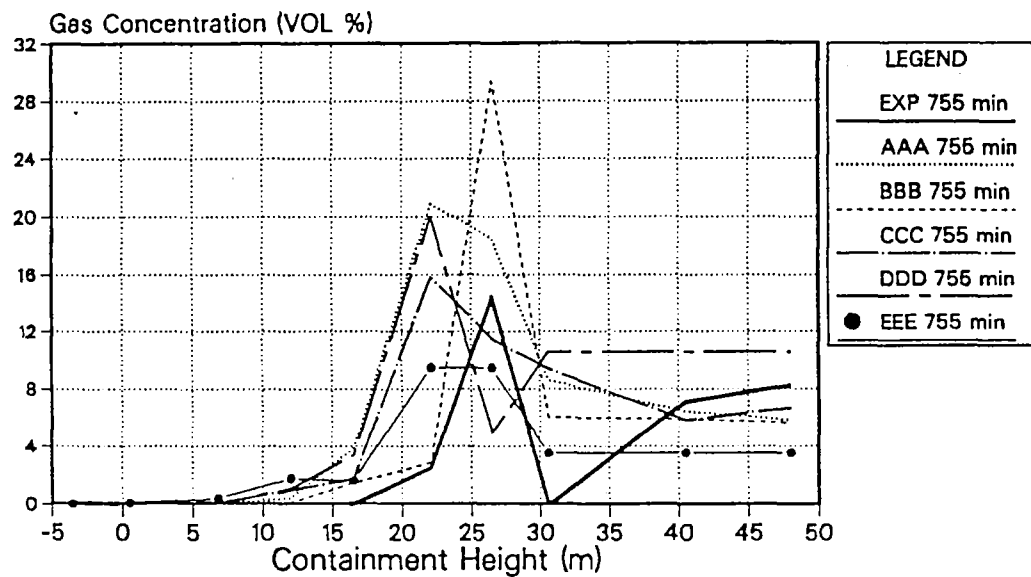


Fig. 6.28: Calculated Gas Concentration Profiles compared to the Measured Profile 15 min after starting gas release

## OECD Standard Problem ISP-29

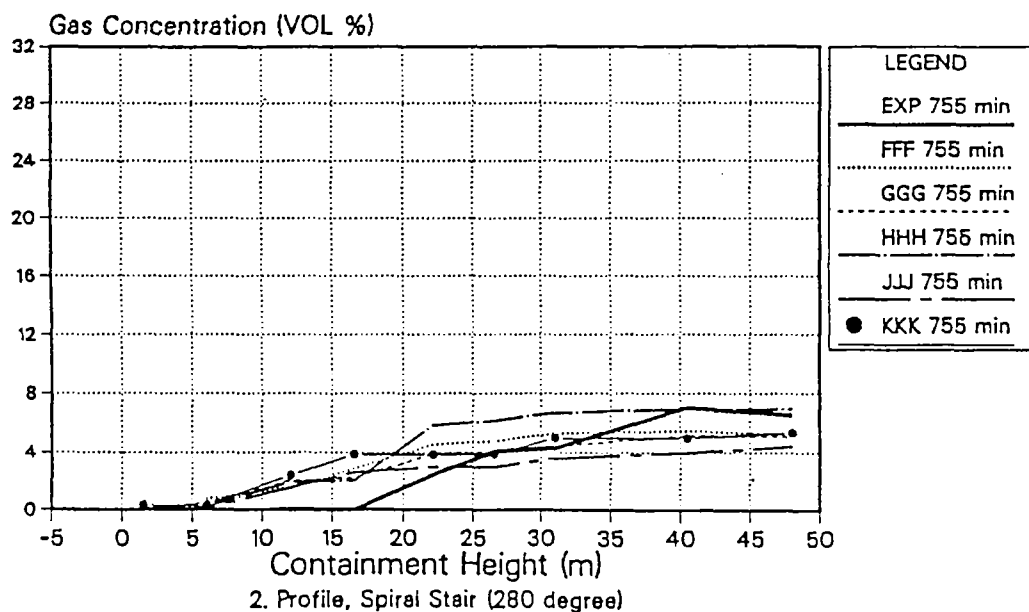
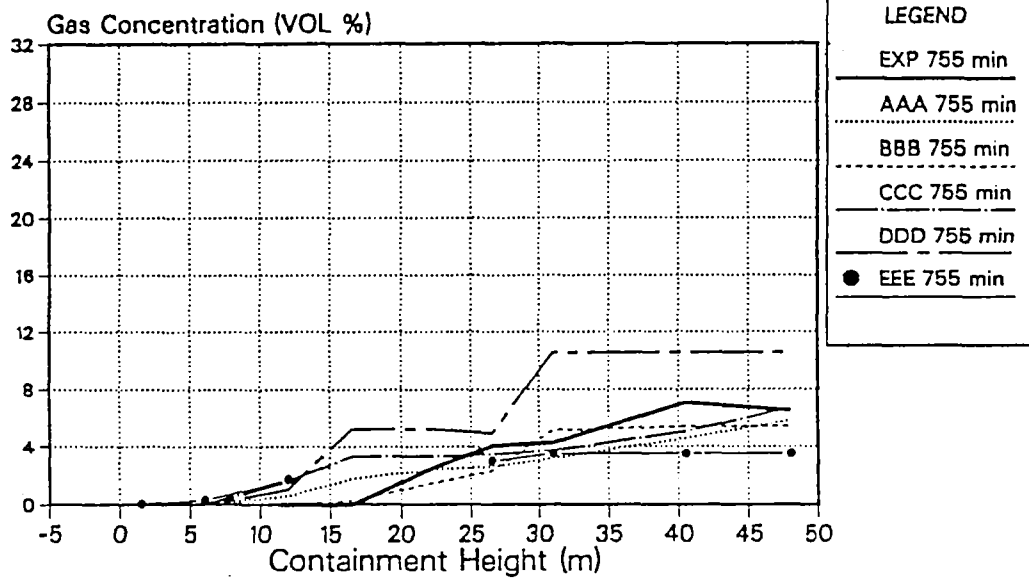


Fig. 6.29: Calculated Gas Concentration Profiles compared to the Measured Profile 15 min after starting gas release

## OECD Standard Problem ISP-29

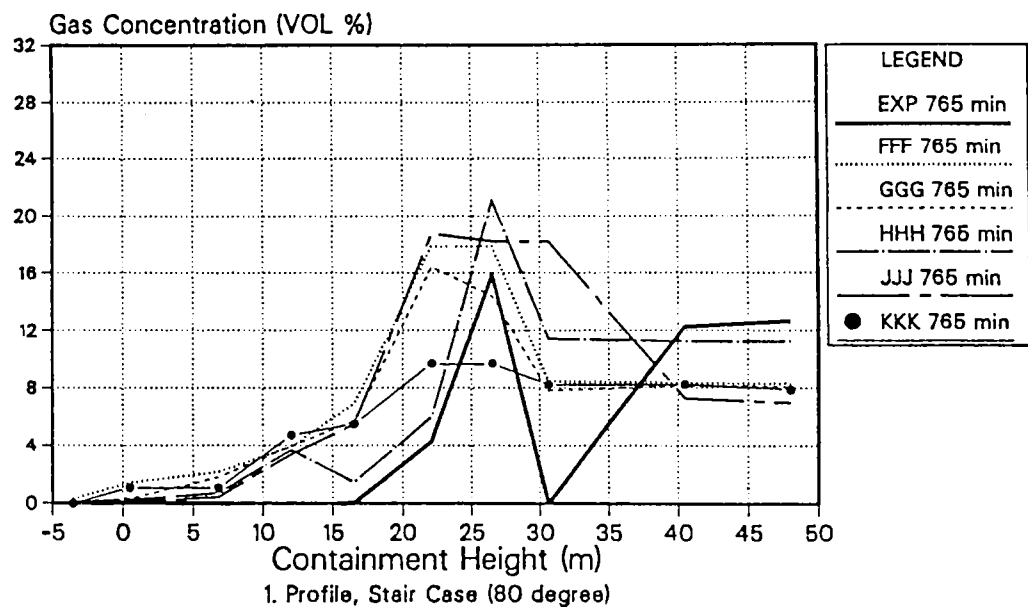
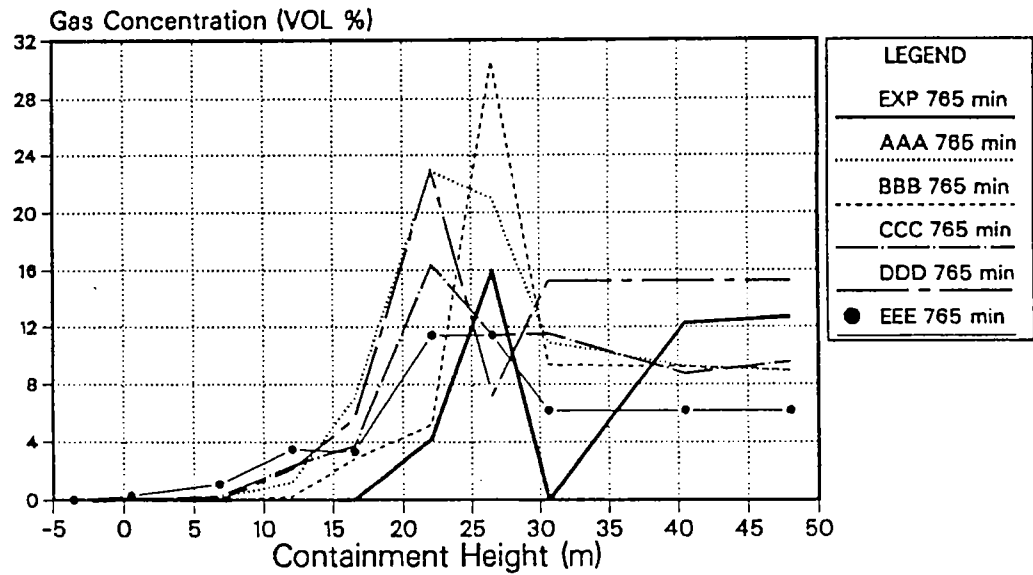


Fig. 6.30: Calculated Gas Concentration Profiles compared to the Measured Profile 25 min after starting gas release

# OECD Standard Problem ISP-29

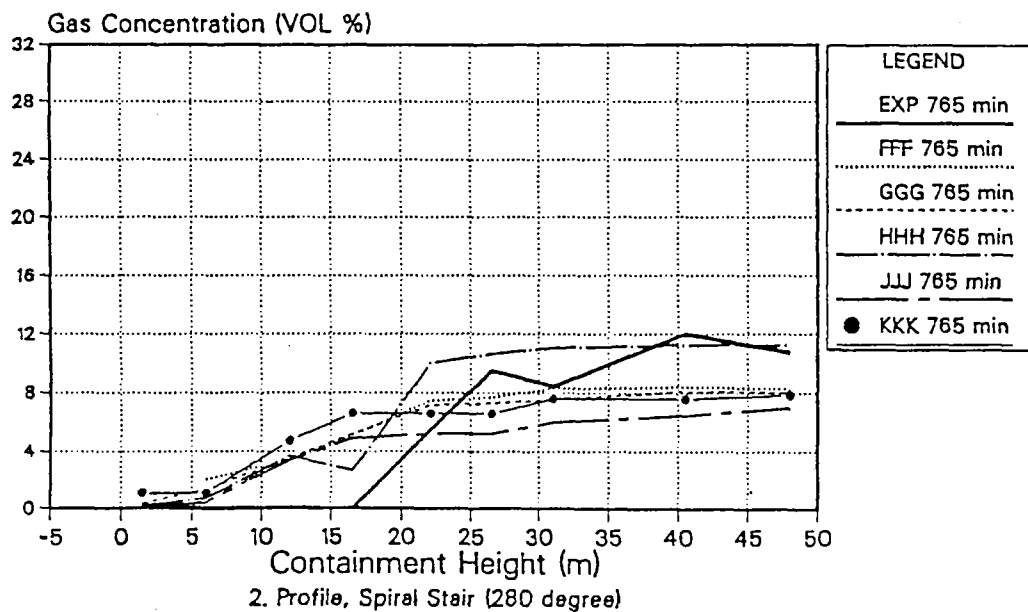
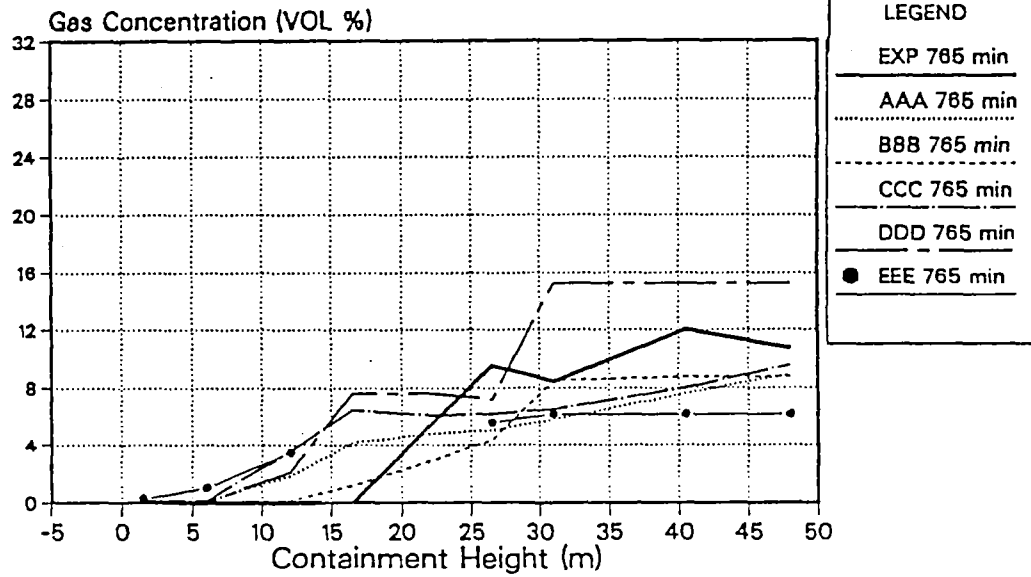


Fig. 6.31: Calculated Gas Concentration Profiles compared to the Measured Profile 25 min after starting gas release

## OECD Standard Problem ISP-29

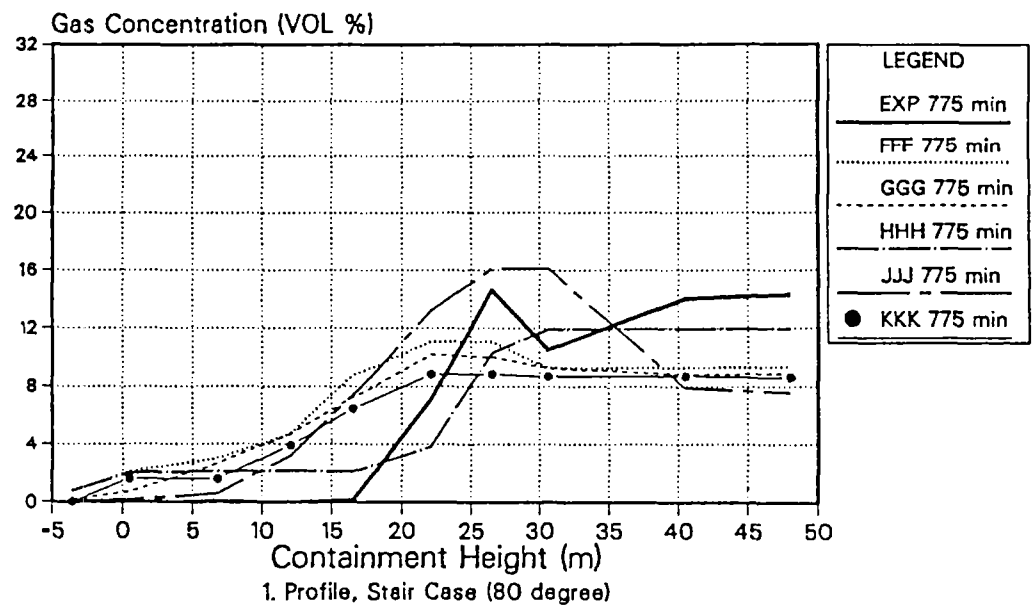
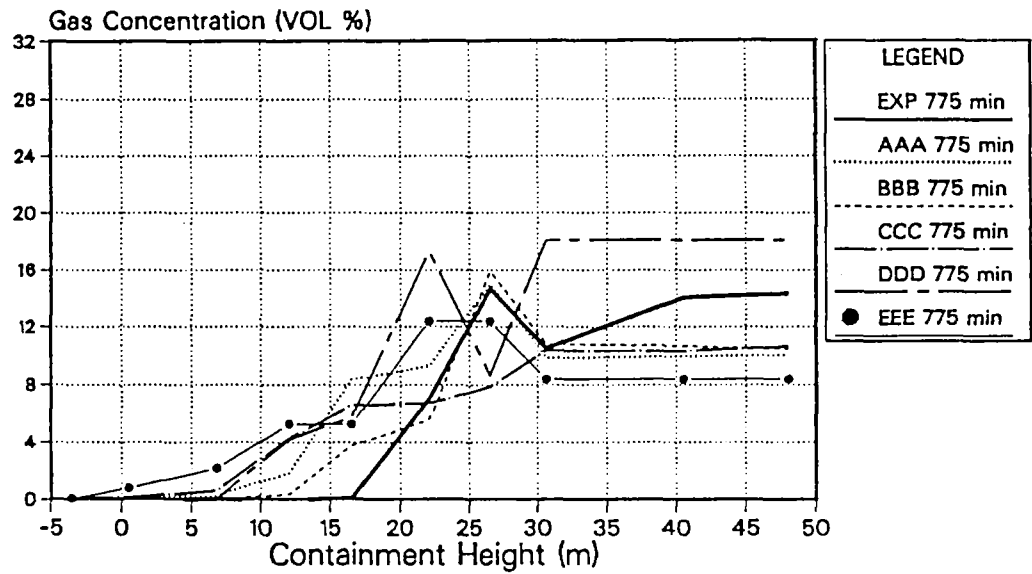


Fig. 6.32: Calculated Gas Concentration Profiles compared to the Measured Profile 35 min after starting gas release

## OECD Standard Problem ISP-29

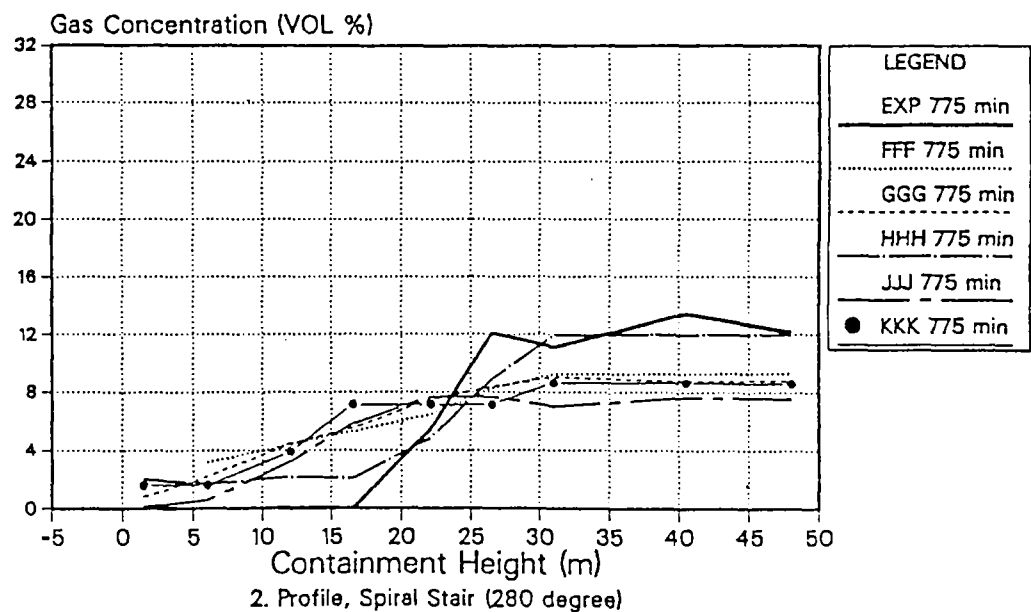
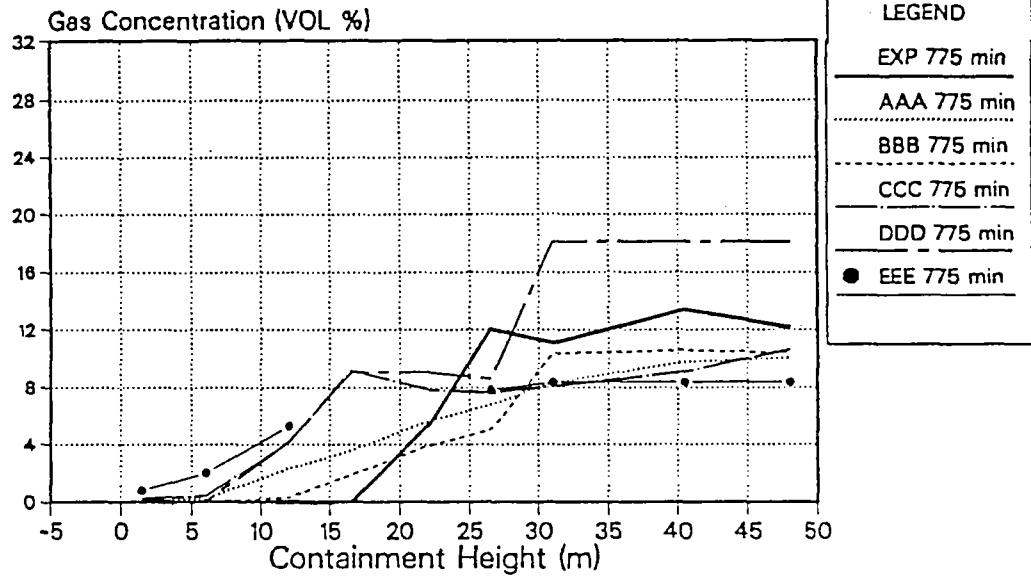


Fig. 6.33: Calculated Gas Concentration Profiles compared to the Measured Profile 35 min after starting gas release



## OECD Standard Problem ISP-29

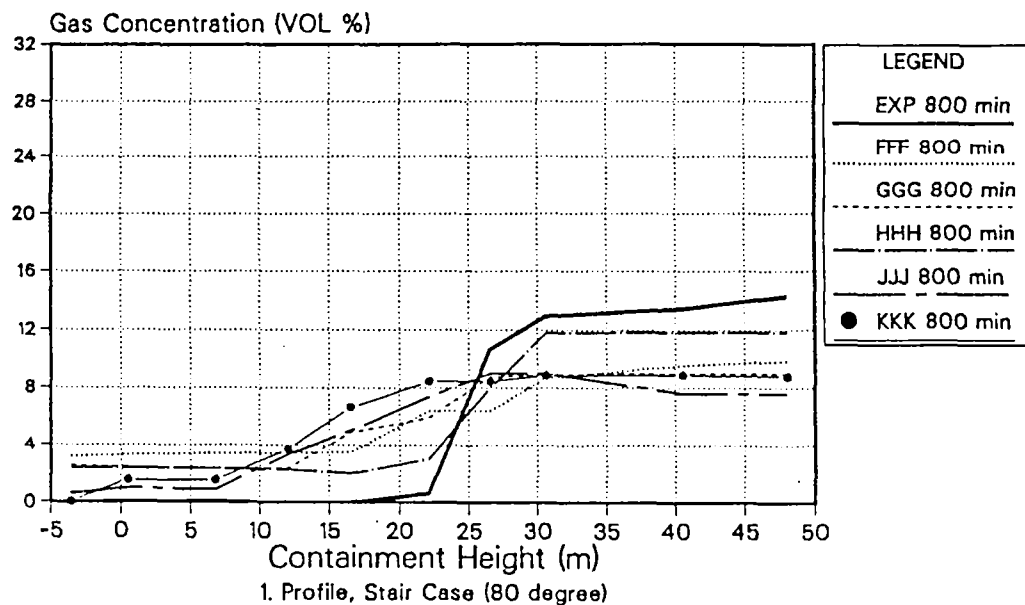
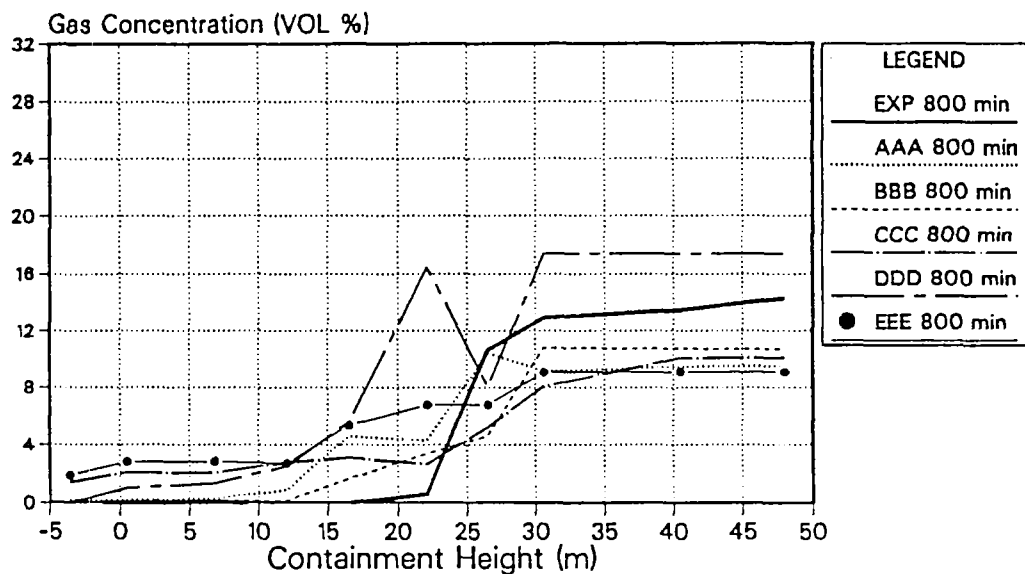


Fig. 6.34: Calculated Gas Concentration Profiles compared to the Measured Profile 60 min after starting gas release

## OECD Standard Problem ISP-29

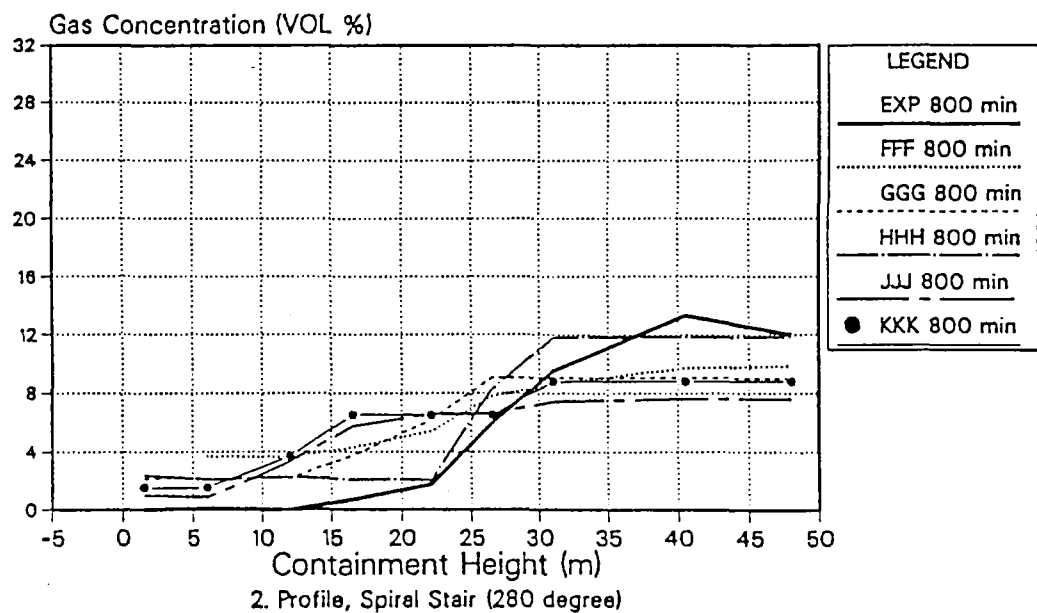
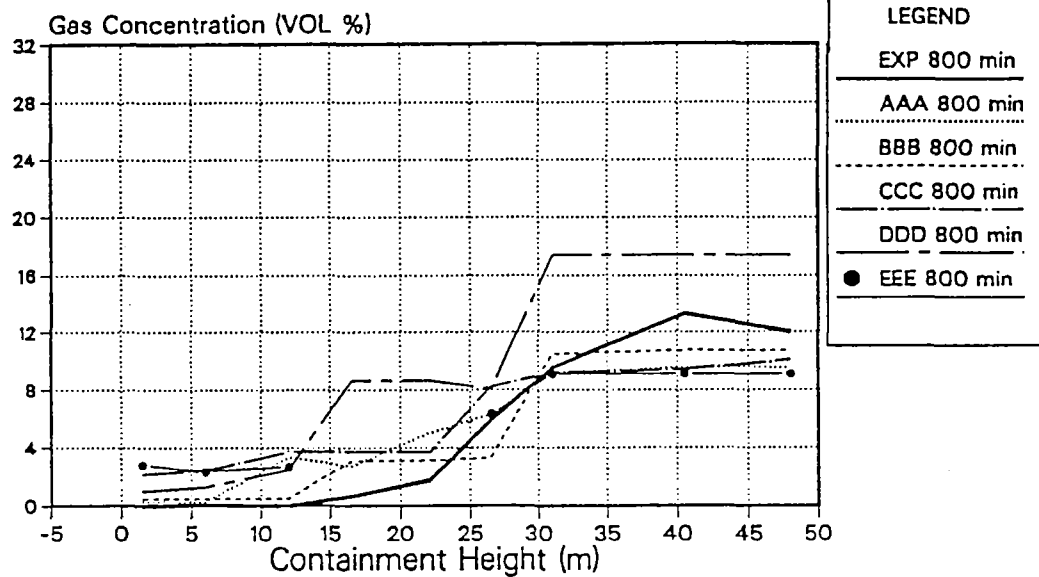


Fig. 6.35: Calculated Gas Concentration Profiles compared to the Measured Profile 60 min after starting gas release

## OECD Standard Problem ISP-29

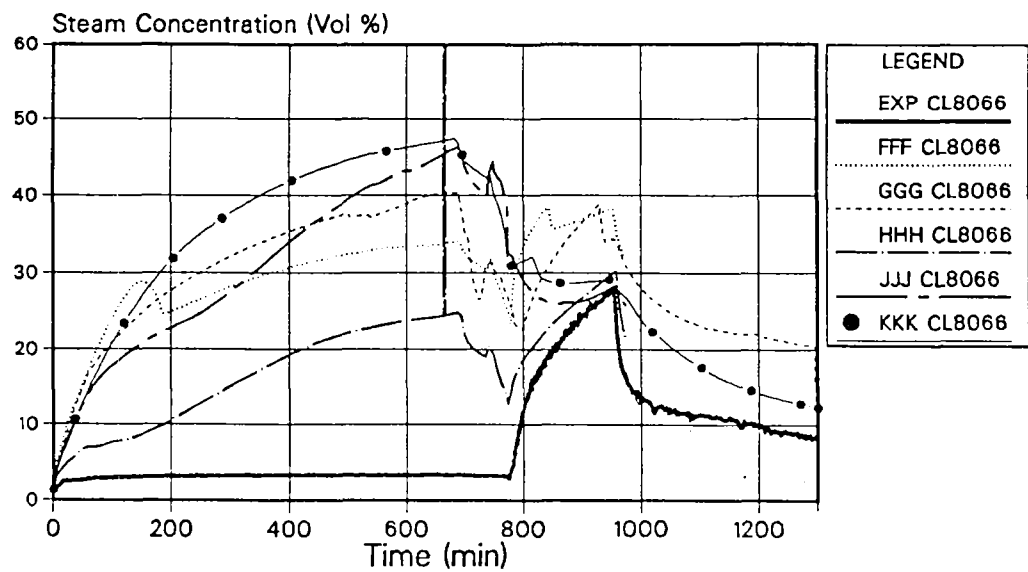
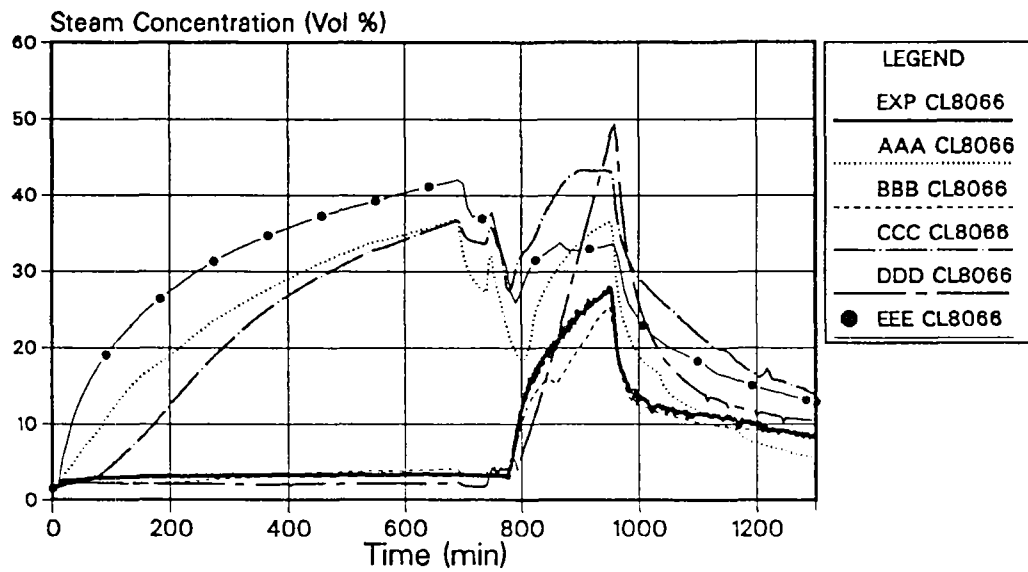


Fig. 6.36

Steam Concentration 12 m Elevation 80 degree

## OECD Standard Problem ISP-29

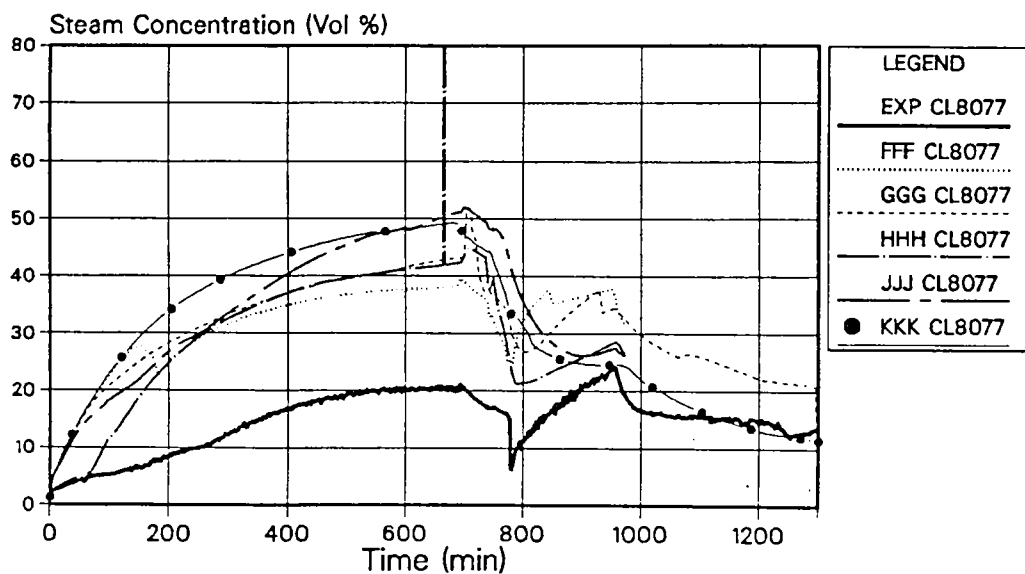
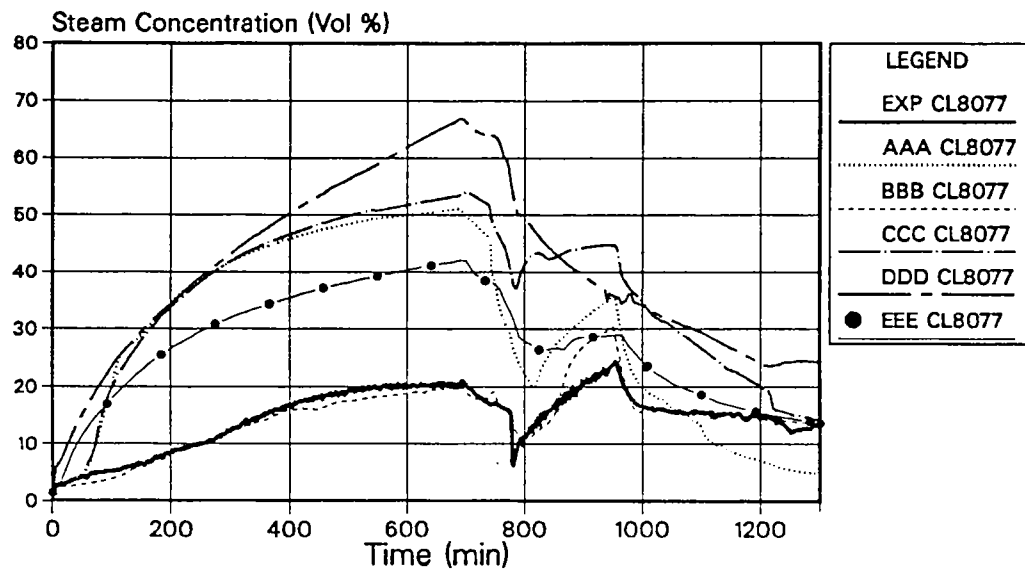


Fig. 6.37

Steam Concentration 16.50 m Elevation 80 degree

## OECD Standard Problem ISP-29

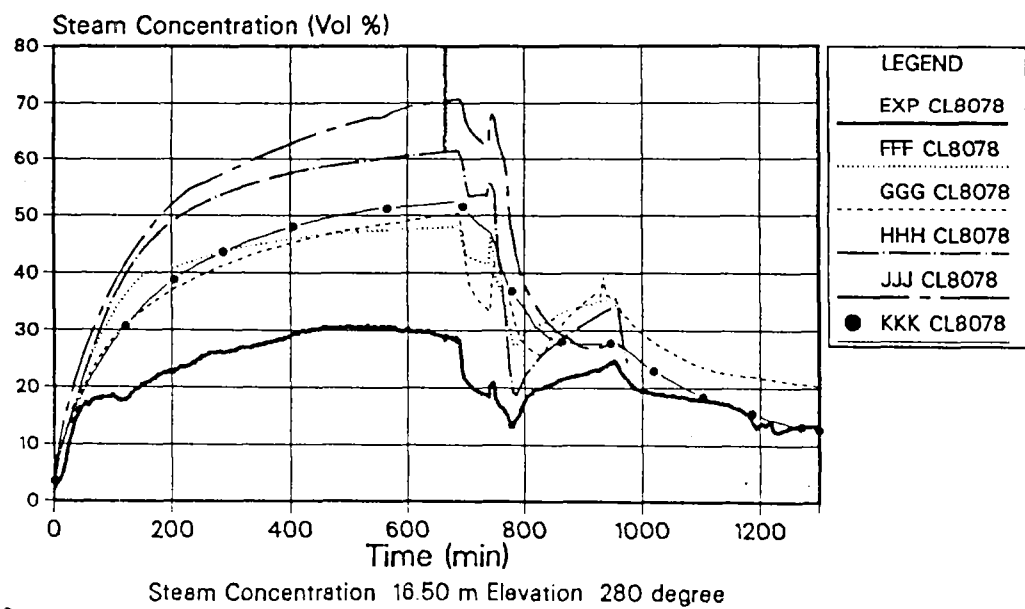
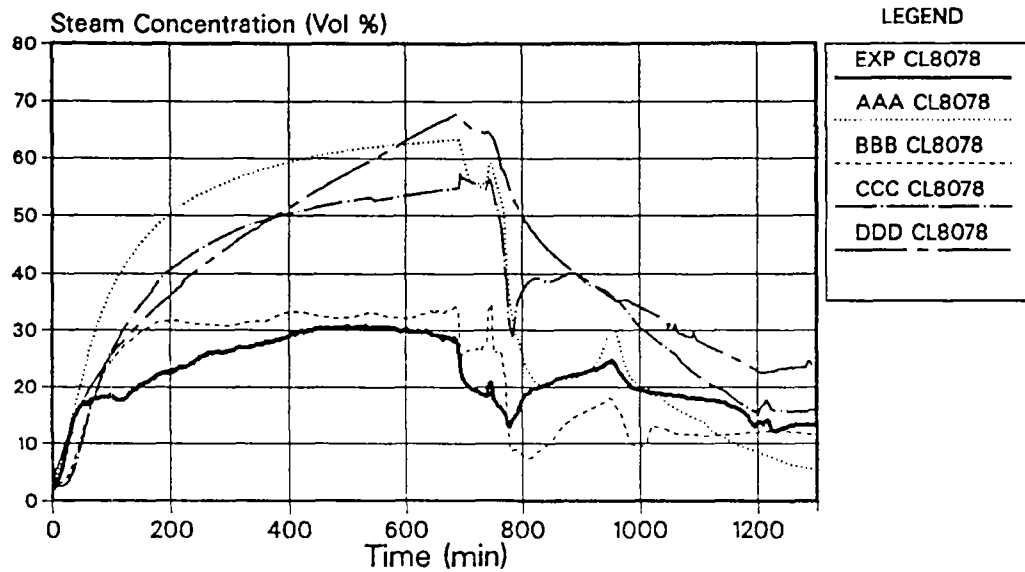


Fig. 6.38

## OECD Standard Problem ISP-29

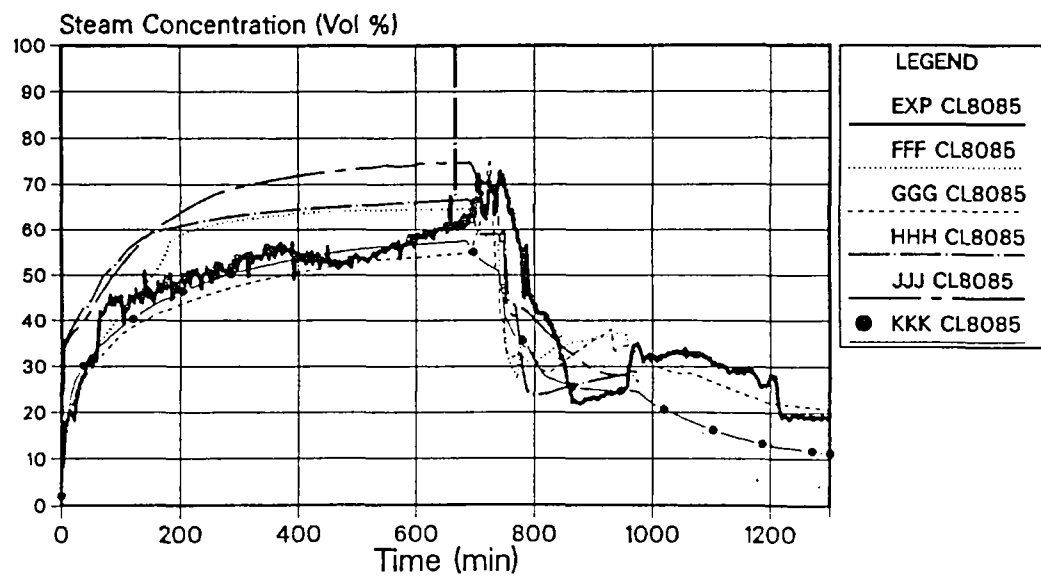
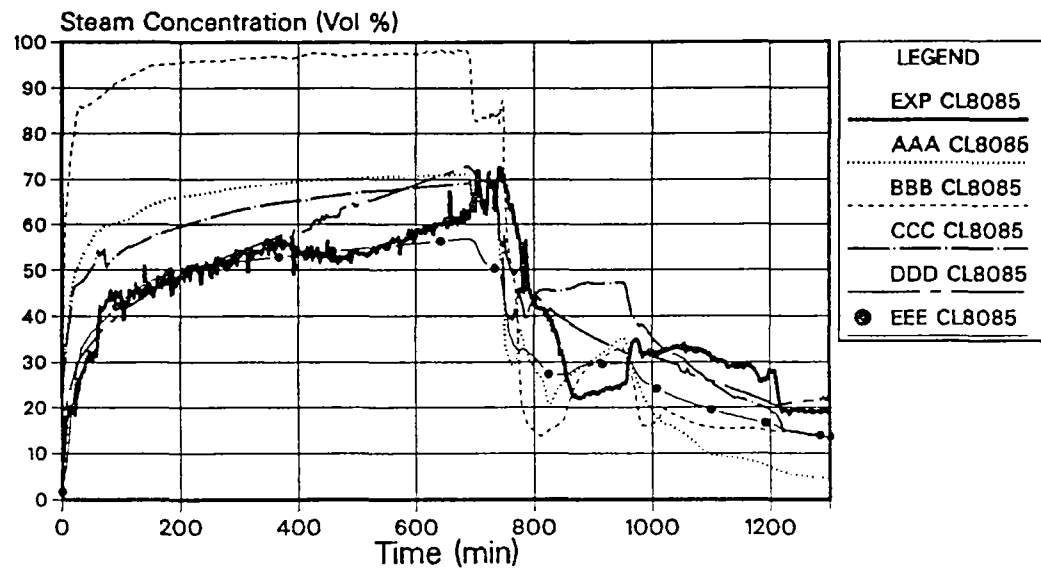
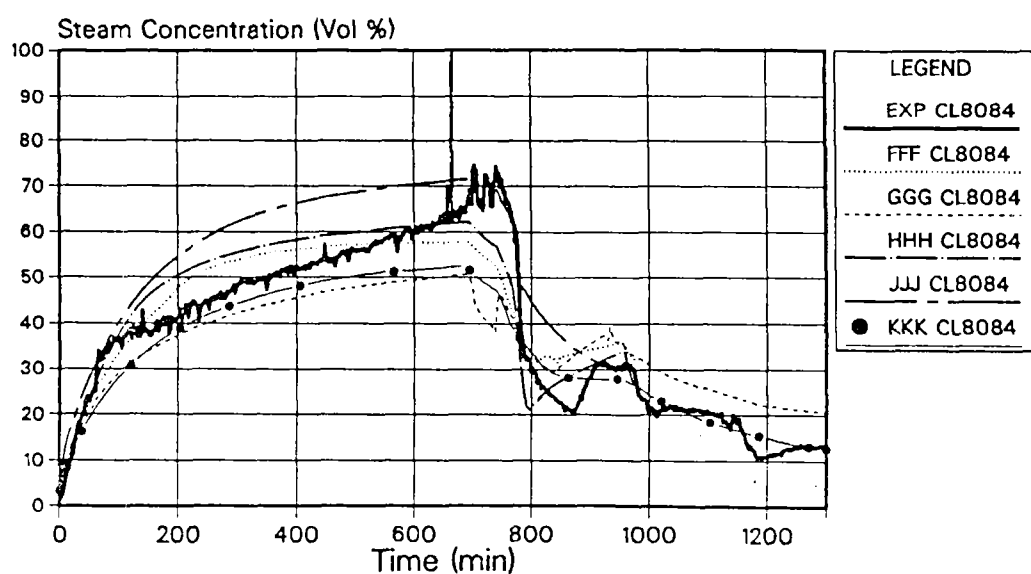
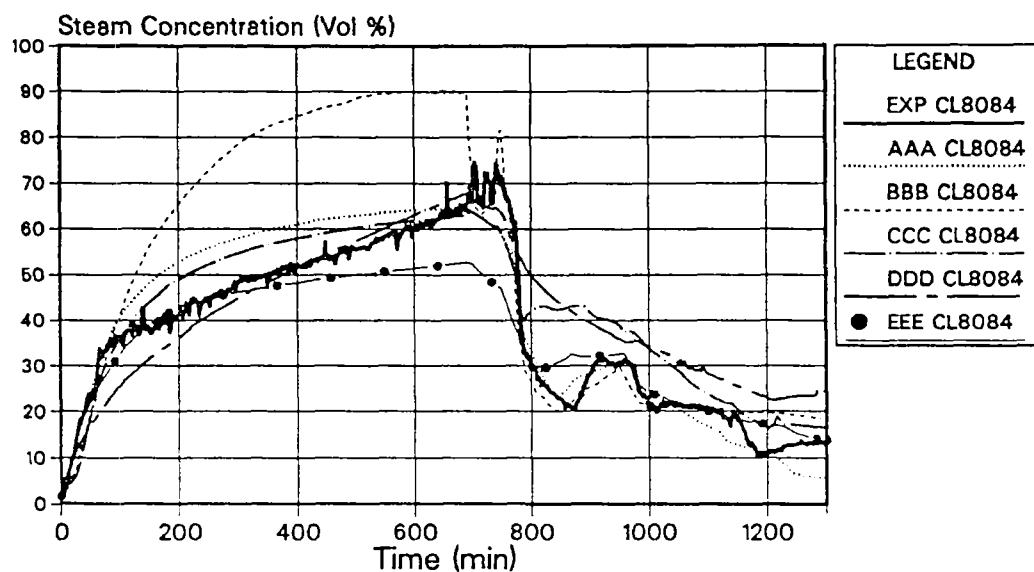


Fig. 6.39

Steam Concentration 22.10 m Elevation 80 degree

## OECD Standard Problem ISP-29



Steam Concentration 22.10 m Elevation 280 degree

Fig. 6.40

## OECD Standard Problem ISP-29

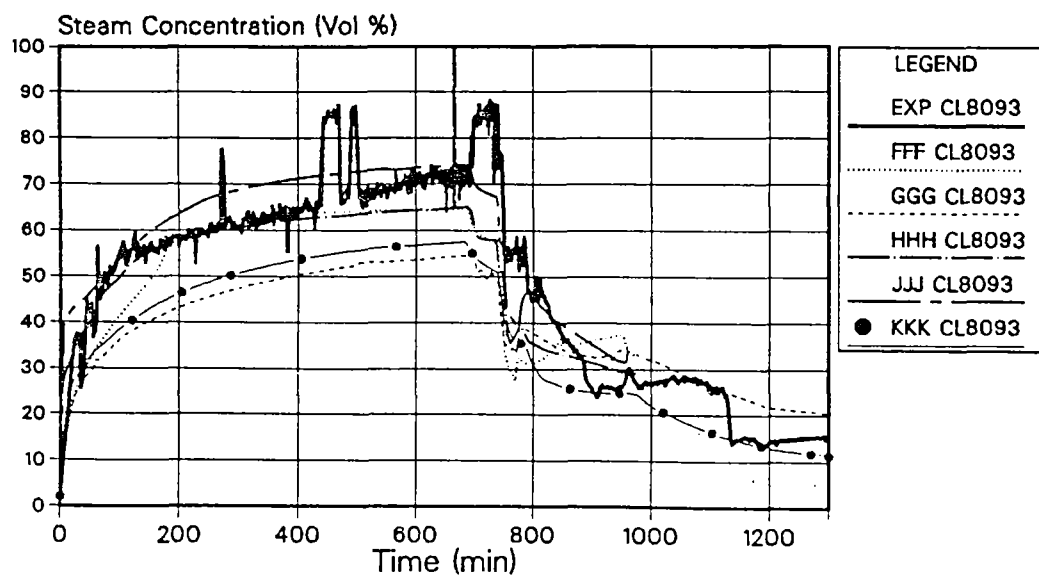
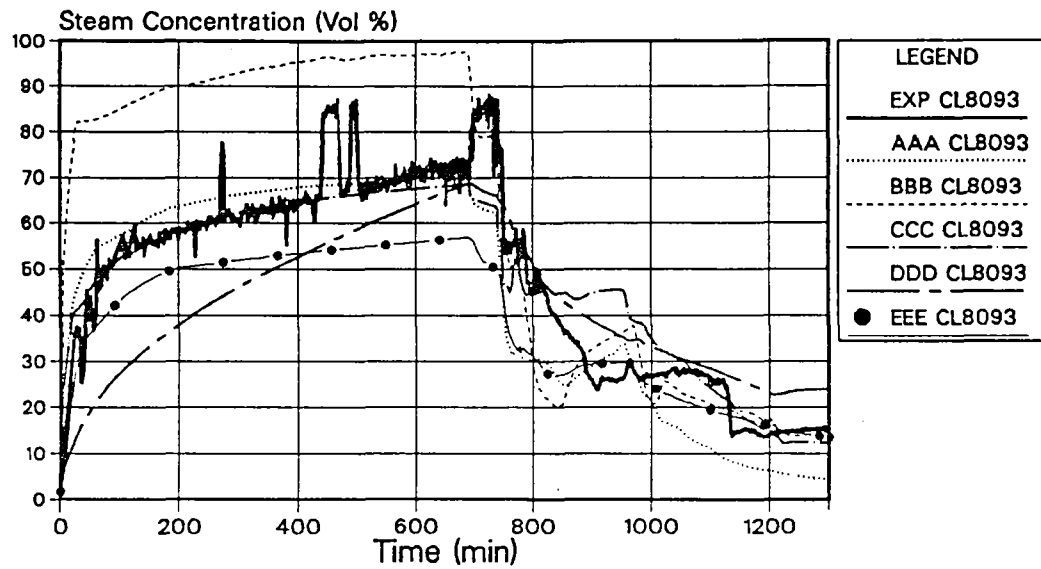
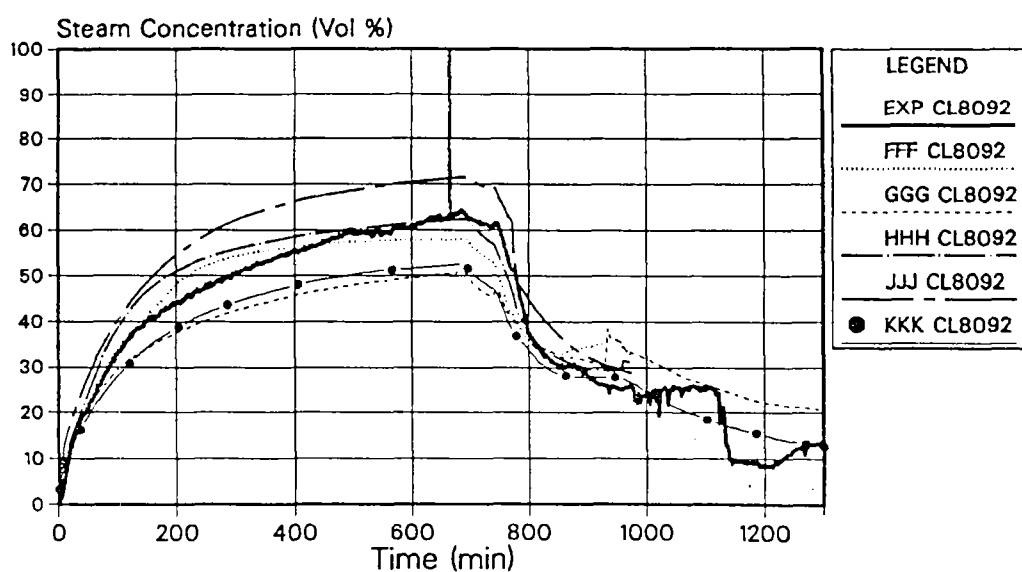
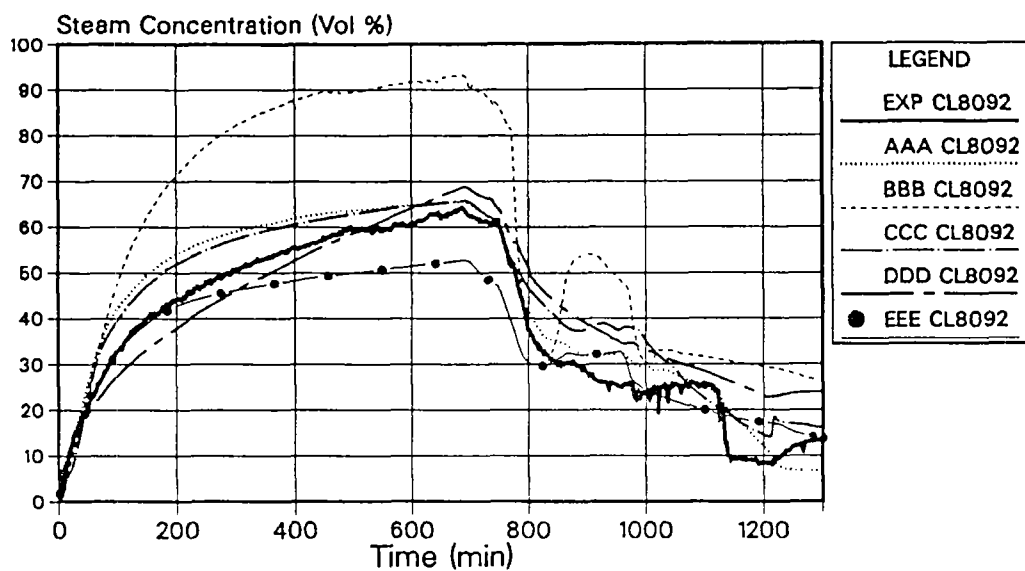


Fig. 6.41

Steam Concentration 26.50 m Elevation 80 degree



## OECD Standard Problem ISP-29



Steam Concentration 26.50 m Elevation 280 degree

Fig. 6.42

## OECD Standard Problem ISP-29

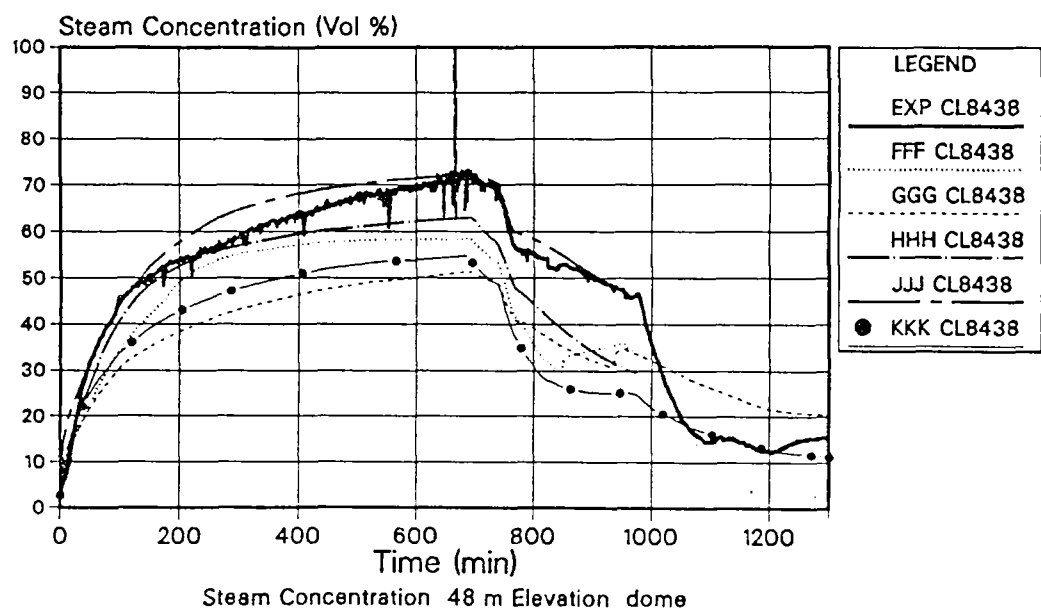
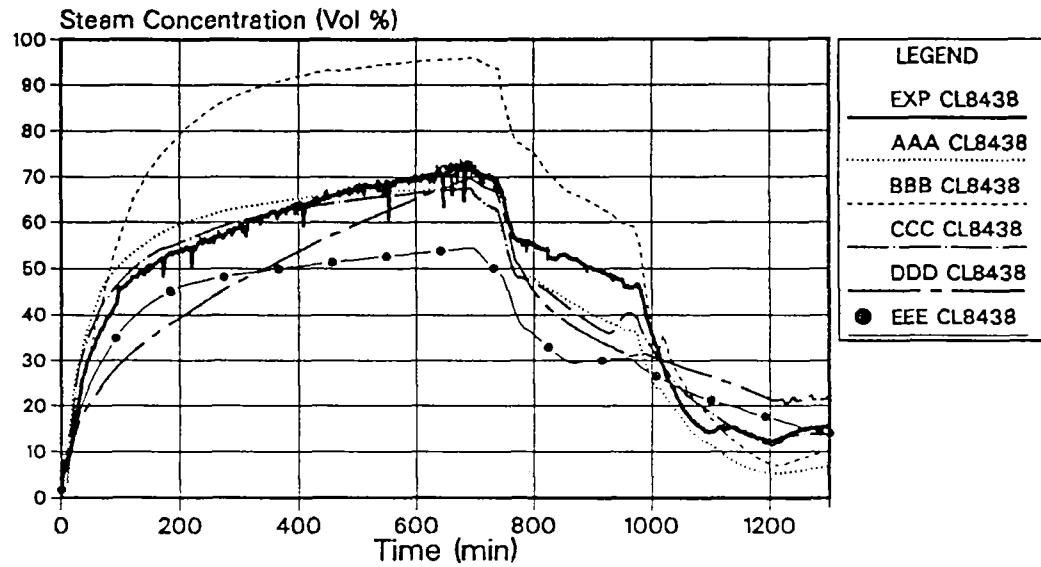


Fig. 6.43

## OECD Standard Problem ISP-29

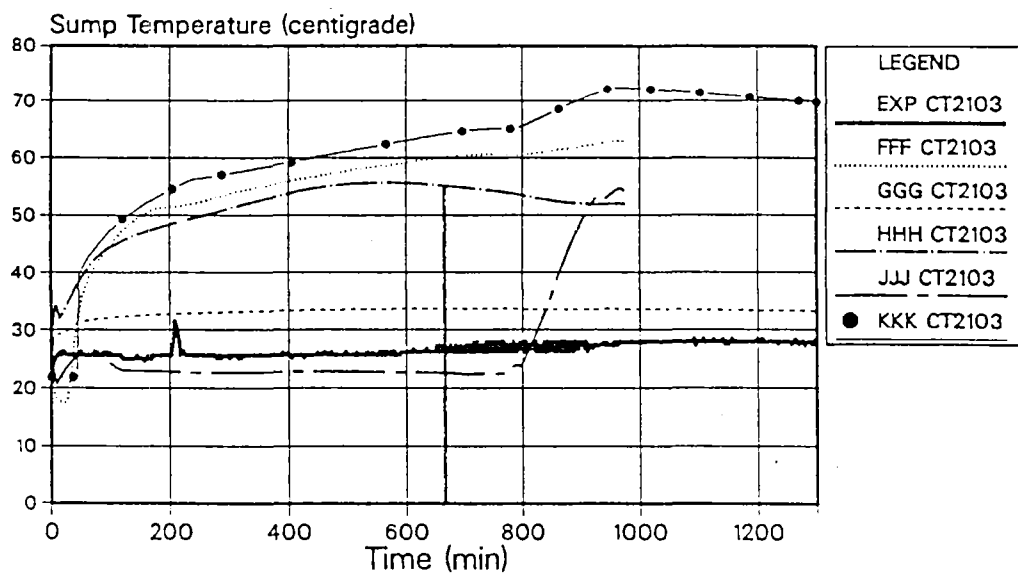
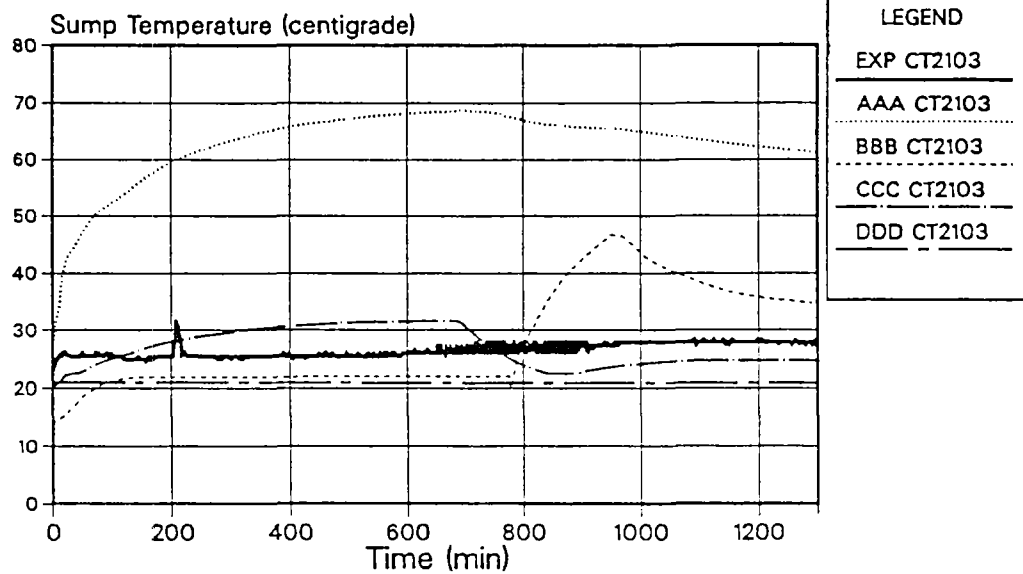


Fig. 6.44

Containment Sump Temperatures - 8.1 m Elevation

# OECD Standard Problem ISP-29

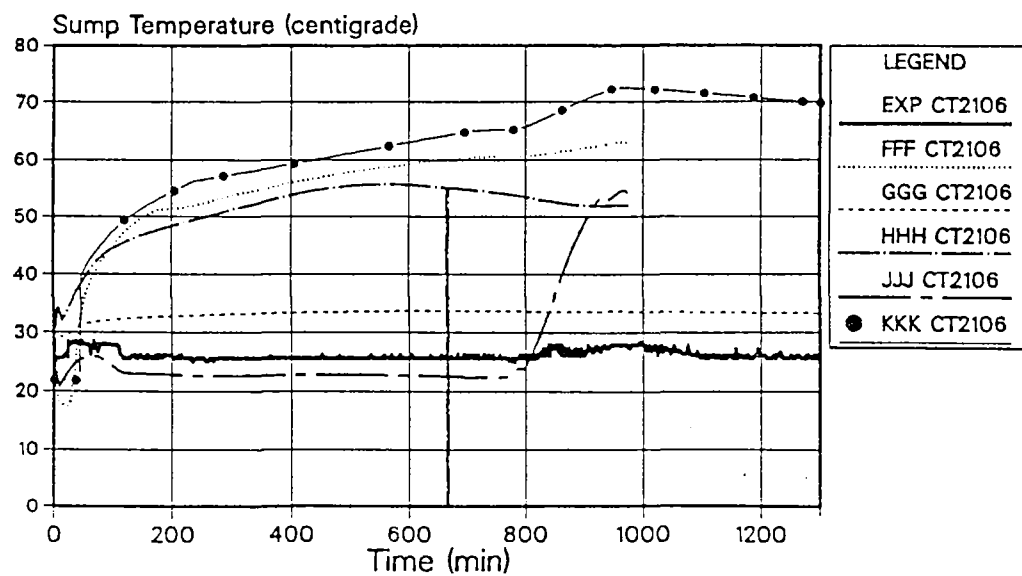
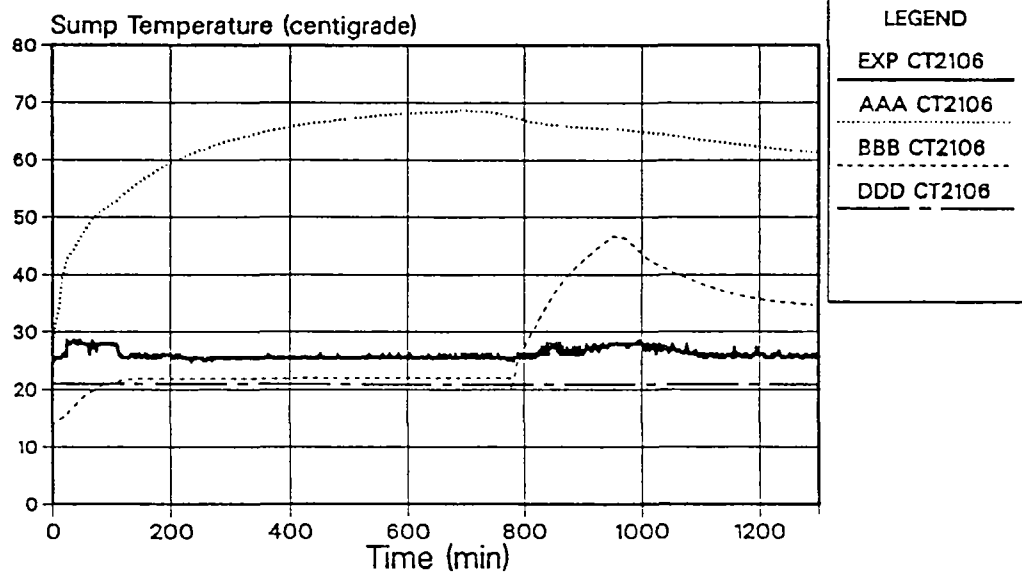


Fig. 6.45

Containment Sump Temperatures - 7.3 m Elevation

# OECD Standard Problem ISP-29

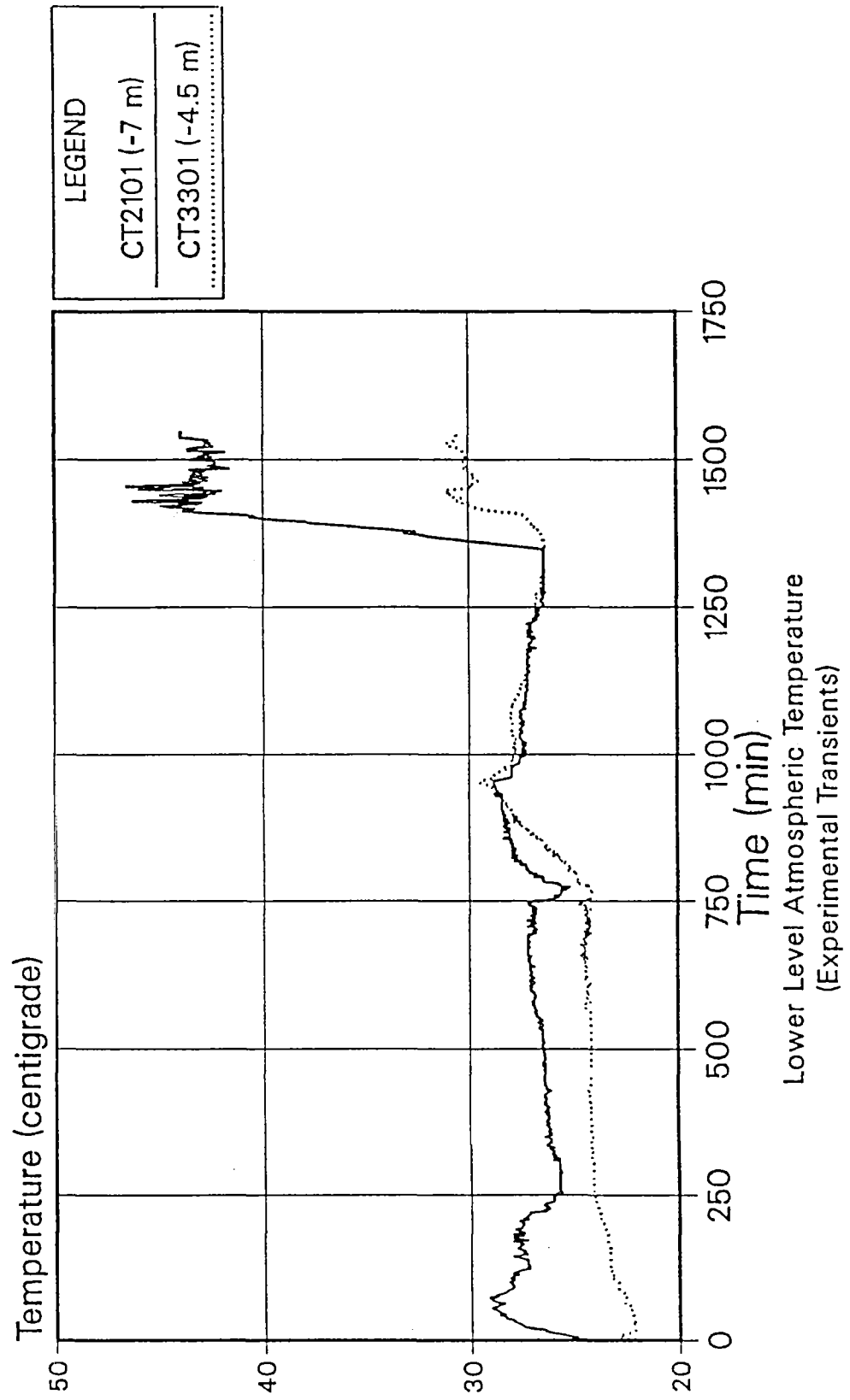


Fig. 6.46

## OECD Standard Problem ISP-29

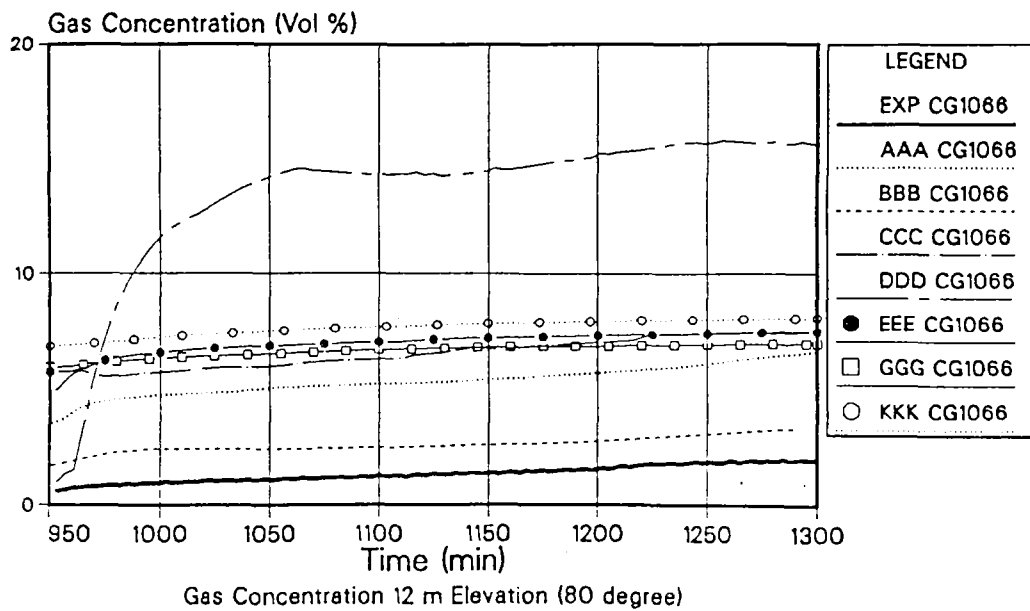
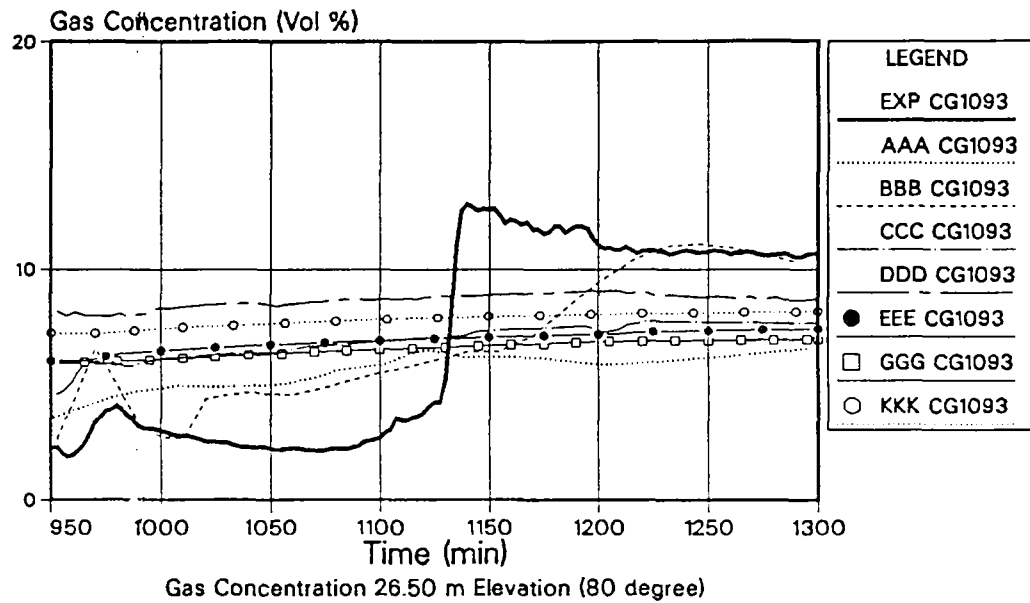


Fig. 6.47: External Shell Cooling Period Gas Concentration Transients

## OECD Standard Problem ISP-29

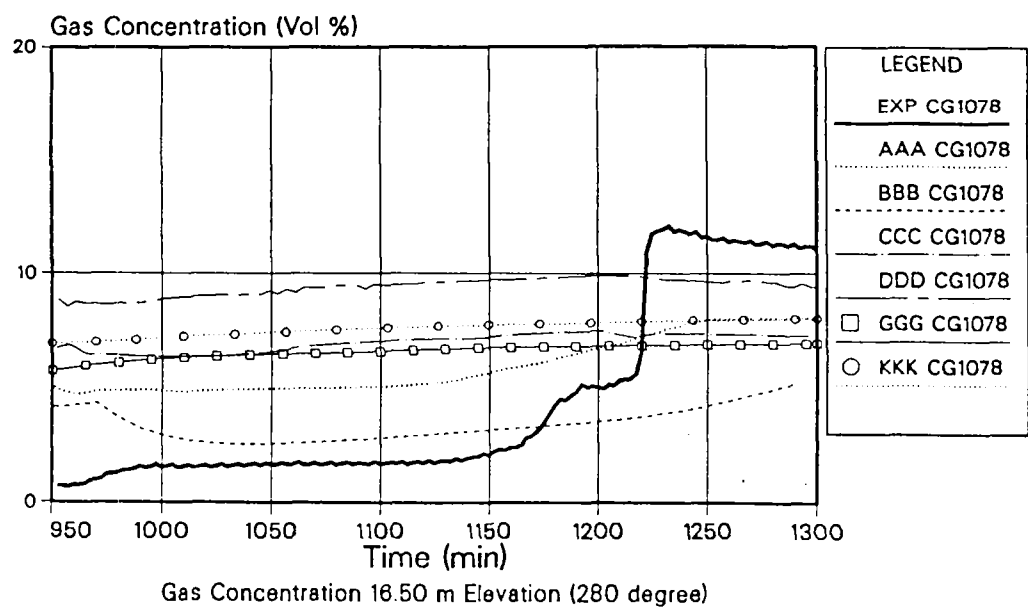
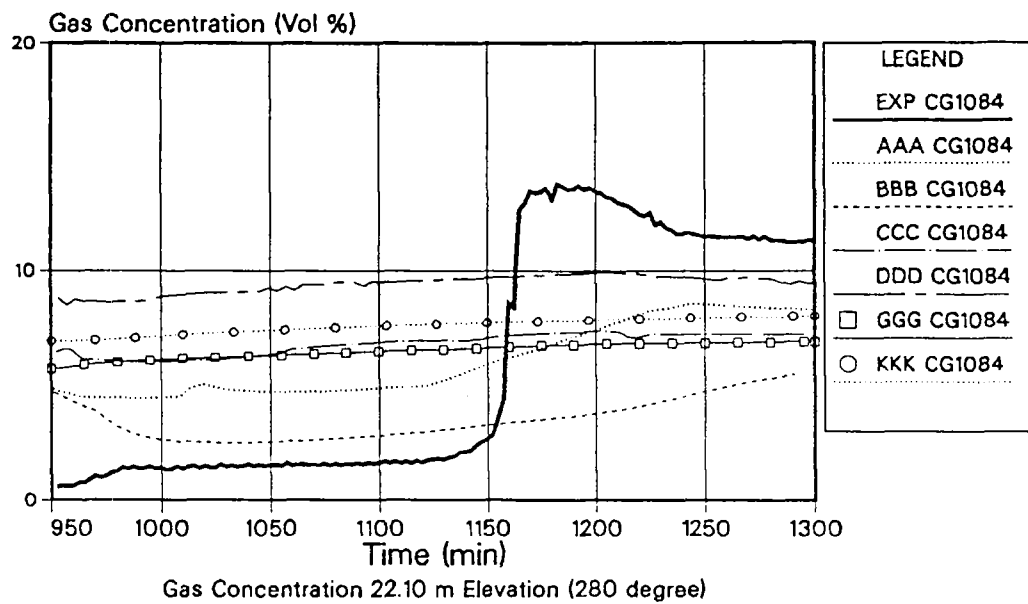


Fig. 6.48: External Shell Cooling Period Gas Concentration Transients

## OECD Standard Problem ISP-29

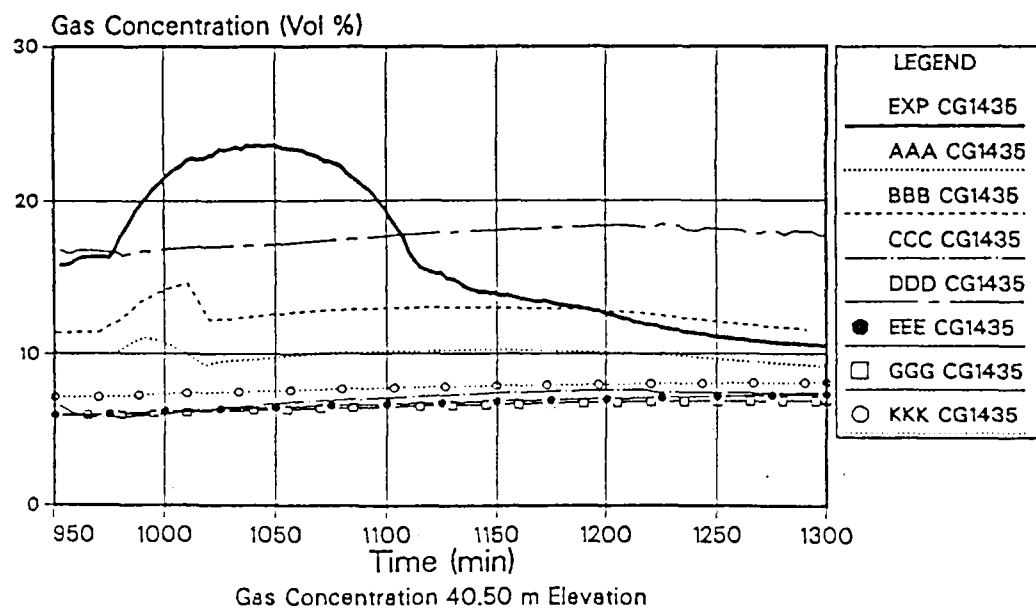
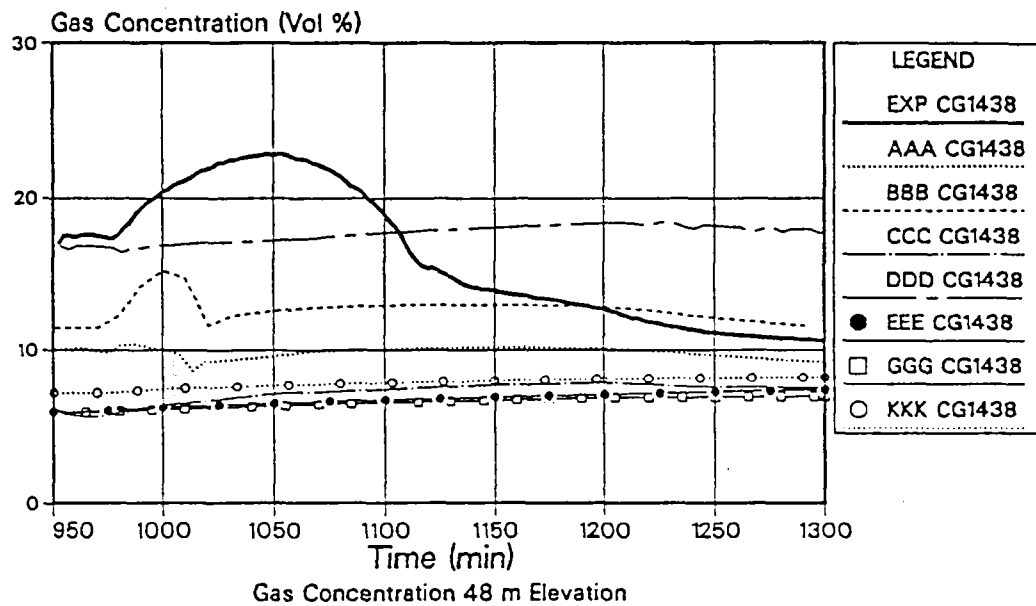


Fig. 6.49: External Shell Cooling Period Gas Concentration Transients



## OECD Standard Problem ISP-29

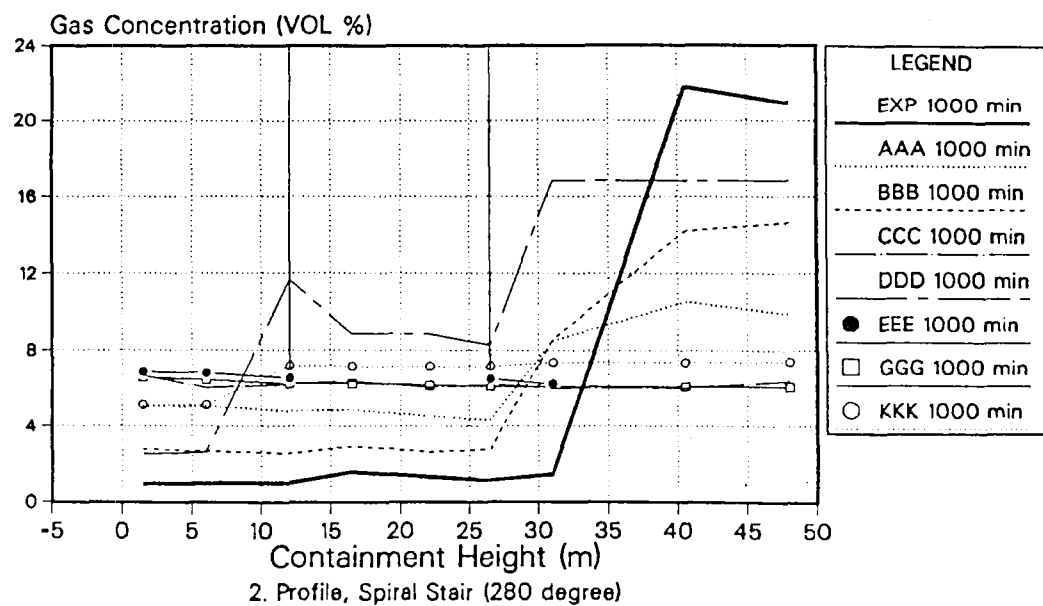
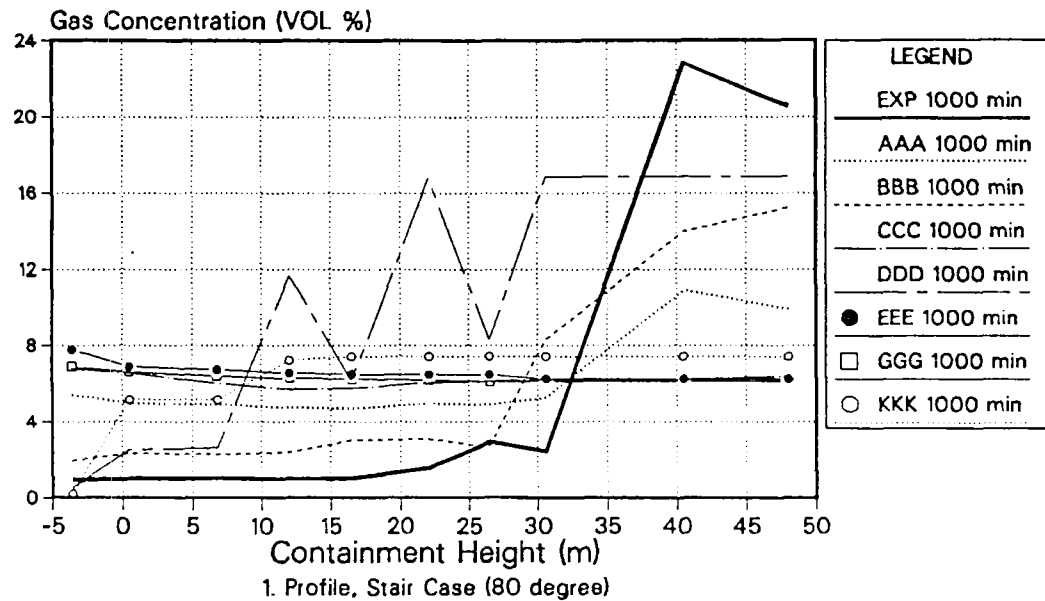


Fig. 6.50: External Shell Cooling Period; Calculated Gas Concentration Profiles at Various Points in Time Compared to Measured Profiles

## OECD Standard Problem ISP-29

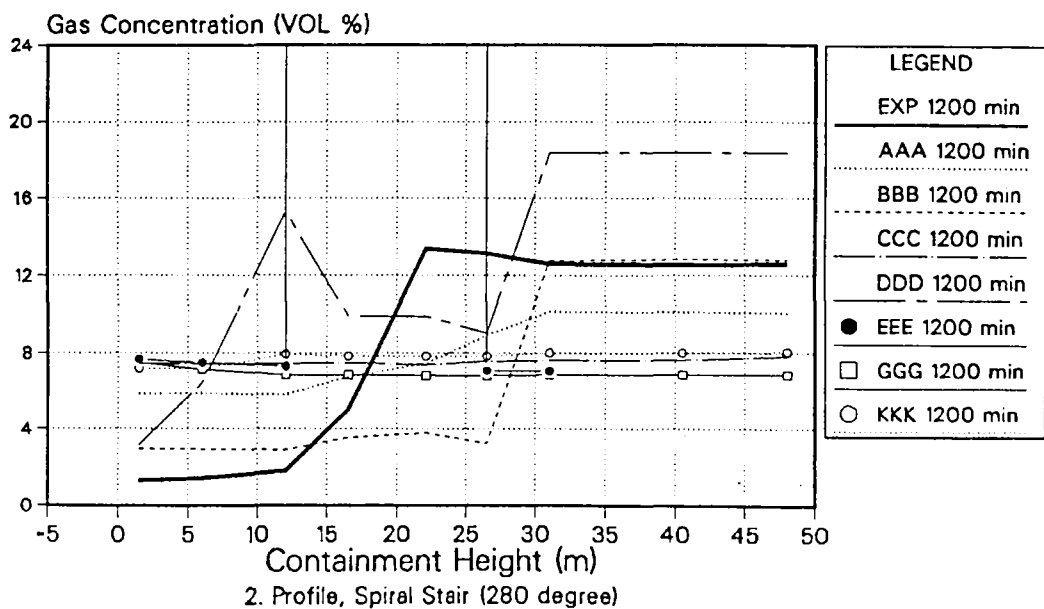
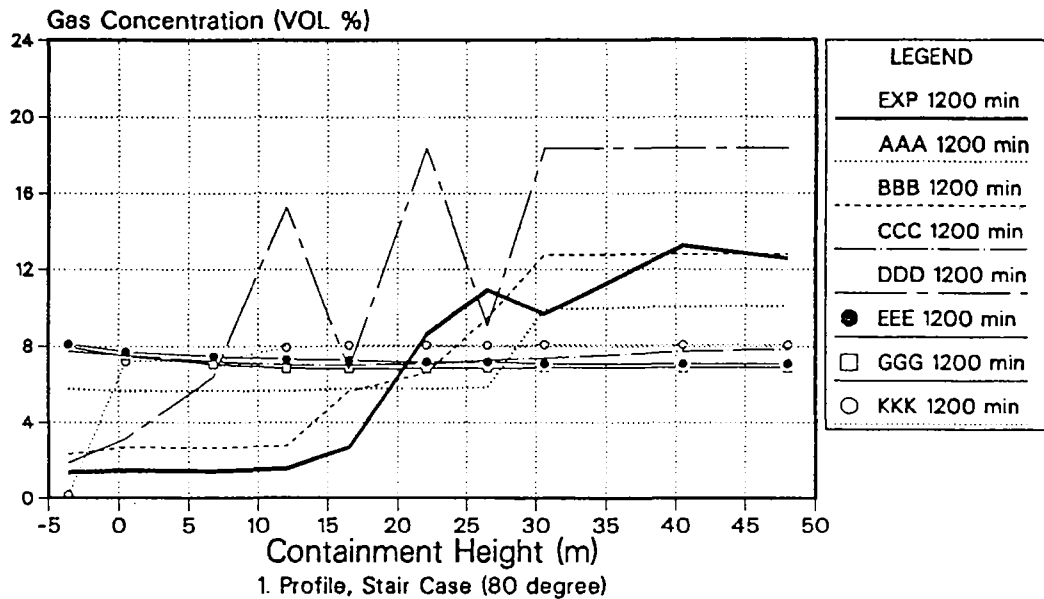


Fig. 6.51: External Shell Cooling Period; Calculated Gas Concentration Profiles at Various Points in Time Compared to Measured Profiles

## OECD Standard Problem ISP-29

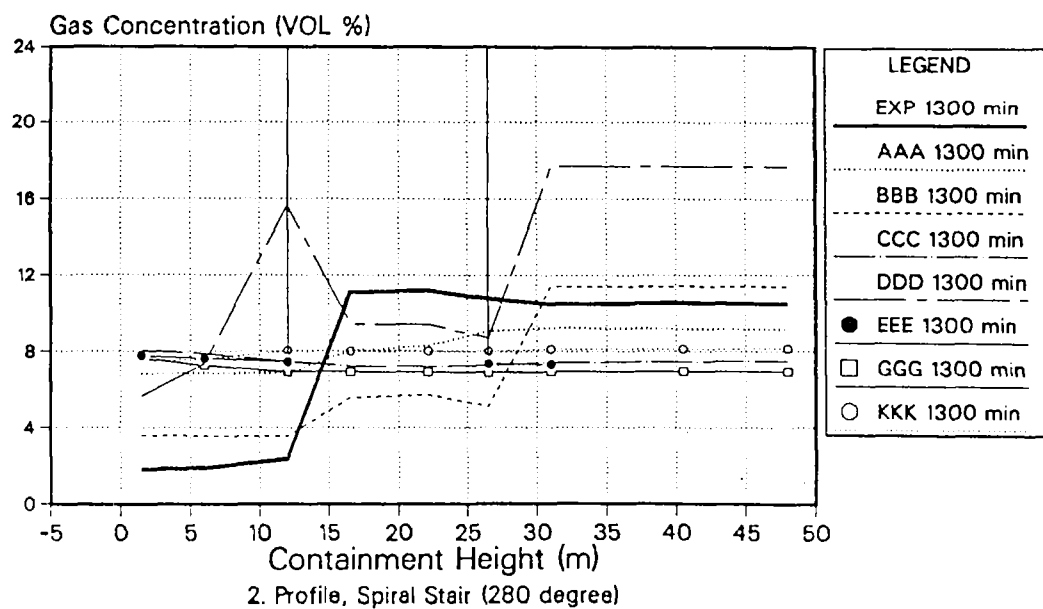
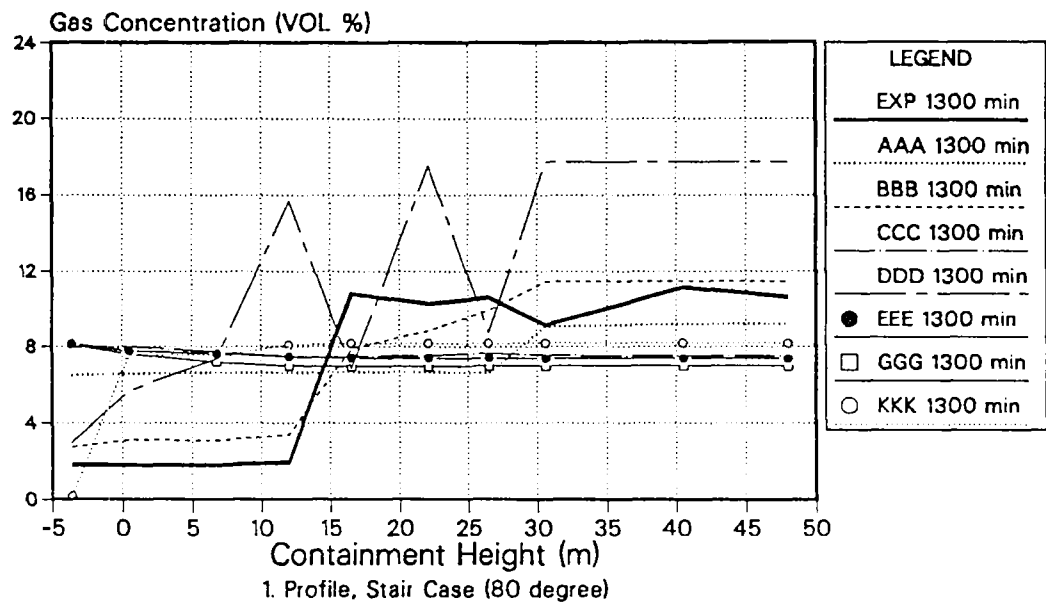


Fig. 6.52: External Shell Cooling Period; Calculated Gas Concentration Profiles at Various Points in Time Compared to Measured Profiles

## OECD Standard Problem ISP-29

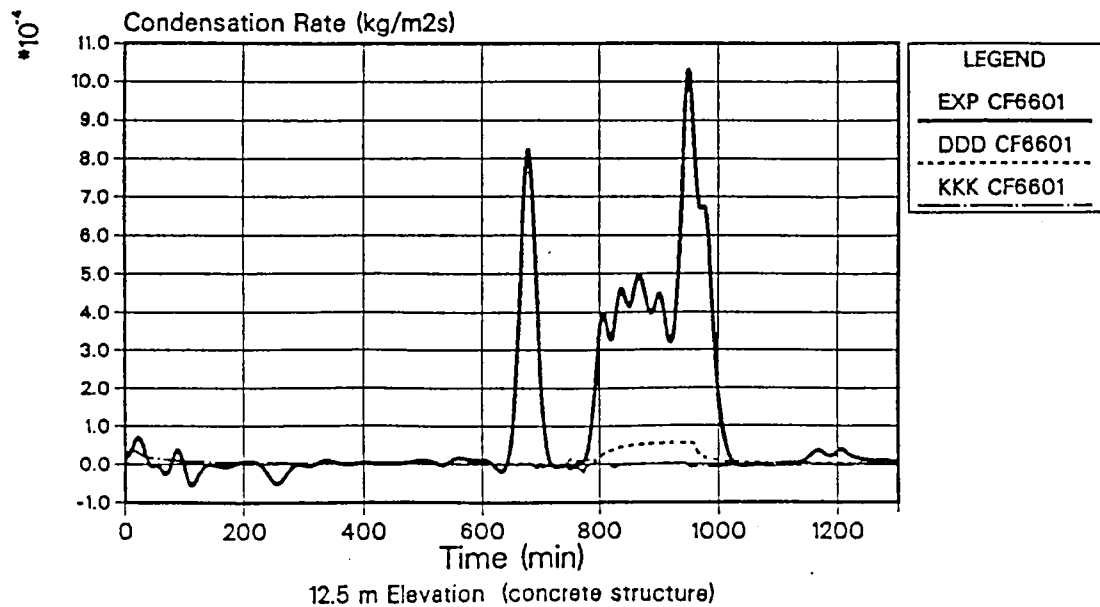
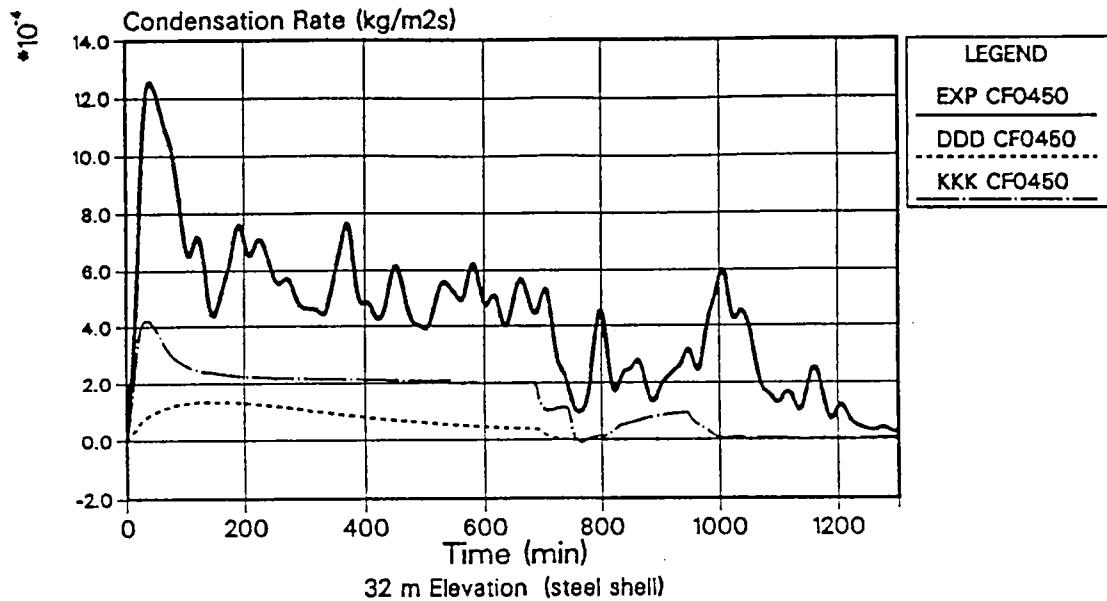


Fig. 6.53

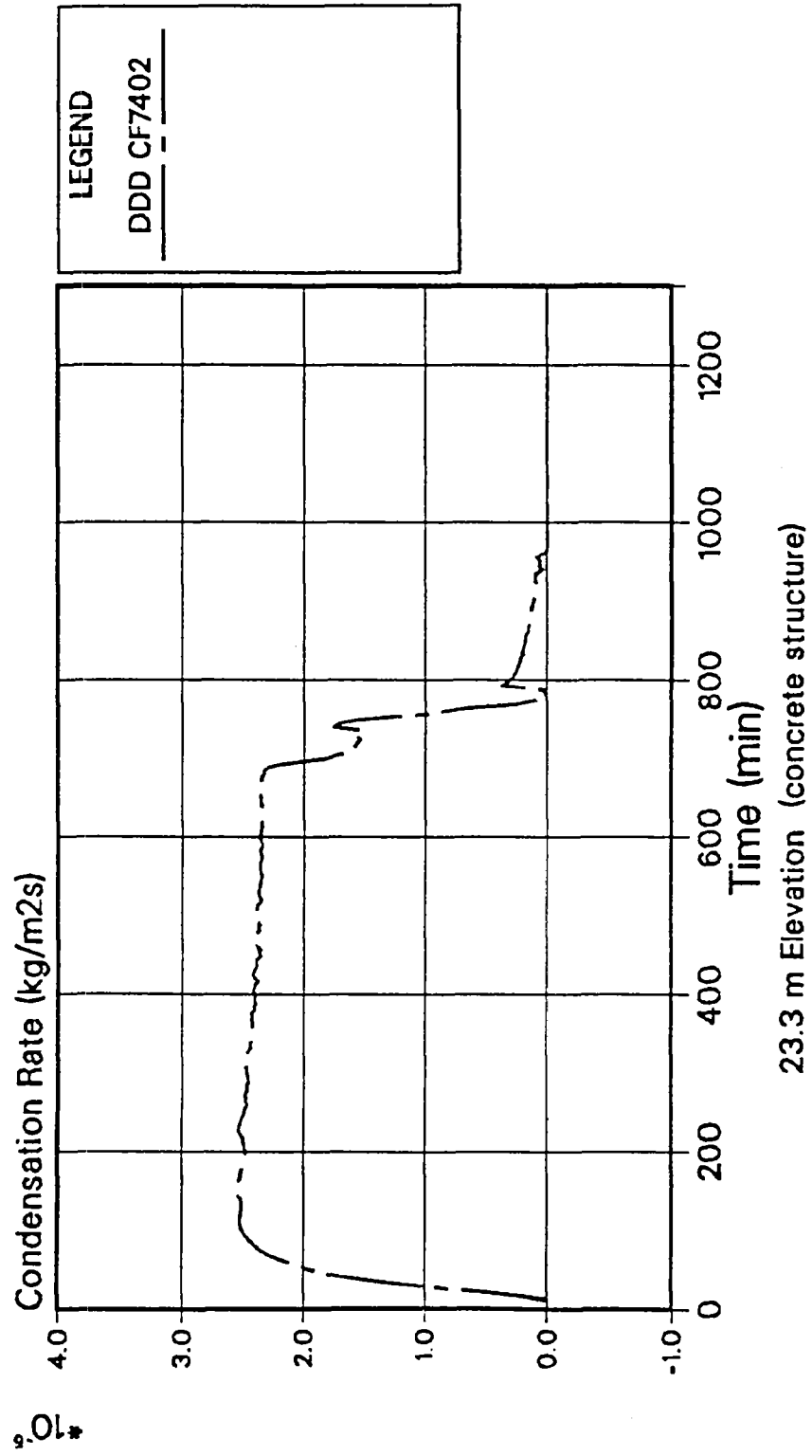


Fig. 6.54

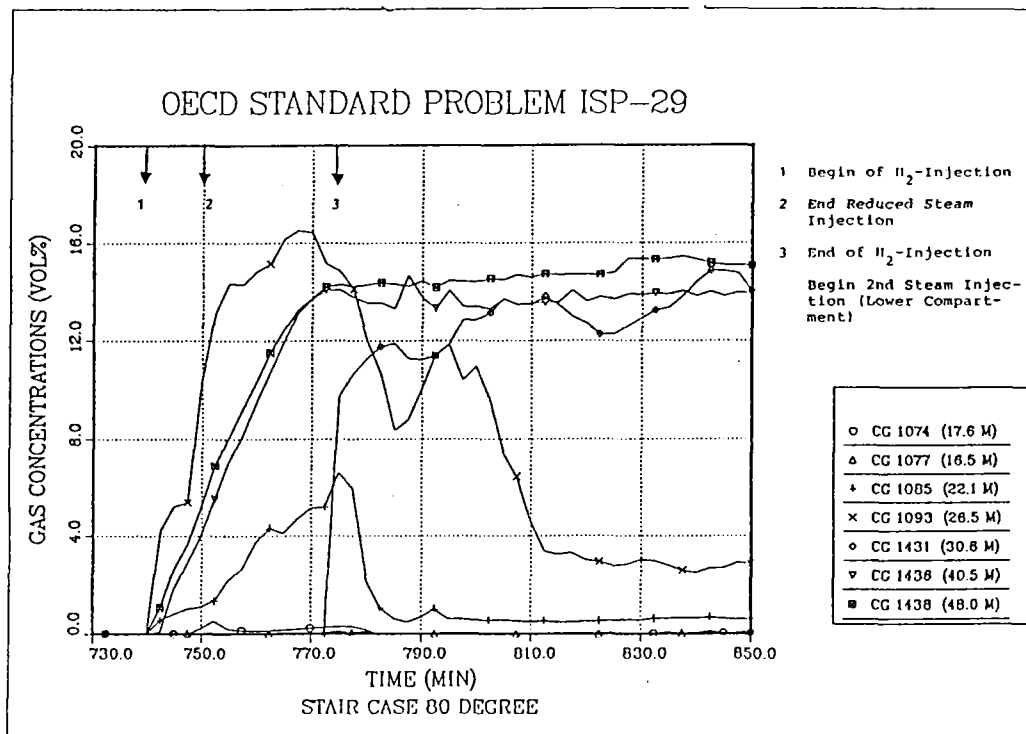


Fig. 6.55: Gas Concentrations Measured at Various Locations during HDR-Experiment E11.2 (Stair Case Side, 80 °)

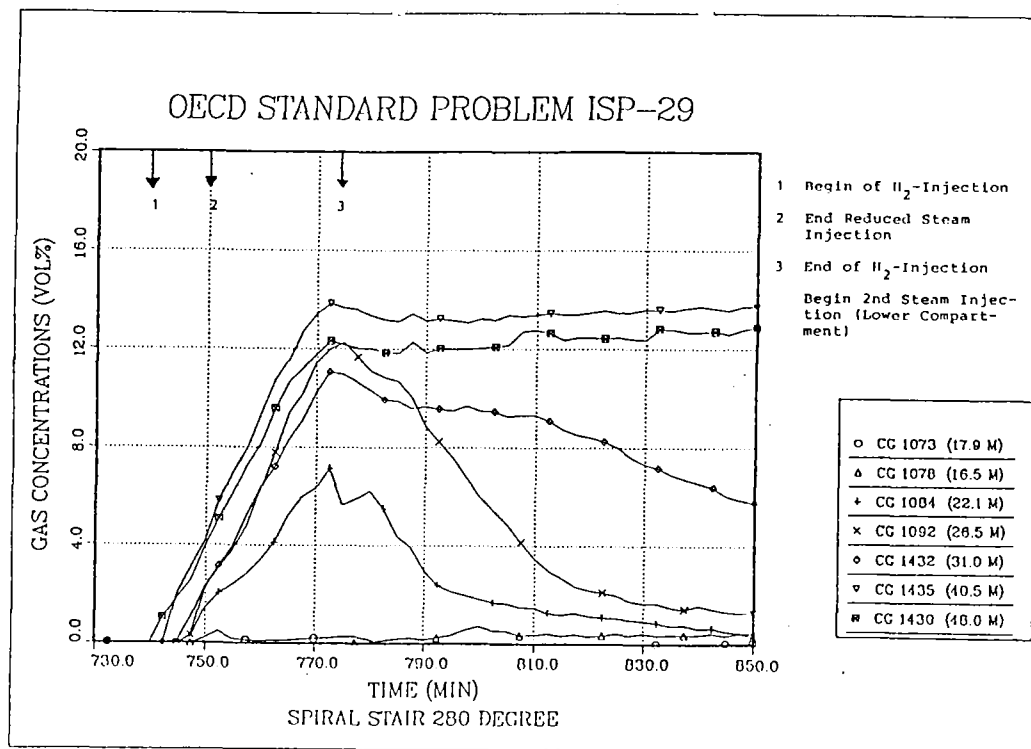


Fig. 6.56: Gas Concentrations Measured at Various Locations during HDR-Experiment E11.2 (Spiral Stair, 280 °)

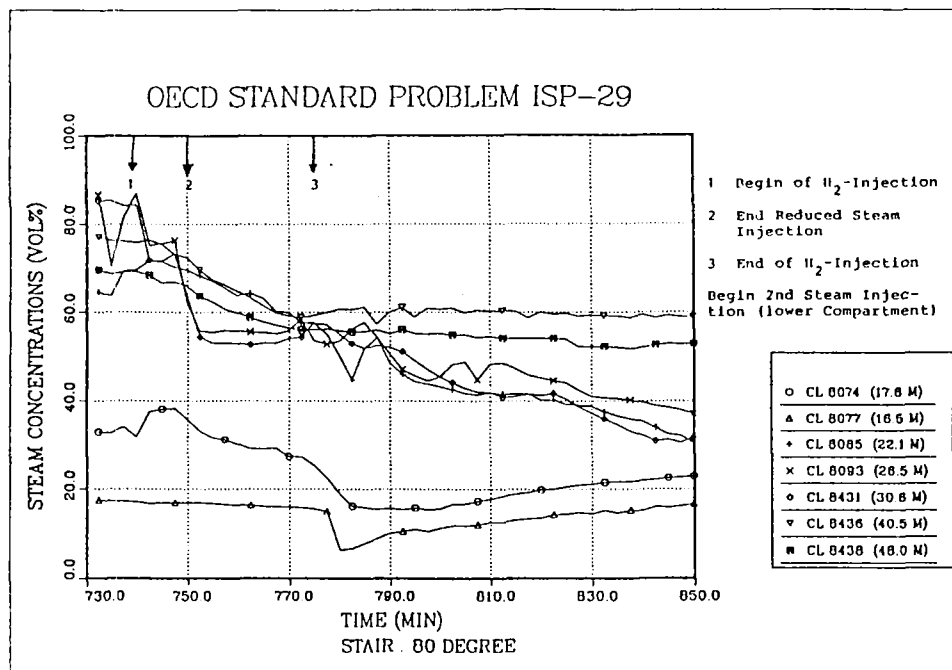


Fig. 6.57: Steam Concentrations Measured at Various Locations during HDR-Experiment E11.2 (Stair Case Side, 280 °)

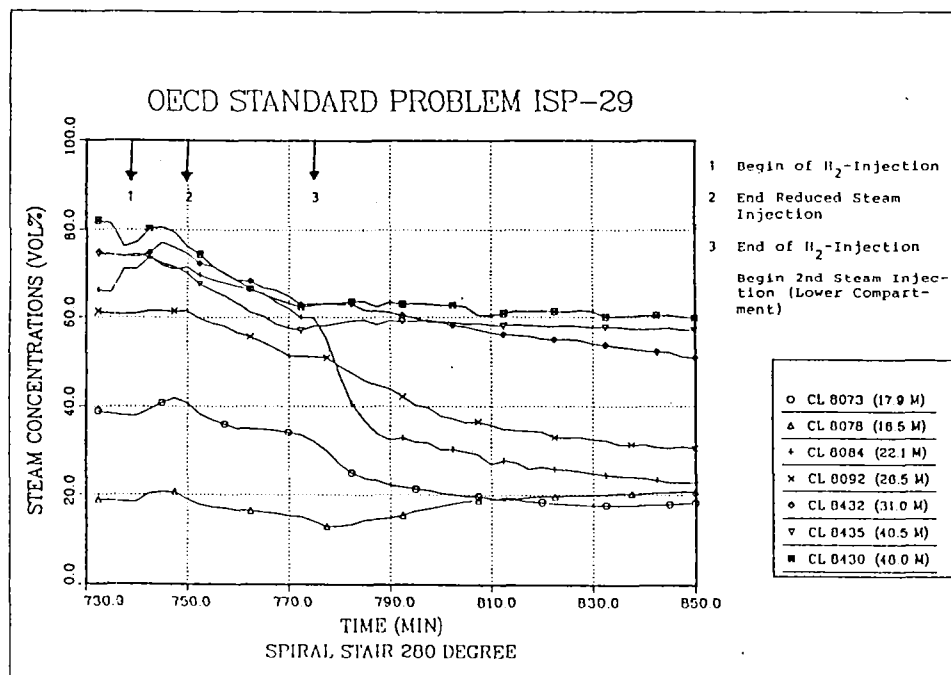


Fig. 6.58: Steam Concentrations Measured at Various Locations during HDR-Experiment E11.2 (Spiral Stair, 280 °)

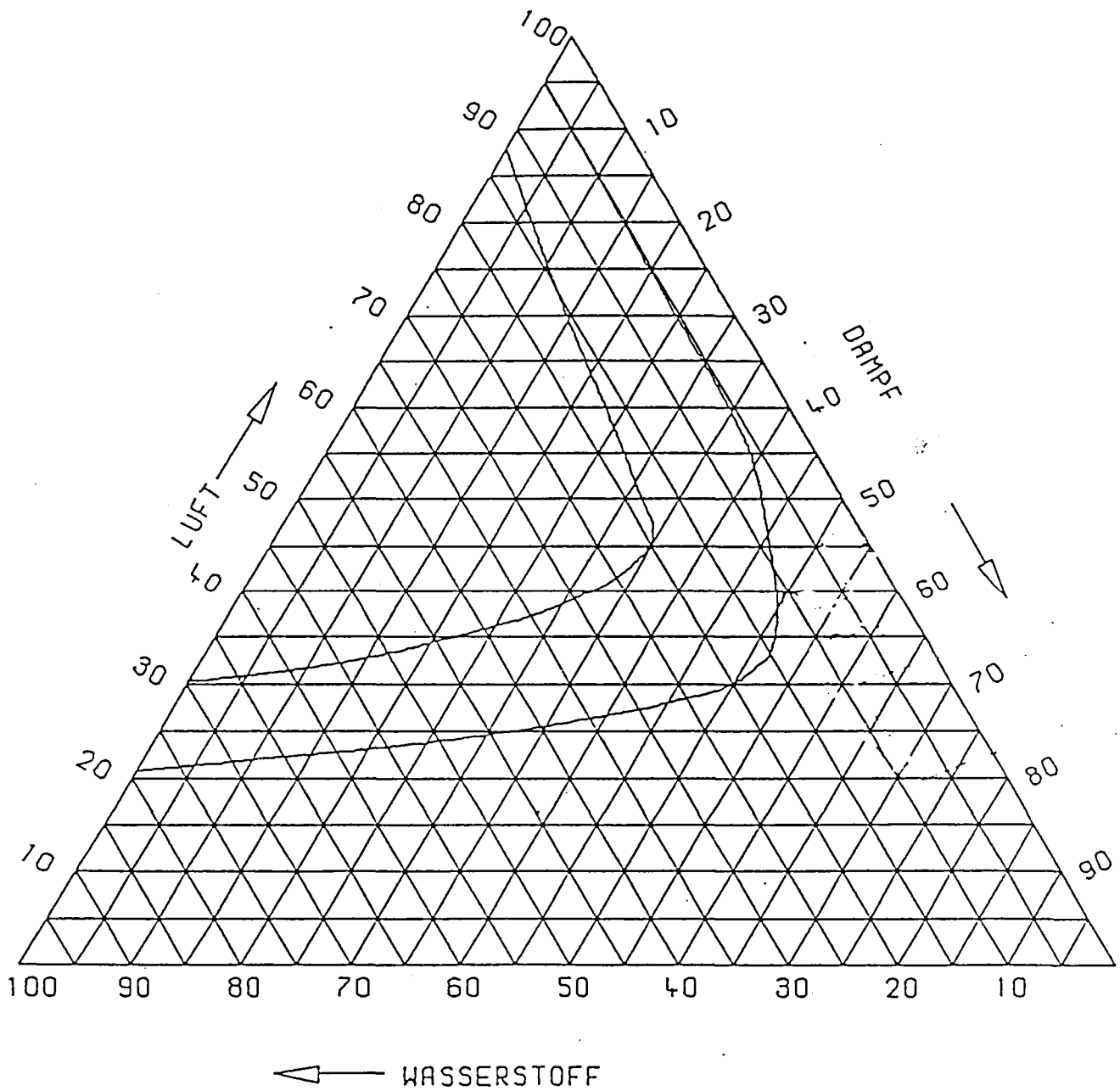


Fig. 6.59: Ternary Flammability Diagram  
Hydrogen - Air - Steam



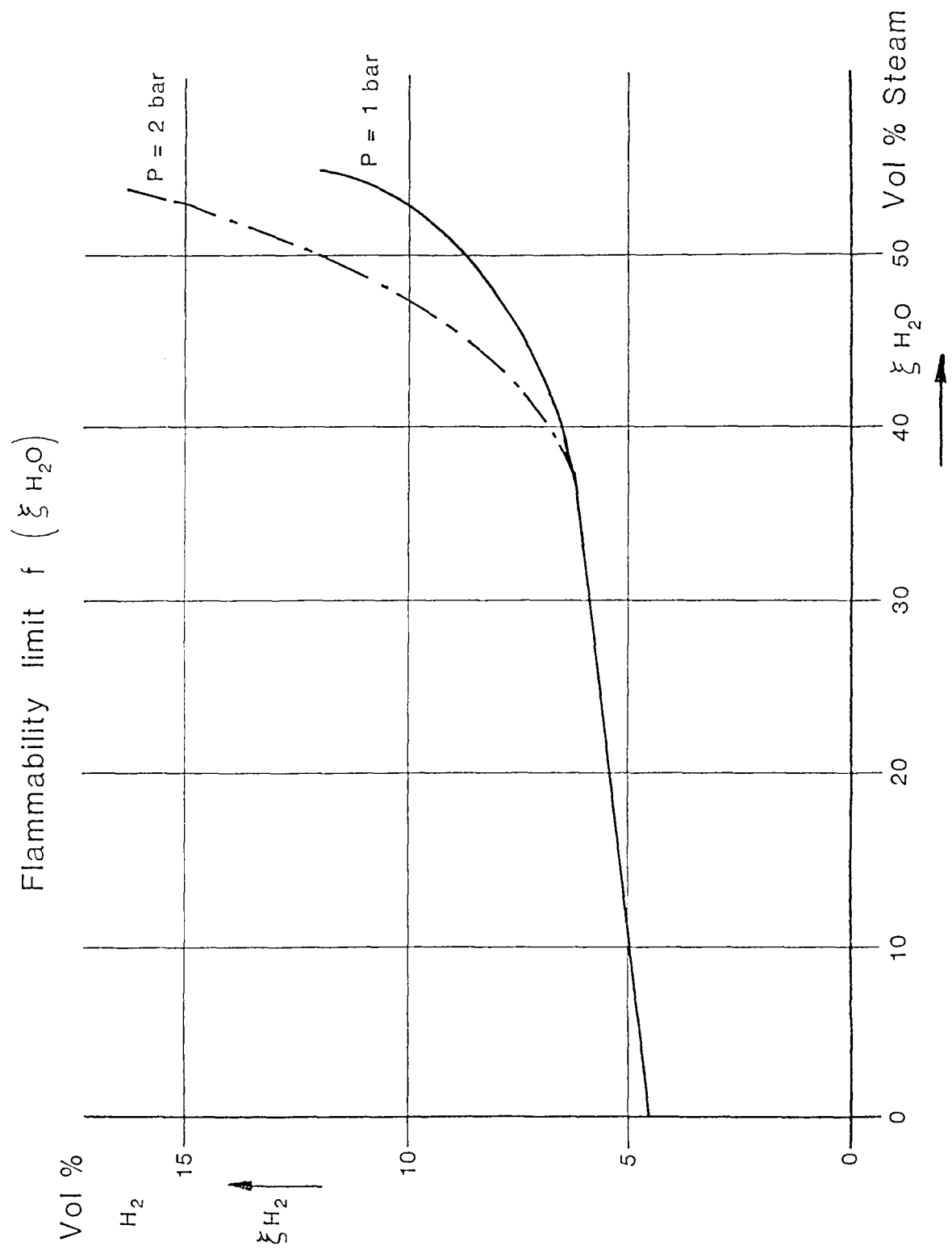


Fig. 6.60: Flammability Limits of hydrogen concentrations in relation to steam concentrations at 1 and 2 bar absolute pressure

# OECD Standard Problem ISP-29

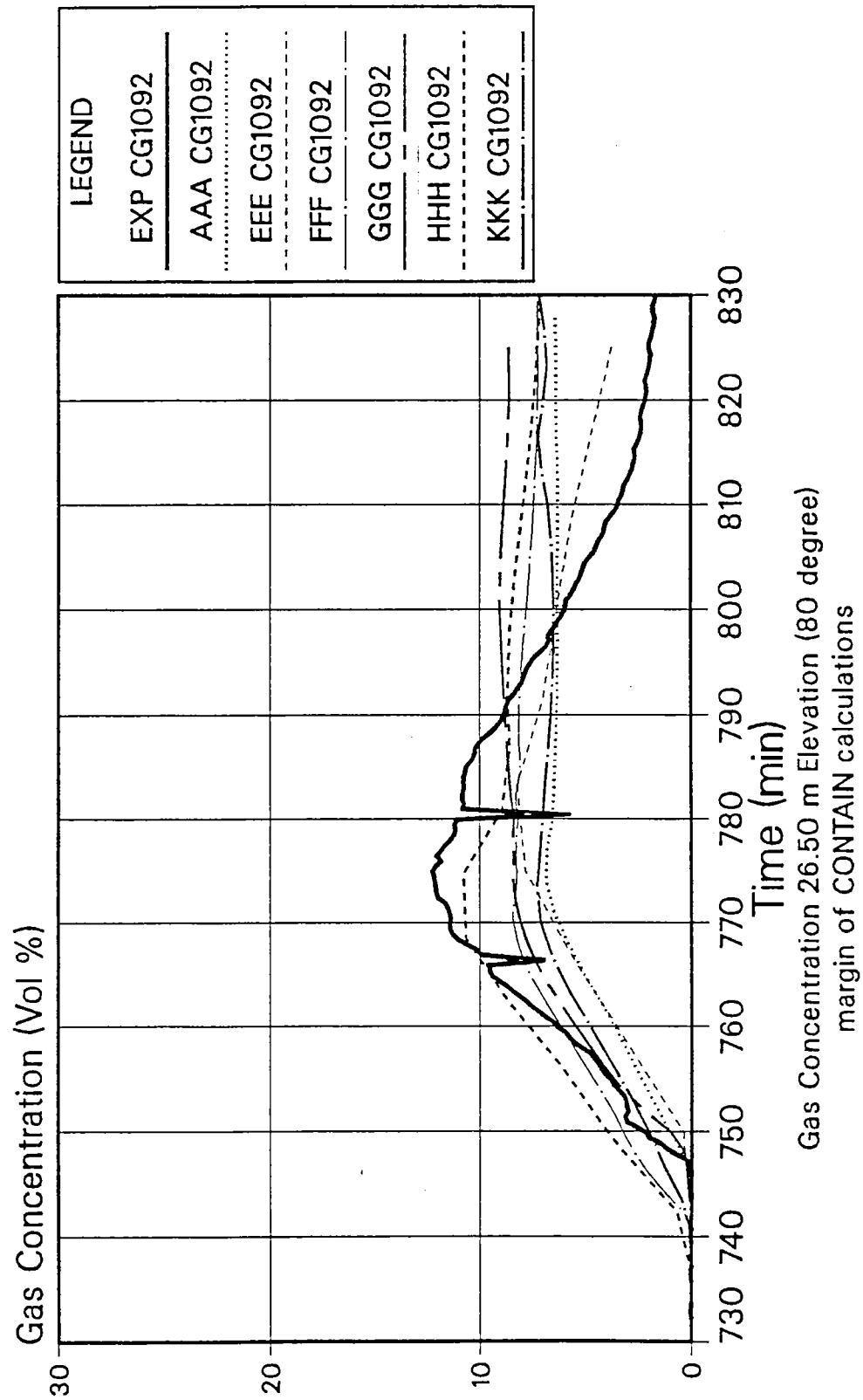


Fig. 6.61

# OECD Standard Problem ISP-29

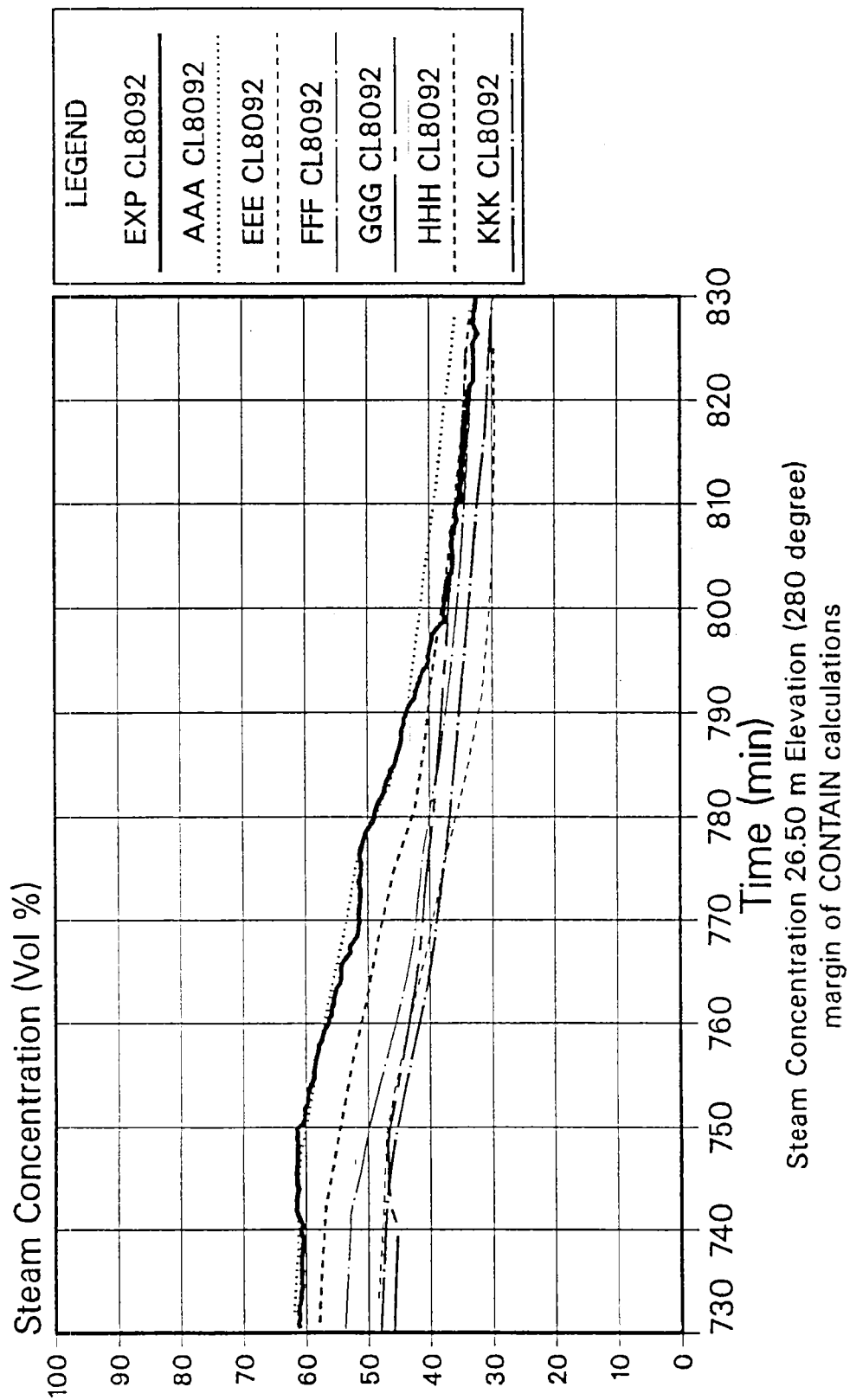


Fig. 6.62

# OECD Standard Problem ISP-29

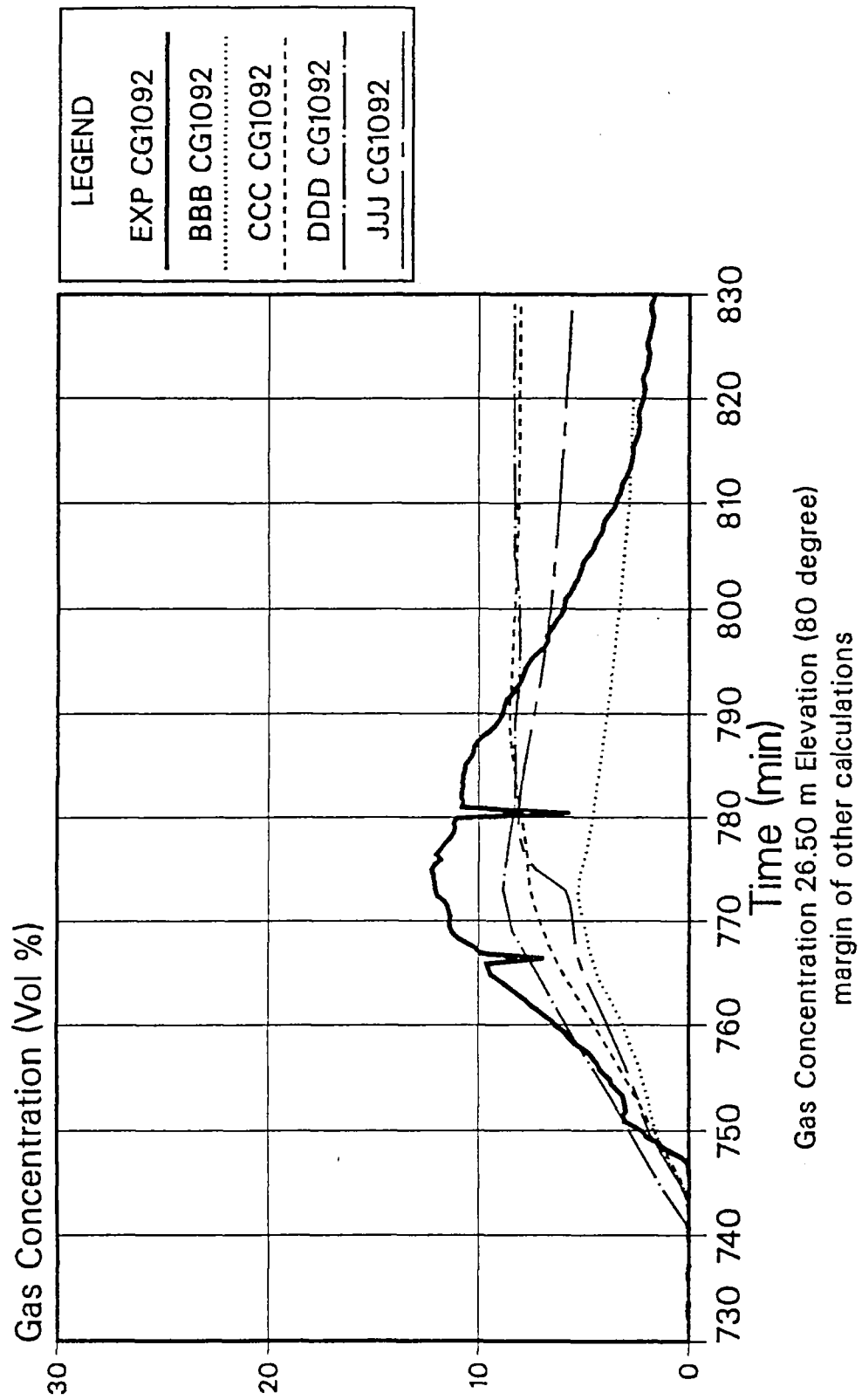


Fig. 6.63

# OECD Standard Problem ISP-29

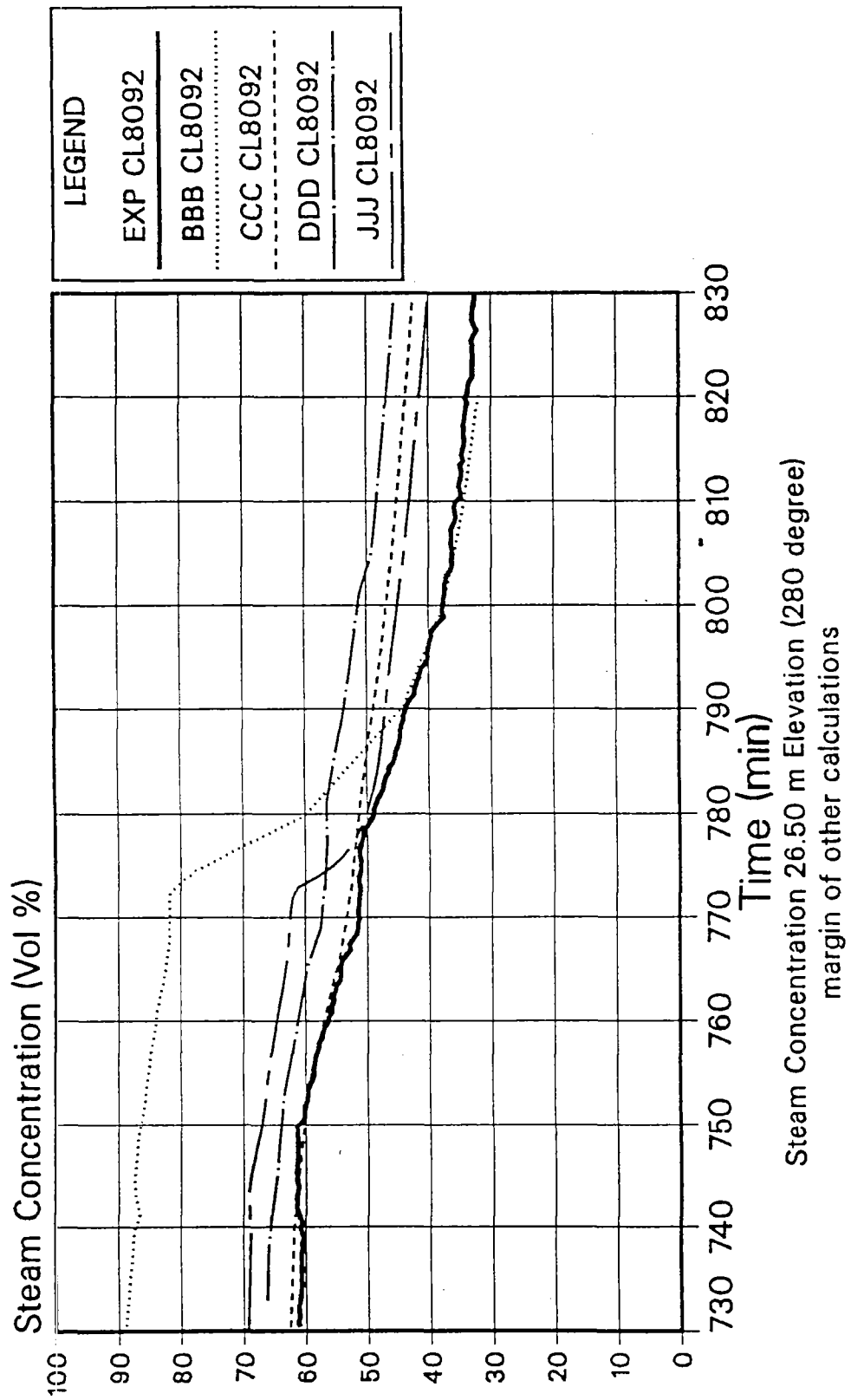


Fig. 6.64

**OECD Standard Problem**

**OECD-CSNI-ISP 29**

**"Distribution of Hydrogen within the  
HDR-Containment under  
Severe Accident Conditions"**

**- Final Comparison Report -  
Appendices**

**H. Karwat  
Lehrstuhl für Reaktordynamik  
und Reaktorsicherheit  
Technische Universität München**

**August 1992**

## Appendix I

### Summary Description of the Involved Codes

Five different codes have been utilized to generate Analytical Simulation Models for the re-calculation of the HDR-experiment E11.2. It appears useful to summarize to a limited extent the main features of the involved codes. For detailed description of the codes the readers are advised to consult the referenced literature.

#### 1. THE FUMO-CODE

The FUMO computer code has been developed at the DCMN of Pisa University (Italy). Its purpose is the study the thermal-hydraulic transient processes following a LOCA or a severe accident in a LWR containment system, through a multicompartment simulation model /A1/. FUMO is derived as a lumped parameter computer code: its fluid-dynamic model is based on mass and energy balances in the control volumes and, for the short and medium term only, also on momentum balance at the junctions linking the nodes. It is possible to simulate the mass and energy blowdown of steam and gas (six different species) and the effects of a spray water injection. Blowdown isentropic or isenthalpic expansions are simulated, together with the associated deentrainment of the liquid droplets.

The thermodynamic conditions in the volume (maximum 100) can be described by the following options:

a stagnant homogeneous mixture of steam, liquid water and air in thermal equilibrium;

a two region model consisting of a homogeneous air/water mixture region (atmosphere) and a liquid pool region. The pool region may or may not be in thermal equilibrium with the atmosphere;

the same model of option 2, but considering a homogeneous mixture of 6 gases instead or air.

Option 1) is used in the first phase of the transient, following the mass and energy into the control volume, that causes homogenization of the control volume through the high induced turbulence. Options 2) and 3) allow one to take into account the separation between the liquid and the vapour phases and their mutual interactions. The code allows to switch between the two options during the transient.

The six simulated gases (Ar, CO, CO<sub>2</sub>, H<sub>2</sub>, N<sub>2</sub> and O<sub>2</sub>, chosen among the most significant in a severe accident scenario) could be present in the control volume from the beginning or their production could be simulated with input blowdown tables.

The control volumes are linked together by "junctions" (maximum 200): the flow area can be time dependent. It is also possible to model:

- pressure dependent junctions, which are opened by pre-set values of the pressure differences between the two volumes linked by the considered junctions;
- junctions that have the inlet or/and the outlet submersed by the water sump eventually present in the source or/and in the receiver control nodes. This option permits an analysis of the pressure suppression containment systems or the description of the water management in the new more intrinsically safe and simplified LWRs.

The junction flow rate is calculated as follows:

The Bernouilli equation is solved for the evaluation of pure water flow rate.

The momentum balance equation (usually used in DBA computer codes) is solved for transients characterized by rapid thermo-fluiddynamic variations. The method requires small time-steps and therefore it is not advisable in a long term transient owing to the need for considerable CPU time. The flow rate through the junctions is evaluated choosing one of the following models:

- Moody critical flow;
- homogeneous inertial flow;
- orifice polytropic flow.

In order to study the long term phase of the simulated accident, a model is used which considers the pressure differences among the control volumes as negligible; the junction flow rates are evaluated in such a way that the pressure in the connected compartments is balanced. This option turns the FUMO programme into a fast running code. A large number of control volumes, connected even in complex ways, can be used to describe the containment.

A natural circulation model allows to consider the buoyancy driven flow, both in serial volumes as in complex loops that are present inside the system. For two serial volumes



the flow rate at the junction is given by:

$$Q_{nc} = \frac{A}{2} w \rho_h = \frac{A}{2} \rho_h \sqrt{2g \frac{\rho_c - \rho_h}{\rho_h} \frac{H}{1 + \lambda \frac{H}{D} + \sum \lambda_i}}$$

For a complex loop the flow rate formula structure depends on the loop volumes number; i.e. for four volumes, the loop mass flow rate is given by:

$$Q_{nc} = A \sqrt{\frac{2g \bar{\rho} (\rho_{34} \Delta H_{34} - \rho_{12} \Delta H_{12})}{1 + \lambda \frac{H}{D} + \sum \lambda_i}}$$

where:

A	=	junction area
D	=	junction hydraulic diameter
g	=	gravity acceleration
H	=	differential elevation
$Q_{nc}$	=	natural circulation mass flow rate
$\rho_c$	=	cold fluid density
$\rho_h$	=	hot fluid density
$\rho_{ij} \cdot \Delta H_{ij}$	=	integral of density along the branch i-j
$\rho$	=	average density at the junction
w	=	fluid velocity at the junction
$\lambda$	=	distributed pressure drop coefficient
$\lambda_i$	=	local pressure drop coefficient

Additionally, a simplified model that simulates the hydrogen vertical distribution in a control volumes is implemented in the code. This model is utilized in the natural circulation scheme, to modify the hydrogen mass fraction of the junction flow rate related to the elevation of the junction of the source volume.

Particular care is given in the code to the flexibility in modelling the heat structures and the heat transfer coefficients. The temperature distribution inside a single thermal structure is evaluated solving the Fourier equation by a finite difference method or with a coarse-mesh method, specifically developed at the DCMN of Pisa University /A2/.

## 2. THE CONTAIN-CODE

CONTAIN is an integrated analysis tool for the physical, chemical and radiological conditions inside a containment building, following the release of radioactive material from the primary system in a severe reactor accident /A3/.

The code is a modular code (based on the lumped parameter concept) which can simulate problems which are either quite simple or highly complex. It is also able to model both Light Water Reactors (LWR) as well as liquid metal reactors. The interactions among the various thermal hydraulic phenomena, aerosol behaviour and fission product behaviour are also taken into account.

The code includes atmospheric models for steam/air thermodynamics, intercell flows, condensation/evaporation on structures and aerosols, aerosol behaviour, hydrogen burning, sodium/atmosphere chemistry, sodium-spray fires and sodium-pool fires. It also includes models for reactor cavity phenomena such as core/concrete interactions and coolant-pool boiling. Heat conduction in structures, fission product decay and transport, radioactive heating and the thermal hydraulic and fission product decontamination aspects of engineered safety features are also modelled. In particular, containment sprays, fan coolers and ice-condensers are incorporated in the engineering safety systems together with storage tanks, pumps, orifices, pipes and valves which can restrict the supply of the sprays etc.. A safety relief valve discharge model is also included.

The code can also be used to predict the source term to the environment.

Similar to other codes, CONTAIN uses a system of control volumes and interconnecting flow paths to model a containment building. Each control volume is specified by a volume and a height relative to other control volumes. The control volume may have a coolant pool specified in which coolant is collected from structure runoff and bulk condensation. The atmosphere of the control volume may contain steam, non-condensable gases, airborne aerosols (comprised of solid, liquid, soluble and insoluble aerosol components) and radioactive particles.

Intercell flows are calculated using a one-dimensional flow equation which incorporates inertia, friction losses and gravitational heat terms. The equations are solved using an implicit

algorithm (which includes all the thermodynamic and aerosol interactions), and this is coupled explicitly to the heat transfer to the structures.

The mass and heat transfer simulation applied in the code is taking into account conduction, condensation/evaporation, convection (forced and natural) and radiation. Structures can have their surfaces connected to different control volumes, simulating the conduction of heat from one control volume to another. Structures can also be connected together.

### **3. THE MELCOR-CODE**

MELCOR is a fully integrated, relatively fast-running code which models the progression of severe accidents in Light Water Reactor nuclear power plants. Characteristics of severe accident progression that can be treated with MELCOR include the thermal hydraulic response in the reactor coolant system, reactor cavity, containment, and confinement buildings. MELCOR has been developed at Sandia National Laboratories for the US Nuclear Regulatory Commission (NRC) to succeed the Source Term Code Package /A4/.

MELCOR uses a control volume and junction approach to model the coolant thermal hydraulics of both the reactor coolant system and containment. Coolant includes liquid water, steam and non-condensable gases.

A pool of water and an atmosphere may reside in each control volume. The pool fills the portion of the control volume and may consist of either single phase liquid water or a two phase mixture of steam and water. The atmosphere occupies the remainder of the control volume and may contain steam, non-condensable gases, and suspended aerosols composed of liquid water (fog), non-radioactive solids and radioactive solids. The geometry within each control volume is defined by a table that the coolant volume as a function of altitude. This volume altitude is changed as other materials move into or out for the control volume.

Control volumes are connected by flow paths. The manner in which control volumes may be connected is not restricted; a given control volume may be connected at various locations to an arbitrary number of other control volumes, and parallel flow paths between control volumes are permitted. There is no mass, energy, or residence time associated with a flow path. Mass and energy subtracted from the upstream control volume are immediately added to the downstream control volume.

If a pool only partially covers the entrance to a flow path, pool water and atmosphere flow may simultaneously pass through the flow path allowing different velocities including countercurrent flow situations. The flow velocities are calculated based on control volume pressures, gravitational heat terms, fluid inertia, and flow path friction losses. Kinetic energy and the related momentum flux term in the flow equation are neglected.

The equations for pool and atmosphere flow in a flow path are obtained from line integrals of the acceleration equations along a stream line from the center of the "from"-volume to the center of the "to"-volume. The results (in non-conservative form) are:

$$\rho_{\phi} L \frac{dv_{\phi}}{dt} = \Delta P + \rho_{\phi} g \Delta z + K \rho_{\phi} \frac{|v_{\phi}| v_{\phi}}{2} - FLv_{rel} + \Delta P_{pump}$$

where:

$\rho$	is the average density,
$\phi$	refers to the material under scrutiny, pool water or atmosphere constituent,
$L$	is the inertial length of the flow path,
$v$	is the average velocity in the flow path,
$\rho g \Delta u$	accounts for static head terms across the flow path,
$K$	is a loss coefficient that includes all form loss and wall friction terms,
$FLv_{rel}$	represents the interfacial force between the pool water and the atmosphere constituents
$\Delta P_{pump}$	accounts for any pumps in the flow path.

Natural circulation flow patterns are calculated by MELCOR based on the control volume and flow path input data and the driving forces predicted by the thermal hydraulic models. A choked flow model is included.

Heat structures simulate the thermal response of the structures and mass and heat transfer between structures and the pools and/or atmospheres present within a specified control volume. Conduction, condensation, convection and radiation are taken into account. Degassing of unlined concrete is also modelled. The MELCOR heat structure package calculates heat conduction within an intact, solid structure and energy transfer across its boundary surfaces into control volumes.

Finite difference equations are used to approximate the heat conduction equation within each specified heat structure and at its boundary surfaces. These equations are obtained from the integral form of the one-dimensional heat conduction equation and boundary condition equations utilizing a fully implicit numerical method.

#### 4. THE GOTHIC-CODE

GOTHIC is a general purpose thermal hydraulics computer program for design, licensing, safety and operating analysis of nuclear containments and other confinement buildings. The code is the result of a long term effort that began with the development of COBRA-NC /A5/, continued with the addition of modelling features and capabilities in FATHOMS /A6/, and is now under EPRI sponsorship for further development and assessment. GOTHIC is currently being used by many utilities and research facilities in a wide variety of applications. The code includes a graphical pre- and post-processor that makes GOTHIC especially useful on PCs and engineering work stations.

GOTHIC solves mass, momentum and energy balances for three separate phases, vapour, liquid and drops. The vapour phase can be a mixture of steam and non-condensable gases and a separate mass balance is solved for each component of the vapour mixtures. An ice phase is also included for ice-condenser containment analysis. The phase balance equations are coupled by mechanistic models for interface mass, energy and momentum transfer that cover the entire flow regime from bubbly flow to film/drop flow as well as single phase flows. The interface models allow for the possibility of thermal non-equilibrium between the phases and un-equal phase velocities.

The code can be used for three-dimensional analysis of the thermal hydraulic behaviour of containment atmospheres and structures. A containment compartment can be modelled using a 1-, 2- or 3-dimensional rectangular grid. Many containment problems cover long periods of real time so that a finely noded multidimensional model may be impractical. For these problems a simpler lumped parameter analysis may be used. Lumped parameter volumes are connected by junctions that employ a one-dimensional model for flow between containment compartments. A combination of lumped parameter and three-dimensional analysis is also possible, with regions of special interest modelled in more detail while lumped parameter volumes are used to model the remaining regions.

GOTHIC includes full treatment of the momentum transport terms in multidimensional models with an optional one parameter turbulence model for turbulent shear and mass and energy diffusion. Thermal conductors model heat transfer surfaces in the containment. Wall heat transfer correlations are incorporated for a wide range of heat transfer situations, including condensation heat transfer with the effects of non-condensable gases. Special models for engineered safety equipment including pumps, fans, valves, heat exchangers, coolers and vacuum breakers are included. Trip logic is used to control the action of the safety equipment in response to changes in the containment atmosphere.

The main model features of the code GOTHIC are listed as follows:

- 4 conservation of mass equations
- 3 conservation of momentum equations for each of the 3 directions for the 3-D field model
- 3 conservation of energy equations
- conservation of mass for every gas component
- semi-implicit finite difference procedure with time-step size limitation given by Courant conditions
- pressure, density, temperature, concentrations cell centred (volume-averaged) velocities at cell interfaces
- mass and energy balances are performed for control purposes at every time-step
- implicit heat conduction solver

A variety of code elements for geometric modelling is available (sections, channels, vent flows, multiple connections are possible between zones, control volumes, unheated thermal conductors, heated conductors)

Several components and process simulators can be utilized for the analysis (spray system inside containment, fans, coolers, heat exchangers, pumps, valves, vacuum breakers, pools, pressure-suppression systems, reactor pressure vessels, ice-condenser, structures, non-condensable gases, metal-water reactions).

## 5. THE CODE RALOC-MOD 2.2

The code RALOC /A7/ was originally developed to calculate Radiolysis and local Gas-Concentrations within the containment. It is a so-called lumped parameter code where in a single zone the fluid has uniform thermodynamic properties and the fluid components have individual but homogeneous concentrations within a zone during each time step.

Changes of the states which are related to location and time will be traced back to a purely time dependent behaviour within one node.

In between the code has been further developed and frequently applied to calculate thermodynamic loads and local gas concentrations in multicompartimented containments or buildings of various kinds of facilities but especially for LWR nuclear plants during

- LOCA (DBA)
- Severe Accidents
- Fires

Also calculations of fluid release through possibly opened flow paths or leakages out of the containment during severe accidents have been performed.

For the description of the physical processes as for example the process of hydrogen distribution or impacts of fire, arbitrary compartment arrangements and geometries can be simulated by control volumes (subdivision is arbitrary, but presently limited to 100 volumes). These volumes (nodes) will be connected with junctions. The number of junctions is arbitrary but presently limited to 200. For the simulation of heat transfer and heat conduction through the walls and internals, an arbitrary number of structures (presently limited to 500 heat slabs) can be assigned to the nodes. The inner walls, pipelines and other internals, partitions and outer walls can all be modelled.

The nodes are defined by a set of data (volume size, relative positions (height location of the volume centre), initial state (temperature, pressure etc.) and mutual connections of the zones). The junctions between the nodes are defined with the declaration of type of junction (gas, liquid), nodes connected, cross sections, junction length, different flow loss coefficients for positive and negative flow directions, and the specification of options for opening at given differential pressures. Heat slabs are defined with the declaration of the nodes

coupled to both sides of the defined structures, the type of structural geometry (plate or cylinder), its surfaces, thickness, layer arrangements and material properties.

For the definition of the states of the volumes, the following model assumptions have been made:

- 4 gas components can be considered: steam as a real gas with the changes of states according to steam table. 3 arbitrarily chosen other gases are considered as ideal gases. These gases can be fixed with their inputs of molecular weights, their gas constants, their diffusion constants and with their specific heats.
- Steam will be considered as gas and/or liquid (water) corresponding to the states of the zones. Superheated as well as saturated conditions are possible.
- Gas components within the zones are assumed to be homogeneously mixed. They are in thermodynamic equilibrium i.e. they all have the same temperature.
- Thermodynamic non-equilibrium with the water phase can be simulated with the definition of a separate sump node.

Equations of mass- and energy balances are solved for each zone yielding the transient mass- and temperature changes for all components.

Mass transport between the zones is calculated for both, gas and liquid flow, with the momentum equation (unsteady) considering the geodetic elevation differences. Partial mass flows of components result from the compositions of the source zones. Furthermore, the mass exchange resulting from the diffusion processes is considered. The diffusion will be calculated separately under steady-state conditions for all the components existing in gas form.

In order to describe the energy transport from the zones to structures, the heat transfer is simulated considering

- convection according to the correlation of Gröber, Erk, Grigull /A8/
- radiation of the gas due to the correlation of Schack, Hottel and Egbert /A9, A10/
- condensation according to Fick's law regarding diffusion processes through the boundary layer



as functions of the changing properties of the zones and structures.

Heat conduction is described in one dimensional form by the solution of the Fourier equation. Any material can be simulated by the input of heat conductivity, specific heat capacity and the specific density.

Walls and internals can be characterized by the geometries of plates and/or cylinders. A structure can be built with maximum 3 different materials and can be separated from each other with variously thick air layers. Each material can be subdivided into an arbitrary number of layers of different densities. Subdivisions of layer thickness can be treated either automatically and equidistant or automatically with progressive growth towards the centre of the structure or by free subdivision according to input.

Also simulations of technical systems are possible as: pumps, heat exchangers, fans, vent pipes, weirs, valves, doors, spray systems, thermal recombiners. The numerical solution is either explicit or implicit and the code has a restart capability.

RALOC-MOD 2.1 meanwhile has been developed further into version MOD 2.2. The essential characteristics of this further development are:

- Heat transfer to the structures will now be solved simultaneously with other differential equations.
- Water transport can be calculated non-steady state with the momentum equation. Strong changes of the mass flow rate are damped by special functions.
- Injection or removal of two simultaneous and independent energy and steam sources.
- It is possible to simulate the door and flap opening process taking into account inertia effects.

## References

- [A1] A. Manfredini et al.  
Il codice GUMO: descrizione e manuale d'uso  
Dipartimento di Costruzioni Meccaniche e Nucleari - Pisa RL 416(89)
- [A2] W. Ambrosini et al.  
A One Dimensional Coarse-mesh Method for Conduction in Heat Structures  
International Journal of Heat and Technology, Vol. 6, 1988
- [A3] K.K. Murata et al.  
User's manual for CONTAIN 1..1, A computer code for severe nuclear reactor containment analysis revised for revision 1.11  
NUREG/CR-5026, SAND7087-2309, 1991
- [A4] R.M. Summers et al.  
MELCOR 1.8.0: A computer code for nuclear reactor severe accident source term and risk assessment analyses  
NUREG/CR-5531, SAND90-0364, Jan. 1991
- [A5] C.L. Wheeler et al.  
COBRA-NC: A thermal hydraulic code for transient analysis of nuclear reactor components  
NUREG/CR-3263, Vol. 1, 1986
- [A6] T.L. George, M.J. Thurgood  
CAP, Containment analysis package user's manual,  
Numerical Applications, Inc., 1987
- [A7] H. Jahn, E. Hofer  
Description of the MOD 2/85 Version of the RALOC/FIPLOC family  
Part 2: Physical modelling of thermal hydraulics and integration methods  
GRS-A-1426 (März 1988)
- [A8] Gröber/Erck/Grigull  
Die Grundgesetze der Wärmeübertragung  
3. Auflage, 1963 Springer
- [A9] H.C. Hottel and R.B. Egbert  
The Radiation of furnace gases  
Trans. Am. Soc. Mech. Eng., 1941
- [A10] K. Schack  
Berechnung der Strahlung von Wasserdampf und CO<sub>2</sub>  
Chem. Ing. Technik, 1970

## **Some sensitivity analyses of HDR hydrogen distribution experiment E11.2 with the CONTAIN 1.12 code**

**Ari Silde  
Technical Research Centre of Finland (VTT)  
Nuclear Engineering laboratory  
P.O.Box 208  
SF-02151 Espoo, Finland**

**tel. +358 0 4565039  
fax. +358 0 4565000**

## 1. INTRODUCTION

Some parameter studies have been performed at VTT with the CONTAIN 1.12 code to investigate the influence of dome nodalization and flow path modeling on hydrogen distribution in the HDR experiment E11.2.

## 2. COMPUTATIONAL MATRIX

Matrix of the performed parameter studies is shown in Table 1.

Table 1. Matrix of performed parameter studies.

	<u>Case A</u> (ISP-29)	<u>Case B</u>	<u>Case C</u>	<u>Case D</u>
Number of dome cells	12	44	44	44
Area of horizontal flow junctions in the dome	15 m <sup>2</sup>	5 m <sup>2</sup>	5 m <sup>2</sup>	1 m <sup>2</sup>
Modeled horizontal flow junctions between the dome cells	all	all	restric- ted *)	restric- ted *)

\*) "Restricted" means here that all of the horizontal flow junctions of the dome are not taken into account.

In addition, one analysis was performed with the same assumptions as Case A, but using the same value of flow loss coefficients for the whole containment.

## 3. SOME RESULTS

### 3.1 Flow loss coefficients

Investigations have shown that use of the same value of coefficients for the whole containment yields totally wrong direction of the flow in the stair case and spiral case during the steam injections in the lower part of the HDR containment. This may be caused partly due to the lack of modeling detail geometry, specially near the injection location. In the CONTAIN calculations a relatively high value of 20,0 was thus used for loss coefficient of some flow junctions to prevent a wrong-direction flow pattern (the flow will be greatest in the path of least resistance). Experimental and predicted flow velocities at the +20 m elevation in the spiral case are presented as example in Figure 1 using equal loss coefficients for the whole containment and using modified coefficients. The influence of loss coefficients on the predicted flow direction can be seen also in Figure 2. Generally, the determination of

loss coefficient is very difficult for a very complicated geometry like the HDR containment has.

### 3.2 Dome modeling

In the blind calculation for E11.2 performed with the HECTR code at VTT the gas space conditions of the dome were predicted to be totally homogeneous. This was not the case in the experiment. These discrepancies are assumed to be caused partly by the unrealistic high circulating flows predicted.

The influence of circulating flows on gas mixture behaviour has been investigated by reducing the horizontal gas mixing in the dome area. This can be easily done in CONTAIN e.c 1) by increasing the flow loss coefficients for horizontal junctions, 2) by decreasing the flow areas of the junctions or 3) by decreasing a number of modeled horizontal junctions.

Predicted upper dome (elevation +48 m) gas mixture concentrations of all investigated cases are compared with the experiment in Figures 3 and 4. Gas concentrations at the lower dome elevation of +31 m just above the stair case are presented in Figure 5.

In the ISP-29 calculation (Case A) a relatively high values of loss coefficient (20,0) was given for the horizontal dome junctions. Some gas mixture stratification was predicted in the dome area, but the degree of stratification was still clearly underestimated. No gas enrichment was predicted during the external spray cooling.

In Case B the dome was renoded by increasing a number of dome cells from 12 to 44 (Fig 6). Because relatively large junction areas may cause computational problems, the original flow areas in the dome were reduced by factor 5. Note that all of the modeled flow junctions are not presented in Figure 6. 44-cell dome model was used in all of the examined cases, except in Case A, which had 12-cell model. Containment nodalization below the dome area was similar in all analysed cases.

As seen in Figure 3 the 44-cell dome predicted some gas enrichment, but the 12-cell did not. Gas concentration is, however, clearly too low in both cases and gas stratification is underestimated in the dome area.

In Case C only some of the horizontal junctions were modeled in the dome area (Fig. 6: the horizontal junctions at the elevations with parentheses are not taken into account).

In Case D unrealistic small value of 1,0 m<sup>2</sup> was used for the flow area of the horizontal junctions. Only some of the horizontal dome junctions were modeled as in Case C. Case D was expected to have least horizontal dome gas mixing of all cases. Figure 4 shows that Case D predicted highest upper dome gas

concentration of all analysed cases, also during the external spray phase. Upper dome gas concentration is predicted fairly well just after the gas injection phase at 773 minutes, but after that the concentration is still underestimated.

Gas mixture concentrations of the experiment, ISP-29 calculation, and the Case D are presented in Figures 7, 8, 9 and 10 as a function of height in the containment stair case. Gas concentration profiles are presented at four different time points; 800, 975, 1050 and 1200 minutes. The profiles show that the results with the 44-cell dome model (Case D) match at each presented time points better the experimental data than the results with 12-cell dome model. Dome nodalization seems to have an slight influence also on the gas concentration in the lower part of the containment (Fig. 11).

Dome nodalization did not have remarkable influence on the stratification of containment temperatures and steam concentrations, when either 12 or 44-cell dome model was used.

Increase of the number of computational cells from 52 to 84 in the whole containment (corresponding the number of dome cells from 12 to 44) increased the computer-CPU-time requirement in the Cray X-MP computer by factor from 2.2 to 2.7, depending on the flow junction modeling.

#### 4. CONCLUSIONS AND RECOMMENDATIONS

Some conclusions of the performed parameter studies can be drawn as follows:

- a) CONTAIN underestimated the gas mixture concentration in the dome area and overestimated the concentration in the rest of the containment.
- b) 44-cell dome model predicted the gas concentrations in the whole containment, specially in the dome area, better than the 12-cell dome model did. 44-cell dome model predicted also some gas enrichment in the dome area during the external spray phase, but the gas concentration was still too low in the upper dome. Case D, which had least horizontal gas mixing in the dome, yields the highest gas concentration of all analysed cases in the upper dome.
- c) The discrepancies between the prediction and the experiment could not be solved with the dome nodalization.
- d) Uncertainties in instrument cooling power distribution and difficulties in determining flowpath loss coefficients may be some reasons for the discrepancies between the experiment and prediction.
- e) Use of the same value of the flow loss coefficients for the whole containment did not yield correct flow pattern in the HDR containment.

Based on the CONTAIN analyses the following recommendation

emerge:

- a) Influence of nodalization should be investigated in the whole containment, not only in the dome area as was done in the studies presented in this report.
- b) Strategies of flow path modeling e.g estimation of relevant loss coefficients for lumped-parameter code need more investigation.
- c) Experiment E11.2 was an extremely difficult task for computer codes (e.g relative high location of steam injection with the complicated multi-compartment geometry). It would be therefore useful to analyse also some other large-scale experiments to draw some overall conclusions of the code capability to analyse hydrogen distribution sequences in the geometries like the commercial nuclear power plant containments have.
- d) Because disagreement between the experiment E11.2 and calculations is partly due to the lumped parameter representation, the possibility to use also other than lumped-parameter codes (e.g 3-D FEM programs) for prediction of large-scale experiments should be more investigated.

## 5. WORK IN THE NEAR FUTURE

CONTAIN 1.12 will be used during summer 1992 in Kernforschungszentrum Karlsruhe to analyse also HDR experiment E11.3 and/or E11.4. A model of external dome spray system will be implemented on the CONTAIN code in the near future.

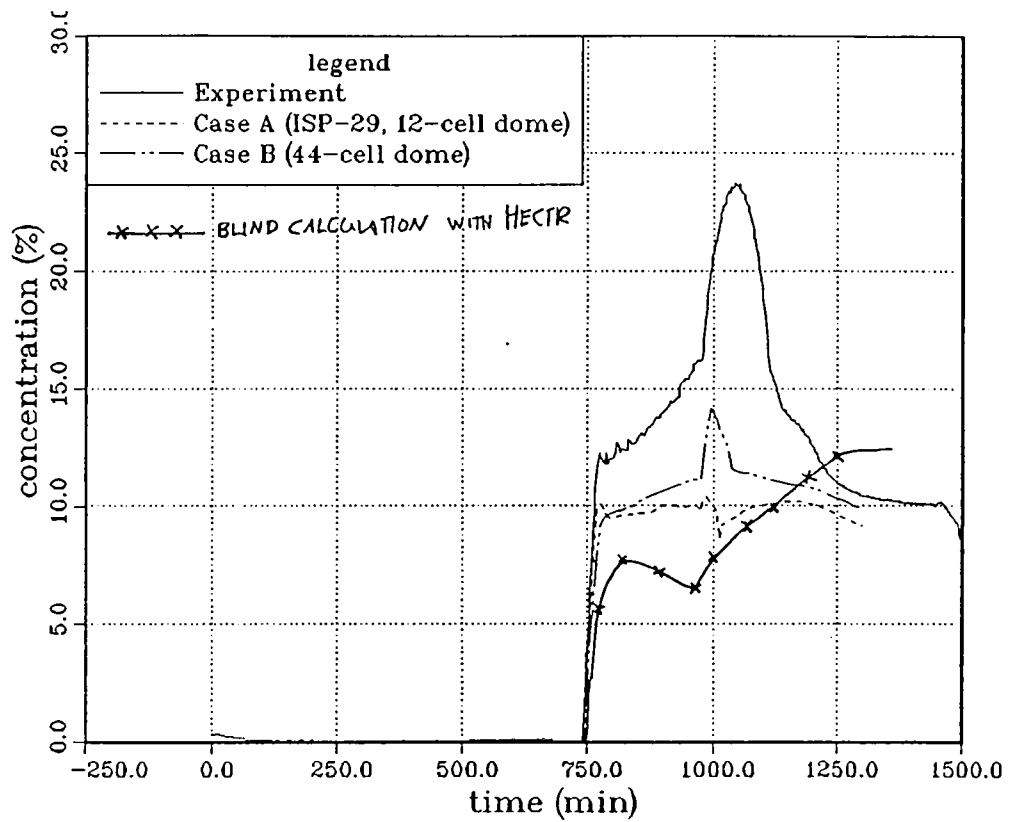


Figure 3. Gas concentrations in the upper dome (+48 m), Cases A and B.

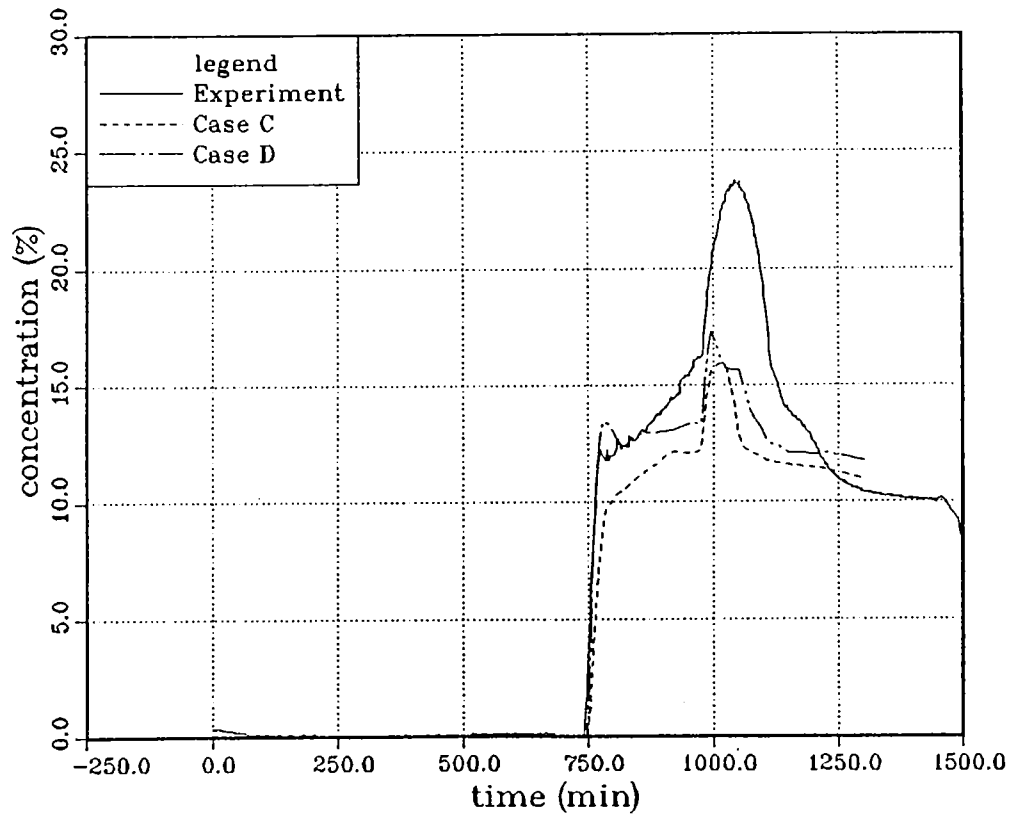


Figure 4. Gas concentrations in the upper dome (+48 m), Cases C and D.





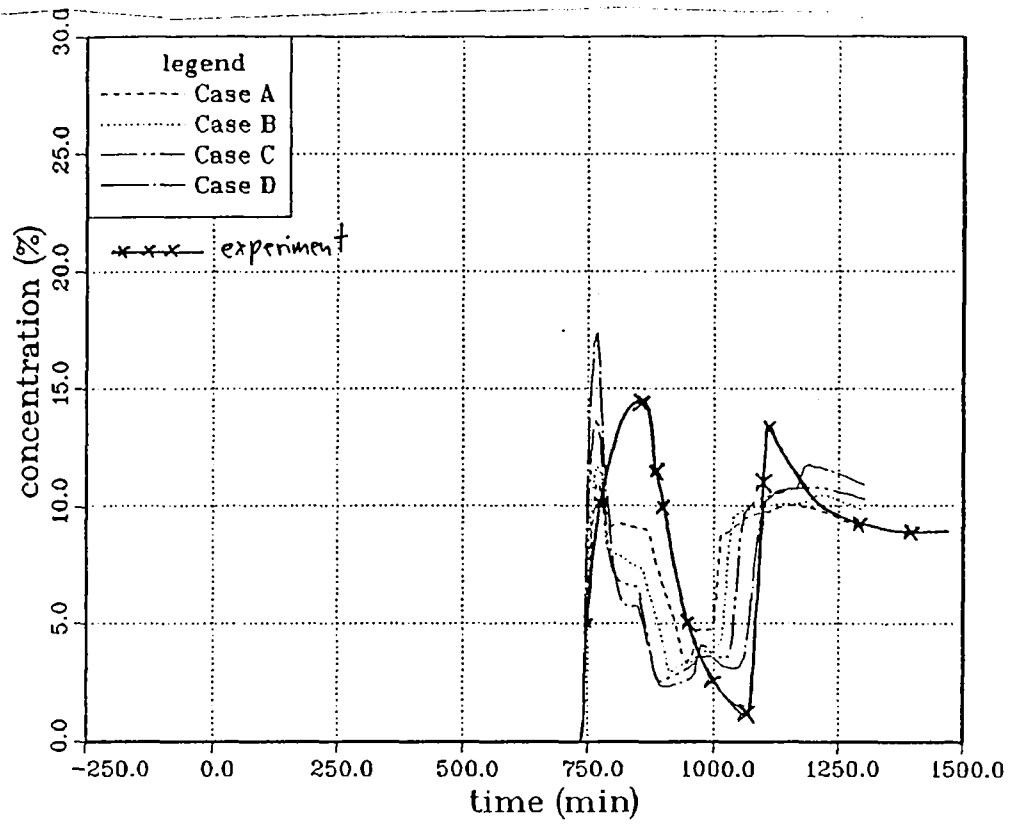


Figure 5. Gas concentrations in the lower dome (+31 m)

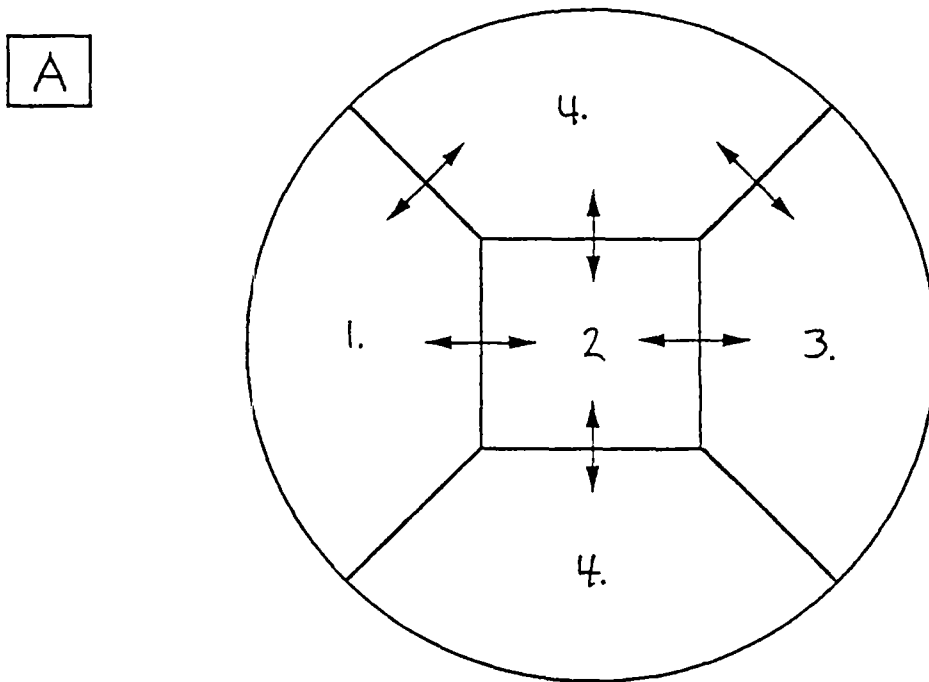
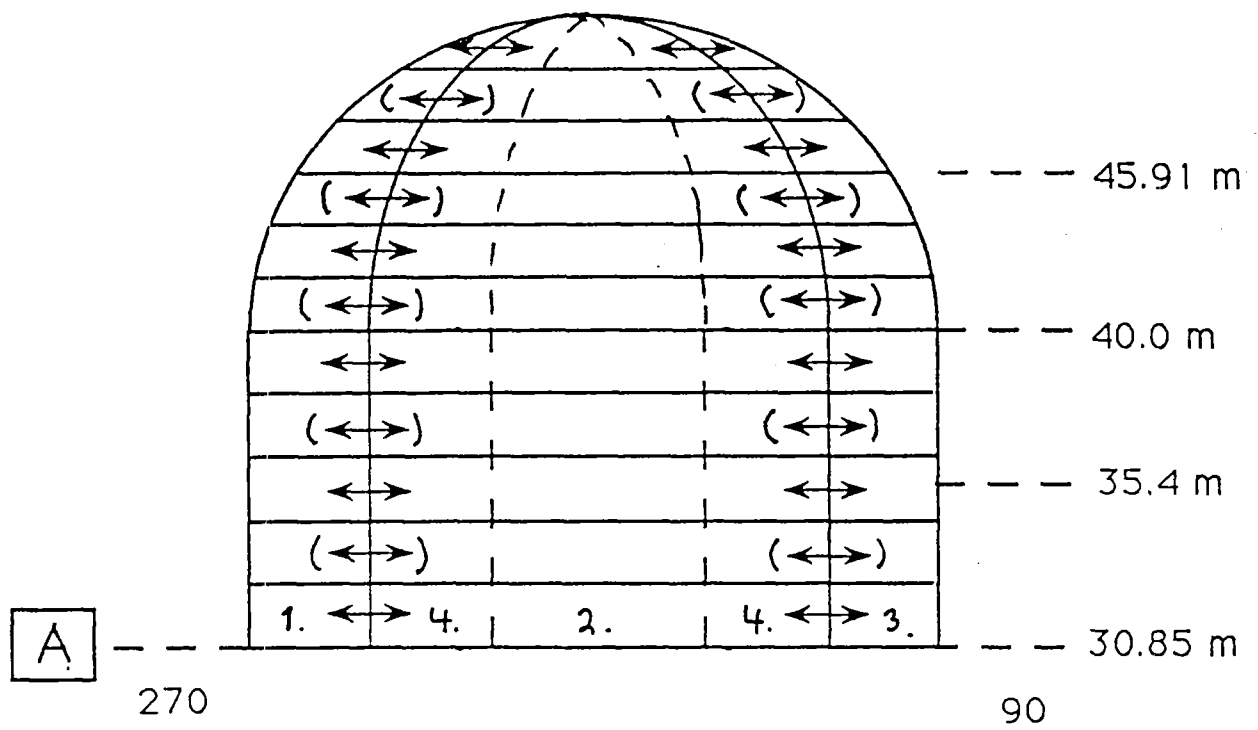


Figure 6. 44-cell dome nodalization.

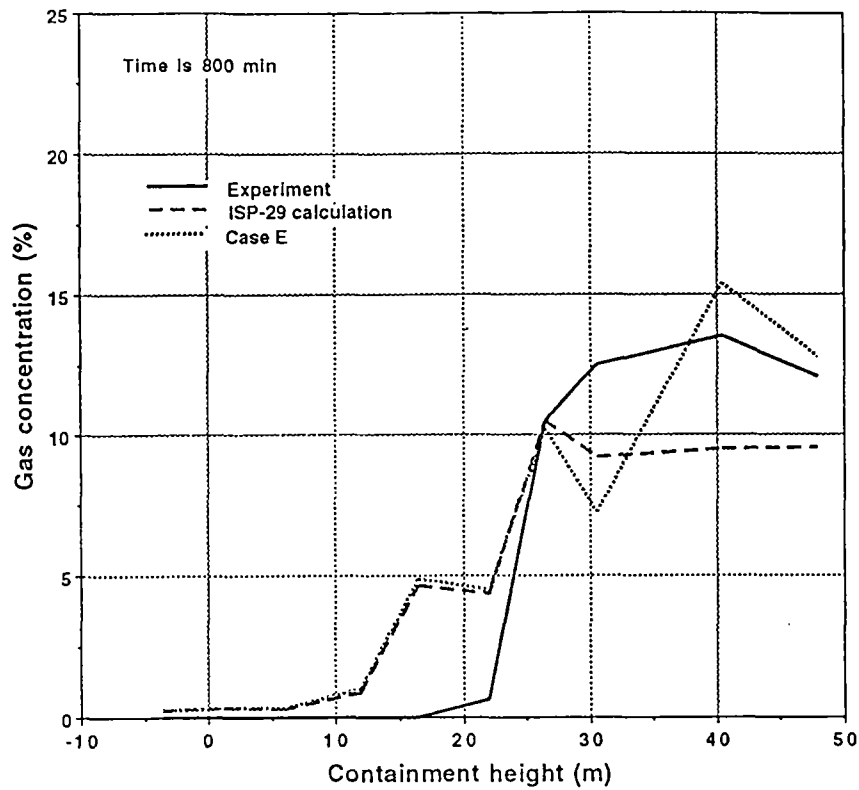


Figure 7. Gas concentrations in the stair case as a function of containment height (at 800 minutes).

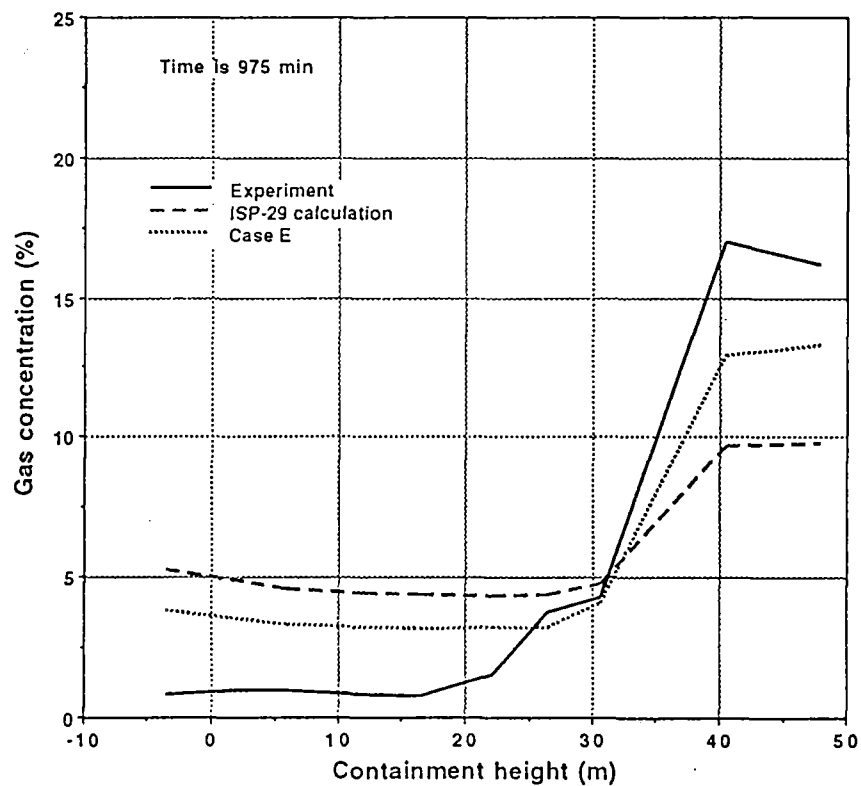


Figure 8. Gas concentrations in the stair case as a function of containment height (at 975 minutes).

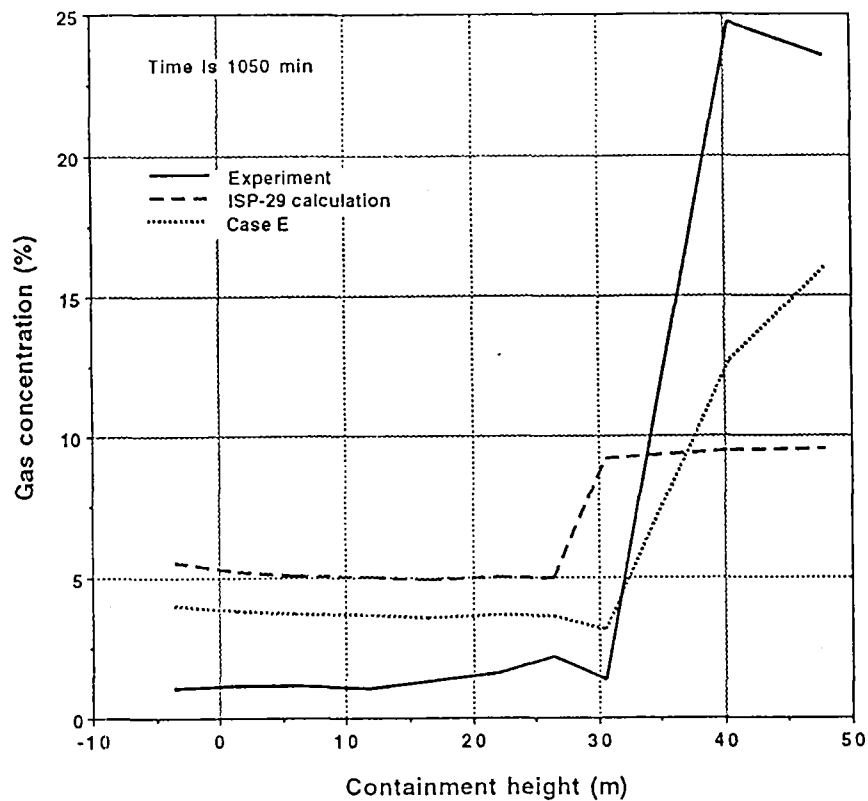


Figure 9. Gas concentrations in the stair case as a function of containment height (at 1050 minutes).

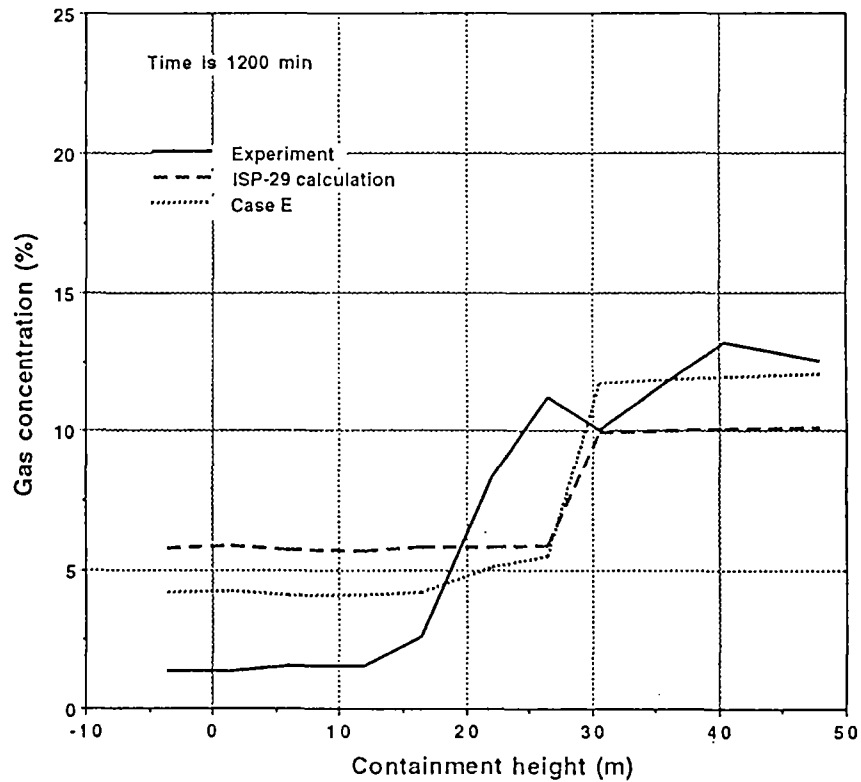


Figure 10. Gas concentrations in the stair case as a function of containment height (at 1200 minutes).

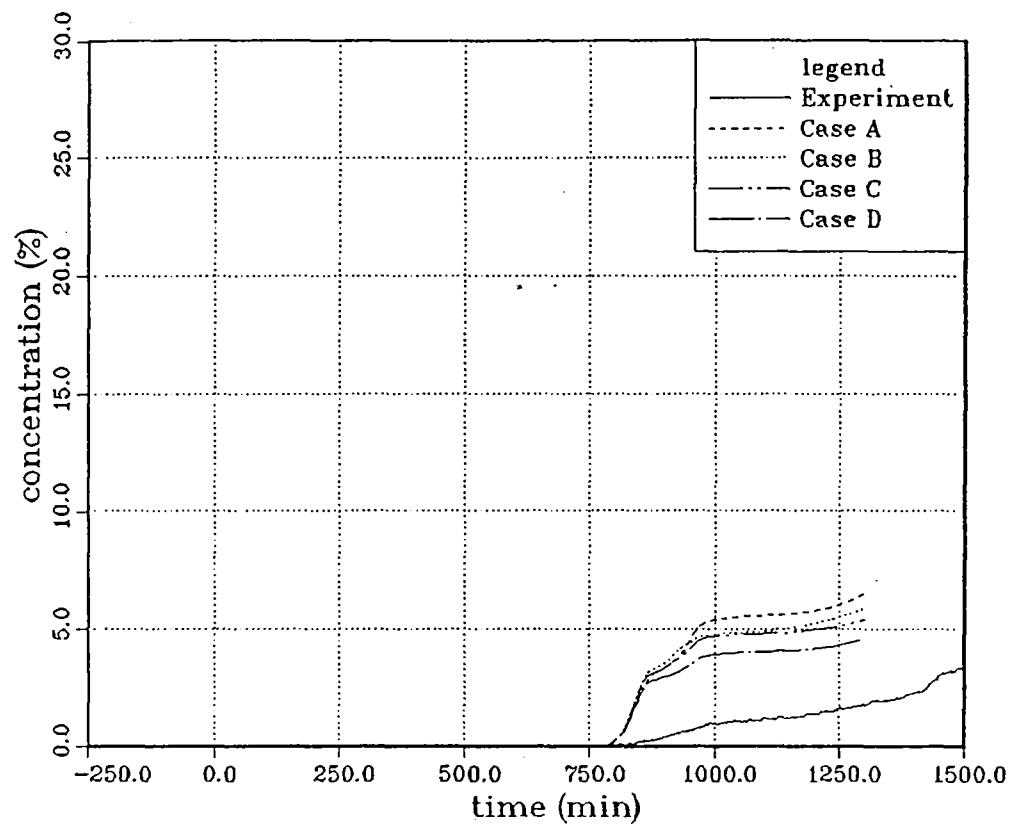


Figure 11. Gas concentrations in the lower containment (-4,5 m)

**Parametric Calculations  
for HDR-Tests E11.2 and E11.4  
with the  
GOTHIC-Code**

**Battelle-Institut e.V.  
Frankfurt am Main**

This appendix contains some results of parametric calculations for the HDR-tests E11.2 and E11.4.

The parameter studies are based on the blind post test calculations and have been performed to investigate the influence of some parameters on pressure, temperatures, and steam- and gas-distribution in the containment.

The investigated parameters were

- steam flow rates
- cooling power of instrument cooling system
- distribution of cooling power
- modelling of steel shell heat slabs
- HTC to internal structures
- HTC to annulus gap
- flow path modelling

The characteristics of the parameter studies are given in Table 1 for test E11.2 and in Table 2 for test E11.4.

Some of the most interesting results are shown in Fig. 1 - Fig. 10 for E11.2-studies, resp. in Fig. 11 - Fig. 15 for E11.4.

The full information about the parameter studies is given in Ref. /1/. Some results are also published in Ref. /2/.

### References

- /1/ H. Holzbauer  
Parametrische Nachrechnungen und Analysen zu den HDR-Wasserstoffverteilungsversuchen E11.2 und E11.4 mit dem Rechenprogramm GOTHIC  
Battelle-Institut e.V., Frankfurt am Main, BF-R67.706-1, Aug. 1992
- /2/ L. Wolf et al.  
Comparisons Between HDR-H<sub>2</sub>-Distribution Experiments E11.2 and E11.4  
19th US NRC WRSIM, Bethesda, MD, USA, Oct. 1991



**Table 1:****PARAMETRIC CALCULATIONS FOR TEST E11.2**

Run	Characteristics
Blind Post Test Calc.	HTC: To internal structures: Uchida * 3 To annulus gap: 100 W/m <sup>2</sup> K Total surface of steel shell in contact with containm. atmosphere External steam flow rates too high Without instrument cooling system
NA 1	Ext. steam flow rates corrected
NA 2	Instrument cooling system considered
NA 3	HTC to annulus gap 5 W/m <sup>2</sup> K
NA 4	Steel shell - heat slabs modelled as recommended by PHDR
NA 13	Junction areas along major flow paths 1/3 A <sub>nominal</sub>
NA 14	Junction areas along major flow paths 1/10 A <sub>nominal</sub>
NA 15	All junction areas 1/10 A <sub>nominal</sub>

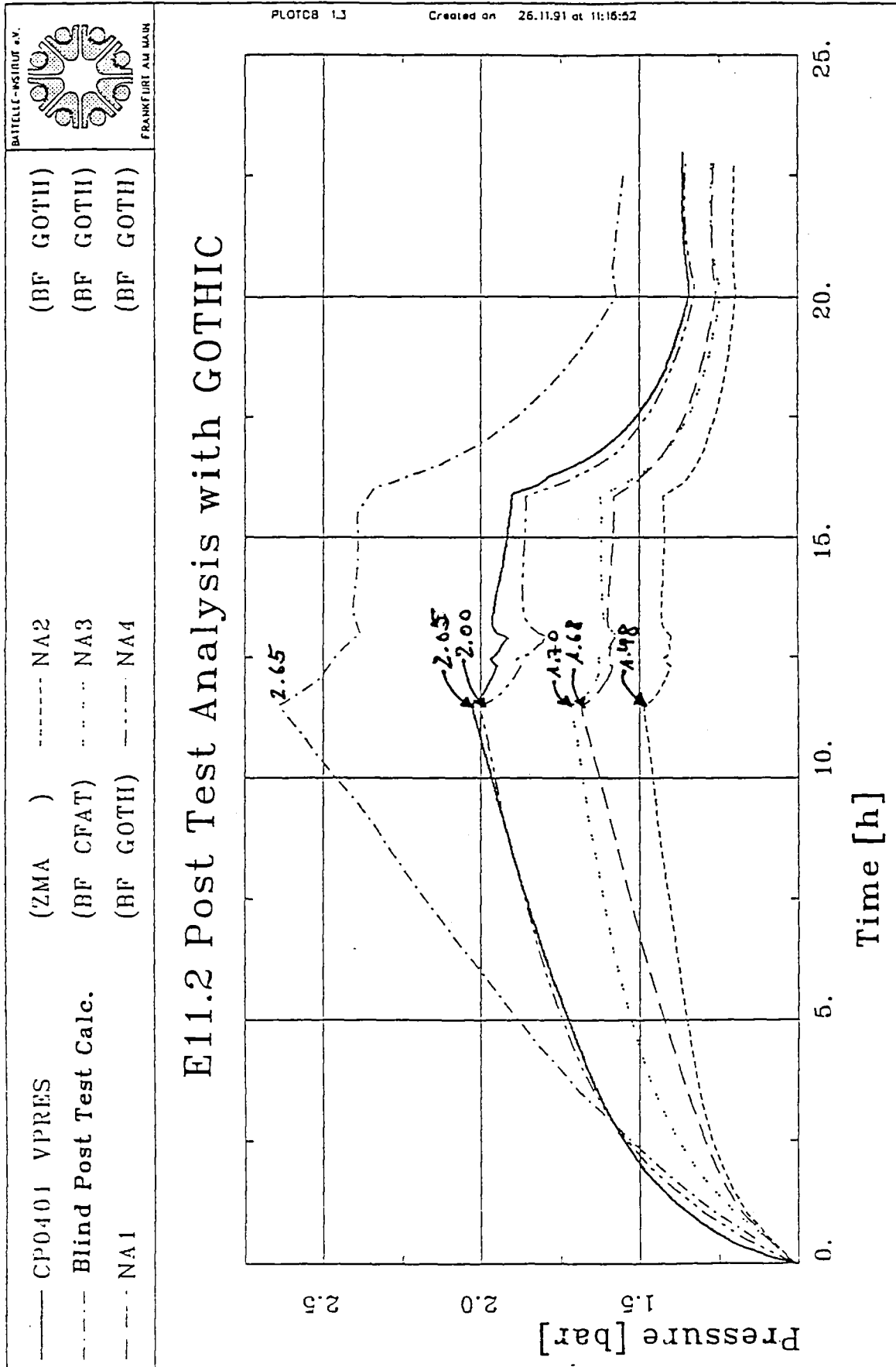
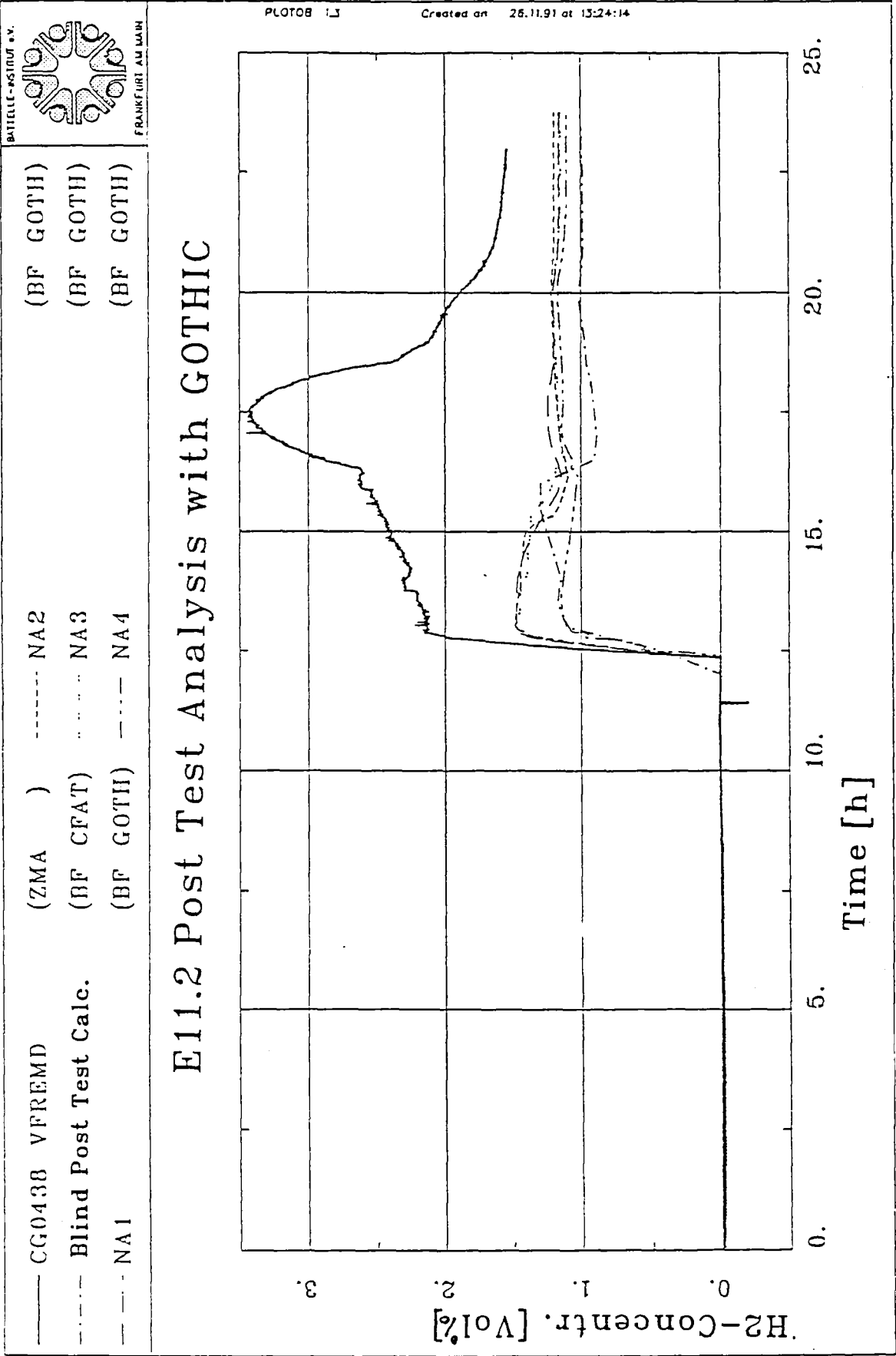


**Fig. 1 Pressure**



E11.2 Post Test Analysis with GOTHIC

Plot of H2-Concentr. [Vol%] vs Time [h]

Legend:

CG0438 VFREMD

Blind Post Test Calc.

NA1

(ZMA )

(BF CFAT)

(BF GOTH)

NA2

NA3

NA4

(BF GOTH)

(BF GOTH)

(BF GOTH)

Y-axis: H2-Concentr. [Vol%]

X-axis: Time [h]

Plot area showing multiple curves representing different simulation results over time.

Created on 26.11.91 at 13:24:14

PLOT08 13

Fig. 2 Hydrogen Concentration +48m (Dome)

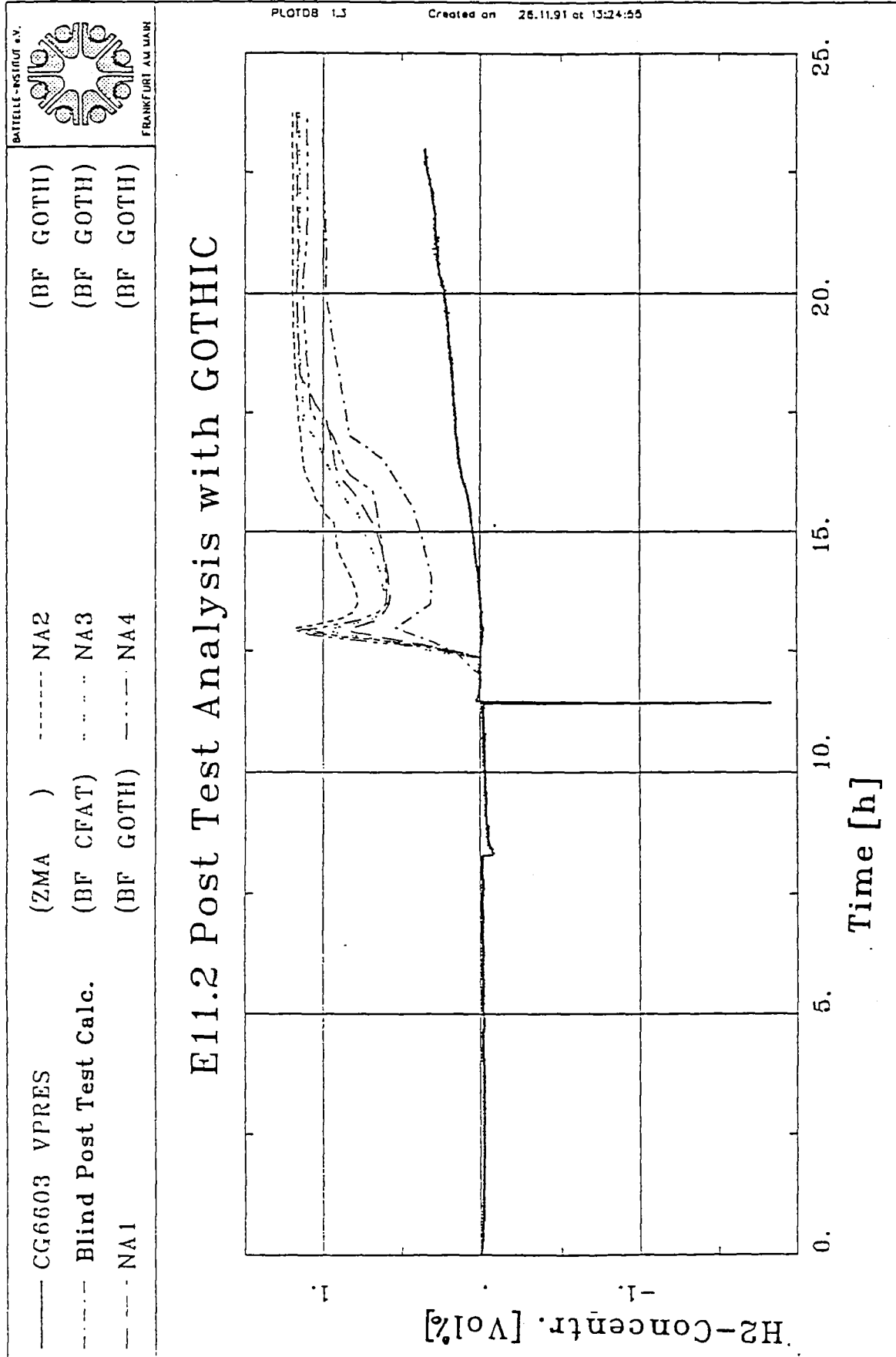


**Fig. 3** Hydrogen Concentration +12m

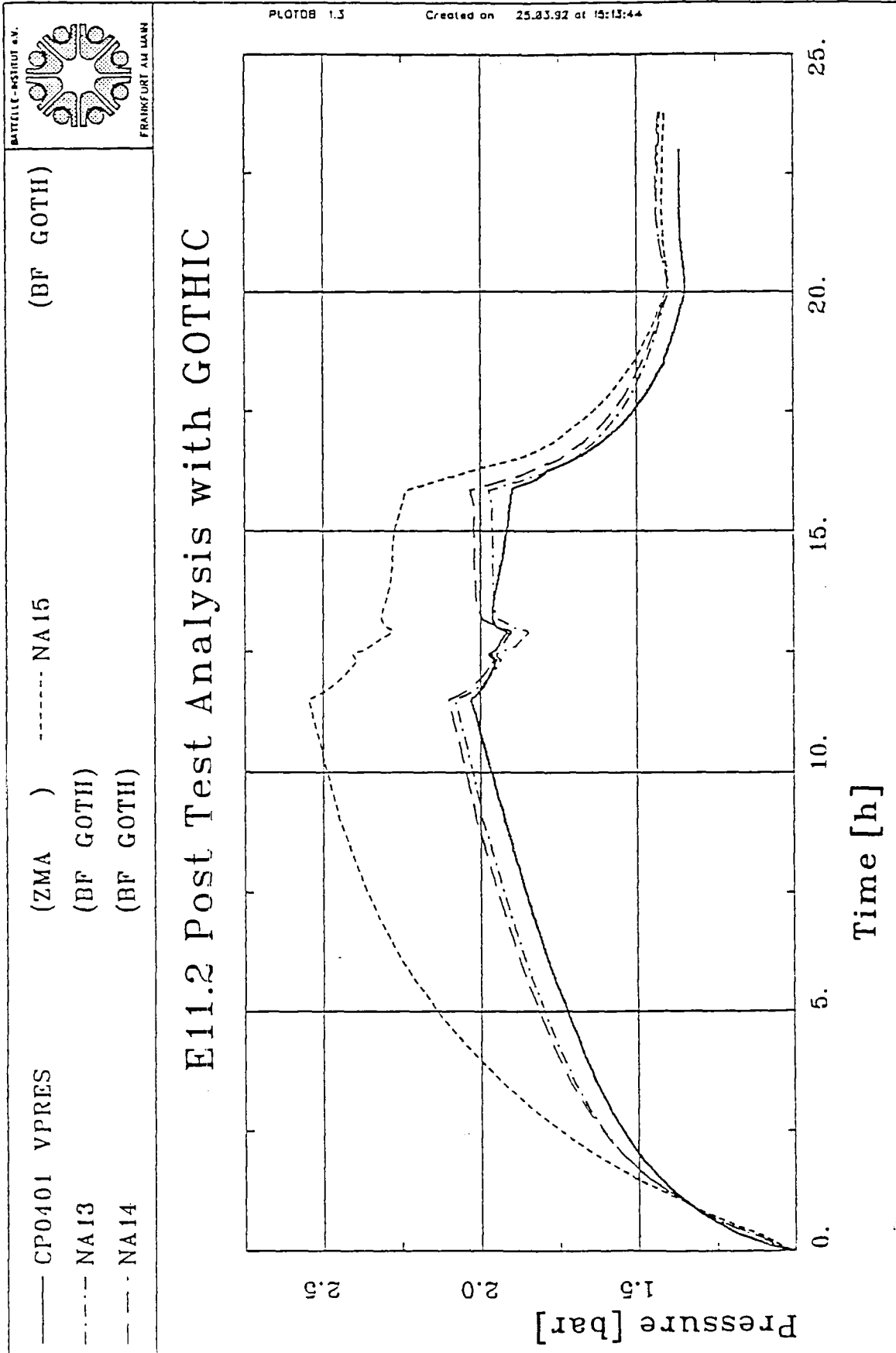


Fig. 4 Pressure

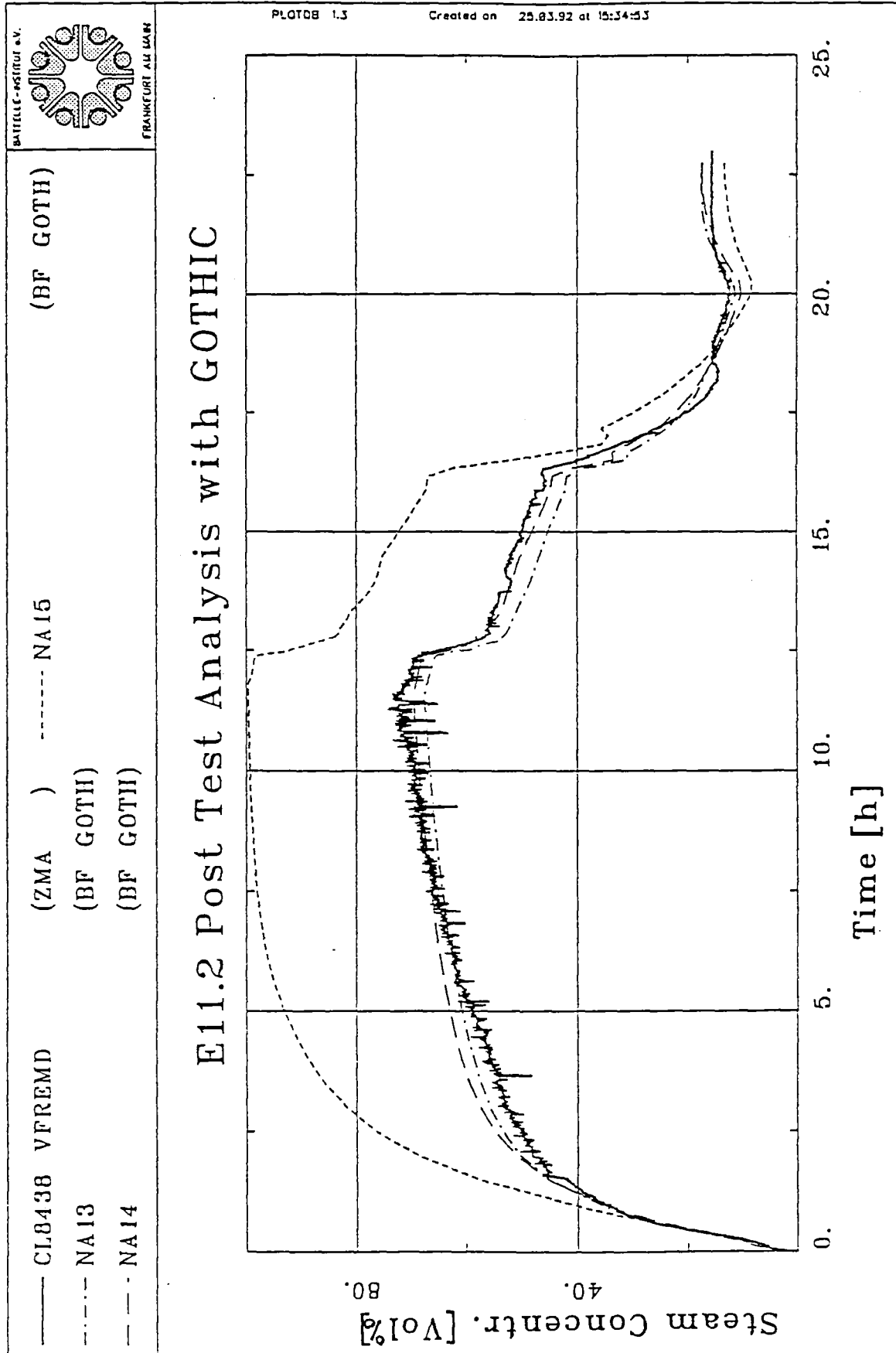


Fig. 5 Steam Concentration +48m (Dome)

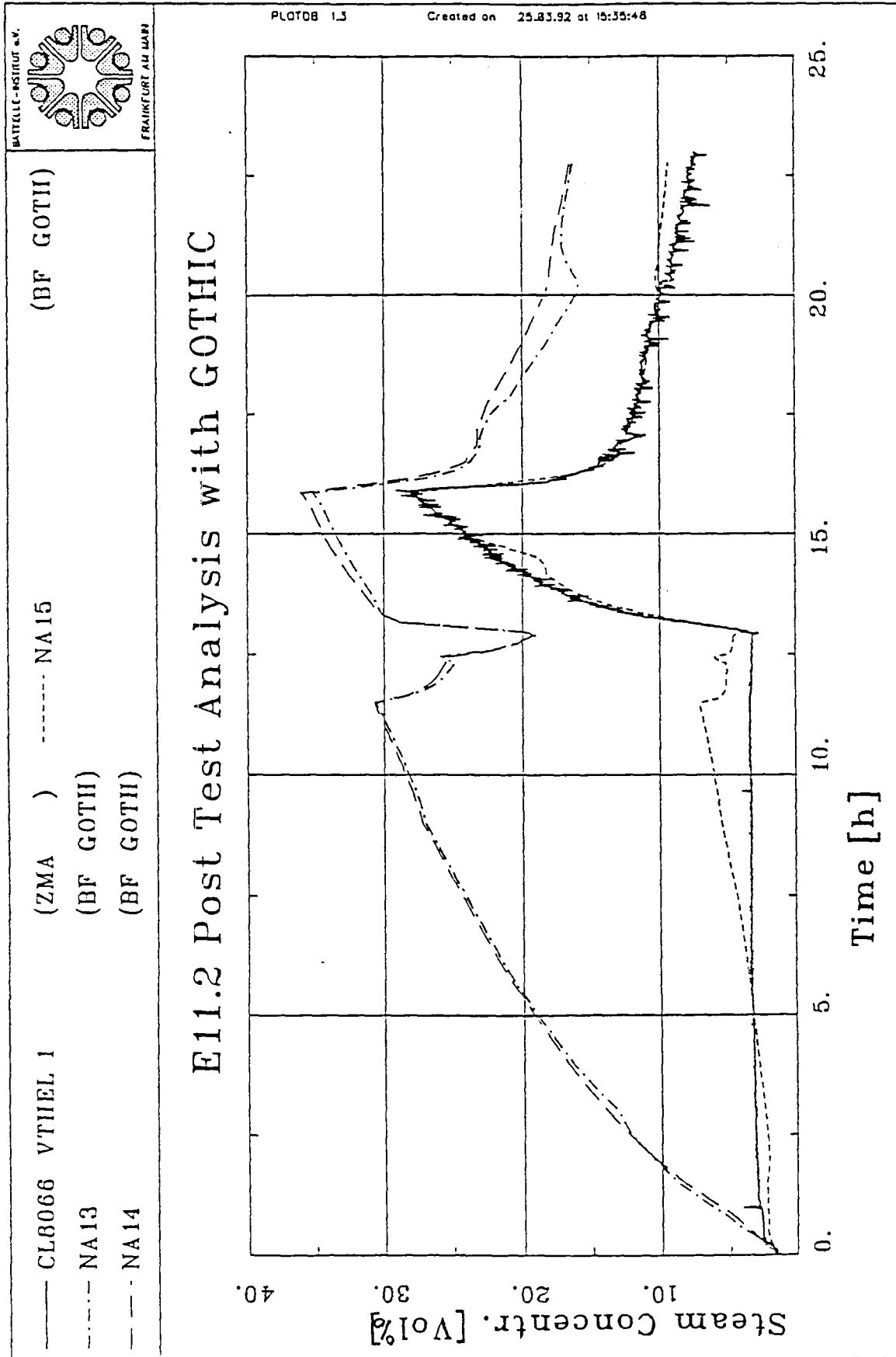
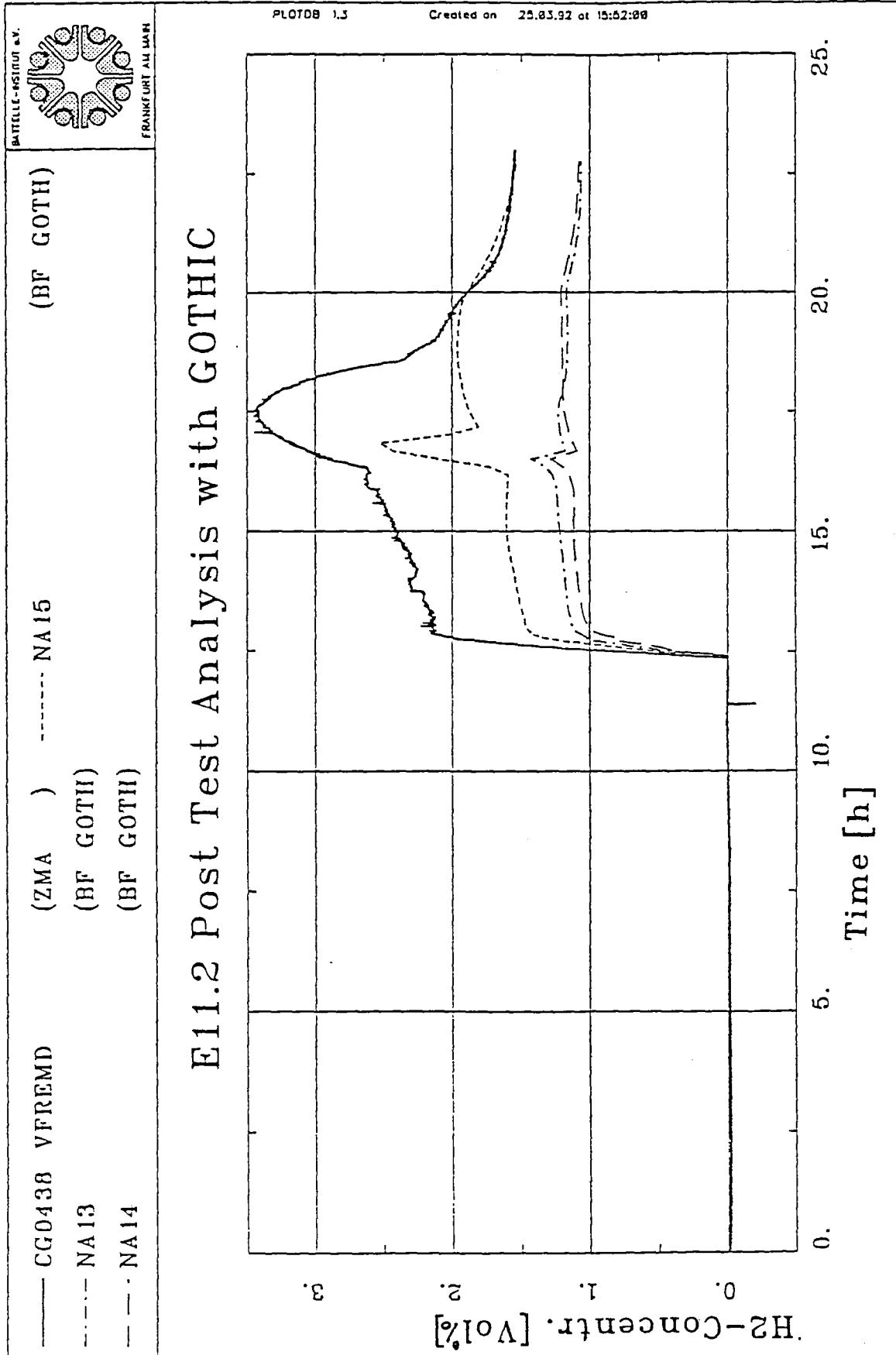


Fig. 6 Steam Concentration +12m



**Fig. 7** Hydrogen Concentration +48m (Dome)



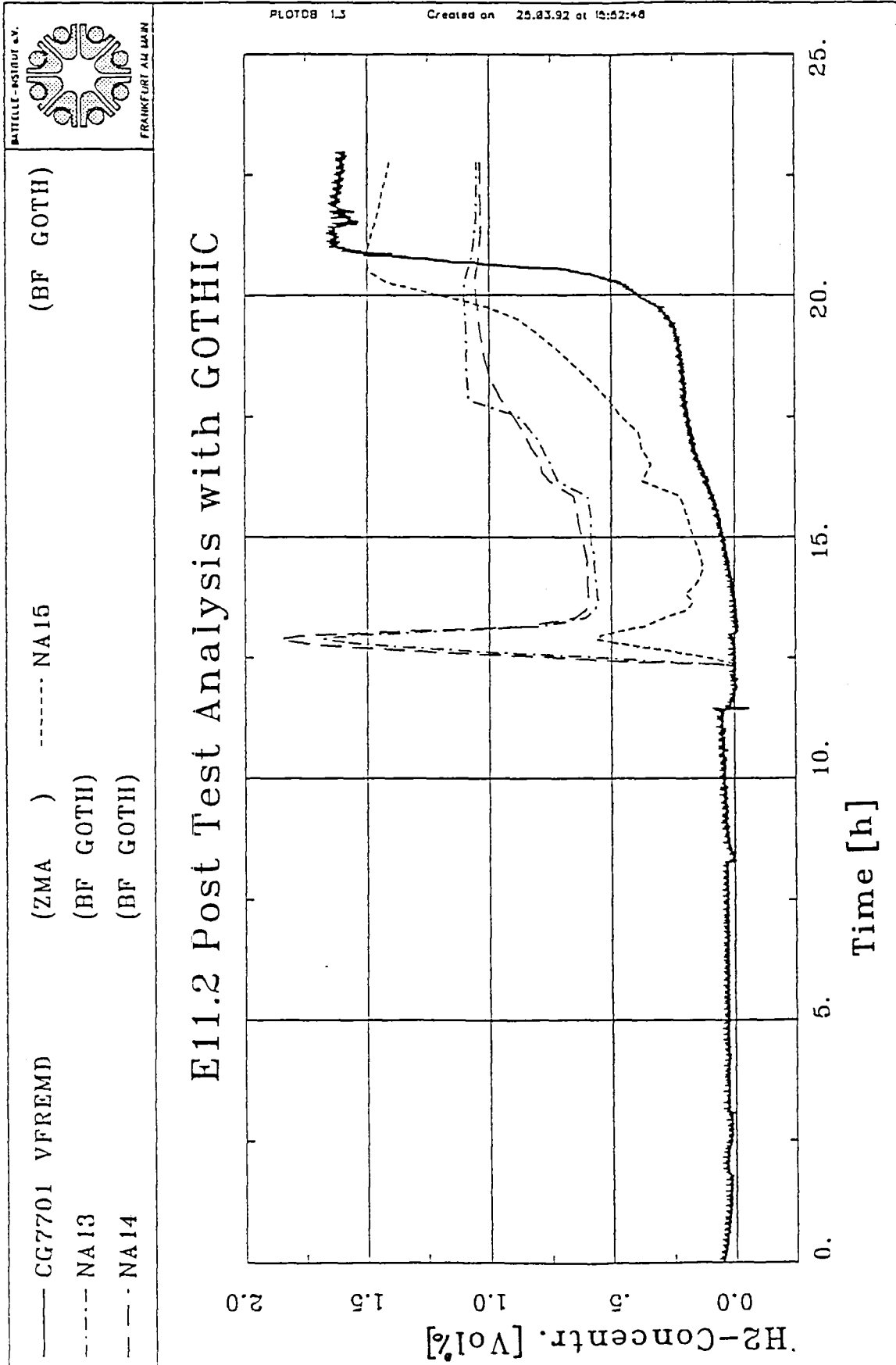
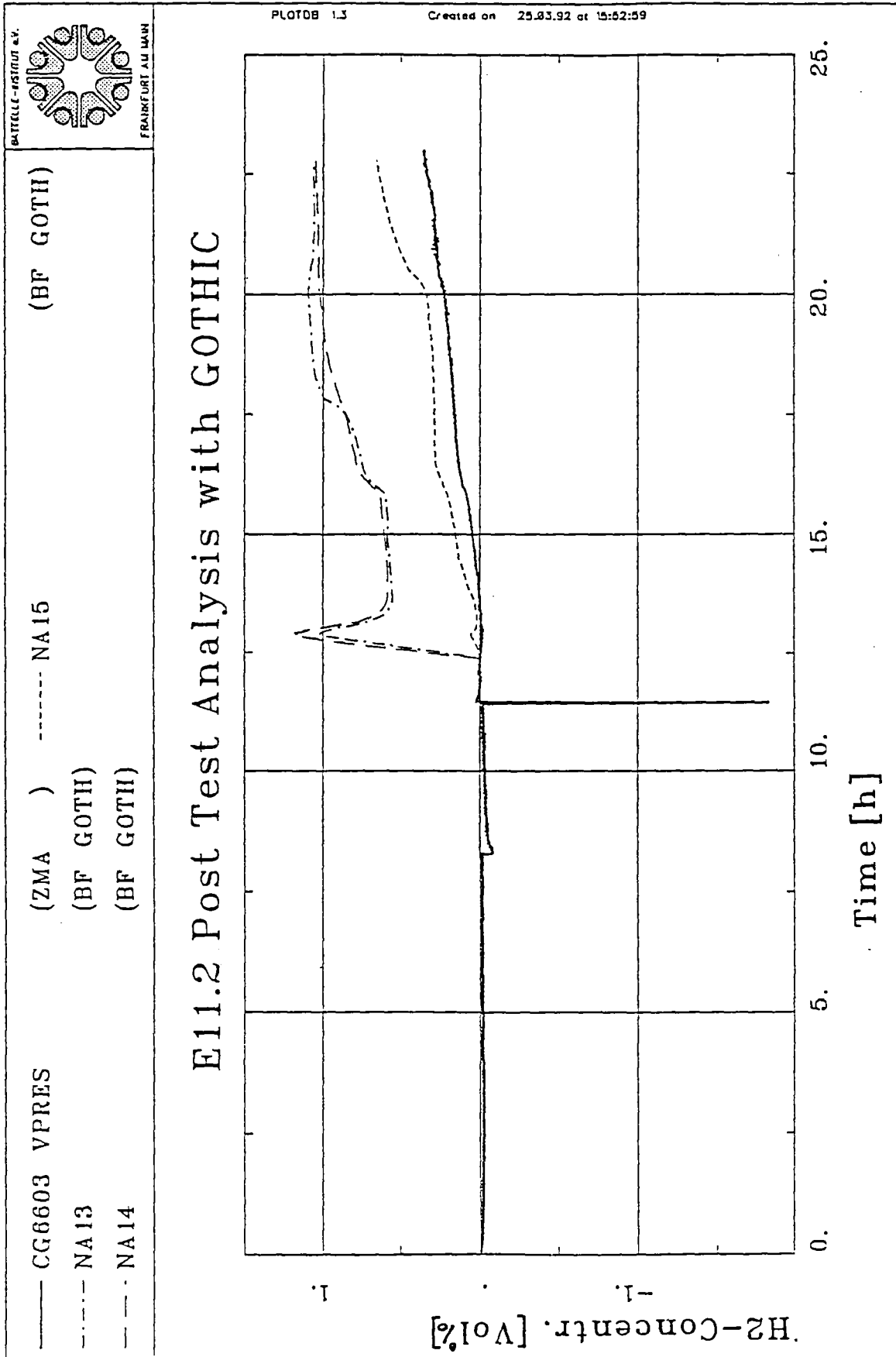


Fig. 8 Hydrogen Concentration +16.5m



**Fig. 9** Hydrogen Concentration +12m

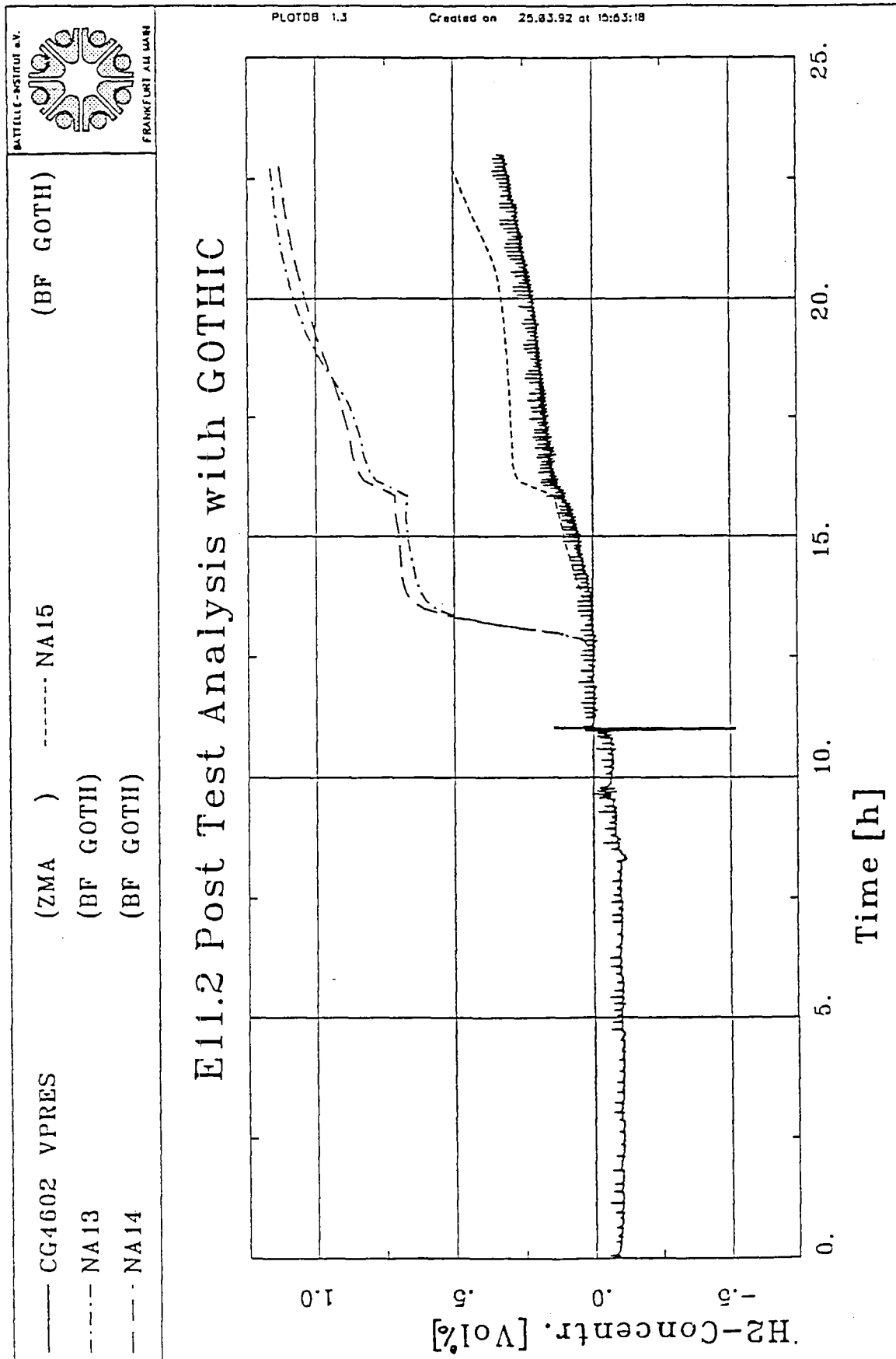


Fig. 10 Hydrogen Concentration +0.5m

**Table 2****PARAMETRIC CALCULATIONS FOR TEST E11.4**

<b>Run</b>	<b>Characteristics</b>
<b>Blind Post Test Calc.</b>	<b>HTC: To internal structures: Uchida * 3 To annulus gap: 100 W/m<sup>2</sup>K Total surface of steel shell in contact with containm. atmosphere External steam flow rates too high Without instrument cooling system</b>
<b>NA 1</b>	<b>Ext. steam flow rates corrected, instr. cooling system considered, steel shell-heat slabs modelled as recommended by PHDR, HTC to internal structures: Uchida, HTC to annulus gap: 10/m<sup>2</sup>K</b>
<b>NA 2</b>	<b>HTC to annulus gap: 25 W/m<sup>2</sup>K</b>
<b>NA 3</b>	<b>HTC to internal structures derived from measured values</b>



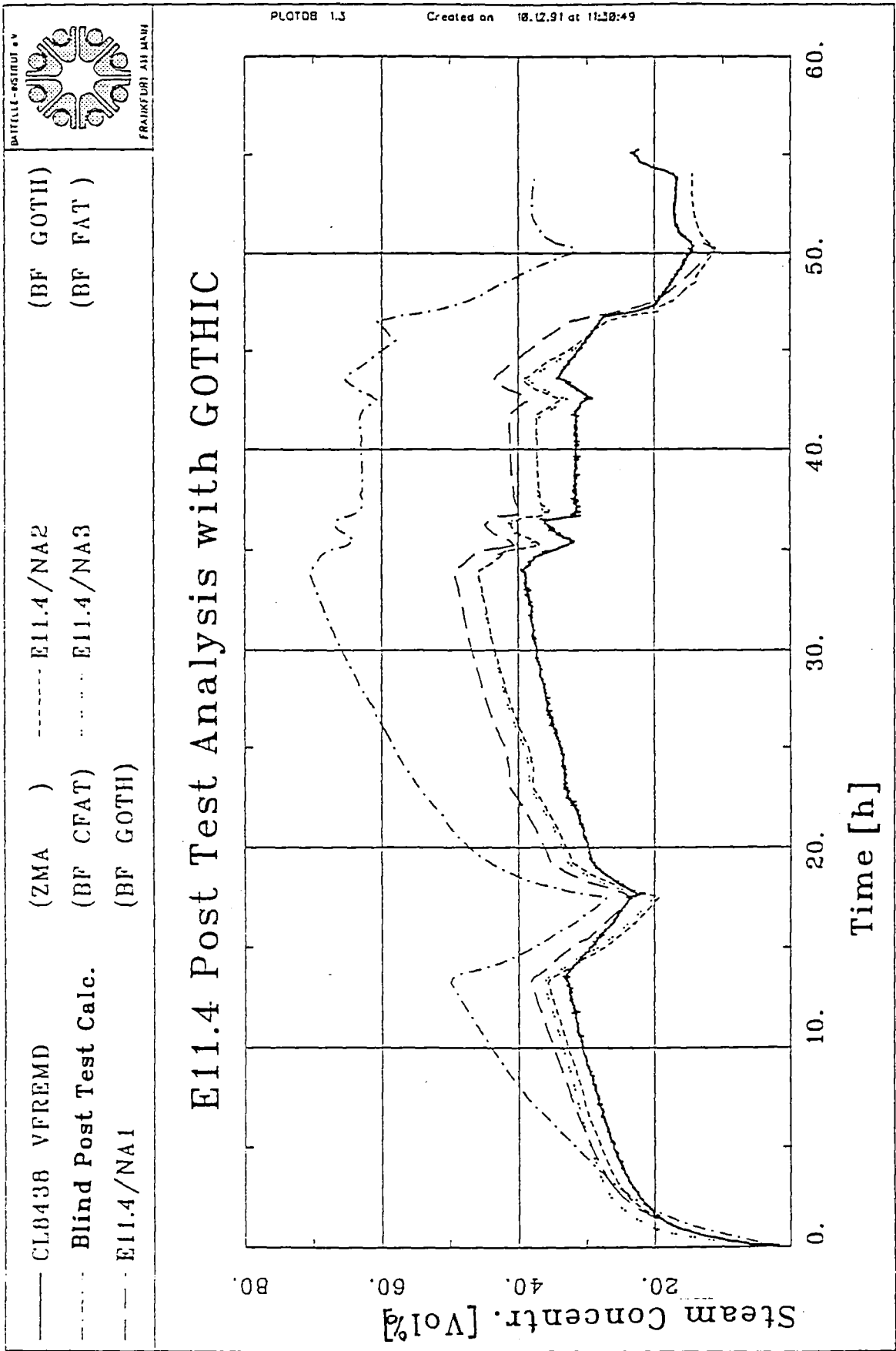


Fig. 12 Steam Concentration +48m (Dome)

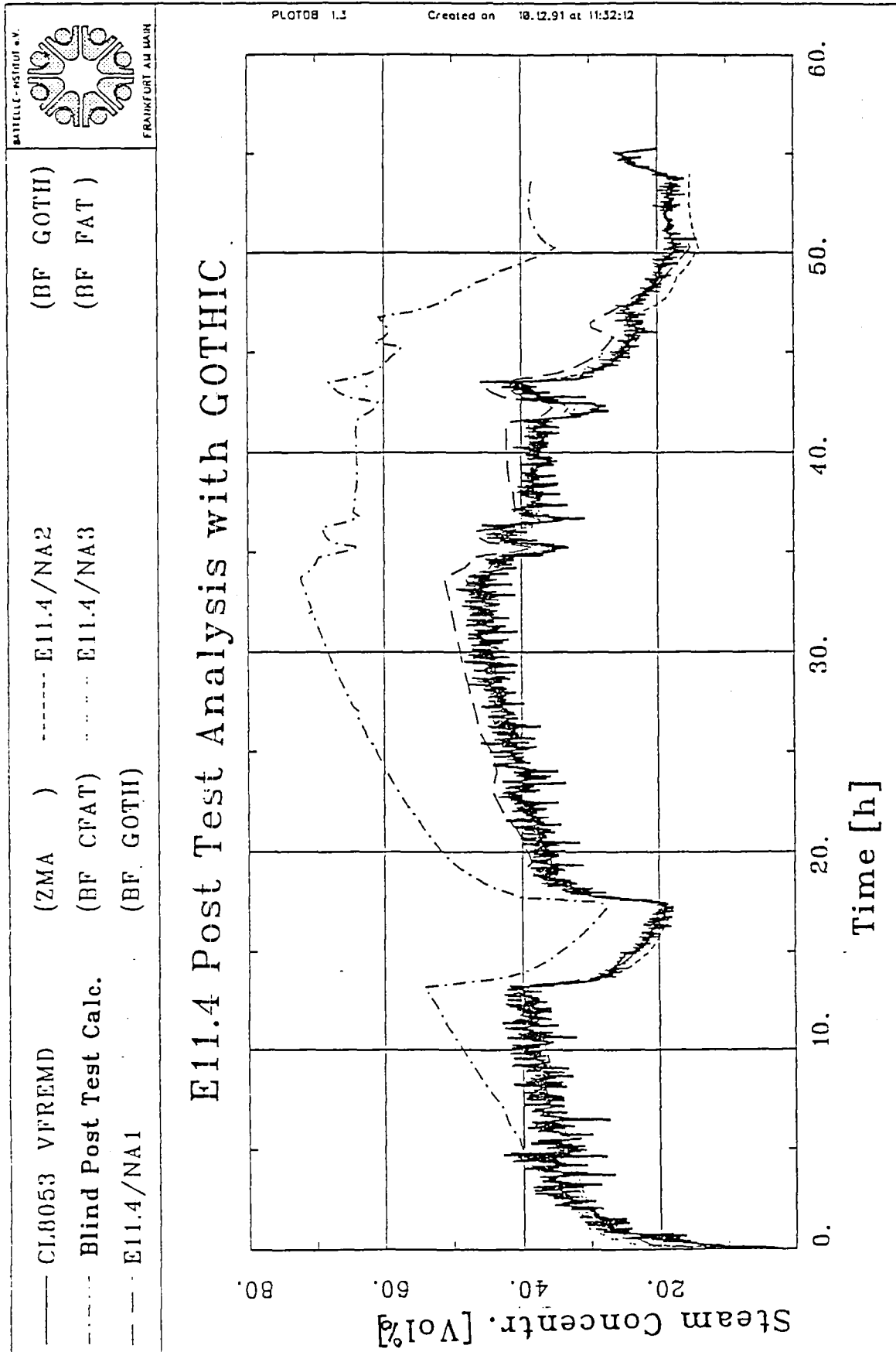


Fig. 13 Steam Concentration +6m

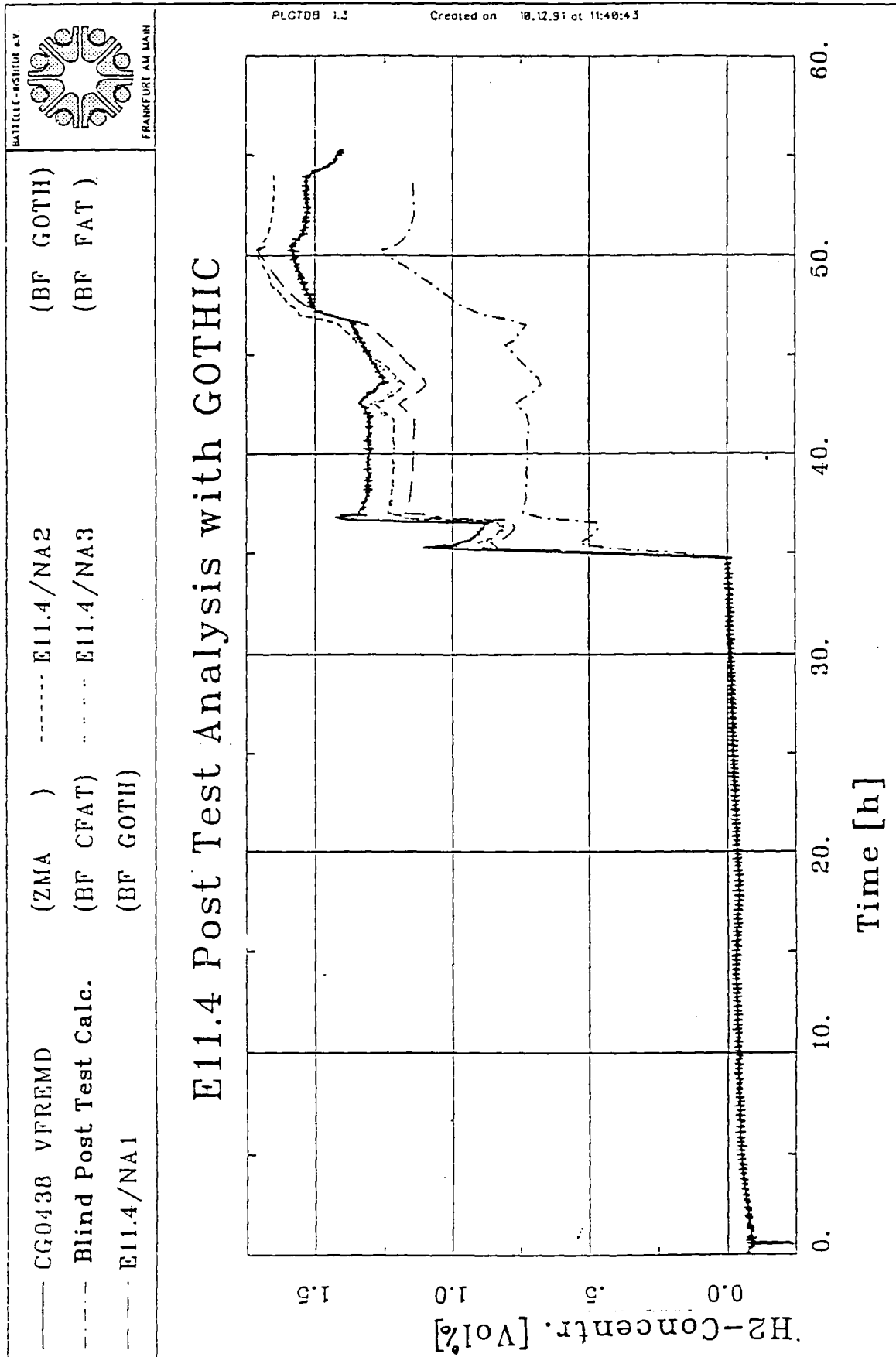


Fig. 14 Hydrogen Concentration +48m (Dome)



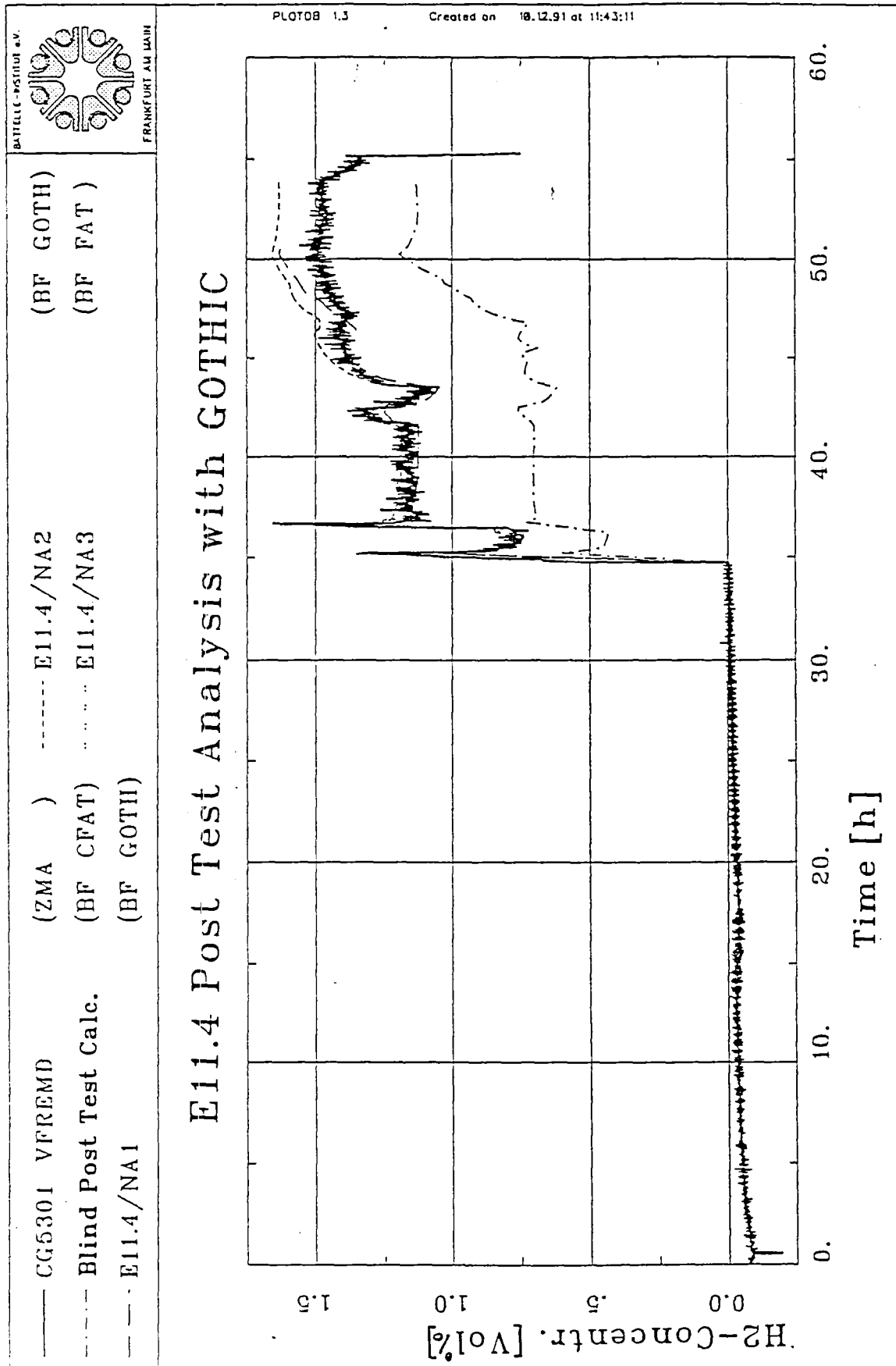


Fig. 15 Hydrogen Concentration +6m

## CONCLUSIONS

### E11.2

- o Flow path modeling using the real geometric areas in combination with "typical" loss coefficients overestimated the energy and gas transport to lower containment sections
- o Increase of flow restriction results in better simulation of stratification effects
- o Well simulated stratification pattern results in overestimation of pressure
- o Flow path modeling needs more investigation
- o Use of distributed parameter models may be helpful for improved predictions

### E11.4

- o GOTHIC-results are in excellent accordance with the experiment
- o Scenarios with homogeneous containment atmosphere can be simulated accurately with lumped parameter models

## Appendix-C

### 1 The convection velocities in E11.2

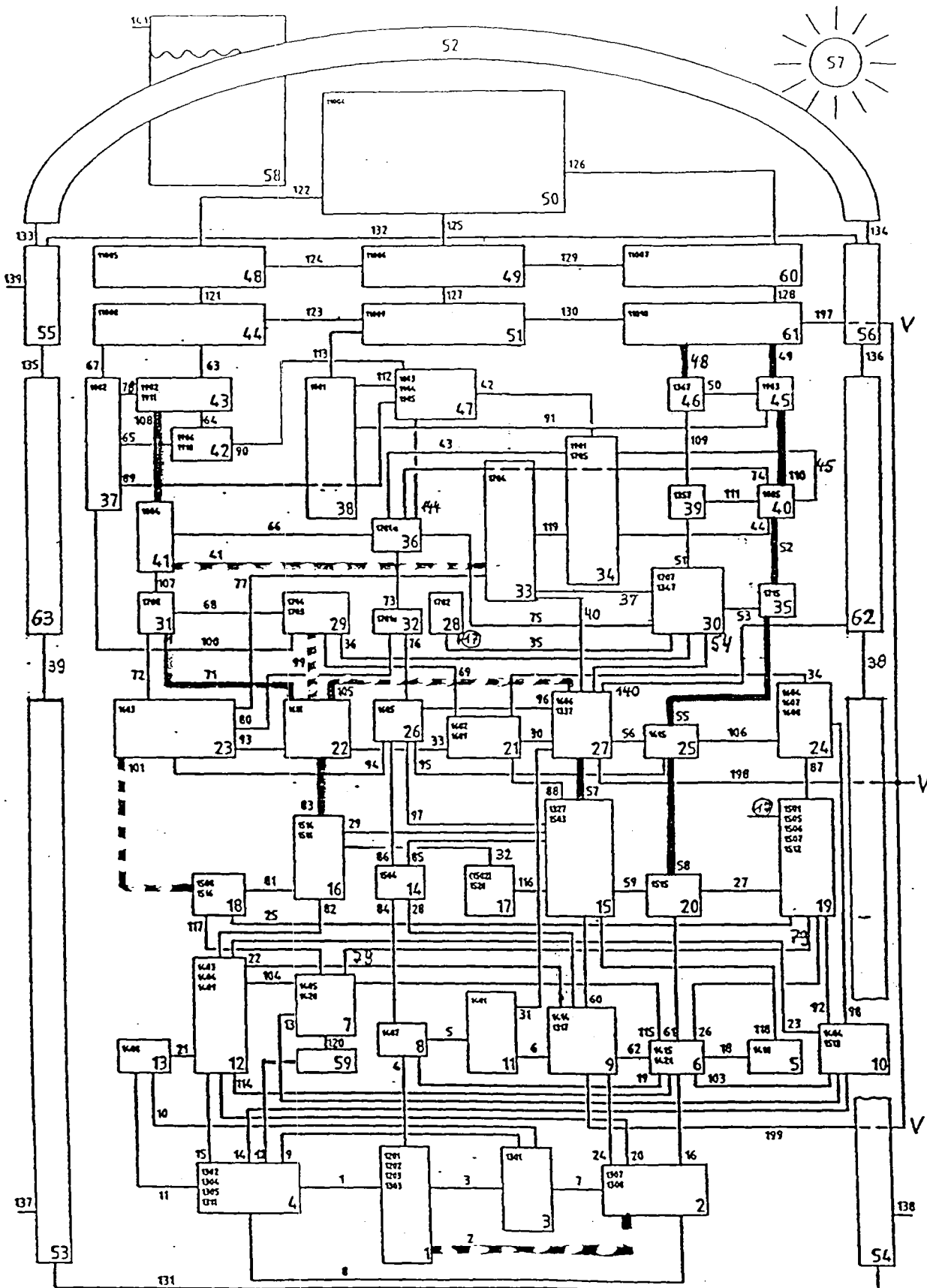
(C = Calculation      M = Measurement      J = Junction )

- From the few useful velocity - measurements in the major flow paths, indicated in Fig 1, one can see that there is a measured upward flow in the stair case junctions (s. Fig. 2, 3, 4, RALOC J/57, J/58, J/55) during steam injection in room 1405. In the C there is in the contrary an indication of a small downward flow. In J83 a downward flow was measured (see Fig. 5) whereas the C shows at the same time a flow into the other direction. No convection is measured during that time in the J108 (s. Fig. 6) and J71 (s. Fig. 7) in the spiral stair case, but the C shows a downward flow.
- Summarizing one can say that there are not sufficient velocity - measurements to explain the convection loops in the containment but the C-loops reveals to be upside down to the M-loop during steam injection in room 1405. Until now we think that there are two reasons for that behavior:
  1. the too high heat up for the zones 16, 18,22, 23 before 1405 injection is reducing the density in that zones. It reduces the weight of the fluid column at that locations and opens the convection loop there.
  2. the flow area documentation from PHDR of (V234) in the breakroom 1405 ceiling, gives an area, which might be 50 % too large. This was identified during our E11.4 verification testrun.

That may be an indication to check other junctions too, which had been changed for the E11. test serie.

## 2 Selected Results of E11.4

The presented results are shown to underline the RALOC capabilities and to find a further judgement basis. Just to understand, what has been done during E11.4-test the picture 8, which indicates the history of the injections is attached. The calculation with the same above documented input deck was run over about 55 hours problem-time and gave excellent results for nearly all locations (s. Fig. 9-25) and thermodynamic values in the HDR-containment. Deviations occurred next to and mainly directly above the break room 1405 as one can see in Fig. 11 (too low temperature), Fig. 13 (too high temperature). There we found an obviously wrong documentation of the V234 junction. The conclusion is, that RALOC is capable to calculate this experiment with well mixed conditions very exactly and the input deck as well as the majority of the pressure-, temperature- and concentration-measurements are o. k.. Velocity measurements have to be analysed critically.



63-room nodalisation and the atmospherical junctions for the post-test-calculation of the HDR test E 11.2 with R A L O C ISP29

--- Indication of useful measurements

Fig.:1

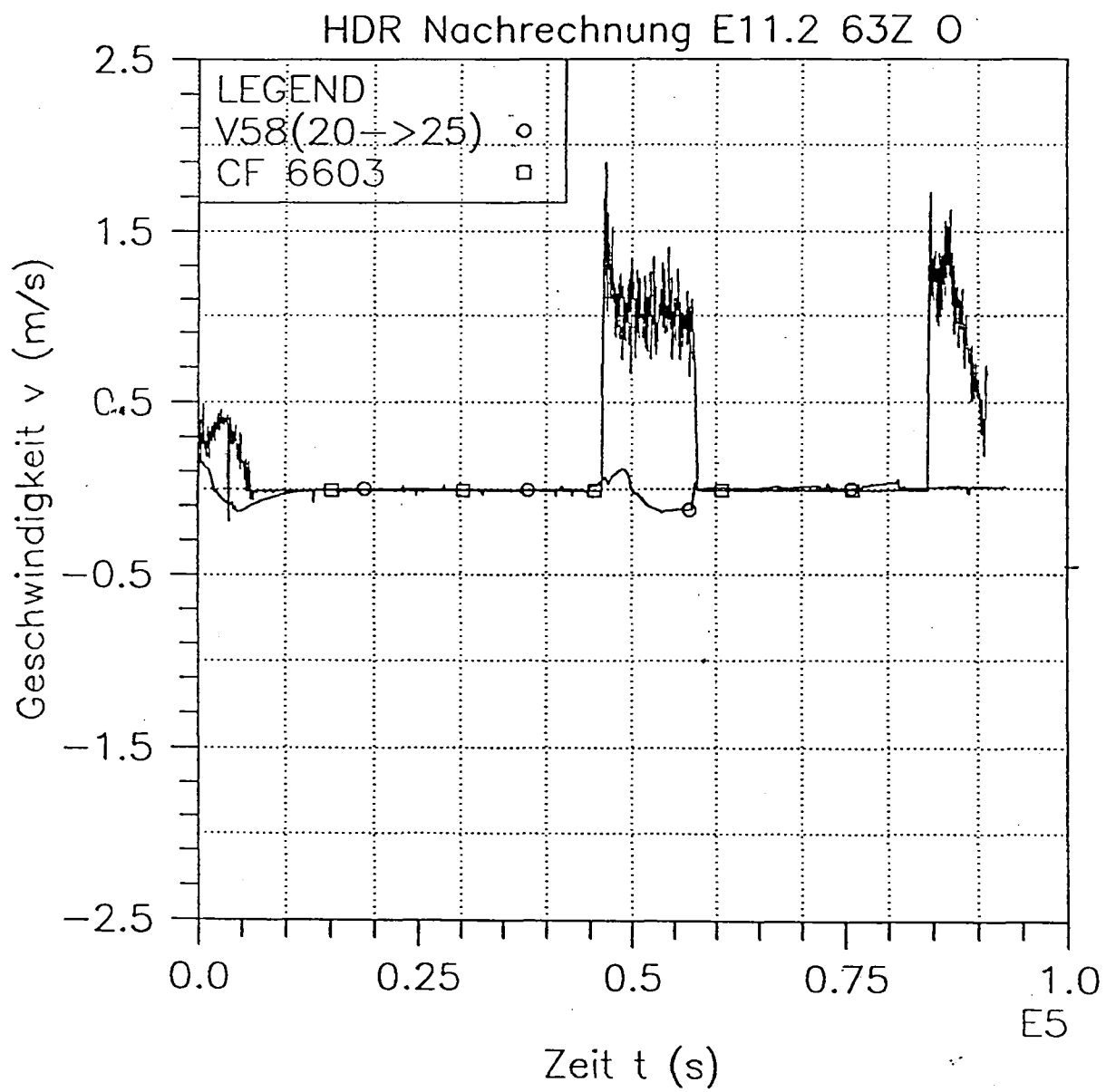


Fig.: 2

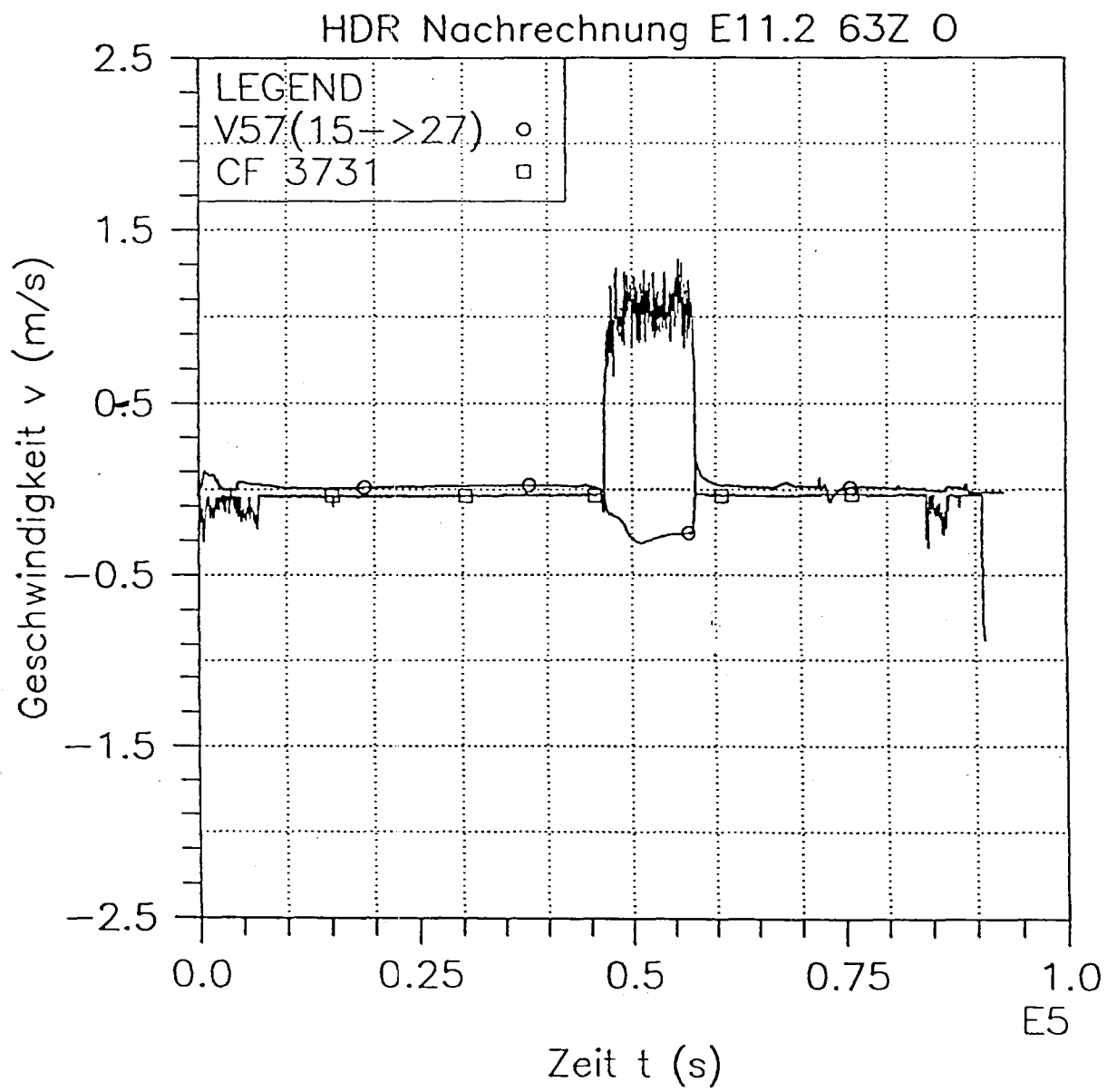


Fig.: 3

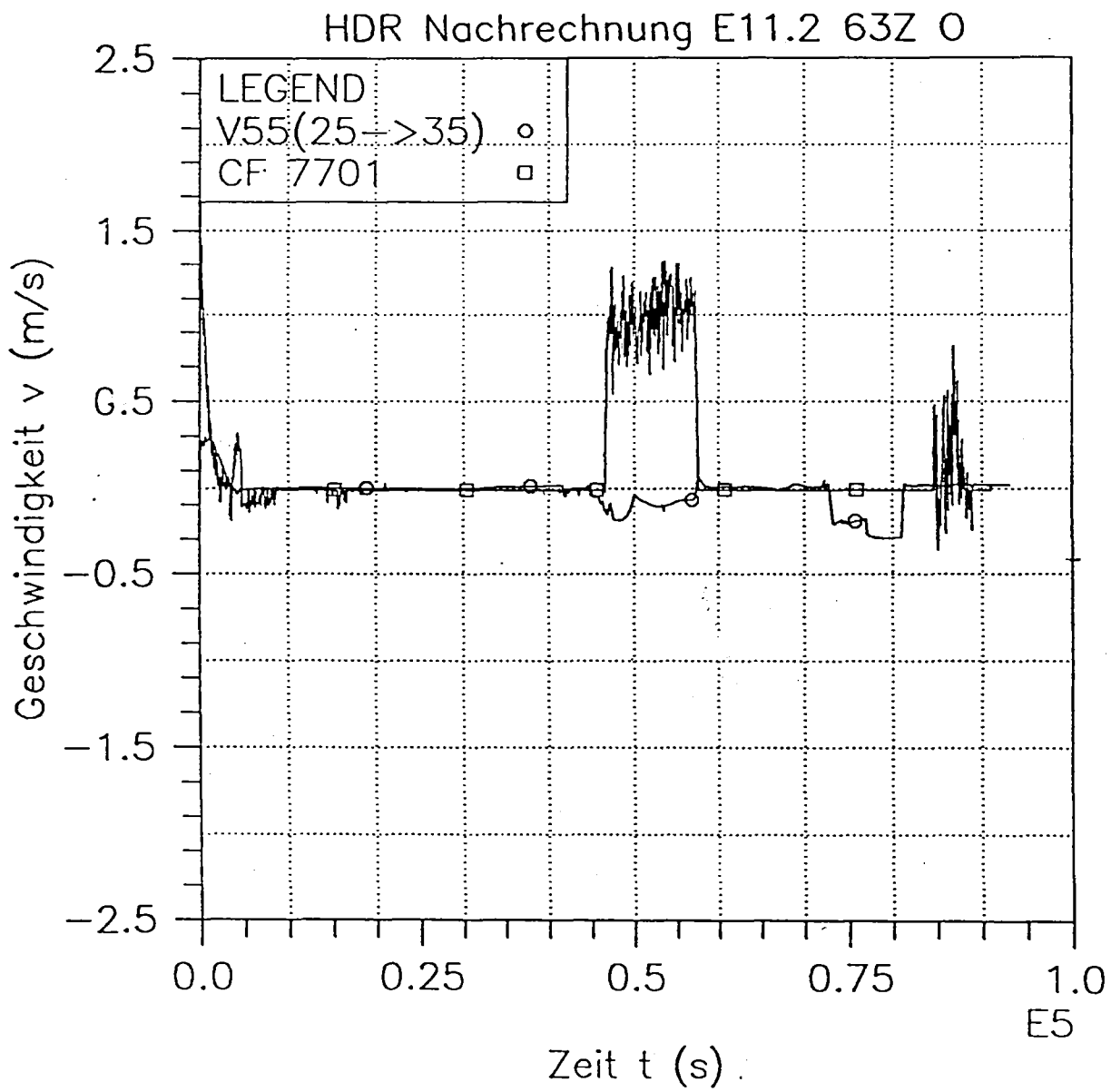


Fig.: 4



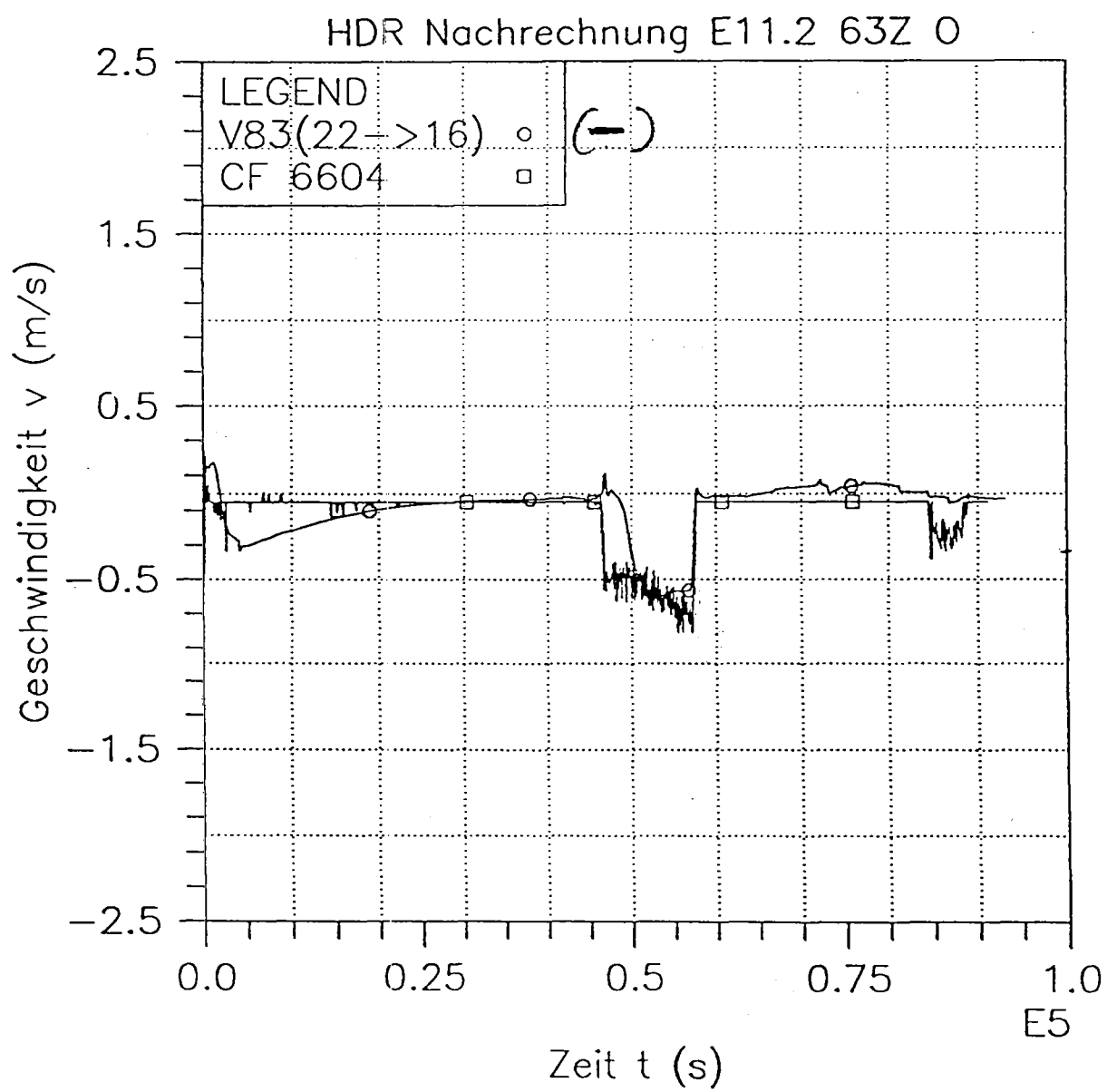


Fig.: 5

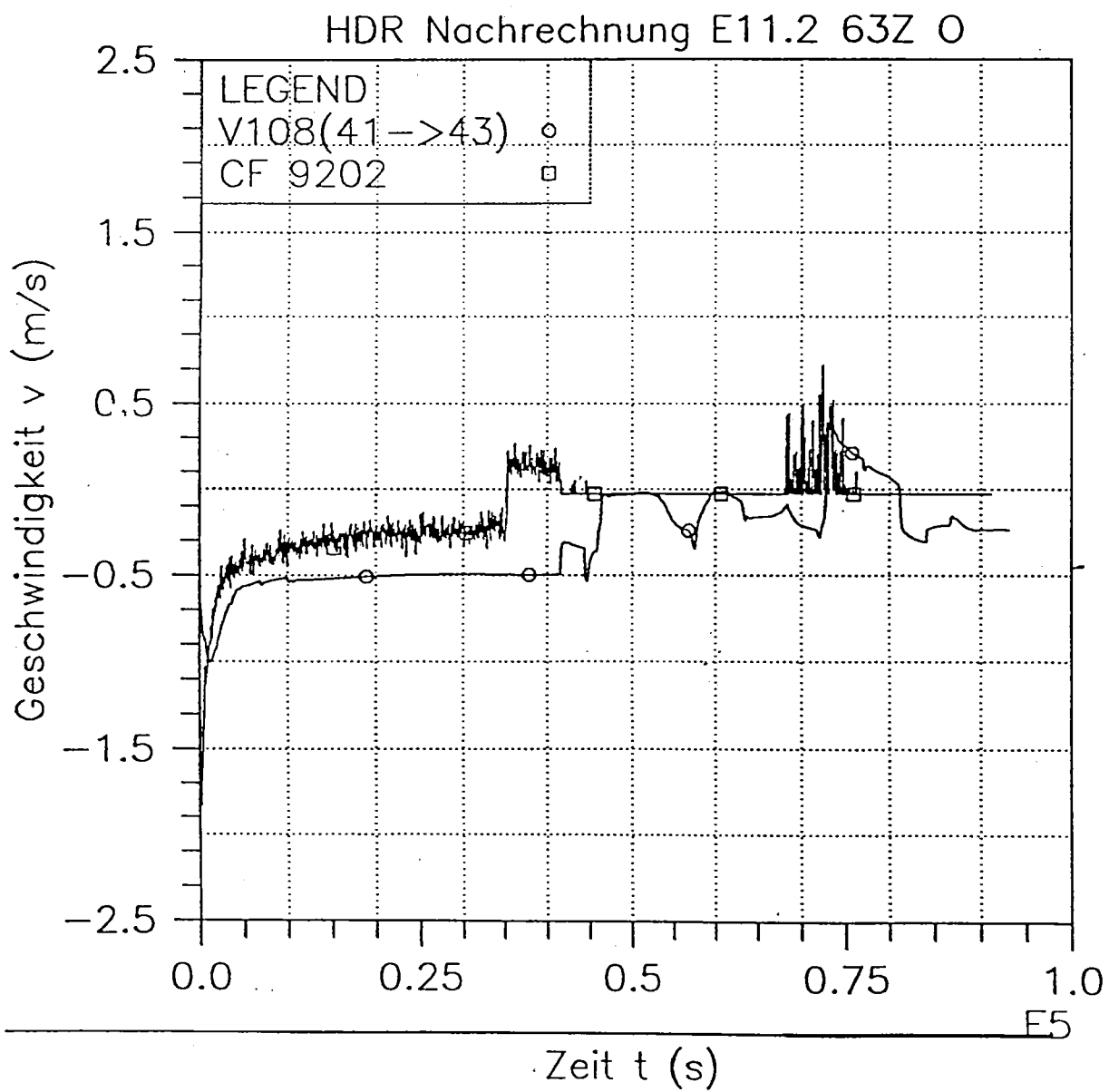


Fig.:6

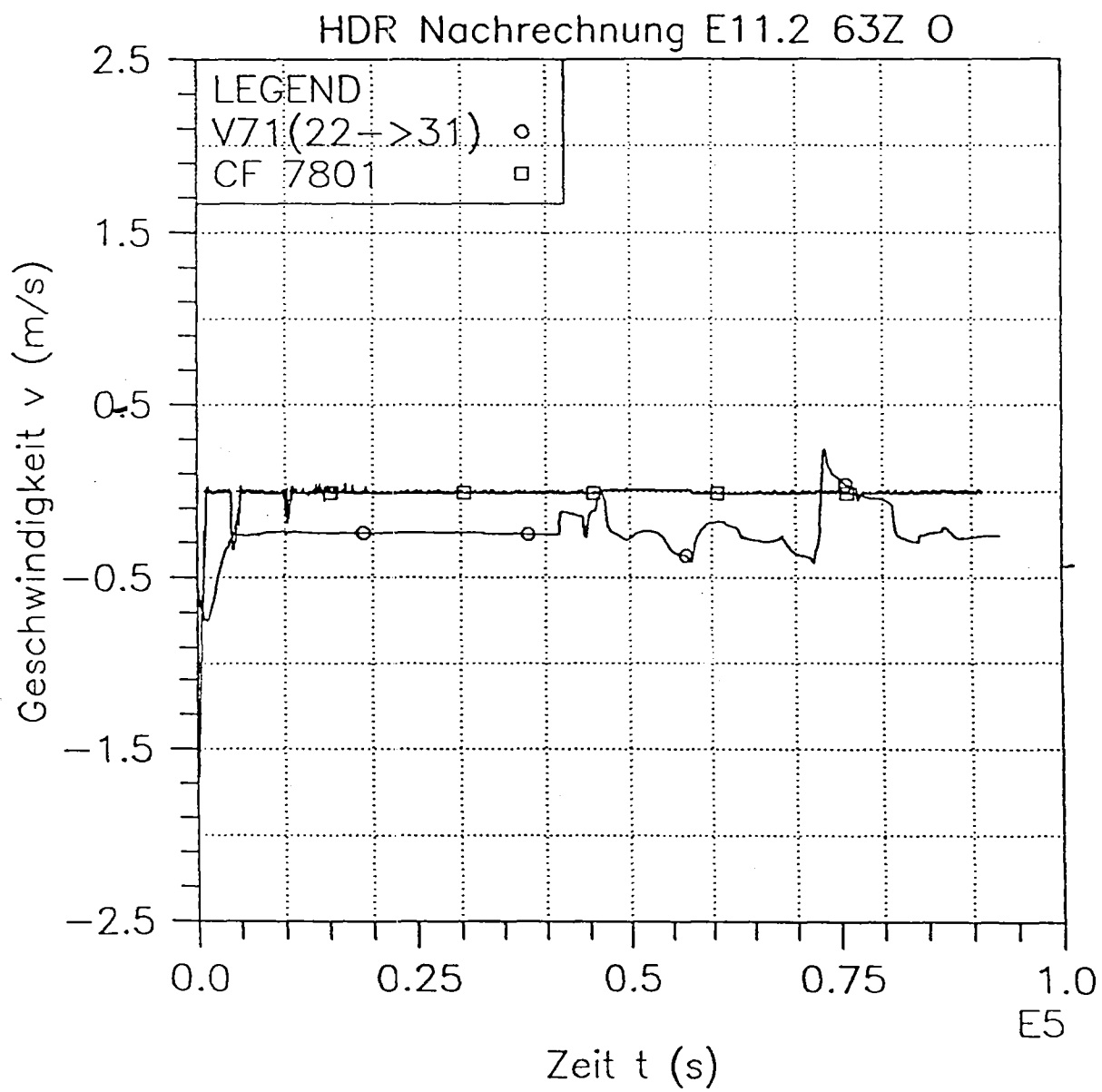
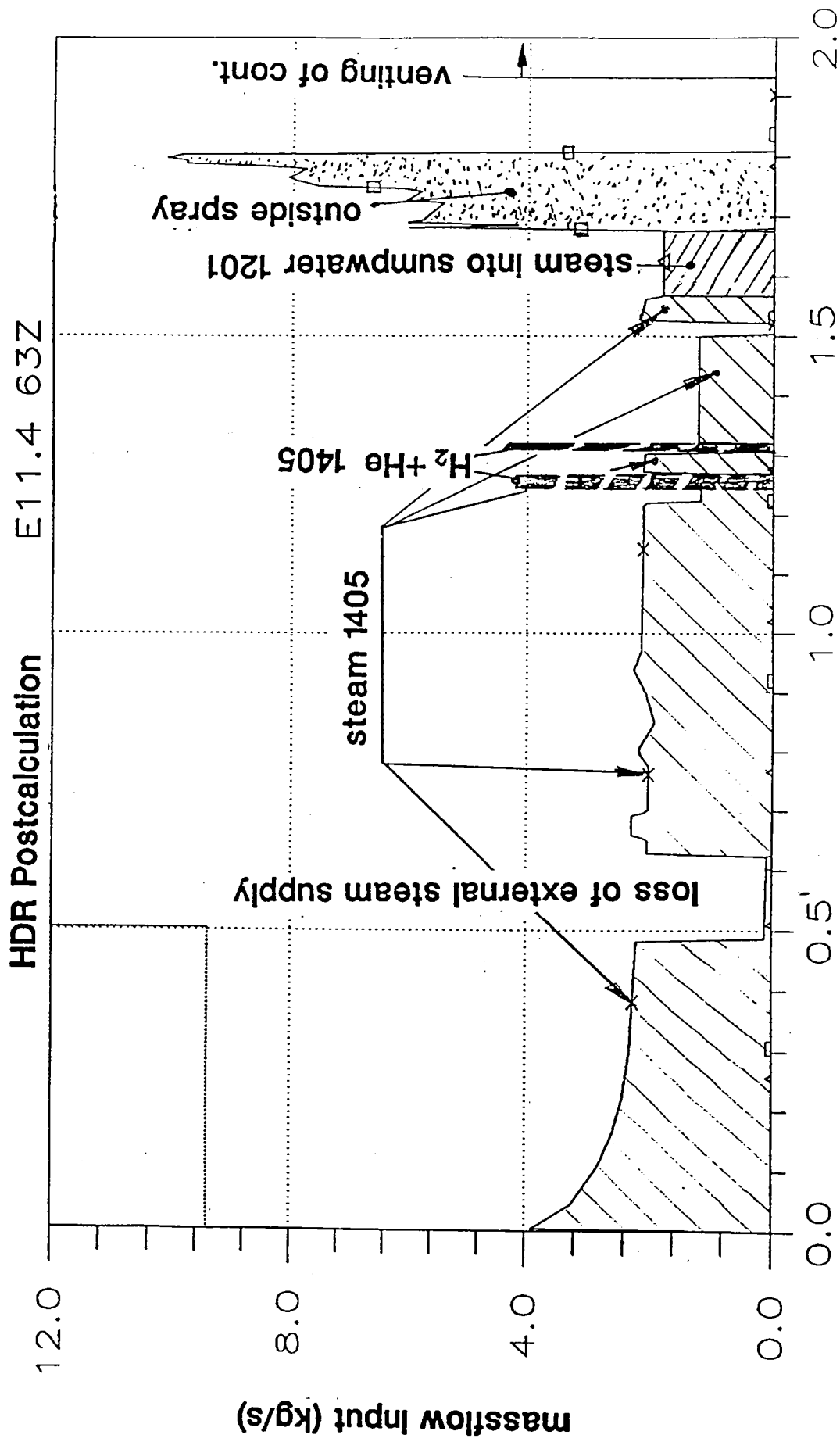


Fig.: 7



Sources of E11.4 time(s) \* 10 \*\* 5 Fig.:8

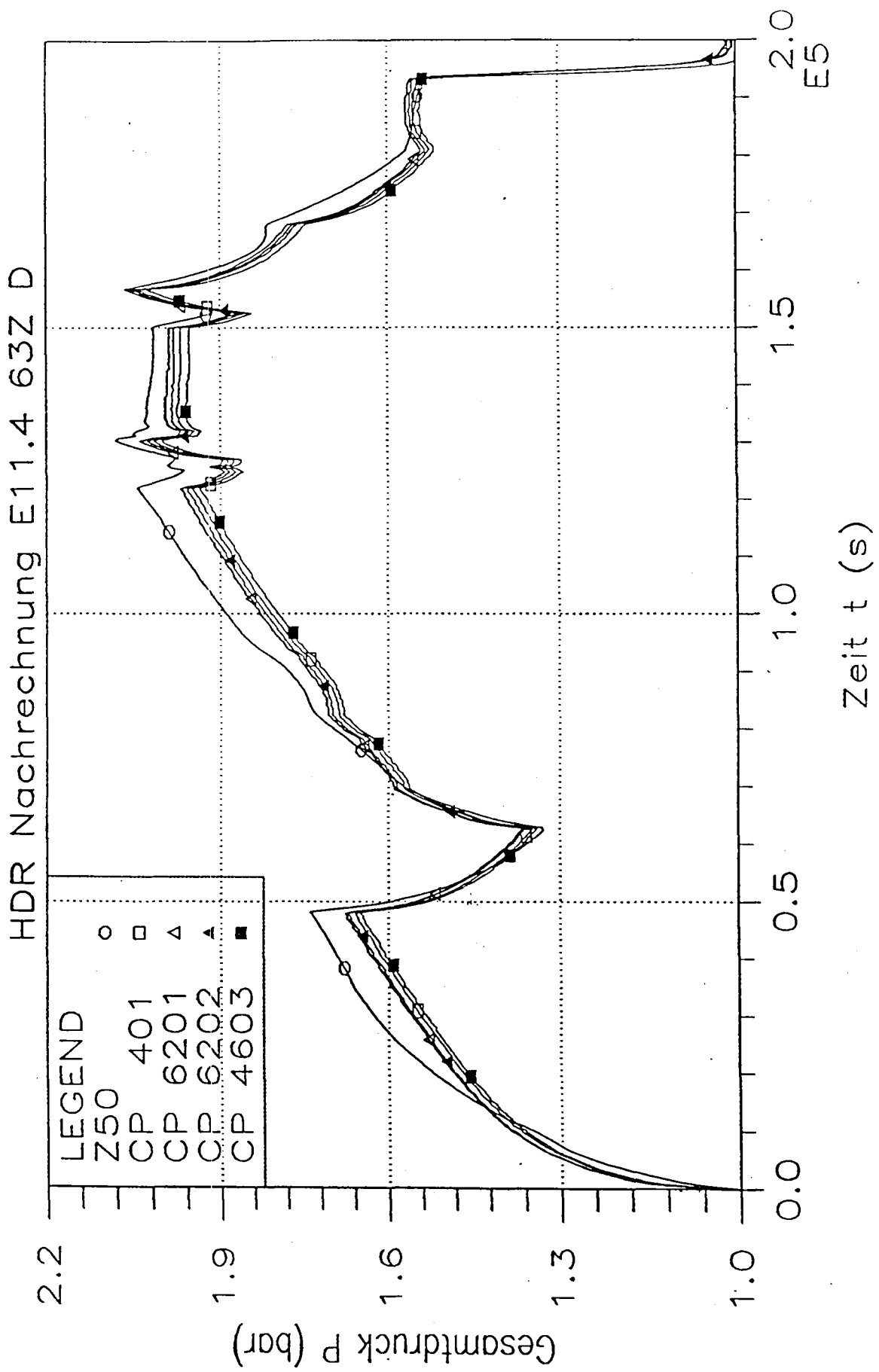


Fig.: 9

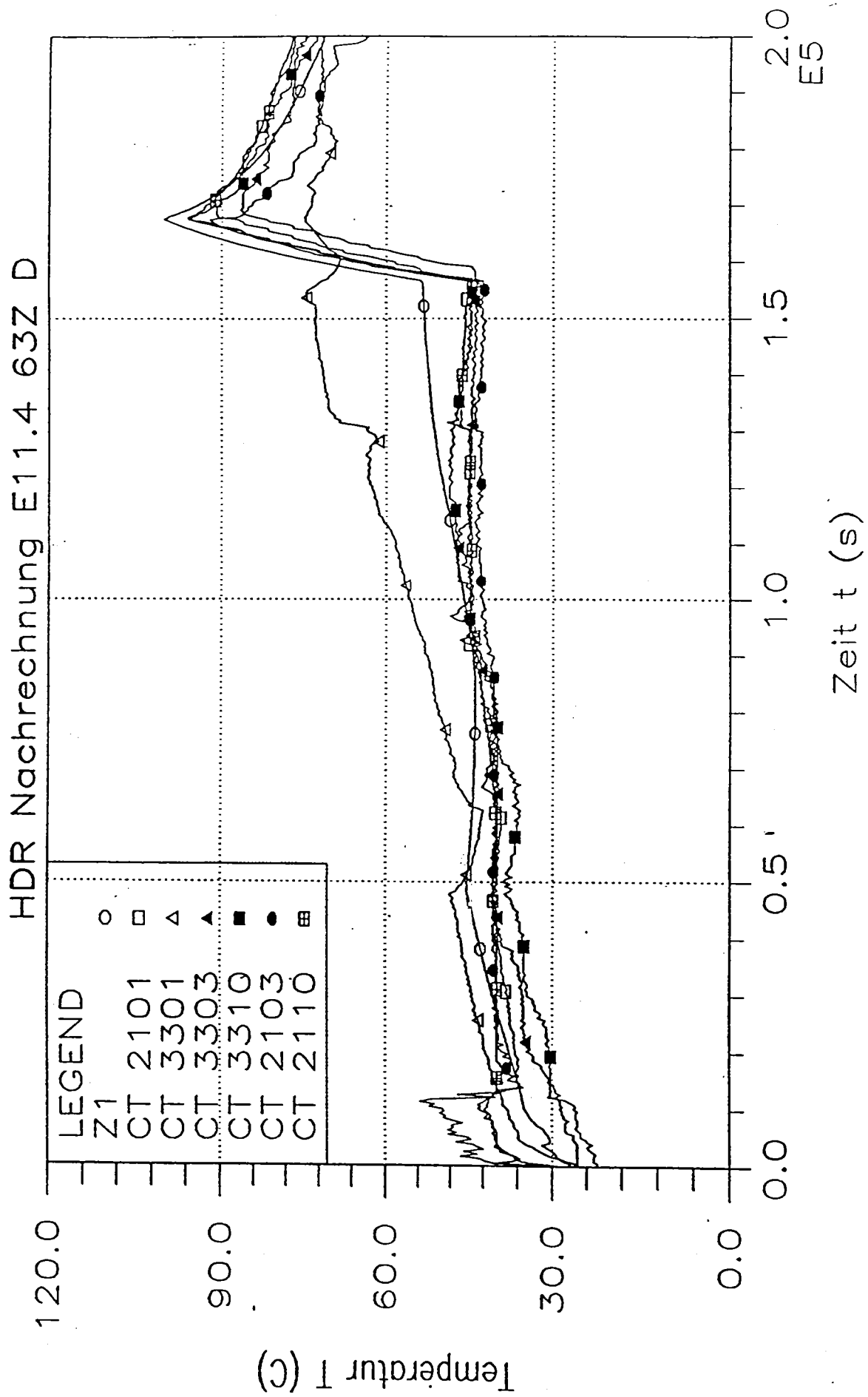


Fig.:10

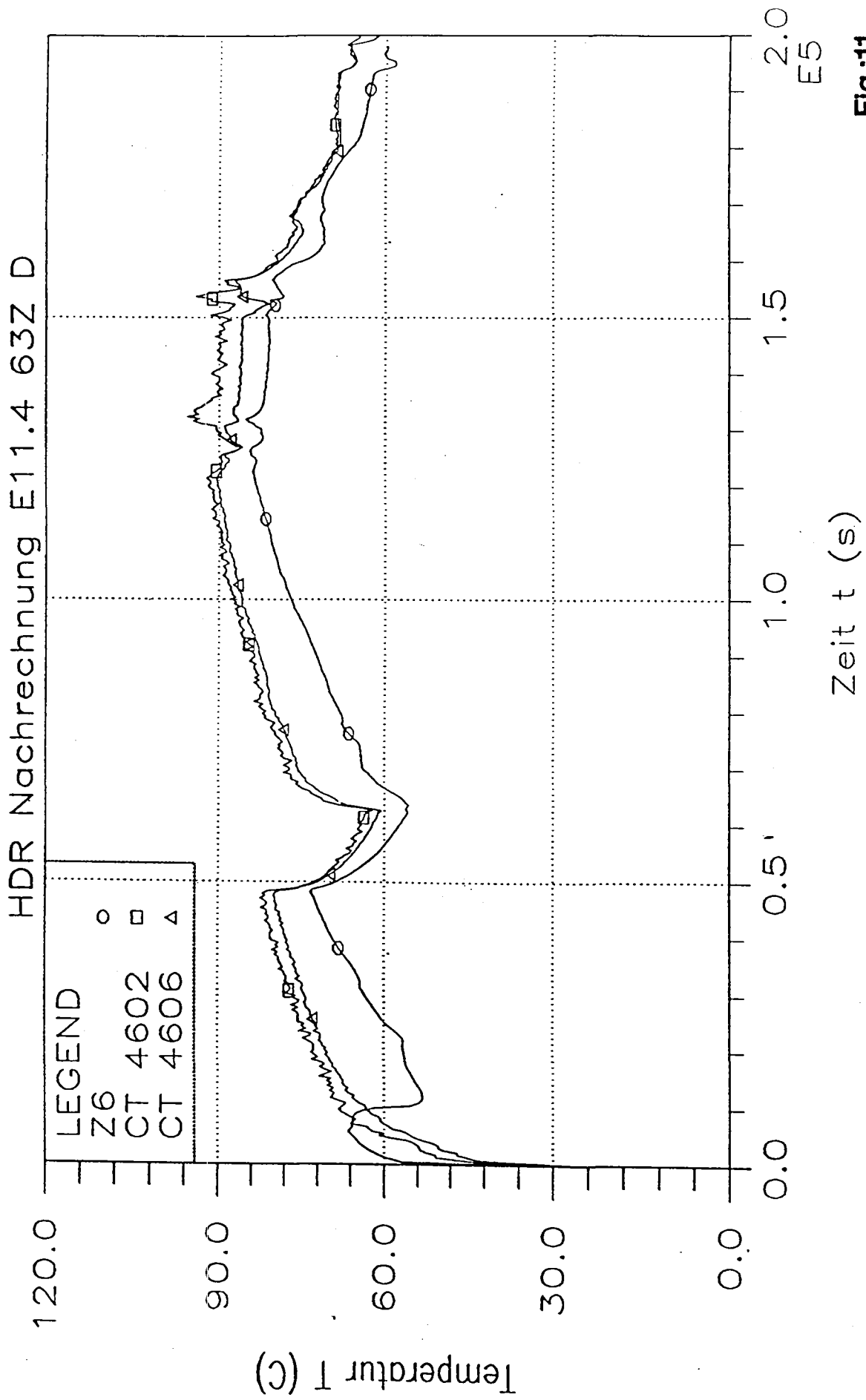


Fig.:11

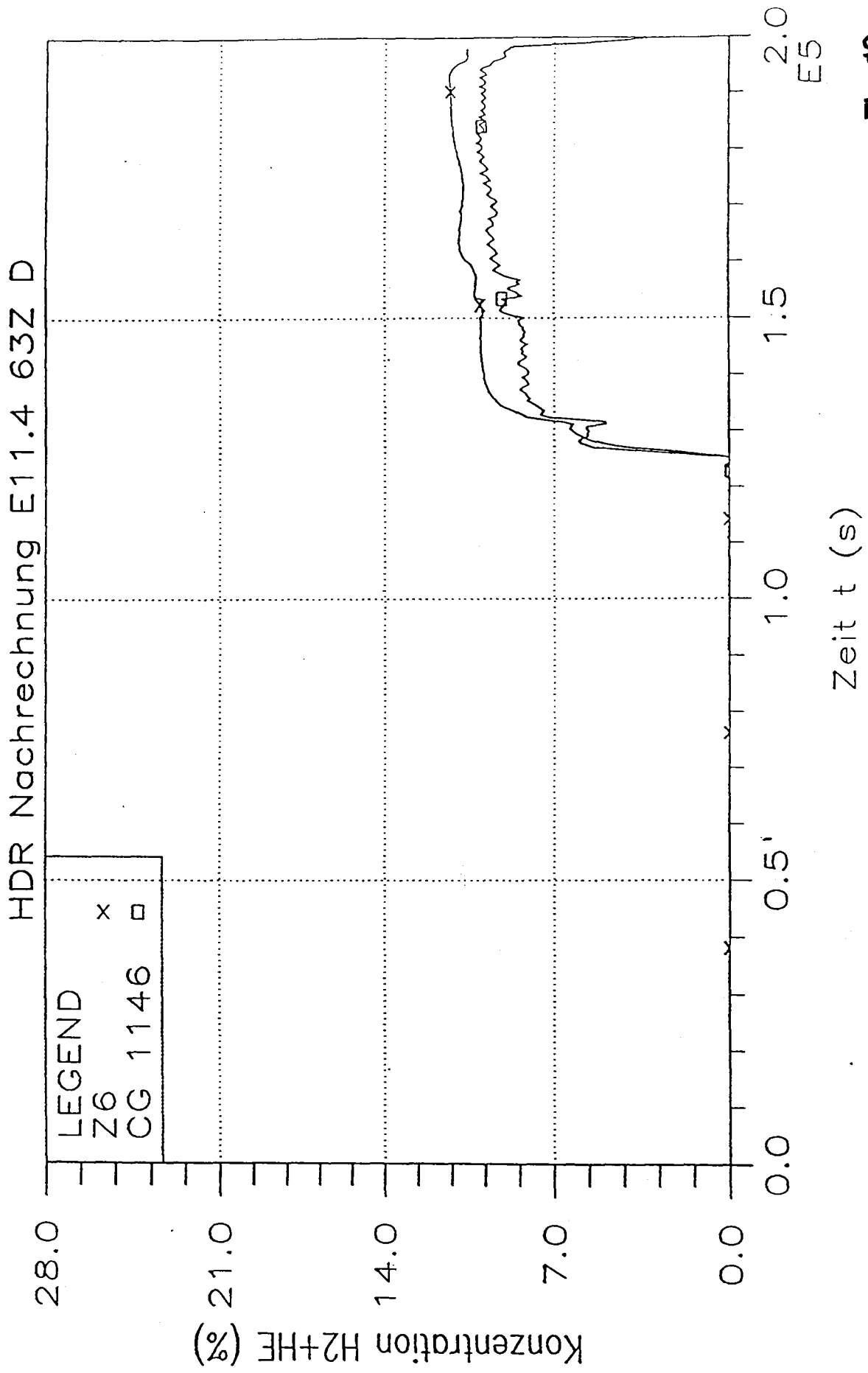


Fig.:12



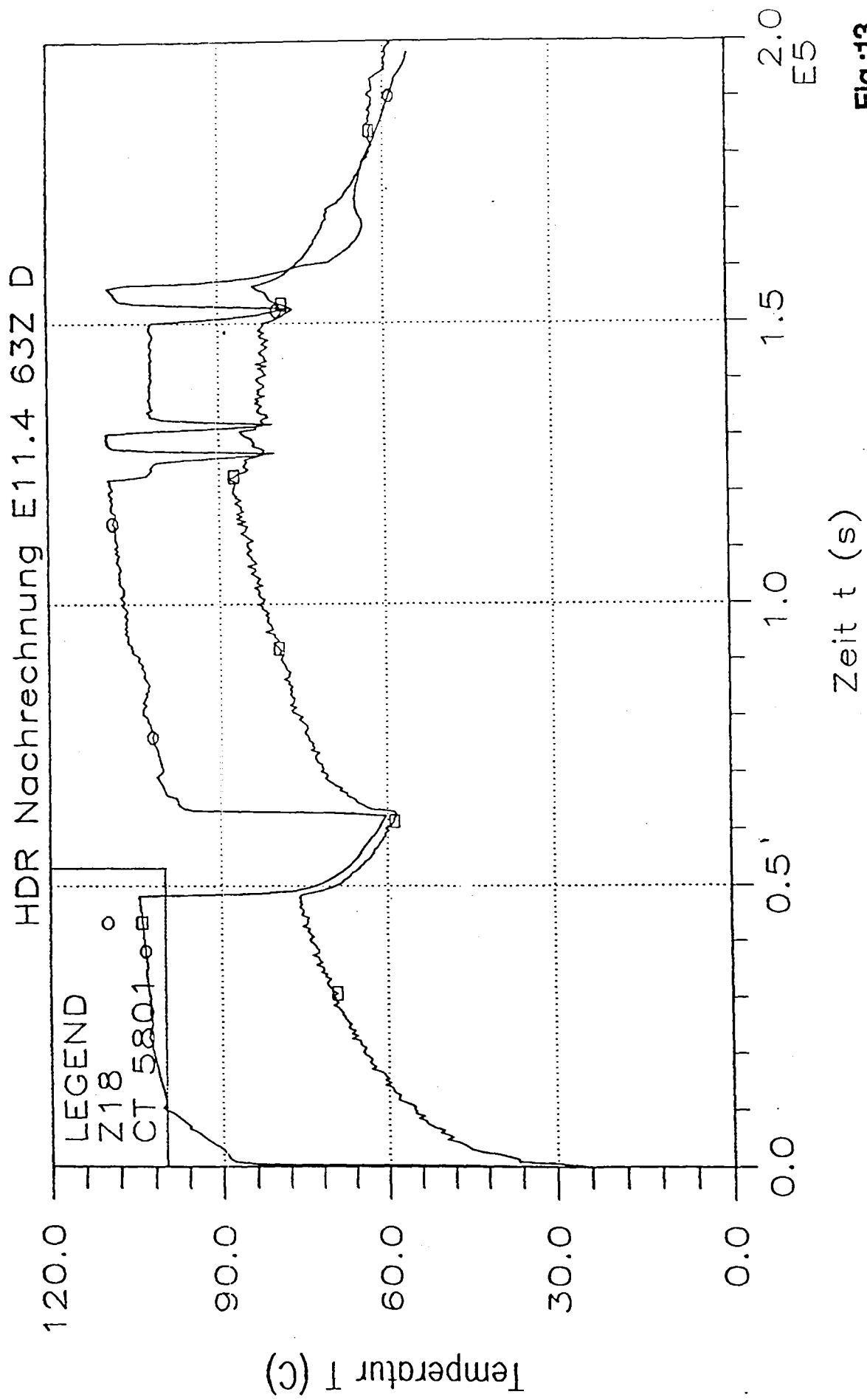


Fig.:13

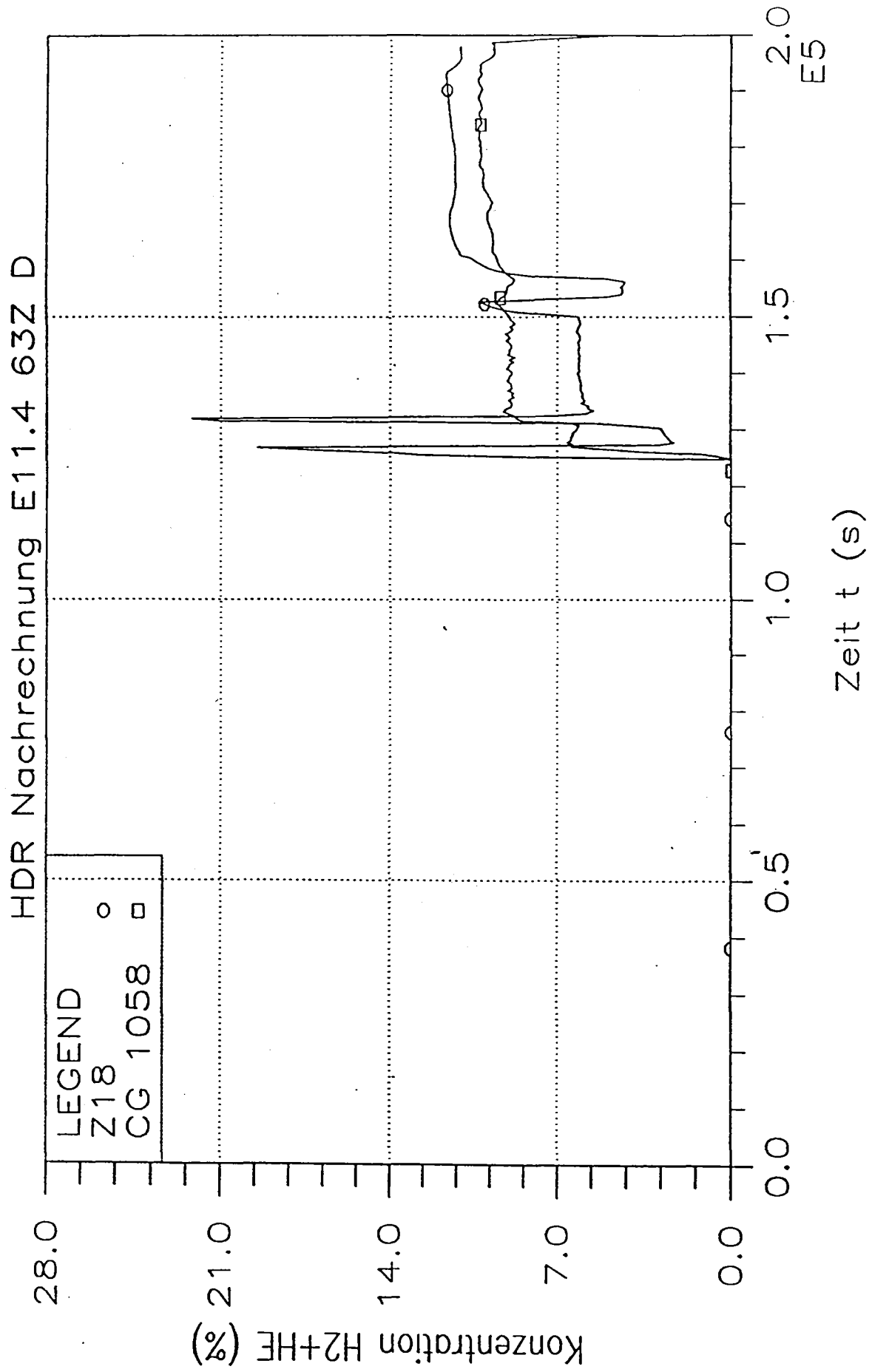


Fig.:14

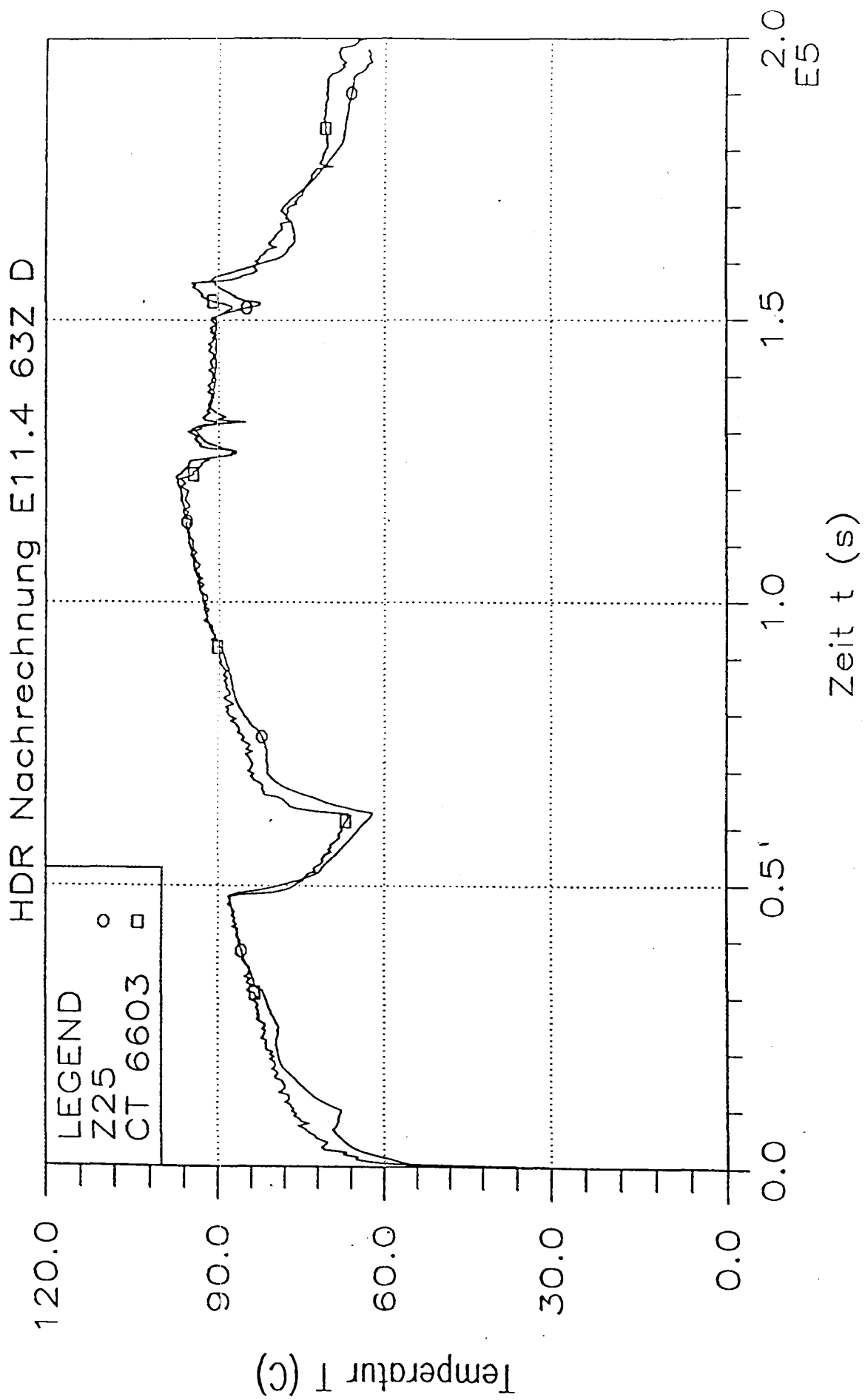


Fig.:15

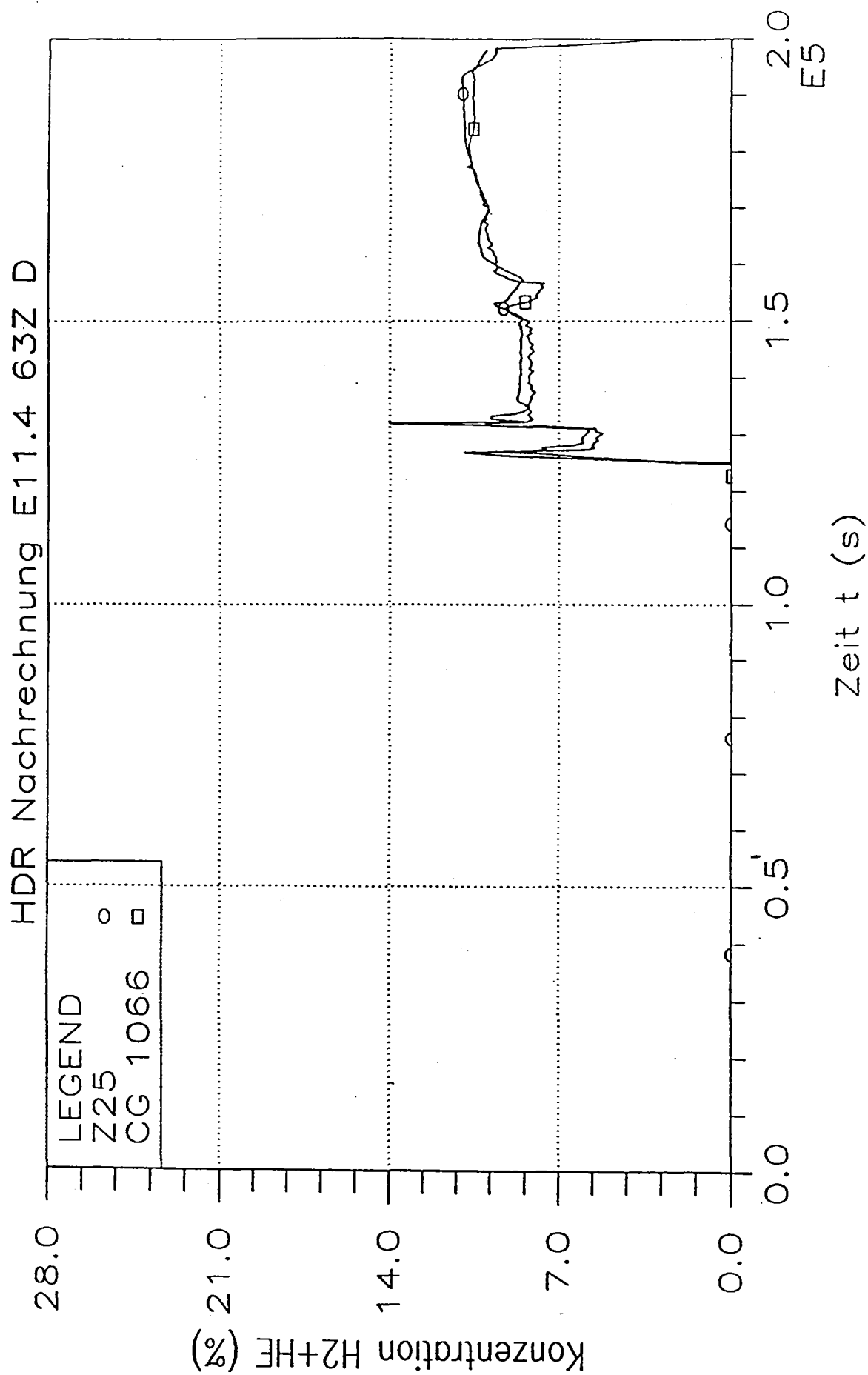


Fig.:16

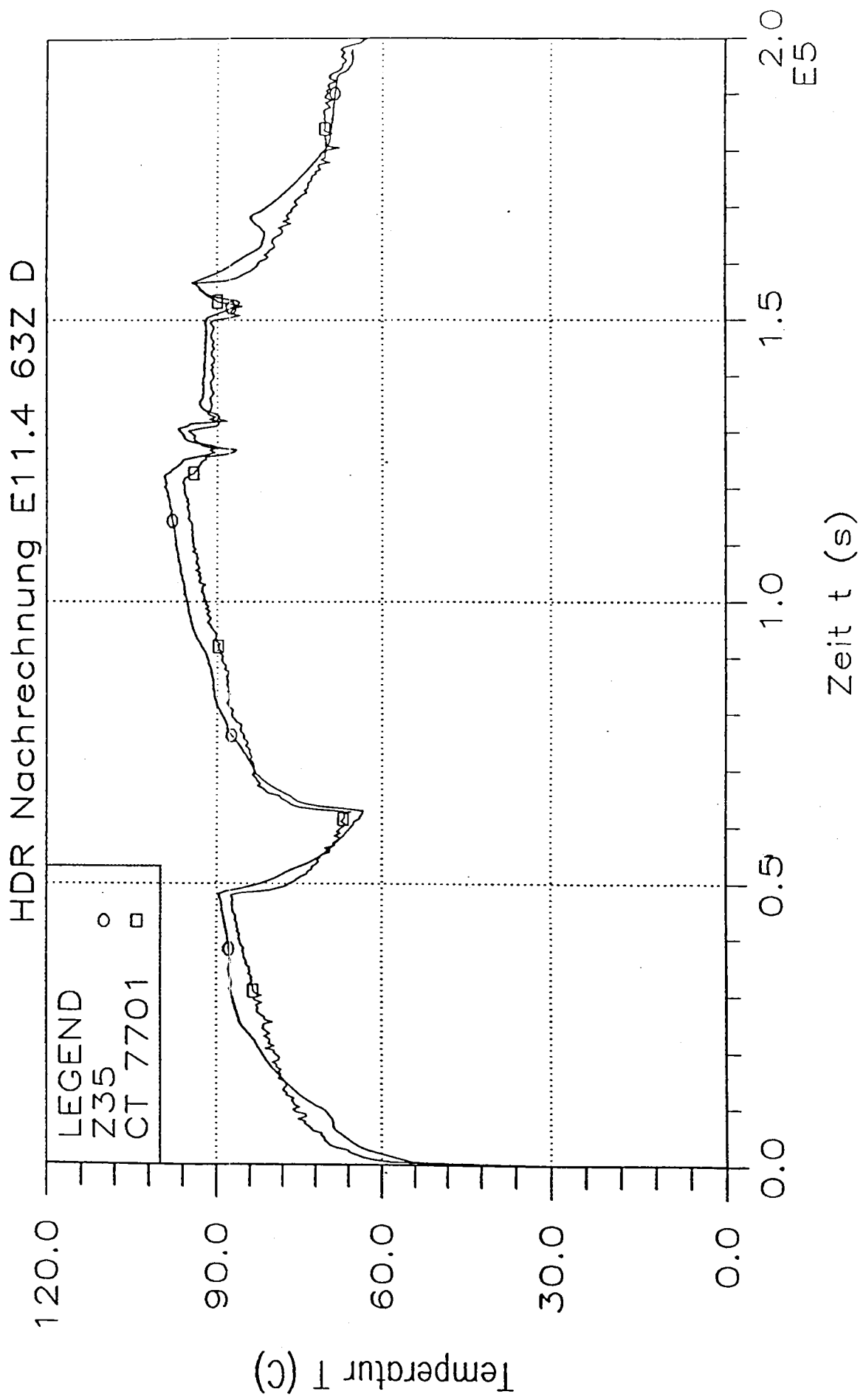


Fig.:17

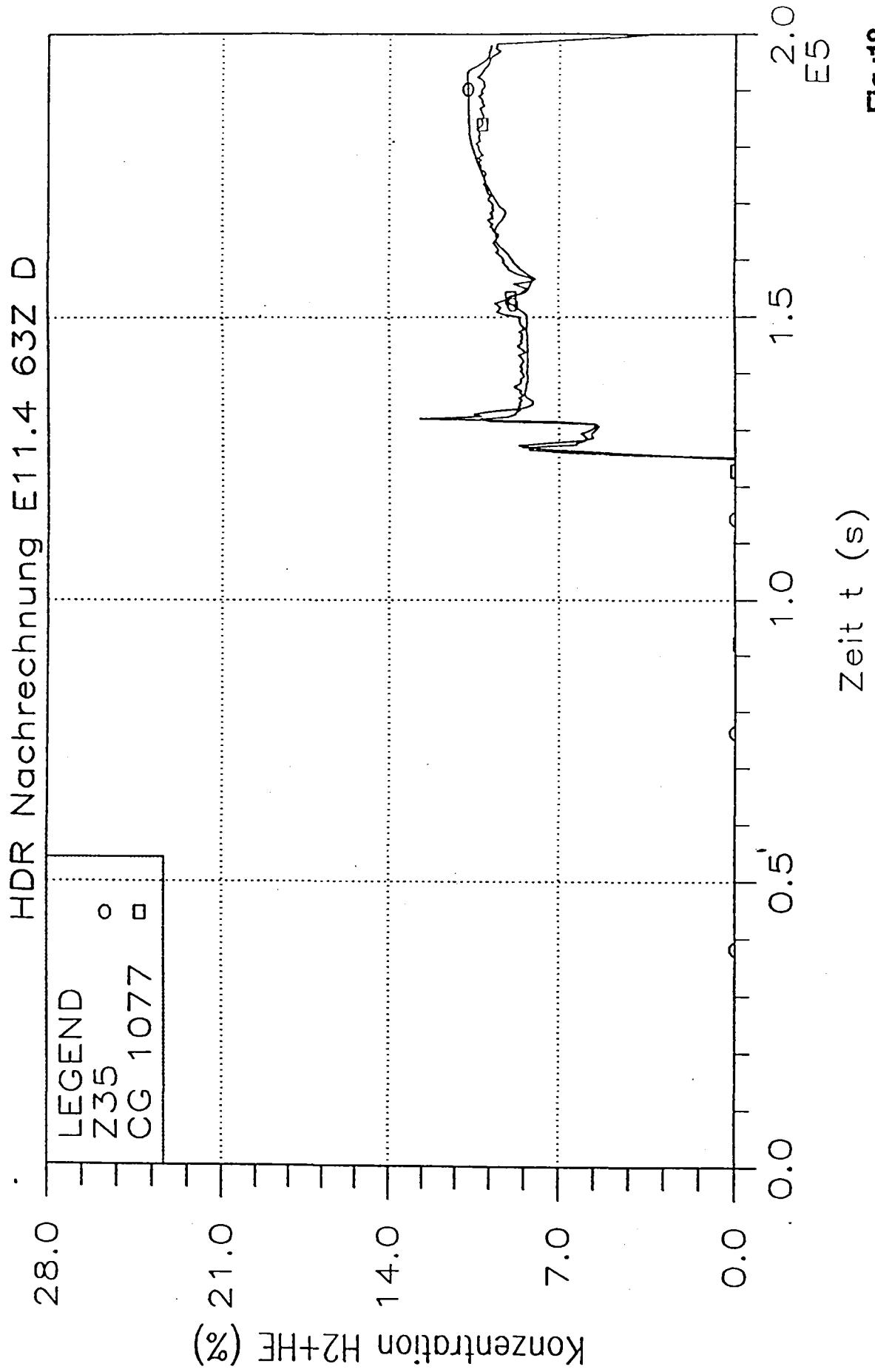


Fig.:18

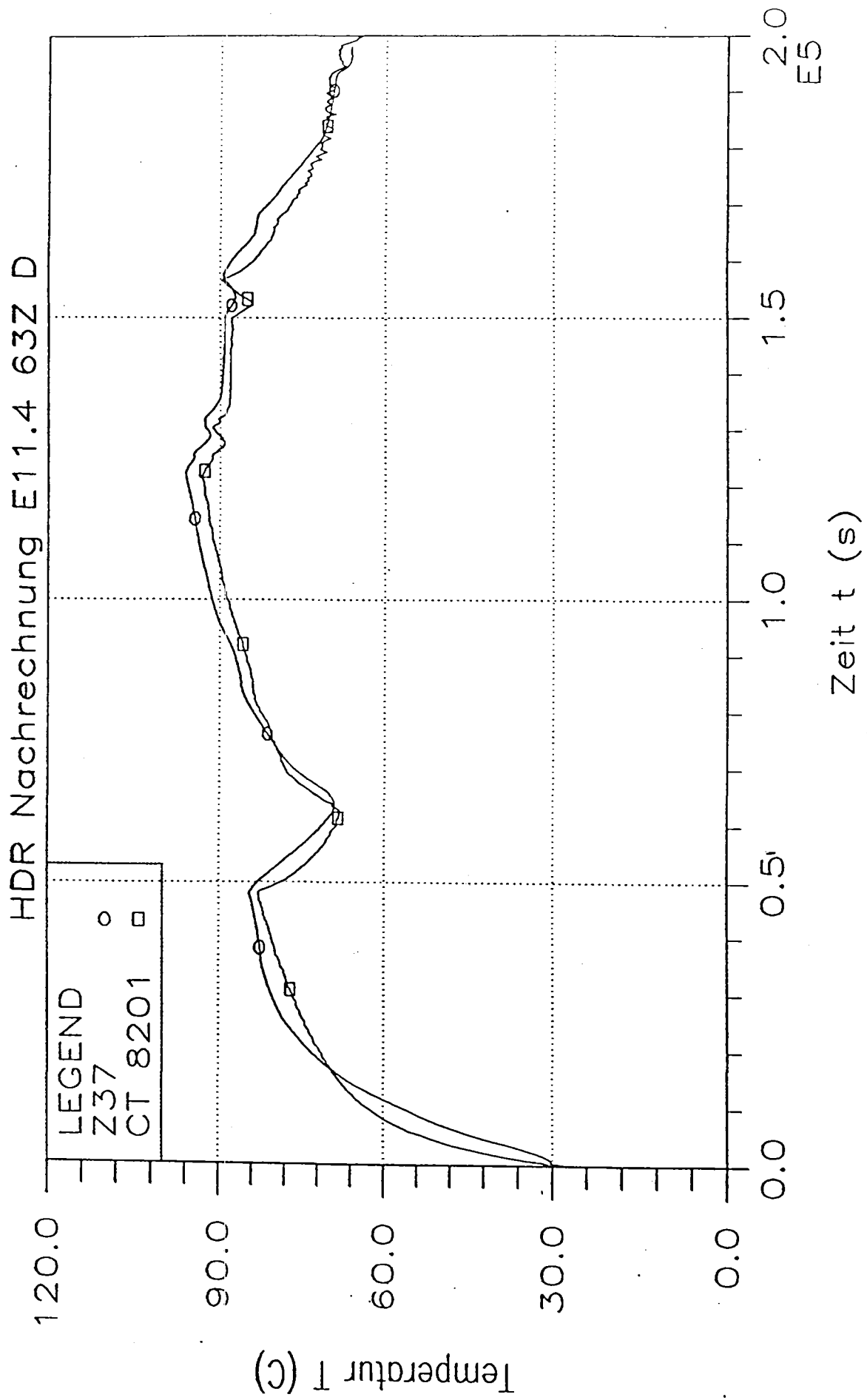


Fig.:19

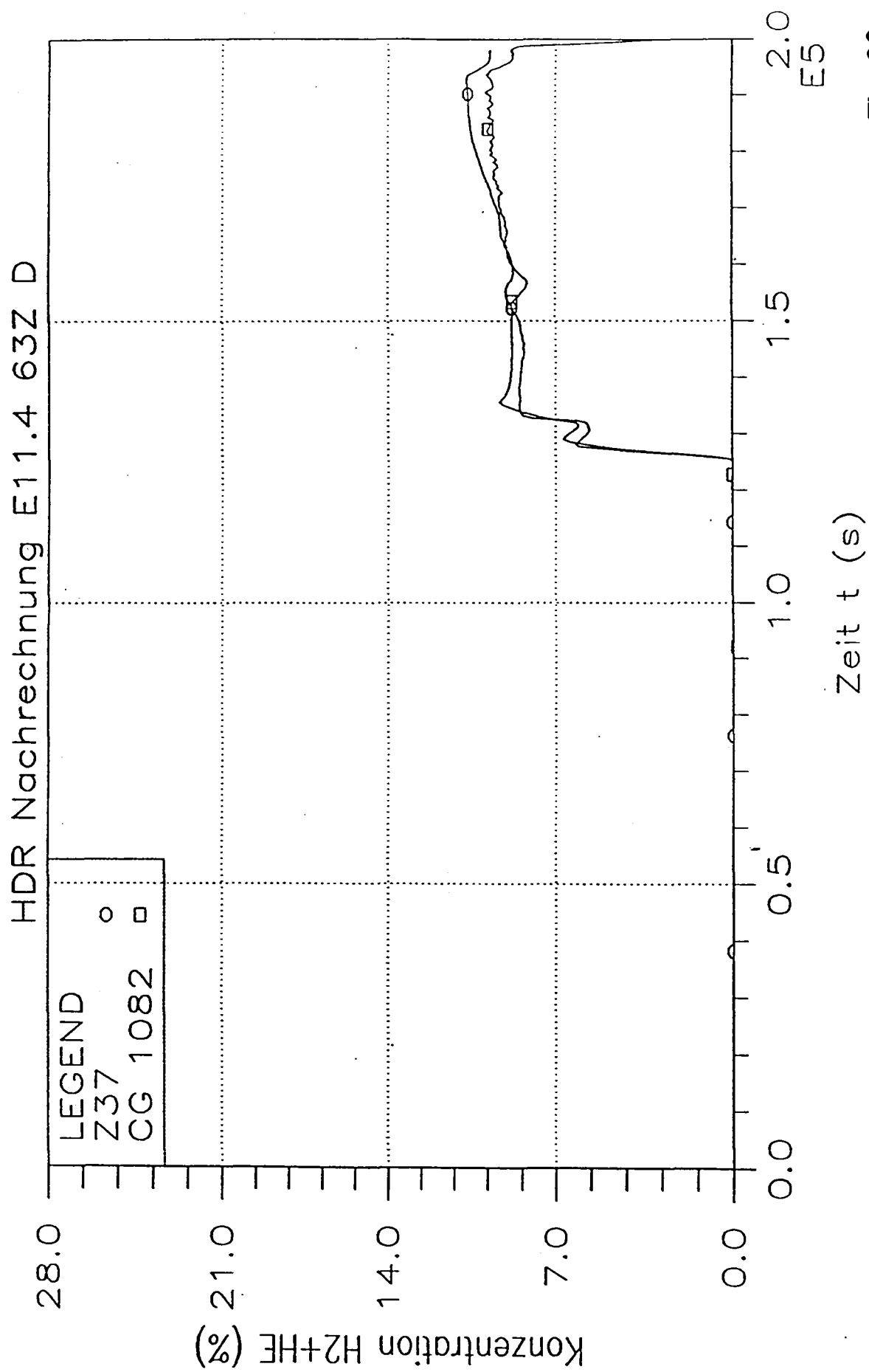


Fig.:20



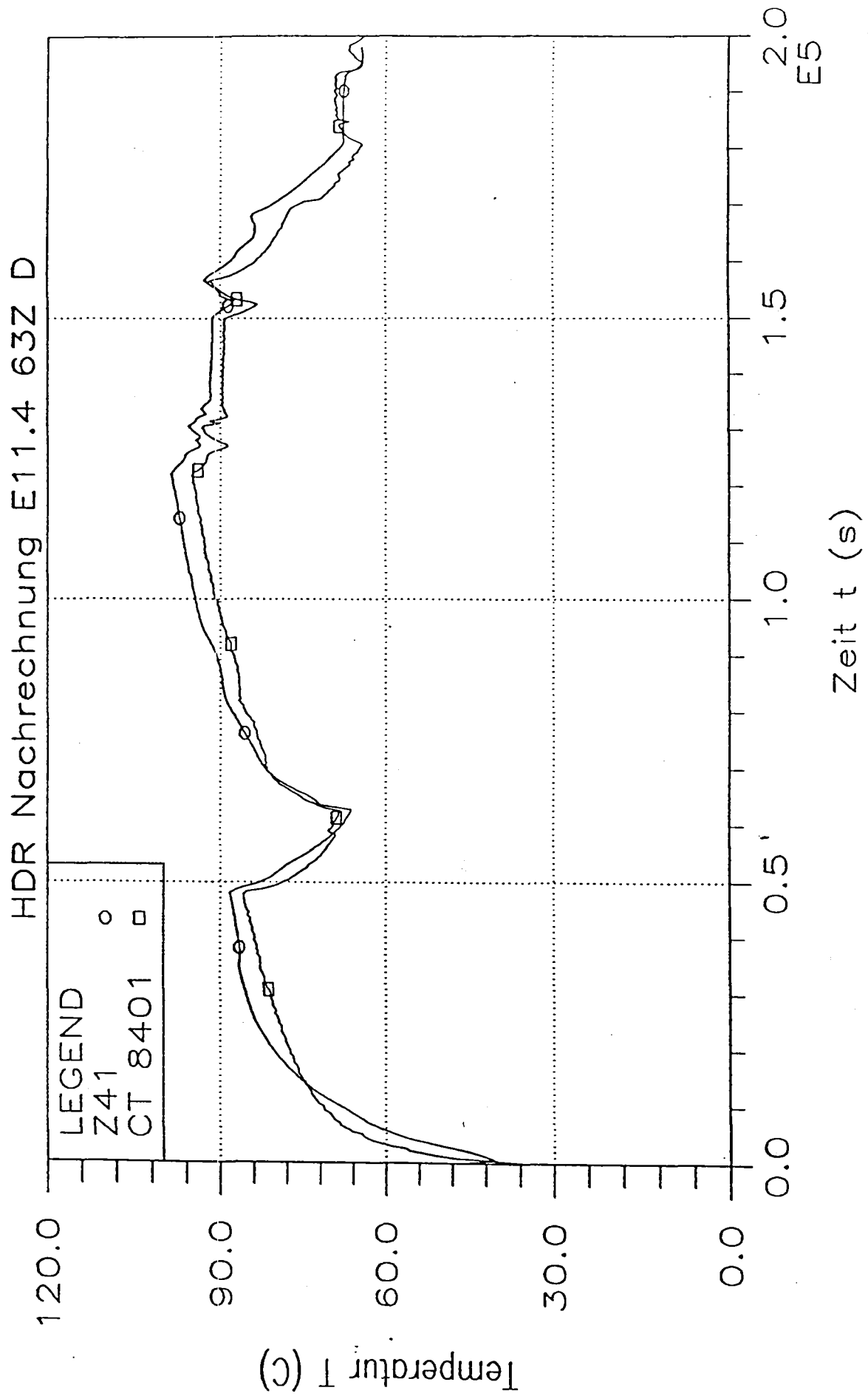


Fig.:21

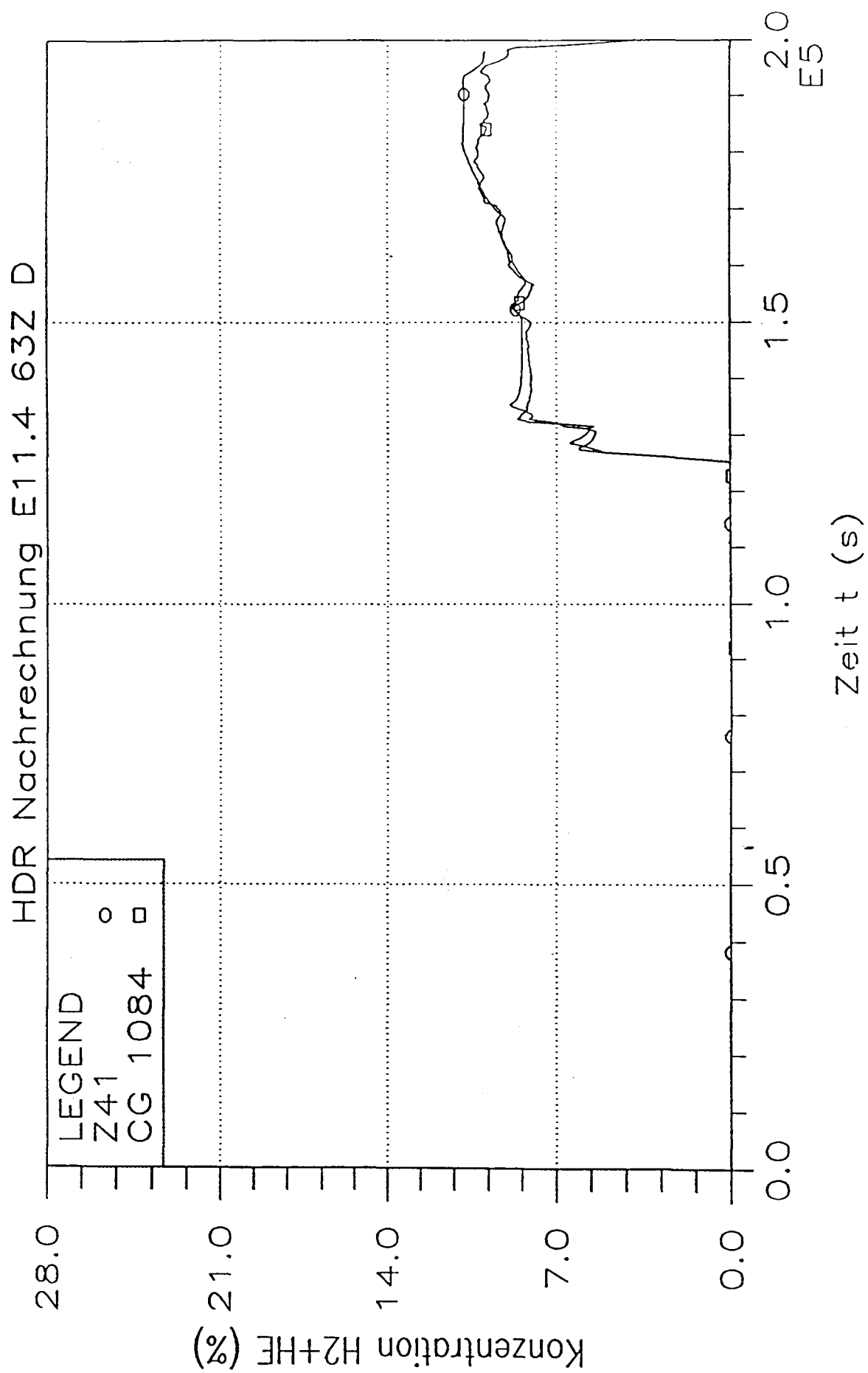
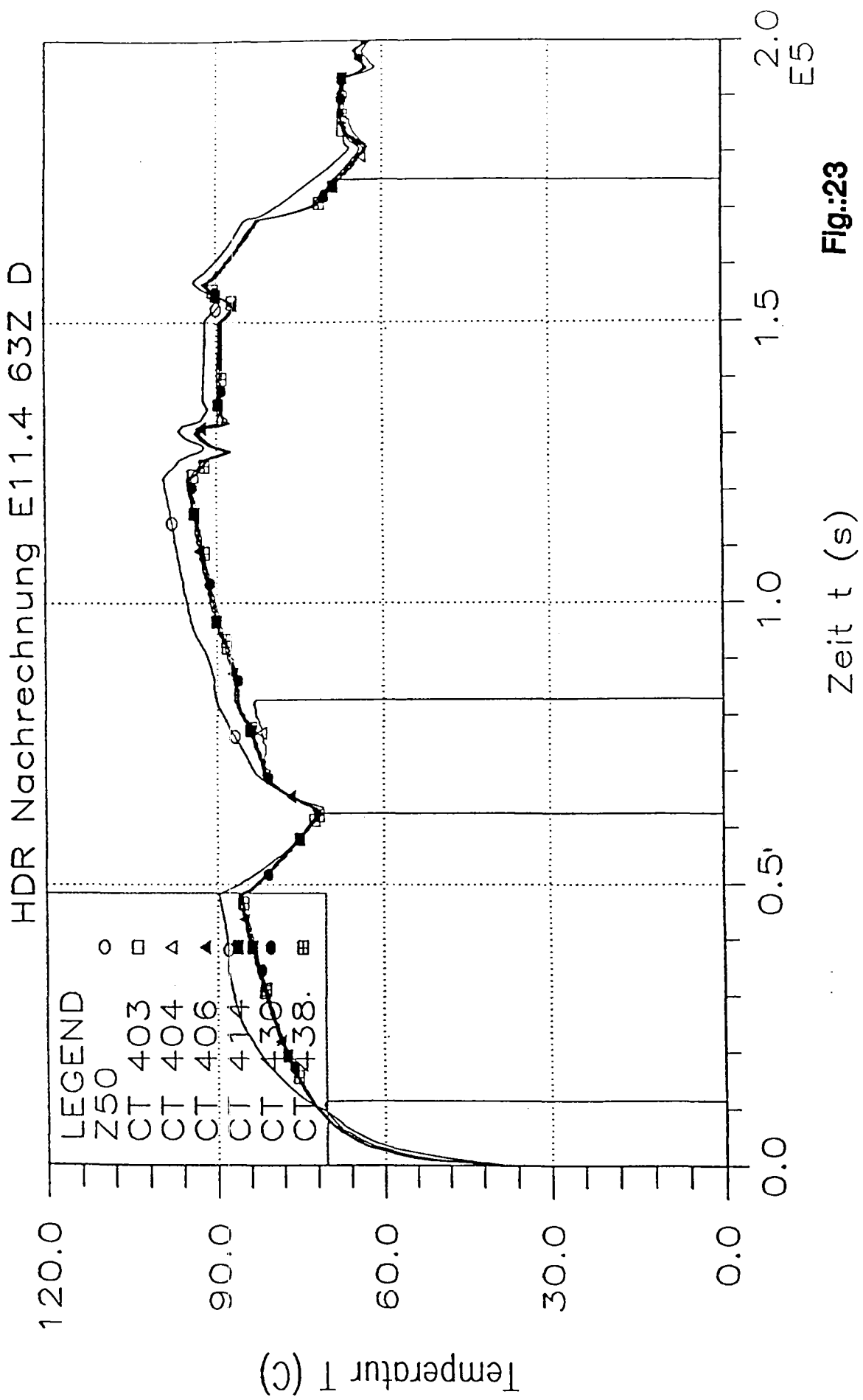


Fig.:22



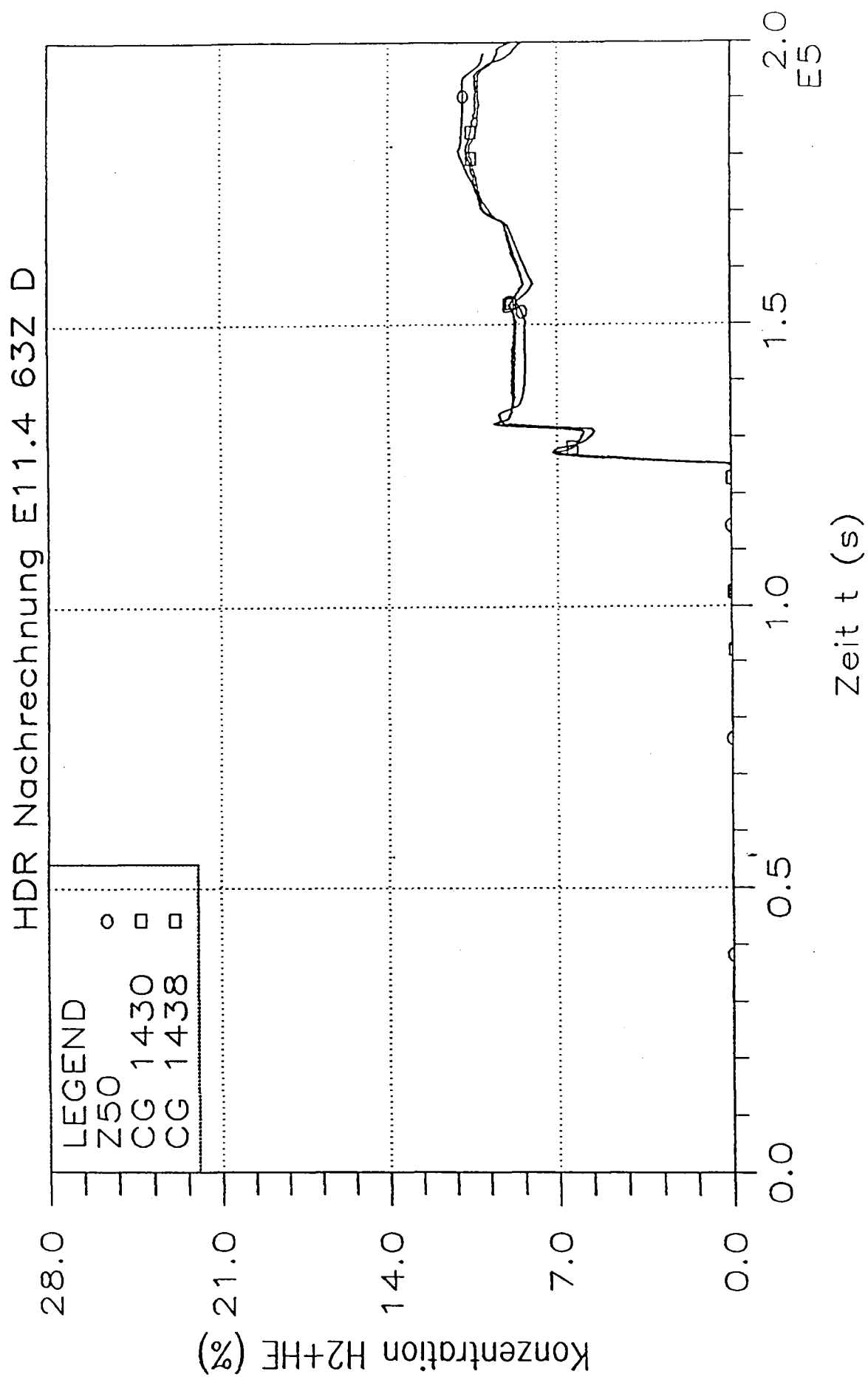


Fig.:24

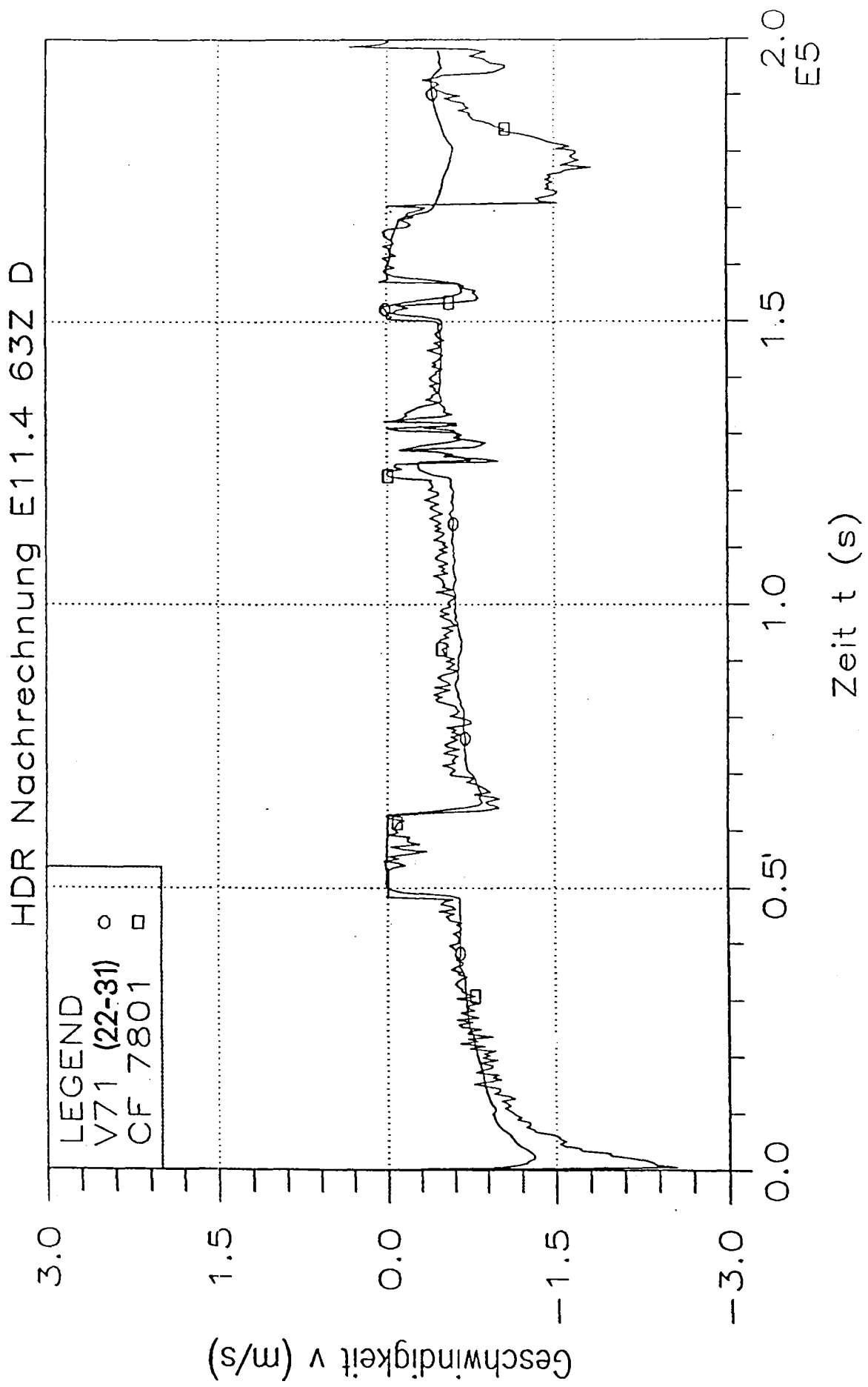


Fig.:25

Appendices were listed according  
to submissions received. There are  
no appendices II D, E, F, G.

### Appendix – AEE Winfrith

This Appendix briefly describes two sensitivity studies, which demonstrate the effect of flow resistance and cooler power distribution on the degree of predicted stratification and the predicted pressure.

#### Flow Resistance

It was noticed in several calculations that the following circular flow path was an important flow path in terms of predicting stratification :

1805 → 1903 → dome → 1902/4 → 1804 → 1704/1901 → 1701o → 1805

and so the flow coefficients (CFC in CONTAIN) were increased from 0.75 to 5.0 in this loop. So that all flow paths from the source cell (1805) had flow coefficients of 5.0, two further flow paths had their flow resistance increased :

1805 → 1367 (the source cell and stairway)

1805 → 1700's (the flow path connecting 1805 to the lower cells)

Figure 1 shows the predicted temperature stratification at 8 hours for the case with the loop flow coefficients set to 5.0, the base case presented in the main part of this report in which the flow coefficients are set to 0.75, and the recorded data. It can be seen that the trends for both calculations are very close to the experimental results, but that the calculation using the higher flow coefficients predicts a higher stratification, closer to that observed experimentally.

Figure 2 shows the same calculations, but at a later time. In this plot, the results at 11.5 hours, the point of maximum stratification, are presented. It can be seen that similarly, a higher degree of stratification is predicted with the increased flow coefficients. In both cases, however, the predicted stratification, although strong, is not as complete as that observed experimentally. The main differences are between the 10m and 15m parts of the containment, where experimentally, very little steam penetration is seen, in contrast to the predicted results.

Figure 3 shows the predicted light gas stratification at 13.33 hours. As in the case of the temperature stratification, the trends for both calculations are similar to that observed experimentally, although again, the case with the higher flow coefficients predicts a greater degree of stratification. The calculations again, do not show the level of stratification observed experimentally, with some light gas penetrating the lower parts of the containment, although in both cases, the predicted concentration levels are at or below 2% by volume.

Figure 4 shows the time history of the dome light gas concentration for both calculations. The predicted initial peak of about 12% by volume is in good agreement with the average experimental dome concentration at this time. The later stratification of

the experimental dome light gas concentration is not observed in either calculation, but instead a well mixed dome is predicted. This shortcoming was common to most of the submissions to this exercise.

The effect on the pressure of respecifying just 8 of 80 flow coefficients can be seen in Figure 5. The experimental pressure is bounded by the two calculations. The difference between the two calculations is relatively large, however. A difference of 0.17 bar can be seen, which when compared with an overall pressure rise of 1 bar, is significant.

### **Cooler power distribution**

The uncertainty in the cooler power distribution has been the subject of many sensitivities. The base case calculation presented in the main part of this report, had the cooler power located in room 1701u, the reactor pressure vessel room. In order to see the effect of locating the power elsewhere, a calculation was run in which the cooler power was distributed in the upper part of the containment, proportional to the number of sensors in the rooms. It is thought that the cooler power arises because water is circulated around the containment to keep the sensors cool. This raises a problem when interpreting the shape of the cooler power curve (Figure 6), because at say 16 hours, when the containment is very much hotter than at the beginning, the cooler power is determined to be not much greater than at the beginning, although it would be expected that the sensors require very much more cooling. Distributing the cooler power proportional to the sensors in a room is, however, the approach suggested in the data specification for this exercise.

Figure 7 shows the predicted dome light gas concentration for the case with the distributed cooler power. It can be seen that eventually, a uniform distribution results. When compared with the base case, with all the cooler power located in room 1701u, it is clear that the location of the cooler power is a very sensitive parameter.



## Model Description

39 Cells      35 + 3 + 1

85 Flowpaths      80 + 5

218 Heat sinks      215 + 3  
                          – (grouped by material type)

- Forced Convection in source cells
- Air gap with flows of  $3m^3s^{-1}$  to the environment
- Outer concrete wall
  - to model conduction to environment
- Material properties as specified by PHDR
- Sump in single cell
  - (will result in high pool temperature)
- Flow Coefficients (CFC in CONTAIN) set to 0.75
  - (sensitivity : 8 paths set to 5.0)
- Cooler power all in Room 1701u
  - (problem interpreting shape of power curve)
- Sources from revised data report
  - (except hydrogen injected into 1903)

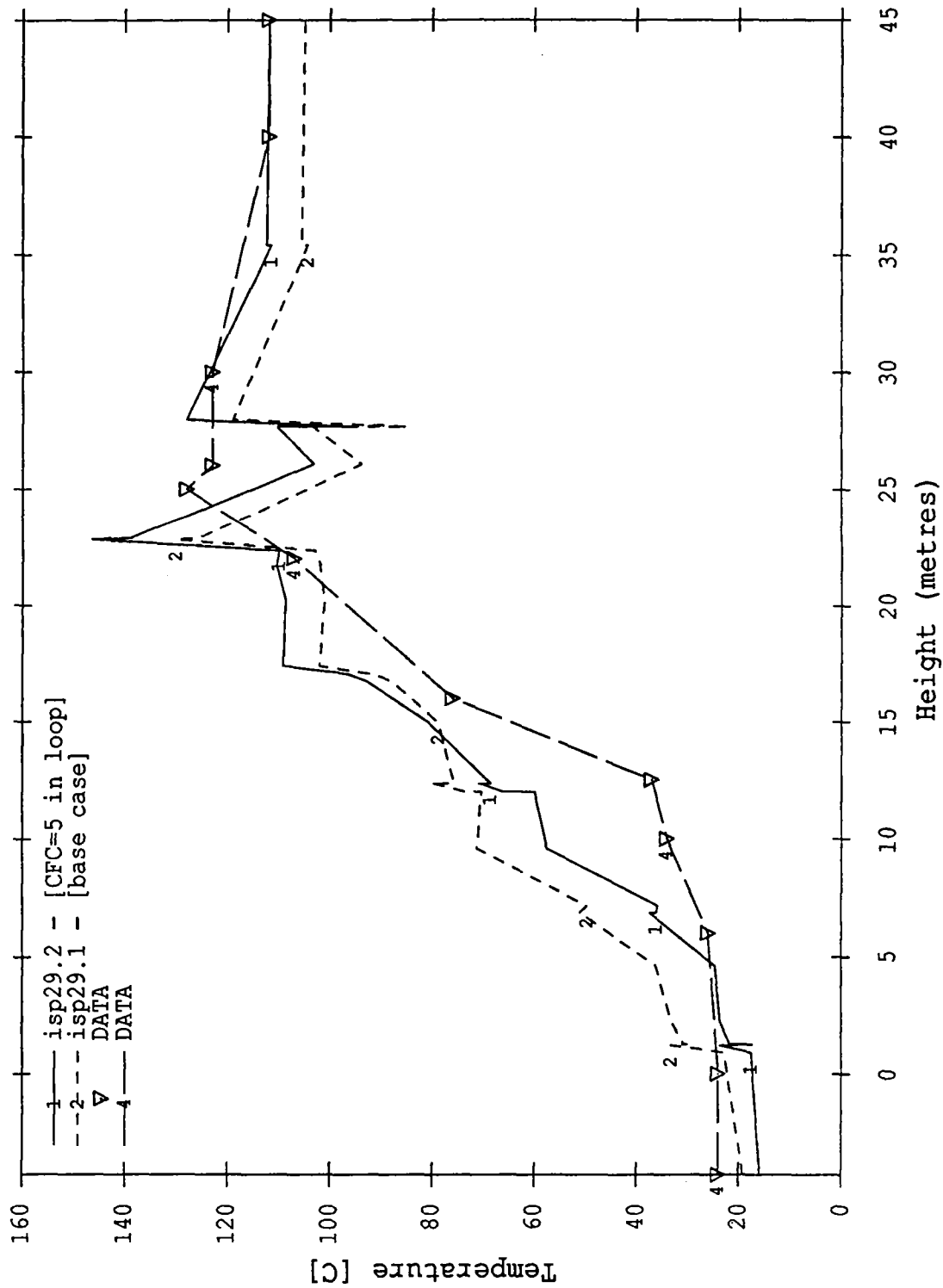


FIGURE 1: Temperature stratification at 8.0 hours

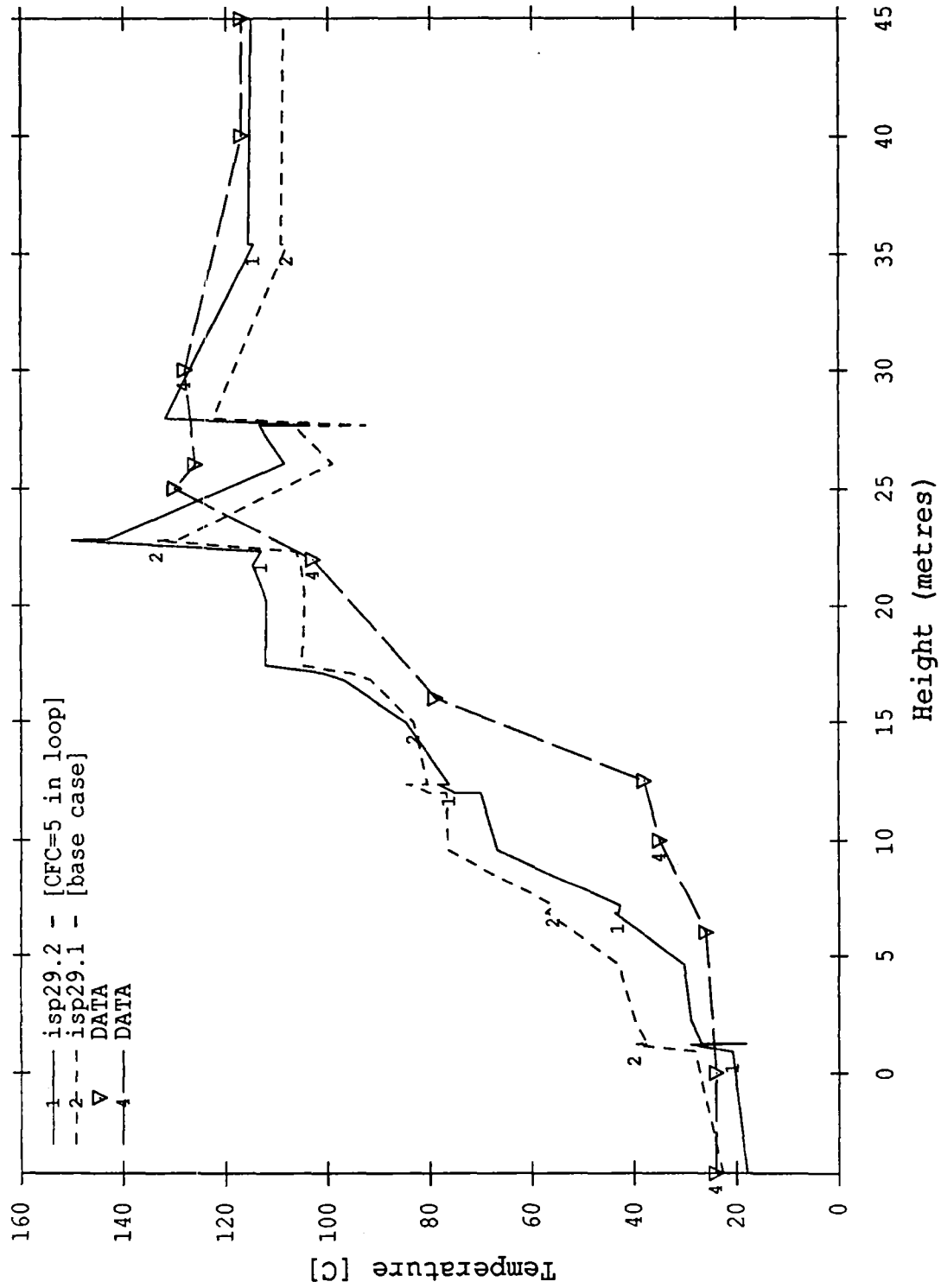


FIGURE 2: Temperature stratification at 11.5 hours

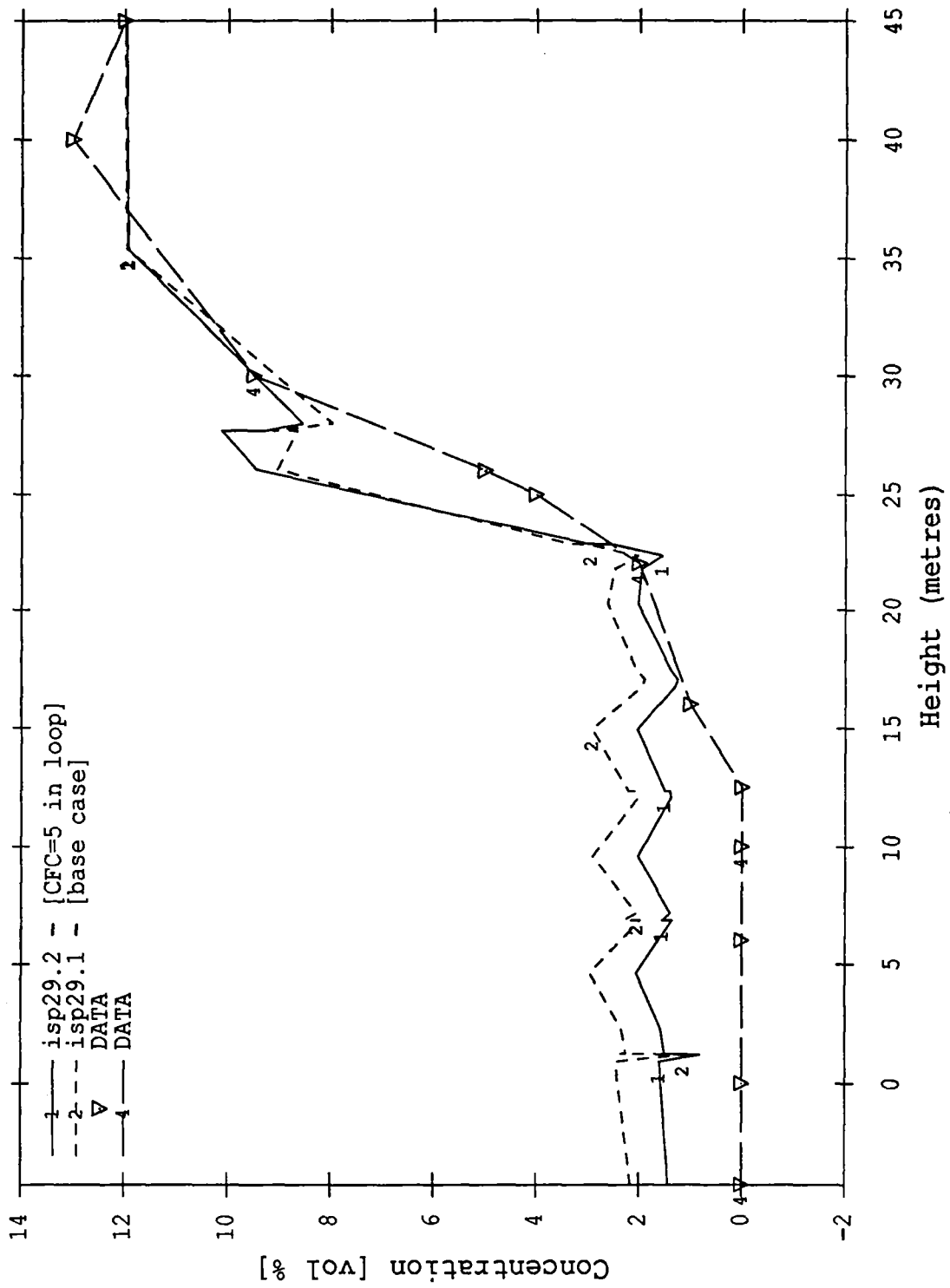


FIGURE 3: light gas stratification at 13.33 hours

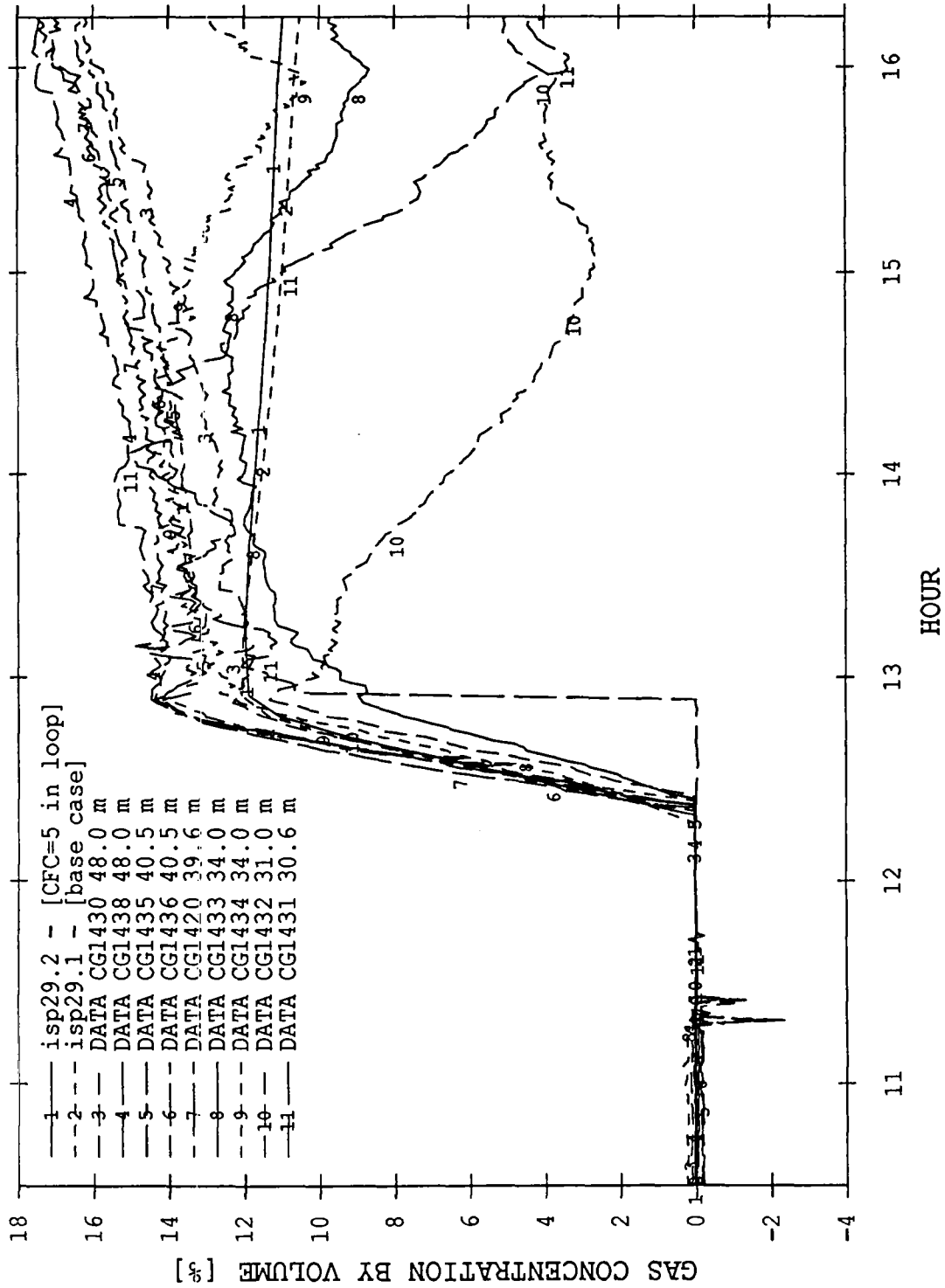


FIGURE 4: Comparison of calculated and measured light gas distributions at various heights in the dome

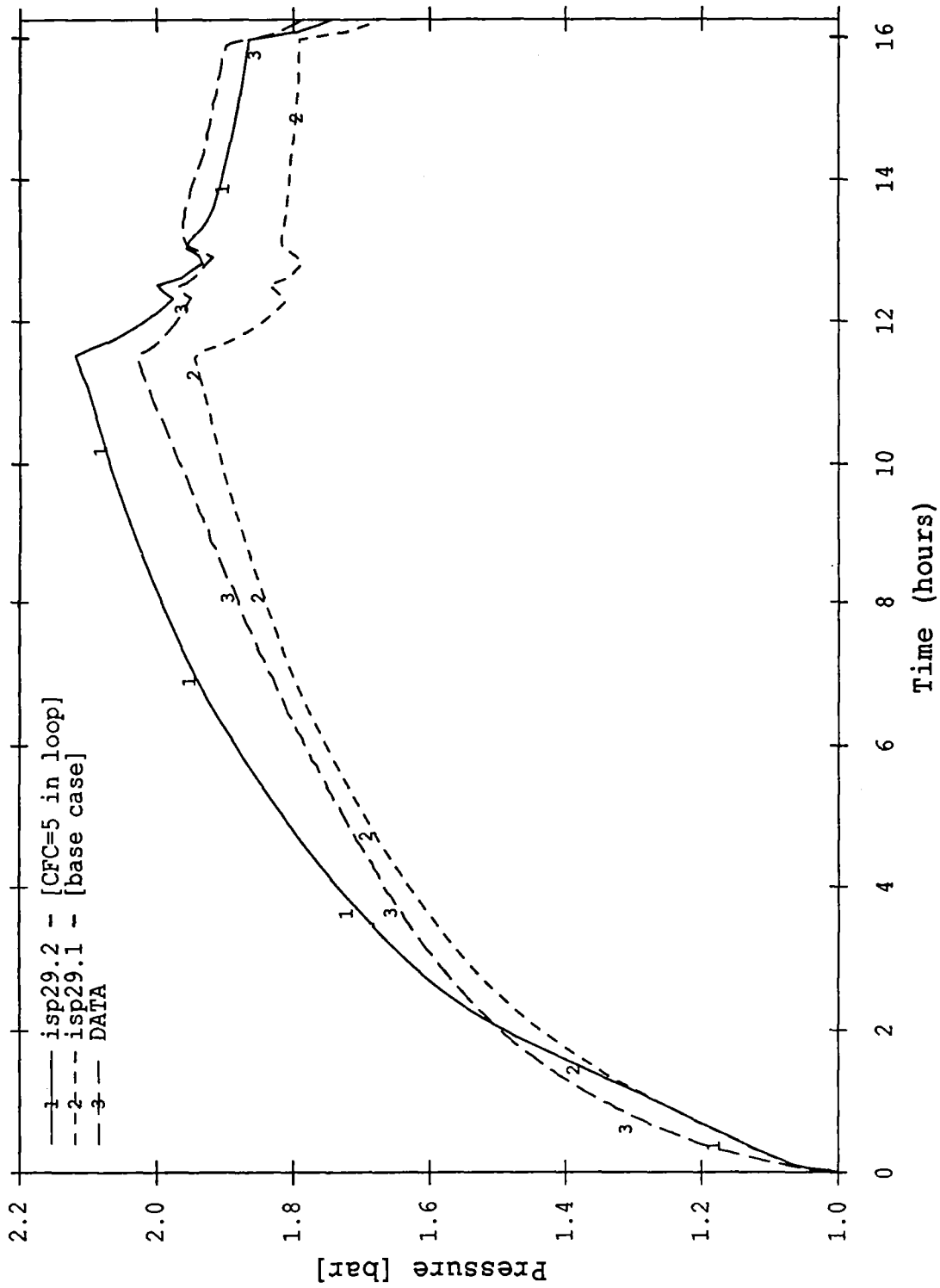


FIGURE 5: Plot of the predicted pressure for calculations ISP29.1 and ISP29.2 against the experimentally observed pressure

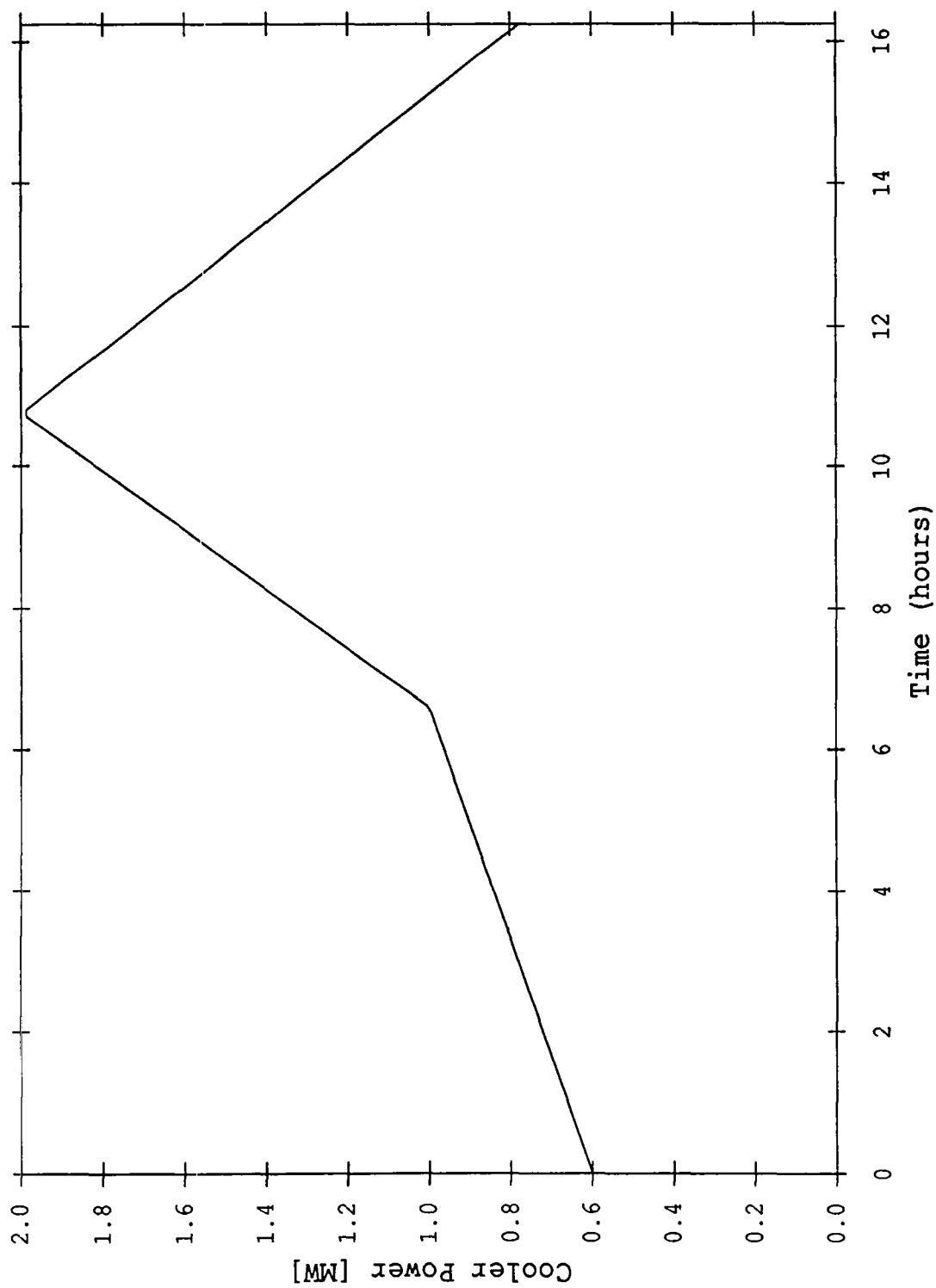


FIGURE 6: Plot of the cooler power used in ISP-29

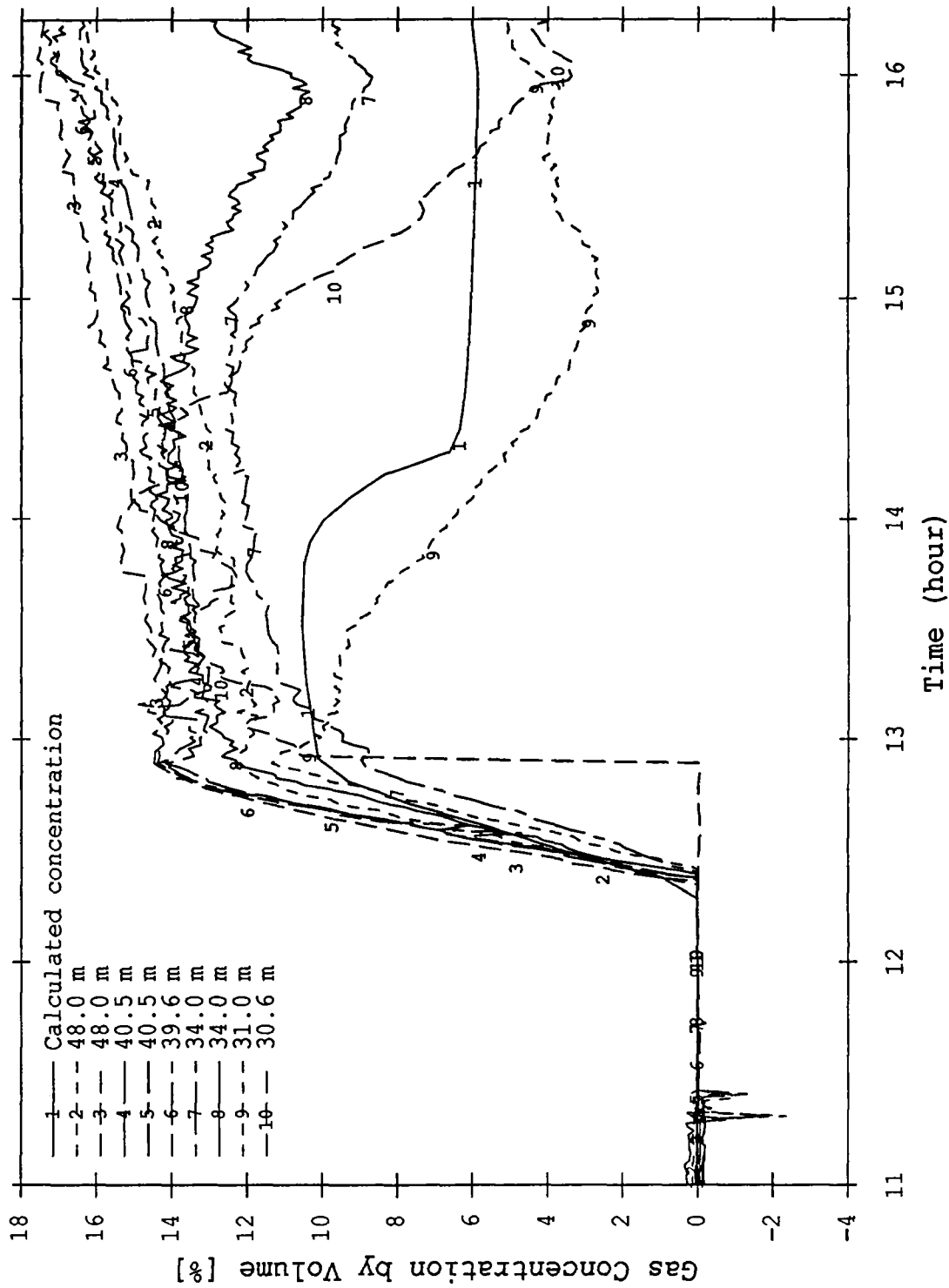


FIGURE 7: Plot of the predicted light gas concentrations in the dome for a distributed cooler power against the experimental measurements

AEE winfrith - CONTAIN 1.11 (UK)



Appendices were listed according  
to submissions received. There is  
no appendix II I.

## MELCOR Calculations for ISP-29

This Appendix contains extracts from a full report of our work for ISP-29 :

"MELCOR Calculations for ISP-29", S J K Bradley and M I Robertson,  
AEA-RS-5236, Reactor Services, AEA Technology, February 1992.

The background to our efforts with MELCOR are presented here and the MELCOR model and calculations described. It is worth noting that the annular gap in the HDR containment was not modelled because it was previously shown [2] that the heat losses from the containment to the annular gap were not important. Finally we have included our conclusions as presented in AEA-RS-5236. The reader is referred to the full report for a more extensive discussion and analysis of the results.

M I Robertson,  
AEA Technology,  
UK.

16 July 1992

## 1 Introduction And Background

The objective of this work is to assess existing methods for containment thermal-hydraulic analysis, particularly their applicability to the assessment of containment integrity threats. The MELCOR code [1] uses the control volume or lumped parameter method and validation calculations have been performed [2] with MELCOR against suitable experimental data. MELCOR is a fully integrated, engineering-level computer code that models the progression of severe accidents in light water reactor nuclear power plants. MELCOR is being developed at Sandia National Laboratories (SNL) for the United States Regulatory Commission (USNRC) as a second-generation plant risk assessment tool and as a successor to the Source Term Code Package.

MELCOR Calculations for the HDR-E11.2 experiment have previously been performed and reported by Robertson [2]. The results reported here are a continuation of this work in light of additional information about the experimental boundary conditions. This test is of particular interest because the distribution of hydrogen gas was measured under simulated severe accident conditions in a large scale containment with complex geometry. Figures 1.1 and 1.2 show vertical cross-sections of the containment facility and indicate the complexity of the internal compartment geometry.

The HDR E11.2 experiment has been selected as the basis for the OECD/CSNI International Standard Problem (ISP-29). The work reported here has been performed as part of this international bench-mark exercise and three calculations have been submitted to the exercise coordinators. In return for participating in ISP-29 we have received the experimental data on magnetic tape. This allows us to make our own comparisons with the experiment. A full comparison report of all the submitted calculations will be produced by the exercise coordinators in the near future.

Earlier calculations for ISP-29, reported by Robertson [2] showed that the containment pressures were grossly over-predicted. This suggested that either there was a problem with the MELCOR code or that there was something wrong with the specified boundary conditions. The latter suggestion was supported by the fact that several other containment thermal-hydraulic codes similarly over-predicted the containment pressures. Investigations of the specified steam boundary conditions by AEA Technology colleagues at Winfrith showed that there were important inconsistencies in the experimental data. In particular they suggested that the specified steam enthalpies were too high. This was investigated by the German experimenters and a report [3] was produced which identified the problem and revised the specified steam enthalpies accordingly.

The calculations reported herein use the same MELCOR model of the containment as was used by Robertson [2] but incorporates the revised steam enthalpy boundary

conditions and investigates the sensitivity of the results to the location of instrument cooling and flow path characteristics.

---

### 3 Description Of MELCOR Model and Calculations

The calculations reported here use the same MELCOR model of the HDR containment structure and internal compartments as used in previous efforts [2] but with the revised steam enthalpies modelled correctly. The containment is represented by a 31 control volumes inter-connected by 66 junctions or flow paths and the external and internal walls are represented by 124 heat structures. Figure 3.1 shows in schematic form how the 31 control volumes are arranged and connected to represent the internal rooms and connections within the containment. Table 3.1 shows which internal rooms were lumped together into which control volume and table 3.2 shows the specification of flow paths between the cells.

Two potentially important areas of uncertainty were identified by Robertson [2] and examined further here. The importance of the instrument cooling and the user specified flow loss coefficients in inter-cell junctions (flow paths) are explored through several sensitivity studies.

#### 3.1 Instrument Cooling

Many experimental transducers in the containment were required to be kept within specific temperature limits. This was achieved by pumping cool water through pipes which lagged the transducers. Special consideration was given to those transducers in areas where the experimenters anticipated higher thermal loads. In HDR-E11.2, this latter treatment was especially true for the central rooms in the facility including those which contained the remnants of the reactor pressure vessel.

It was not anticipated by the experimenters that the sum effect of the instrument cooling would be significant, as has been shown [2] to be the case. Consequently we have no information about the local levels of heat loss associated with the cooling pipes. Instead we have an estimate of the total heat losses from the facility derived from an energy balance on the inlet and outlet cooling water temperatures. The only additional information is the pipe lengths, diameters and locations within the facility. From this limited information it has been left to the modellers to determine how best to model the instrument cooling.

We have performed sensitivity studies on the location of the instrument cooling and the subsequent effects on the predictions. A detailed evaluation of the instrument cooling pipes and their locations was undertaken by Robertson [2] and the control volumes with most pipe volume identified. The cooling was then modelled by apportioning the total heat losses from the facility to appropriate control volumes according to the volume fraction of the total volume of pipes in that cell. For the

sensitivities reported here the total heat losses are assigned to particular regions in the MELCOR model to examine the maximum effect of the location on results, in particular the location of the instrument cooling in the facility was assigned to cells around the blowdown injection point and the inner cells representing the reactor pressure vessel rooms.

### 3.2 Flow Loss Coefficients

There is a large uncertainty associated with the correct choice of flow loss coefficients for flow paths in a complex model such as the one used to represent the HDR facility. Flow loss coefficients are usually determined for small scale experiments involving flow through small diameter pipes. These empirically derived results can be applied to much larger scale systems if the flow characteristics are similar (determined by comparison of relevant dimensionless numbers). A typical flow loss coefficient for the conditions being examined in this experiment is about 2 for flow from one room to another. In the MELCOR model used here, up to 12 rooms are lumped together into a single cell. This type of approach is necessary for computational efficiency. However, it is not at all clear how an equivalent flow loss coefficient should be derived for flow paths connected to cells in the MELCOR model which represent several different rooms of the facility and which are in turn inter-connected by parallel and serial paths. Intuitively we would expect the net resistance for flow into a lumped cell to be increased and this can be modelled by increasing the flow loss coefficients for any flow paths into such control volumes. To the best of our knowledge however there is no established methodology for deriving the value which should be used.

The original calculations performed with MELCOR for HDR-E11.2 [2] used a model which was based on one used by the code developers at Sandia National Laboratories (SNL) for ISP-23, [4]. This standard problem was based on the HDR-T31.5 experiment which measured the containment thermal-hydraulic conditions following a simulated large loss of coolant accident (LOCA). The MELCOR best-estimate calculations for this test were performed with a model where the flow loss coefficients of all inter-cell junctions were set to 2. Subsequently these values were retained for the earlier calculations reported by Robertson [2] for HDR-E11.2. For the sensitivities reported here we have explored the effect of increasing the flow loss coefficients in flow paths into cells representing several rooms by up to 2 orders of magnitude from the original value of 2.

---

## 5 Conclusions

We have investigated the lumped parameter method for modelling containment thermal-hydraulics by comparing the results from the MELCOR code against experimental data from the HDR-E11.2 test. Extensive sensitivity studies have been performed to assess certain outstanding uncertainties associated with an experimental feature and the MELCOR model itself. In particular the location of the instrument cooling and the modelled flow loss coefficients for flow paths into the lower regions of the facility model have been examined. From these studies we can make the following conclusions.

1. The instrument cooling is an important heat sink and it must be modelled otherwise the containment pressures will be grossly over-predicted.
2. Inadequate data is available on how best to model the location of the instrument cooling. Weighting the cooling of certain compartments by the fraction of cooling pipe therein causes the calculation to crash as it freezes those compartments where very little heating is measured. The greatest heat losses will have been from those compartments with cooling pipes and with highest atmospheric temperatures. This is a time dependent problem and modelling it correctly is non-trivial.
3. The location of the instrument cooling in the facility has some effect on the short term results especially for the penetration of the light gas into the lower cells of the model. However, these differences are eroded over a period of 4 hours with similar concentrations throughout the facility predicted at the end of the calculations.
4. The over-prediction of the temperatures in the lower cells of the model result initially from an over-prediction in the amount of steam ingress and this is an inherent limitation of the lumped parameter method. The temperature over-predictions following the late blowdown injection are most likely due to the fact that no cooling is modelled in this region.
5. The nodalisation of the containment facility is inadequate in certain respects. In particular the results for one cell representing six rooms of the facility at about the 10 metres level are quite different from others at a lower level and to which it is connected. A more refined nodalisation of these rooms should be explored.
6. Increasing the flow loss coefficients in those flow paths connecting cells in the lower cells of the model to those higher up restricts steam and light gas ingress

---

into the lower regions. This gives better agreement with the experimental values in the lower cells but results in over-predictions of the pressures, steam concentrations and consequently temperatures in the upper dome cells.

7. The over-pressures which result from the increased flow loss coefficient approach indicate that this is not an adequate model refinement for better prediction of the containment thermal-hydraulic behaviour.
8. We conclude that the consistent over-prediction of the containment pressures throughout all the sensitivities reported here is due to a problem in the mass/energy balance in the MELCOR code which results in pressures being over-predicted for steam injection into a containment. This is a matter of serious concern and should be addressed by the code developers.
9. MELCOR predicts in all cases that there is no stratification of the atmosphere in the upper dome and that it is continuously well-mixed. This is in contrast to the experiment where significant differences in the steam and light gas concentrations were observed.
10. MELCOR does not predict the light gas distribution in the containment correctly. In the experiment all the light gas rose into the upper dome and stayed there, in contrast MELCOR initially predicts flow up into the upper dome but then distributes the light gas evenly throughout the containment.
11. We conclude that the lumped parameter method is inadequate for accurate prediction of light gas (hydrogen) distribution in a containment under severe accident conditions. We therefore recommend that alternative methods be investigated.



---

## References

- [1] Summers, R.M., Cole Jr., R.K. et al., *MELCOR 1.8.0: A Computer Code for Nuclear Pressure vessel Severe Accident Source Term and Risk Assessment Analyses*, NUREG/CR-5531, SAND90-0364, Sandia National Laboratories, U.S. Nuclear Regulatory Commission., January 1991.
- [2] Robertson, M.I. and Wheatley, C.J., *Validation Of The Control Volume Method As Applied In The MELCOR Code, For Calculating LWR Containment Thermal-Hydraulics During Severe Accidents*, AEA-RS-5108, Reactor Services, AEA Technology, April 1991.
- [3] Wenzel, H.H, Wolf, L., Valencia, L., Bader, H.J., Grimm, R., Jansen, K., *Quality Considerations Of Major Direct And Indirect Measured Quantities During The Experiments Of Test Group E11*, PHDR-Working Report No. 10.025/91, June 1991
- [4] Karwat, H., *International Standard Problem, ISP-23. Rupture of a Large Diameter Pipe in the HDR Containment. Volumes 1 and 2.*, CSNI-Report No. 160., OECD/NEA/CSNI., December 1989.
- [5] Bradley, S.J.K., Ketchell, N., Robertson, M.I., *MELCOR Aerosol Review*, GNSR(DEn)/TWP/P(91)82, AEA Technology, January 1992

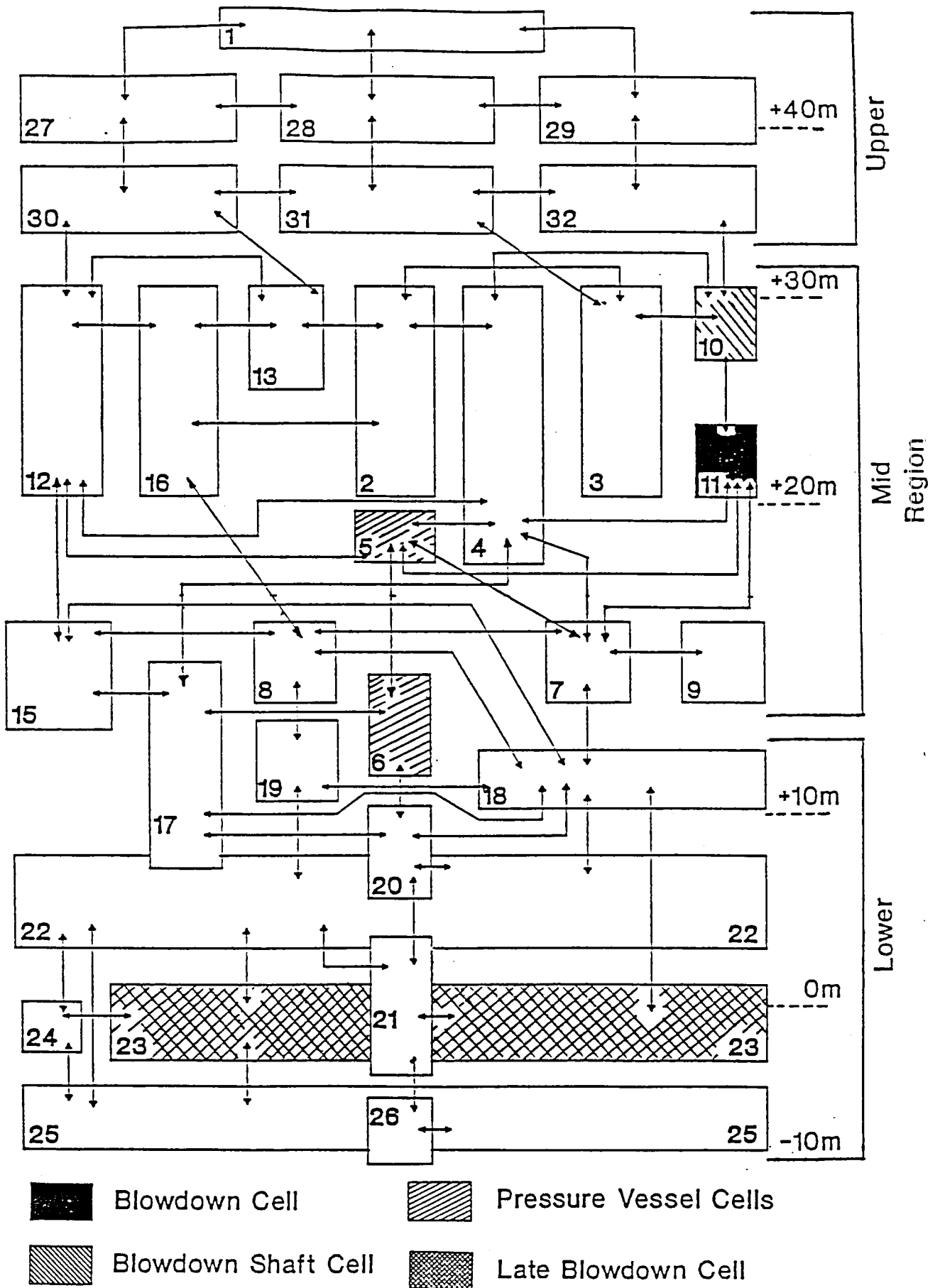


Figure 3.1  
MELCOR Model Of HDR Test E11.2  
Used For ISP-29 Calculations

Table 3.1  
MELCOR Nodalisation Of HDR Test E11.2  
For ISP-29 Calculations

CELL NUMBER	HDR ROOMS	COMMENT
1, 27, 28, 29, 30, 31, 32	11004	Upper dome split into 7 nodes.
2	1803 1904	
3	1801 1905	
4	1704	
5	1701o	
6	1701u	
7	1347 1707	
8	1703 1706	
9	1702	
10	1367 1903	
11	1357 1805	Blowdown cell
12	1804 1902	
13	1906	
15	1708	
16	1802	
17	1603	
18	1337 1604 1606 1607 1608 1611	
19	1602 1609	
20	1605	
21	1407 1504	
22	1327 1501 1502 1503 1505 1506 1507 1508 1511 1512 1513 1514	
23	1317 1401 1403 1404 1405 1406 1409 1410 1420 1421	Late blowdown cell
24	1408	
25	1201 1301 1302 1304 1305 1307 1308 1311	
26	1202 1203 1303	

**Table 3.2**  
**Specification Of Flow Paths Used In MELCOR Model**  
**Of HDR Test E11.2 For ISP-29 Calculations**

FLOW PATH NUMBER	FROM CELL NUMBER	TO CELL NUMBER	AREA OF FLOW PATH (m <sup>2</sup> )	LENGTH OF FLOW PATH (m)	FLOW PATH NUMBER	FROM CELL NUMBER	TO CELL NUMBER	AREA OF FLOW PATH (m <sup>2</sup> )	LENGTH OF FLOW PATH (m)	FLOW PATH NUMBER	FROM CELL NUMBER	TO CELL NUMBER	AREA OF FLOW PATH (m <sup>2</sup> )	LENGTH OF FLOW PATH (m)
1	31	3	35.0	0.5	30	7	11	12.51	0.5	56	21	22	0.0825	1.0
4	32	10	9.62	0.5	31	7	18	11.69	0.5	57	21	23	1.039	0.1
5	30	12	4.1	0.5	33	8	15	0.06	0.5	58	21	26	0.337	0.8
6	30	13	0.03	0.1	34	8	16	0.072	0.5	59	22	23	15.9	1.0
7	2	3	15.0	0.5	35	8	18	0.304	0.56	60	22	24	0.276	1.0
8	2	4	0.0148	0.5	36	8	19	0.06	0.5	61	22	25	0.93	5.0
9	2	13	0.075	5.0	37	10	11	12.83	0.5	62	23	24	0.119	0.8
10	2	16	0.06	5.0	38	12	13	0.197	0.5	63	23	25	10.835	1.0
11	3	10	0.42	5.0	39	12	13	2.91	0.3	64	24	25	3.142	0.5
12	4	5	1.62	1.6	40	12	15	4.99	0.5	65	25	26	3.027	1.0
13	4	7	1.5	2.38	41	12	16	3.11	0.4	66	1	16	1.824	0.4
14	4	10	0.31	5.0	42	13	16	0.061	0.5	67	30	27	100.0	1.0
15	4	11	0.168	1.24	43	15	17	0.43	2.27	68	31	28	100.0	1.0
16	4	12	0.4515	2.27	44	15	18	6.98	0.5	69	32	29	100.0	1.0
18	4	17	1.648	0.5	45	17	18	4.104	0.8	70	27	1	100.0	1.0
22	5	6	1.7	3.0	46	17	20	0.19	0.5	71	28	1	100.0	1.0
23	5	7	0.0327	3.0	49	18	19	3.085	0.32	72	29	1	100.0	1.0
24	5	11	0.0806	2.0	50	18	20	2.27	1.5	73	30	31	100.0	1.0
25	5	12	0.24	2.0	51	18	22	13.137	2.0	74	31	32	100.0	1.0
26	6	17	3.313	4.0	52	18	23	0.22	10.0	75	27	28	100.0	1.0
27	6	20	13.95	2.0	53	19	22	0.1	0.27	76	28	29	100.0	1.0
28	7	8	1.69	0.28	54	20	21	0.557	2.0					
29	7	9	1.44	0.2	55	20	22	0.163	5.0					

## Appendix A - Description Of The MELCOR Calculations

The table below list all the MELCOR calculations carried out for ISP-29. Calculations CB-D1 are reported elsewhere [2], and calculations E1-J2 are described in this report.

Calculation	Description
CB	Blind post-test calculation
M1	Liquid water flow prevented in vertical flow paths
B1	Corrected steam enthalpies
C1	Instrument cooling modelled
D1	Heat losses due to annular ventilation modelled
E1	Corrected steam injection rates, no instrument cooling, liquid water flow prevented in vertical paths, annular ventilation
F1	Instrument cooling modelled and occurs in the blowdown cell (11)
F2	As F1 but with lower cell flow loss coefficients of 20
F3	As F1 but with lower cell flow loss coefficients of 200
F4	As F1 but with lower cell flow loss coefficients based on HDR
G1	Instrument cooling modelled and equally partitioned between the pressure vessel cells (5,6)
G3	As G1 but with lower cell flow loss coefficients of 20
G4	As G1 but with lower cell flow loss coefficients based on HDR
H2	Instrument cooling modelled and equally partitioned between the blowdown cell and the pressure vessel cells with flow loss coefficients of 20 in the lower cells
I1	Instrument cooling modelled, all in the blowdown shaft cell (10)
I2	As I1 but with lower cell flow loss coefficients of 20
I3	As I1 but with lower cell flow loss coefficient of 200
I4	As I1 but with lower cell flow loss coefficients based on HDR
J2	Instrument cooling modelled and equally partitioned between the blowdown cell and the pressure vessel cells with flow loss coefficients of 20 in the lower cells

Table A.1 : MELCOR Calculations For ISP-29

All calculations were performed with MELCOR 1.8BC on a SUN Sparc1 Workstation. The maximum time step chosen for each calculation was 5 seconds.